Characterization of procedural memory neuronal substrates : role of corticostriatal networks dynamics

Nagham Badreddine

THÈSE

Pour obtenir le grade de

DOCTEUR DE L'UNIVERSITE GRENOBLE ALPES

Spécialité : **Neurosciences Neurobiologie**

Arrêté ministériel : 25 mai 2016

Présentée par

Nagham BADREDDINE

Thèse dirigée par **Sophie ACHARD, DR, CNRS, LJK**,
et
co-encadrée par **Elodie FINO, CR, CNRS, INMED**

préparée au sein du **Laboratoire « Dynamiques intracellulaires et neurodégénérescence », GIN, Inserm, U1216**
dans **l'École Doctorale Chimie Sciences du Vivant**

Caractérisation des substrats neuronaux de la mémoire procédurale : rôle de la dynamique des réseaux corticostriataux

Thèse soutenue publiquement le **8 décembre 2020**,
devant le jury composé de :

Mr Rémy SADOUL
Professeur des Universités, Université Grenoble Alpes, Président du jury
Mr Eric BURGUIERE
Chargé de recherche CNRS, ICM, Rapporteur
Mr Paolo GUBELLINI
Directeur de recherche, IBDM, Rapporteur
Mr Nicolas MALLET
Chargé de recherche CNRS, Université de Bordeaux, Examinateur
Mme Sophie ACHARD
Directrice de recherche CNRS, LJK Grenoble, Directrice de thèse
Mme Elodie FINO
Chargée de recherche CNRS, INMED Marseille, Co-encadrante de thèse, Invité

إلى أمّي و أبي

To my parents

Remerciements

Je souhaite tout d'abord remercier les membres du jury, pour avoir accepté d'évaluer ce travail de thèse. Je remercie le Dr. Eric Burguière et le Dr. Paolo Gubellini d'avoir accepté d'être rapporteurs de cette thèse, le Dr. Nicolas Mallet et le Dr. Rémy Sadoul d'avoir accepté de participer en tant qu'examinateurs. Je remercie spécialement le Dr. Rémy Sadoul de m'avoir encouragé à faire une thèse.

Je tiens à remercier les membres des comités de suivi de thèse, le Dr. Nicolas Mallet et le Dr. Mireille Albrieux pour leurs conseils pertinents et leurs esprits critiques vis-à-vis du projet.

Je remercie Frédéric Saudou de m'avoir acceptée dans son équipe pour la réalisation de ma thèse.

Je remercie Emmanuel Barbier de m'avoir accueillie dans les bureaux de son équipe et de m'avoir permis de finir ce travail dans de très bonnes conditions.

Elodie, merci pour tout. Merci pour ton encadrement et d'avoir accepté de diriger ce travail de thèse. Merci d'avoir toujours été présente (même quand tu étais à 2 doigts d'accoucher !). Merci pour toutes les discussions scientifiques où on se lançait des idées par rapport au projet et à ce qu'on pouvait encore faire. J'ai vraiment apprécié ces moments, je peux sincèrement dire qu'ils furent mes moments préférés. Merci pour la confiance que tu m'as accordée quant au projet. Merci pour toutes les discussions sur le voyage, la découverte de nouvelles cultures et sur la vie en général. Merci d'avoir continué à me parler malgré tous les 'mercis libanais' (je n'explique pas plus que ça !). Merci pour ta patience, ton ouverture d'esprit et d'avoir instauré une ambiance de travail très agréable au sein de notre petit groupe.

Sophie, merci d'avoir accepté de diriger ce travail de thèse malgré une répétition peu convaincante avant le concours. Merci d'avoir toujours été présente et d'avoir géré tous les problèmes administratifs et les situations difficiles.

Florence, la bienveillance incarnée. D'abord merci pour ton aide et ta présence permanente pour l'utilisation du 2P. Merci pour les discussions scientifiques qu'on avait et qu'on a encore par rapport aux analyses à faire et au projet en général. Merci de m'avoir écouté quand je me plaignais de tout et n'importe quoi. Mais surtout merci pour les fous rires qu'on se tapait les vendredis soir (aka les moments de craquage). Merci d'avoir été ma partenaire pour au moins 150 brevets innovants dans tous les domaines qui puissent exister (il faudra d'ailleurs qu'on fasse un recensement de toutes ces idées, je suis sûre qu'il y en a au moins une qui pourrait passer !).

Gisela, muchas gracias. Merci pour ta bonne humeur constante pendant ces 3 dernières années. Merci d'avoir partagé le travail tout le long de la thèse, et surtout l'entrainement des

souris au Rotarod. Je ne peux que penser à toi en enchaînant comportement et perfusion. Merci pour tous ces soirs où on n'entendait que ta voix chanter dans les couloirs.

Guillaume B, merci pour ton aide et ta patience chaque fois que je t'envoyais un mail pour te demander 'je clique où maintenant'.
Nicolas T, merci pour ta patience et les poses de yoga face aux problèmes administratifs.

Evidemment un grand merci à tous les membres de l'équipe.
Eve, merci pour ton intelligence et l'intérêt que tu portais à tous les projets. Merci pour toutes les discussions pendant les soirs passés à analyser. Merci pour les cours de français. Et surtout, merci pour le génotypage !
Aurélie, ma Mary Poppins préférée. Merci pour ta disponibilité. Merci pour ta gentillesse qui n'a pas de fin. Merci pour tes passages dans le bureau pour nous faire des câlins ou nous donner à manger.
Hélène, merci pour les times story qui tombaient chaque fois un dimanche soir où il pleuvait (on finira par finir ce dernier avant nos soutenances ou peut-être après !).
Max (2), merci pour les petits moments à regarder des vidéos de Brooklyn Nine-Nine et Parks and Recreation.
Max (1), merci pour ton esprit critique de très haut niveau et pour tous tes conseils pour rendre le projet plus 'beau'. Merci pour les moments de sagesse en fin de soirée, et pour les discussions sur la vie pendant et après la thèse. Et puisque je sais que tu n'aimes pas, merci cousin !
Anne-Sophie, merci pour ton esprit critique et ton intelligence. Tu as une capacité à poser des questions intéressantes sur n'importe quel type de sujet, ce que j'ai sincèrement apprécié.
Chiara, j'aurais fini ma thèse sans avoir touché à un seul western blot ! Merci pour les barbecues chez toi.
Emeline et Anca, merci pour votre bonne humeur constante.
Nathalie, merci d'avoir toujours pris le temps pour répondre à mes questions administratives et pour ta patience face à mon incompréhension du système administratif.
Aux anciens du labo : Julie-Anne de m'avoir donné l'idée du tiroir de nourriture, Amandine pour tes petites blagues et tes histoires de thèse. Julie, merci pour ton sourire constant. Sylvie d'avoir toujours eu le grand sourire et une très belle vision de la vie. Maria, merci pour ta gentillesse et nos discussions. Tu as apporté un bout du Liban au labo et je t'en remercie. A Caroline, merci pour ton sourire et ton aide. Bien sûr, merci à Pierre, d'avoir été ma première expérience d'encadrement.

Mariacristina, merci pour ton rire que je reconnaissais de loin et qui me faisait sourire. Merci pour ta gentillesse et ton humour.
Rémi, merci d'avoir été la personne la plus posée et la plus stable que j'ai jamais rencontré. Merci pour ta gentillesse, et ton intelligence.
Céline, ma partenaire neurocog. Merci pour les soirées 'la bourse', pour toutes nos discussions sur la vie de thésard et sur la vie en général.
Doris, merci d'avoir toujours été sympa avec moi, et pour ton petit rire mignon.

Sophie, merci pour ton humour noire (je n'ai pu m'empêcher de faire la blague).
Noémie, je ne peux dire que 'Salut Noémie !' Merci pour ta bonne humeur et ton sourire.
Roxanne, merci pour ton énergie sans égale, et pour tous les grands 'salut' accompagnés d'une petite danse contemporaine.

L'équipe Marty et le PIC GIN, merci de m'avoir accueillie dans vos couloirs.
Mathilde B et Laurianne, merci pour les discussions de geek et pour les repas à midi, surtout pendant cette dernière période de rédaction. Merci pour les idées de projets qui valent des millions.
Mathilde C, merci pour ton sourire constant, de m'avoir proposé de faire du parapente et d'avoir été intéressée par l'évolution de ma thèse.
Laurent, Julie, Anne, Isabelle, Yasmina, Jacques, merci pour vos sourires et votre gentillesse.

A l'équipe Buisson, merci de m'avoir laissée utiliser votre étireuse.
Adrien, merci pour tes conseils pour le patch. Merci pour toutes les discussions qu'on avait sur la thèse pendant que tu patchais et que j'étirais.

Merci à l'équipe Depaulis de m'avoir toujours laissée utiliser son matériel.
Emel, merci pour ton intelligence et ton esprit critique (qui m'ont été utiles en tant que ton binôme de TP). Merci pour toutes les discussions qui ne devaient durer que quelques minutes et qui finissaient 1 heure plus tard dans les couloirs de l'animalerie.
Merci à Guillaume, Florian, Lucile et Isabelle pour leur gentillesse et leur aide.

Merci à l'équipe Carnicella.
Sébastien, merci pour l'intérêt que tu as porté à mon projet de thèse et pour tes conseils.
Merci également à tous les membres de l'équipe pour leur gentillesse et d'avoir été arrangeants pour l'utilisation du matériel à l'animalerie et du cryostat.
Magali, merci pour ta présence quand on avait besoin d'aide avec du comportement. Mais surtout merci pour toutes les discussions sur tout et n'importe quoi et pour ton air du Sud.

Merci à l'équipe Barbier de m'avoir accueillie dans leurs bureaux et leurs couloirs.
Merci à Veronica et Fabien qui passaient par l'étape de fin de thèse en même temps que moi, mais qui ont gardé leur bonne humeur.
Jan, merci d'avoir partagé un bureau avec moi et de m'avoir aidée à déménager.

Merci à toute l'équipe administrative pour tout son travail et sa patience.

Sylvain, Fabien, Laure et Flore, merci pour toutes les petites blagues dans les couloirs de l'animalerie et pour votre gentillesse sans équivalent. Merci surtout pour votre aide.

Merci à Georges, Annie et Joséphine. Vos sourires le matin égayaient mes journées.

Merci à Evelyne. Pour le travail à la laverie, et d'avoir toujours pris des nouvelles de mes parents.

Merci à tous les bisontins maintenant grenoblois.
Merci à Antoine pour sa gentillesse et son sourire. A Pierre pour ma première expérience de ski et pour sa patience à chaque fois que je tombais (ce qui arrivait souvent).
Merci à tous les bisontins qui ont rendu mes années de licence agréables.

Merci à Vincent Van Waes pour ma première expérience dans un labo.
Merci à Solène Pedron qui gérait plusieurs étudiantes alors qu'elle était en fin de thèse. Merci pour tous tes conseils et les petits mails ces dernières années.

Vini, merci pour les discussions qu'on avait sur tout et n'importe quoi. Je pouvais vraiment me lâcher en te parlant et c'était vraiment agréable.

Alice, merci pour toutes les discussions au milieu de la nuit et qui ne se terminaient qu'une fois le soleil levé. On n'attendra pas 10 ans pour se revoir cette fois.

Chirine, merci pour tout. Merci pour ta gentillesse, ton sourire, ton intelligence. Mais surtout merci d'avoir toujours été là. Merci pour les petites balades les week-ends après-midi. Merci de m'avoir appris à nouer une cravate (même si je pense qu'aucune de nous deux n'a réussi à le faire à la fin !). Merci pour ton enthousiasme dans la vie.

Wilhelm, mille fois merci. Merci de m'avoir écoutée râler pendant des heures, des jours et des mois cette dernière année. Merci pour tes blagues pourries et ton rire ultrason qui me font éclater de rire. Merci pour ta patience et ton soutien.

A ma famille, le plus grand merci pour leur soutien tout au long de ma vie et plus particulièrement pendant ces années de thèse.
A mes parents, sans qui je n'aurais jamais réussi. Merci de m'avoir fait confiance et de m'avoir soutenue dans tous mes choix.

شكرا أمي و أبي على كل شيء. هذا العمل نتيجة تعبكم و دعمكم.
شكرا خالتي منيفة على اهتمامك بي.

Noureddine (aka za3tar), merci d'avoir été le meilleur grand frère.
Nancy (aka e5te lmoufaddale), merci d'avoir été la personne la plus bizarre qu'on puisse imaginer.
Nathalie (aka nat7alieu), merci pour la nourriture que tu préparais à ta grande sœur puisqu'elle arrive à peine à faire cuire des pâtes.
Ali (aka allouchi), merci pour ton côté ronchon qui équivaut au mien.
Manon (aka MG), pour ta gentillesse et les gâteaux (surtout la galette comtoise !).

Et enfin, merci à toutes les souris sans lesquelles ce projet n'aurait pas pu aboutir.

Summary

Remerciements 5

List of abbreviations 14

Figure Summary 16

Part I: Introduction 17

I- An overview of the different types of memory 18

A) Models of memory 18

B) Short-term memory 21

1) Prefrontal cortex 21

2) Hippocampus 23

C) Long-term memory 23

1) Explicit or declarative memory 23

a- Episodic and semantic memories 24

b- Brain structures involved in declarative memory 24

1. Cortical areas 25

2. Medial temporal lobe and hippocampus 26

2) Implicit or non-declarative memory 27

a- Associative memory (classical and operant conditioning) 28

b- Non-associative memory 29

c- Priming 30

d- Procedural memory 30

II- Anatomy and circuits of the basal ganglia 36

A) Historical overview of the basal ganglia 36

B) Basal ganglia anatomy 36

1) Nuclei of basal ganglia 37

a- Striatum 37

b- The subthalamic nucleus 38

c- Globus pallidus 38
d- The substantia nigra 39
2) Cortico-basal ganglia-thalamocortical loops 39
a- Basal ganglia inputs 40
1. Cortico-striatal projections: funneling and parallel circuits 40
2. Nigrostriatal projections 43
3. Other projections to the striatum 44
b- Basal ganglia outputs 45
3) Anatomy of the striatum 46
a- The striatum on a cellular level 46
1. Projection neurons or medium-sized spiny neurons 47
2. Interneurons 49
b- Striatum: a heterogeneous structure 54
1. Striosome / Matrix dichotomy 54
2. DorsoMedial Striatum (DMS) and DorsoLateral Striatum (DLS) 56

III- Basal ganglia: role in motor control 59
A) Pathways of the basal ganglia 59

B) Role of direct and indirect pathways in motor control 61

IV- Procedural learning and Basal Ganglia circuits 64
A) Procedural learning: BG and striatal circuits 64

B) Behavioral assays to test procedural memory 68

C) Dynamics of striatal networks during procedural learning 70

V- Dysfunctions in the BG pathways: example of Huntington's disease 74
A) Introducing Huntington's Disease 74
1) Genetic aspects 74
2) Triad of symptoms 76
a- Motor symptoms 77
b- Psychiatric symptoms 78
c- Cognitive symptoms 78

3) Neurodegeneration in HD 79
a- Structure degeneration 79
b- Cellular degeneration 82
4) Mouse models of HD 84

B) Dysfunction of cortico-striatal networks 86

Part II: Methods 89
I- Experimental models 90

II- Stereotaxic injections 90

III- Behavioral experiments 91
A) Accelerated rotarod 91

B) Fixed-speed rotarod 92

C) Open-field 92

IV- Brain slices 93

V- *Ex-vivo* two-photon imaging and mutli-patch-clamp recordings 94
A) Two-photon calcium imaging 94

B) Whole cell patch-clamp recordings 95

VI- Retrograde tracing with Cholera Toxin B (CTB) 97

VII- cFos-TRAP experiments 97

VIII- Chemogenetics experiments 98

Part III: Results 100
I- Objectives 101

II- Study 1: Spatiotemporal reorganization of corticostriatal network dynamics encodes motor skill learning 103

III- Study 2: Classification of types of neurons from calcium imaging 183

IV- Study 3: Disruption of motor skill learning and associated striatal network activity in a Huntington's Disease mouse model 192

Part III: General discussion 218

1) Importance of striatal 'engram' cells 219

2) Role of synaptic plasticity in learning 221

3) Local inhibition as a mechanism of reorganization of striatal networks 222

4) Dissecting functional heterogeneity of striatal networks in motor skill learning 225

a- Role of dMSNs vs iMSNs in learning 225

b- Role of matrix and striosomes in learning 227

5) Interaction of different brain structures during motor learning 228

Conclusion 231

References 232

Résumé 266

Abstract 268

List of abbreviations

BG	Basal Ganglia
CR	Calretinin
ChAT	Choline AcetylTransferase
DMS	DorsoMedial Striatum
DLS	DorsoLateral Striatum
GPe	Globus Pallidus external segment
GPi	Globus Pallidus internal segment
GABA	gamma-Aminobutyric acid
HD	Huntington's Disease
LTD	Long-Term Depression
LTP	Long-Term Potentiation
MSN	Medium-sized Spiny Neurons
iMSN	Medium-sized Spiny Neurons of indirect pathway
dMSN	Medium-sized Spiny Neurons of direct pathway
MTL	Medial Temporal Lobe
NMDA	N-Methyl-D-aspartic acid
NPY	Neuropeptide Y
PV	Parvalbumin
SNc	Substantia Nigra pars compacta
SNr	Substantia Nigra pars reticulata
SST	Somatostatin
STN	SubThalamic Nucleus
TAN	Tonically Active Neuron

TBZ	Tetrabenazine
VP	Ventral Pallidum
VTA	Ventral Tegmental Area

Figure Summary

Figure 1: Multi Store Model of memory proposed by Atkinson and Shiffrin in 1968. 18
Figure 2: Multicomponent model of memory developed by Baddeley and Hitch. 19
Figure 3: Tulving's memory model. 20
Figure 4 : Behavioral tasks to test short-term memory in monkeys and rodents 22
Figure 5: Place cells and grid cells. 26
Figure 6: Classical conditioning, based on Pavlov's experiment. 28
Figure 7: Experimental design of a Skinner box. 29
Figure 8: Defining an action as goal-directed and habit. 31
Figure 9: Place response task to test the formation of habits 32
Figure 10: Involvement of the striatum in the formation of a habit with a place response task. 33
Figure 11: Summary of neural correlates for different memories. 34
Figure 12: Basal ganglia pathways and nuclei 37
Figure 13: Model of the basal ganglia based on the information 'funneling' hypothesis. 41
Figure 14: Parallel or segregated loops of the basal ganglia 42
Figure 15: Input and output pathways of the basal ganglia on a sagittal view. 45
Figure 16: Striatal neuronal types. 47
Figure 17: Representation of a medium spiny neuron and its electrical properties 48
Figure 18: Diversity of striatal interneurons 50
Figure 19: Striatal circuits 53
Figure 20: Segregation of the striatum into matrix and striosome compartments 54
Figure 21: Striatal somatotopic map of a mouse body in the DLS but not the DMS. 57
Figure 22: Box and arrow model of the BG. 60
Figure 23: Involvement of the DMS and DLS in procedural learning based on lesion studies 65
Figure 24: Functional segregation of the cortico-BG-thalamocortical loops in humans 66
Figure 25: Chunking of DLS activity in a T-maze task. 68
Figure 26: Behavioral tests for procedural memory 69
Figure 27: Models of associative and sensorimotor circuits during skill learning 72
Figure 28: Correlation between CAG repeats and age. 76
Figure 29: Symptom manifestation in relation to age and CAG repeats 77
Figure 30: Normal vs HD brain 80
Figure 31: Levels of severity of HD and affected structures 81
Figure 32: Corticostriatal circuit in normal and HD conditions. 86
Figure 33: Stereotaxic surgery. 91
Figure 34: Rotarod and learning curve. 92
Figure 35: Open-field test. 92
Figure 36: Brain slices for DMS and DLS recordings 93
Figure 37: Calcium imaging analysis 95
Figure 38: Electrophysiological recordings and analysis 96
Figure 39: Retrograde tracing with CTB.. 97
Figure 40: Cre-lox system. 98
Figure 41: DREADD system. 99
Figure 42: Cortical and thalamic inputs onto different striatal neurons 224
Figure 43: Plasticity of dMSNs and iMSNs during learning 226

Part I: Introduction

I- An overview of the different types of memory

Memory is a function which allows us to integrate, store and reproduce information to interact with our environment. It allows us to store knowledge for later use or recall. Memory is perceived as a unitary system and has long been considered as such. It was proposed by Atkinson and Shiffrin in 1968 that memory can be divided into three major classes: sensory memory, short-term memory and long-term memory. By interacting with our environment, we are confronted to sensory stimuli. This information is stored by sensory memory allowing us to access the information in the future. Short-term memory intervenes when one needs to store an information for a short period of time, it is also known as working memory. This short-term memory allows us to remember the beginning of our sentence when we are speaking, or to store the concept that is discussed on a page we are reading, but not the specific words. Storing these words for a longer period of time requires long-term memory. This memory enables us to store information for a period ranging from days to years. This information may be retrieved consciously (explicit memory) or unconsciously (implicit memory) (Camina & Güell, 2017).

A) Models of memory

Atkinson and Shiffrin proposed a Multi Store Model of memory which divides memory into three classes as mentioned earlier (Atkinson & Shiffrin, 1968). This model described the functioning of memory as a linear passing from one store to the other (Fig.1).

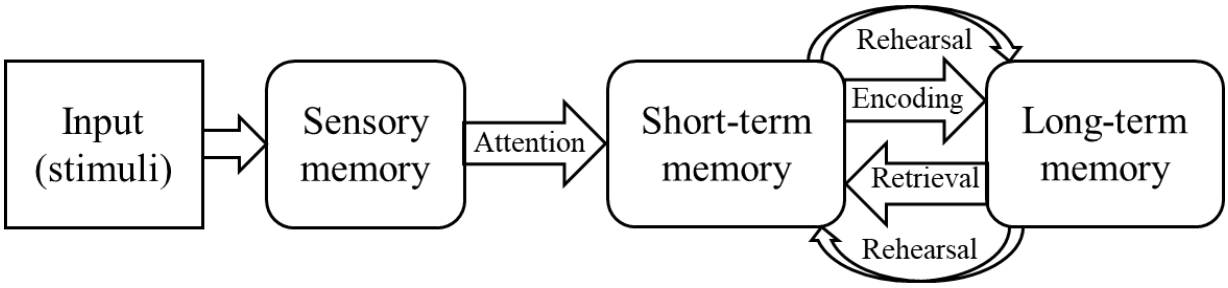

***Figure 1:* Multi Store Model of memory proposed by Atkinson and Shiffrin in 1968**. *This model is linear. A stimulus is received and then stored by sensory memory. By paying attention to that information, it is stored in short-term memory which after rehearsal, can be encoded and stored in the long-term memory store. Adapted from (Amin & Malik, 2014).*

This model was criticized for being too linear and not recognizing the existence of several components of each class of memory. Baddeley and Hitch were among the scientists who criticized this model, especially the short-term memory store of the model (A. D. Baddeley & Hitch, 1974). They presented in 1974 a second model of short-term memory and introduced the term 'Working memory'. This model was characterized by splitting up a memory store into several components. Their model consisted of three main parts: the central executive, the phonological loop and the visuospatial sketchpad. The phonological loop deals with all verbal information storage, whereas the visuospatial sketchpad allows the storage of visuospatial information. The central executive controls both the phonological loop and the visuospatial sketchpad. This Working Memory Model presented by Baddeley and Hitch in 1974 was criticized for only looking into short-term memory and not giving a more comprehensive model of memory explaining the transformation of short-term memory into long-term memory. Considering these criticisms, in 2000, Baddeley and Hitch added another component to the model, an episodic buffer (Fig.2) (A. D. Baddeley & Hitch, 2000). The episodic buffer would then become a temporary storage unit. It is assumed that it can act as a buffer between the phonological loop and the visuospatial sketchpad, but importantly, it also allows an interaction between working memory and long-term memory (Funahashi, 2017).

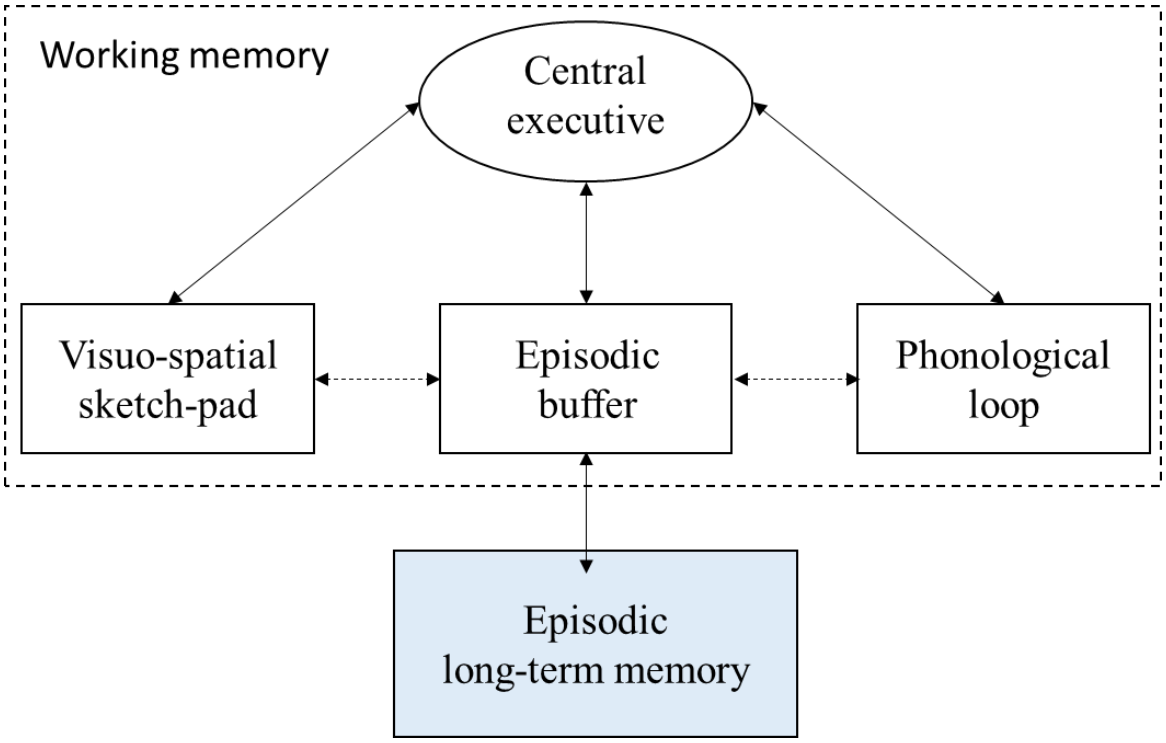

***Figure 2:* Multicomponent model of memory developed by Baddeley and Hitch.** *The episodic buffer was added in the year 2000 to explain the mechanistic process of working memory formation into a long-term memory. The interaction between each of the stores (central executive, visuospatial sketch-*

pad, phonological loop) and the newly added episodic buffer, allows the formation of this memory. Adapted from (A. Baddeley, 2010).

In the models presented earlier, short-term memory was presented with multiple stores. However long-term memory was seen as a whole. During the 1960's, scientists proposed to divide long-term memory into explicit and implicit memory (Fig.3). Explicit memory corresponds to memories that we evoke on purpose, whereas implicit memory corresponds to memories, which do not need any effort in resurfacing. In addition, in 1972, Endel Tulving proposed a new model of memory (Tulving, 1972) suggesting a distinction between two types of explicit memory: semantic and episodic (Fig.3), semantic memory being the memory of general knowledge and episodic memory being the memory of experience. Although this model was later modified, the classification proposed by Tulving remains until this day. Implicit memory on the other hand corresponded to memory that is used unconsciously and was first only composed of procedural memory. During the 90's, this model of implicit memory was updated to include four subtypes of memory (Squire & Zola, 1996).

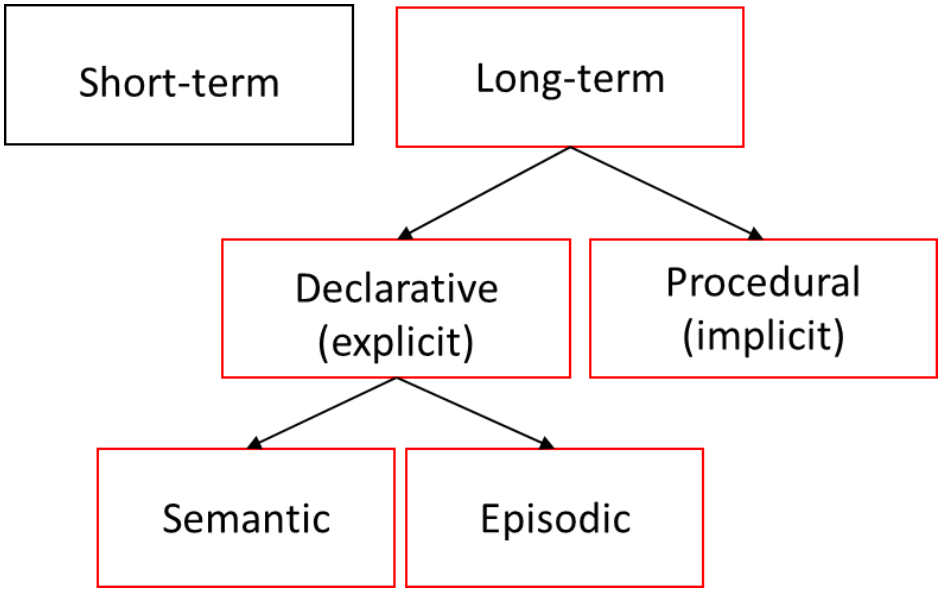

***Figure 3:* Tulving's memory model**. *Short-term and long-term memory constitute two different compartments in this model. Long-term memory is then divided into declarative and non-declarative memory which are in turn divided into other types of memory. In red: Tulving's model involving long-term memory. Adapted from (Kalonaris, 2018).*

Here, I presented a quick overview of different models of memory and their historic background to have a broad understanding of how the current classification started. What is interesting is that in all models, two main classes of memory emerge: short-term and long-term memory. For the rest of this first introductory chapter, I will consider the updated version

of Tulving's model of memory. I will describe in more details each form of memory and present the different brain areas involved in these processes.

B) Short-term memory

Short-term memory is the capacity to temporarily store information. Once information is processed, we talk about working memory. It is the memory that is involved in many events of our daily life. One good example is when we want to dial a phone number that we wrote on a piece of paper: after reading the numbers, they should be maintained for several seconds before we dial them. These numbers were only shortly stored and not consolidated because if we need to redial the number at a later time, we already forgot and we need to take another look at the paper to remind ourselves of the number. Short-term memory is retained for a relatively short time (up to 30 seconds) (Cascella & Al Khalili, 2019). I mentioned earlier how Atkinson and Shiffrin divided memory into sensory, short-term and long-term memory based on the time-scale of retention. Sensory memory is thought to act as a funnel of information into short-term memory (Cowan, 2008; Tripathy & Öğmen, 2018). One good example of short-term memory is George Miller's 'magical' number 7+/-2 which posits that adult humans can repeat without error a list of 7 random numbers (+/-2 for variability) (Cowan, 2015). When more items are present, chunks can be made to group them in only 7+/-2 chunks and thus be retained more easily.

As I described earlier, short-term memory was divided into several compartments. In order to understand how these compartments are organized and how this memory functions, identifying the brain areas that are responsible for this memory and the neurophysiology of these areas is necessary.

1) Prefrontal cortex

From studies attempting to identify the neural basis of short-term memory, the prefrontal cortex (PFC) emerges as playing a central role. First evidence dates back to a study by (Jacobsen, 1935). He trained monkeys on a simple delayed-response task (Fig.4). First, monkeys were shown that food was hidden in one of two identical cups. After a delay of several seconds to minutes while monkeys did not see the cups, they were tested to see if they would choose the right cup where the food was hidden (Fig.4). Jacobsen then performed

bilateral lesions of the PFC which resulted in a severe impairment of the monkeys' performance during this task but not during other tasks. Later studies confirmed these results and narrowed the area of the PFC that is responsible for short-term memory, area 46 of the dorsolateral PFC (Levy & Goldman-Rakic, 2000; Pribram et al., 1952). The Delayed-response task then became a widely used experiment to examine prefrontal cortical functions (Curtis & D'Esposito, 2004; Funahashi et al., 1993; Fuster, 2008; Rosenkilde, 1979). With the success of this task in deciphering the anatomical structures involved in the formation of this memory, a variation of the task, the delayed alternation task, started being used in rat and mice studies (Arime & Akiyama, 2017; Funahashi, 2013; Yang et al., 2014). This task allows an assessment of spatial working memory in a T or Y-maze (Fig.4).

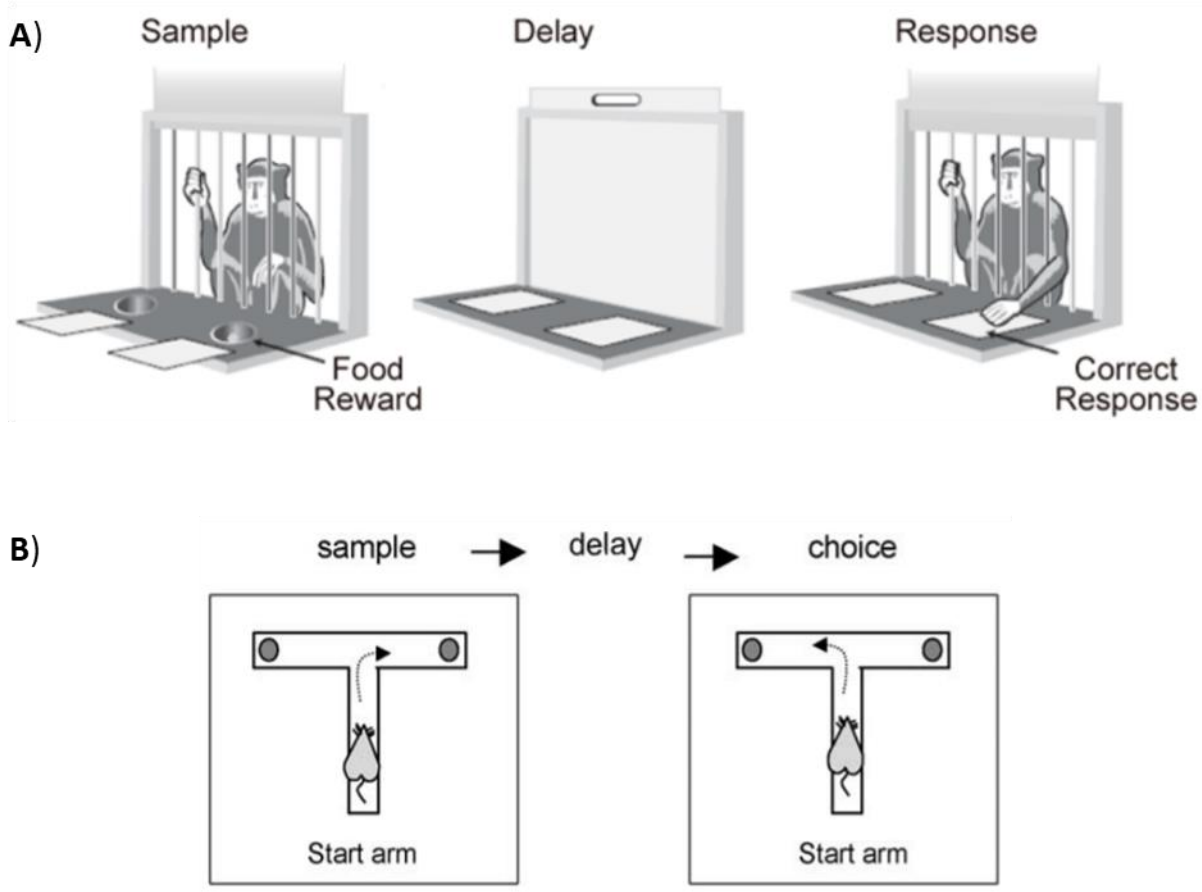

Figure 4 : ***Behavioral tasks to test short-term memory in monkeys and rodents****. **A**) Delayed-response task in monkeys. Experiment based on the study done in 1935 by Jacobsen. Monkeys are placed in a Wisconsin General Test Apparatus. They are shown two cups, one of them containing food. The monkeys cannot see the cups during a period of time. Then they are shown the cups covered and are required to choose which cup contains the food. From* (Tsujimoto & Postle, 2012). ***B****) Delayed alternation task on a T-maze. The animal is first placed in one arm of the maze and allowed to enter one of the arms. The animal is then removed from the maze for a certain time and when it is returned to the maze, it will usually choose the other arm. From* (Dudchenko, 2004).

2) Hippocampus

Another brain region that has recently surfaced as playing a role in short-term memory is the hippocampus. Although this brain region is known for its role in long-term memory consolidation, more and more evidence is starting to show its involvement in the processing and maintenance of working memory (Axmacher et al., 2007; Ranganath & D'Esposito, 2001). Indeed, using an fMRI approach, Ranganarth and D'Esposito showed that the anterior part of the hippocampus was more activated during the presentation of novel faces than when familiar faces were shown. A more recent study showed that patients with hippocampal amnesia were not able to remember the location of novel objects, even in a short period of time (a few seconds) (Jonides et al., 2008; Kumaran, 2008). This shows that short and long-term memory may share similar neural mechanisms.

C) Long-term memory

Long-term memory corresponds to a storage of information for long periods that last days, years and can go up to most of our lives. As far as we know, the capacity of storage of this memory is unlimited. As seen earlier (Fig.3), long-term memory is divided into explicit (or declarative) and implicit (or non-declarative) memory. Explicit memory can be evoked consciously and is divided into two types of memory: episodic memory and semantic memory. On the other hand, implicit memory corresponds to unconscious memories. There are four different types of implicit memory: associative, non-associative, priming and procedural. We will briefly present associative and non-associative memories, and go into detail on procedural memory since it is the one at the center of my work.

1) Explicit or declarative memory

Explicit memory includes memories that can be evoked consciously such as episodic memory and semantic memory. Episodic memory, as the term 'episodic' suggests, corresponds to the memory of event and personal experiences. Semantic memory however, stores memory about facts and knowledge from the moment we are young. With episodic memory, people are usually able to remember even the smallest details of events, what time it was, how they felt, what they were wearing… Semantic memory on the other hand corresponds to all the

information we collected since we were young and they are usually not linked to personal experience.

a- Episodic and semantic memories

Episodic memory is the memory of personal experiences, it involves the ability to learn, store and retrieve this kind of information. This memory holds information about the content (What), its spatial context (Where) and temporal context (When). It was first defined as a distinct memory from semantic memory by Tulving in 1972. He was also the one to describe how this memory was encoded and restored (Tulving, 1983). He created in 1983 another memory model or a processing system of memory that explains how episodic and semantic memories are differentially processed. What episodic memory is characterized by is still debated to this day (Eichenbaum, 2014; Howard & Eichenbaum, 2015), but date and time seem to be key elements. Memories of an event can be modified or distorted, but as long as the spatial and temporal contexts are present, episodic memory persists. Semantic memory on the other hand corresponds to the memory of facts, of knowledge about the world, word meanings etc. (Moscovitch et al., 2005). Tulving precises that restoring an 'episode' is always linked to our subjective consciousness since it is linked to our past, he called this autonoetic consciousness. In the case of semantic memory, there is a noetic consciousness which corresponds to knowledge without a sense of self (Moscovitch et al., 2005; Tulving, 1983). Thus episodic memory was defined as a unique system, distinct from semantic memory. The distinction between these two types of memory was helped by neuropathological cases such as an amnesic patient called KC. This patient had an intact semantic memory but an impaired episodic memory with difficulty remembering an entire lifetime of experiences (Rosenbaum et al., 2005; Tulving, 1985). KC was unable to relive an episodic event that occurred in his past nor was he able to imagine future experiences that he might have. Not only did the case of KC shed the light on the distinction between episodic and semantic memory, it also opened the door for studying the role of episodic memory in future thinking.

b- Brain structures involved in declarative memory

There are several neural components that contribute to the establishment of episodic and semantic memory. A large network of brain areas including neocortical areas and parts of the

medial temporal lobe (MTL), mainly the hippocampus and parahippocampal cortical areas. Each of these structures seems to play a role in the proper functioning of episodic memory.

1. Cortical areas

The prefrontal cortex is involved in the formation of new episodic memories. But it has also been shown to be involved in semantic memories. Each side of the prefrontal cortex seems to be involved in one type of memory. Neuroimaging studies at the end of the last century show that episodic memory activates right prefrontal regions, whereas semantic memory activates left prefrontal areas (Burianova & Grady, 2007).

The hippocampus is a central structure in the formation, processing and recollection of episodic and semantic memories. However, the hippocampus receives inputs from layers 2 and 3 of the entorhinal cortex, which receives inputs from the perirhrinal cortex and parahippocampal cortex (Moscovitch et al., 2016). Declarative memories are encoded by parahippocampal cortical areas. The perirhinal cortex is involved in visual object recognition. The parahippocampal cortex, constituting the biggest part of the medial temporal lobe, is involved in recognizing places and processing information related to that place (Camina & Güell, 2017; Dickerson & Eichenbaum, 2010). Based on MRI studies, the anterior temporal lobe seems to be a crucial neural substrate of semantic memory (Miyashita, 2019).

Thus, cortical areas play an important role in the formation of these types of memory (episodic and semantic). Without these structures, the hippocampus would not be able to integrate information about complex object representations, or about the representation of the environment. The connectivity and the circuits formed between the hippocampus and the different cortical areas should therefore be taken into account when discussing the formation or the recollection of these memories. One good example of the connectivity between the cortex and the hippocampus is the interplay between place and grid cells. The search for behavioral or cognitive correlates started a while back, and in the case of the hippocampus, it started with ‘place cells’. *In vivo* electrophysiological studies showed that the firing of principal cells in the hippocampus of rodents is determined by the location of the animal (O’Keefe & Dostrovsky, 1971), they are active in a single area of an environment, thus earning them the name ‘place cells’ (for review see (Bush et al., 2014)) (Fig.5). Other cells specific of certain behaviors or movements were later discovered. Since the medial entorhinal cortex is a principal input to the hippocampus, more recent studies looked into the role this cortex could

play in spatial localization. Grid cells in the medial entorhinal cortex were identified as they would fire at regular intervals when rodents navigated in their environment. Unlike place cells, grid cells will only fire when the animal visited several locations forming a grid pattern (Fig.5). This discovery earned John O'keefe, May-Britt and Edvard Moser a Nobel Prize in physiology or medicine (Bush et al., 2014). Since both 'place cells' and 'grid cells' activities seem to be driven by movement related input, several models involving both structures and the interaction between both cell types were proposed (Bush et al., 2014). These studies show the importance of the circuits linking the hippocampus and the cortex in the formation of memories.

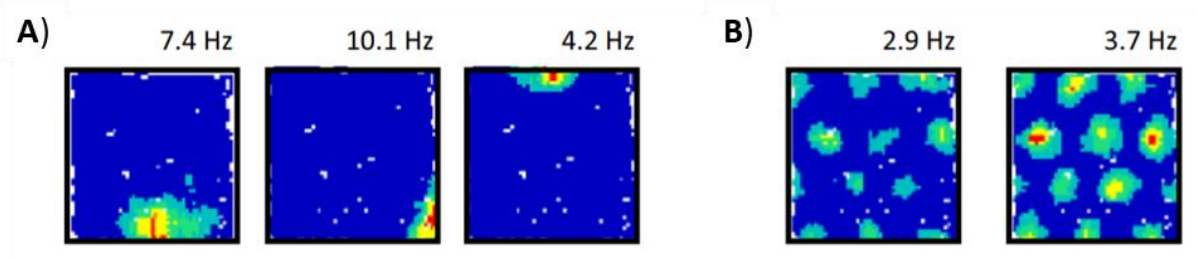

Figure 5: ***Place cells and grid cells****. **A**) Firing maps of 3 simultaneously recorded CA1 place cells, each of them having only one firing location. **B**) Firing maps of two simultaneously recorded grid cells in the medial entorhinal cortex. The formations of a grid-like pattern is clearly visible on these maps. From* (Bush et al., 2014).

2. Medial temporal lobe and hippocampus

Burianova and Grady showed that both types of memory activate common but also unique neural correlates. Both types of memory functionally activated the inferior frontal gyrus, the middle frontal gyrus, the caudate nucleus, the thalamus and the lingual gyrus. However episodic memory and semantic memory activate unique neural correlates. Episodic memory activates the right middle medial temporal lobe (MTL), whereas semantic memory activates the right inferior temporal lobe.

The involvement of the MTL in declarative memory was made clear by a study that span over 50 years of research. Henry Molaison (HM), born in 1926 in Connecticut, was suffering from a type of epilepsy that was causing him seizures for many years. Following his 16th birthday, he started having tonic-clonic seizures. By the age of 27, his seizures worsened despite the anticonvulsant medication he was on. In 1953, a neurosurgeon at Hartford Hospital, William Scoville, localized his epilepsy in the left and right MTLs. A bilateral resection of the MTLs was proposed to HM. He underwent the surgery which resulted in the removal of his amygdalae, the anterior part of the hippocampi, as well as the perirhinal cortex, entorhinal and

parahippocamal cortices. After surgery, HM was unable to form new declarative memories, he was left with severe anterograde amnesia (Scoville & Milner, 1957). Later studies showed that other cognitive faculties were not affected: language, working memory, procedural learning (Corkin, 2002). These results showed that declarative memory is distinct from other abilities and the crucial role that the hippocampus and MTL play in this memory.

In addition to the place cells described earlier for the space dimension, the important role the hippocampus plays in declarative memory is exemplified by the discovery of engram cells. An engram is defined as a physical substrate of memory, or more commonly, a memory trace. Technological advances such as the use of immediate early genes (such as *c-fos* or *arc*), markers of neuronal activity, allowed for the identification of cells that are specifically active in the formation of a memory. After learning, an assembly of cells is activated and they are labeled thanks to an immediate early gene promoter, allowing for the manipulation of these cells with optogenetics for example (for review see (Tonegawa et al., 2018)). These engram cells are supposed to be a neuronal trace of the memory. The storage of this memory for long period of time requires persistent plasticity of these cells. This is evident in the higher synaptic strength and spine density in engram cells compared to non-engram cells (Tonegawa et al., 2015). The presence of these engram cells and their role was demonstrated with other studies either reactivating these engram cells in the case of induced amnesia thus allowing for memory retrieval (Ryan et al., 2015), or reactivating engram cells in different contexts thus allowing the creation of false memories (Ramirez et al., 2013).

Thus, with the discovery of specific cells of different memories, the hippocampus was placed at the center of declarative memory.

2) Implicit or non-declarative memory

As I mentioned earlier, implicit memory or non-declarative memory corresponds to unconscious memories. It is divided into four subgroups: (i) associative memory which requires an association between different items with reinforcement or punishment, (ii) non-associative memory which only requires one association without any reinforcement, (iii) priming which corresponds to the ability to classify and identify an item faster after a first encounter thus improving the efficiency of interaction with a familiar environment, and (iv) procedural memory also known as the memory of habits.

a- Associative memory (classical and operant conditioning)

Associative memory corresponds to the storage and retrieval of information by associating information to other information. This memory is acquired by either classical conditioning or operant conditioning. Classical conditioning corresponds to learning by associating stimuli and behavior. Operant conditioning corresponds to learning by associating consequences to behavior. One of the best known examples of classical conditioning is the experiment by none other than Ivan Pavlov (Fig.6). In Pavlov's experiments, the unconditioned stimulus was the food, and unconditioned response salivation whenever the dog was presented with food. The neutral stimulus was the bell ringing because it was not associated to anything and did not induce any response. After conditioning, the bell ringing becomes a conditioned stimulus because it is now associated to food and will therefore result in salivation (Camina & Güell, 2017; Pavlov, 1927).

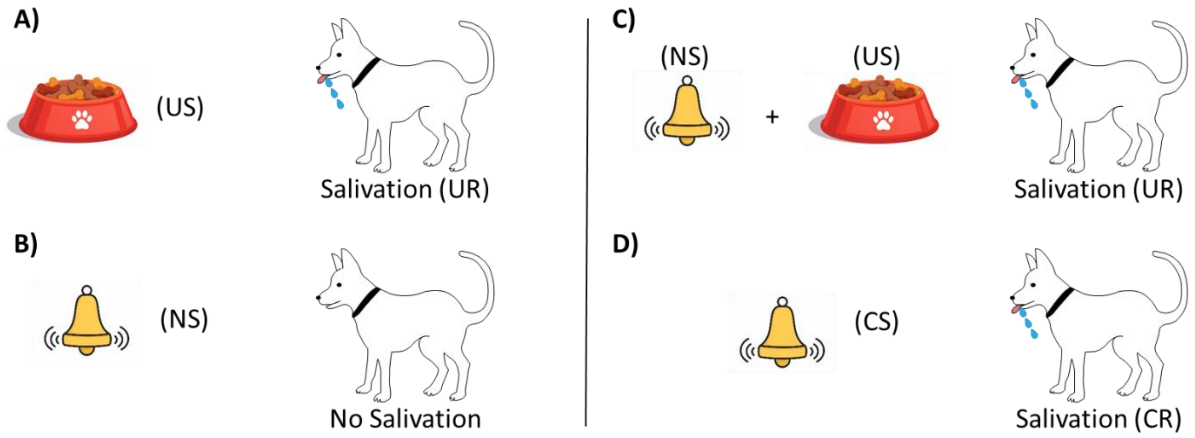

***Figure 6**: **Classical conditioning, based on Pavlov's experiment**. The experimental set up allows a distinction between different stimuli and behavioral responses and their association. **A)** When the dog is shown food (unconditioned stimulus: US), it salivates (unconditioned response: UR). **B)** When a bell rings (neutral stimulus: NS), there is no response. **C)** However, once the bell ringing is followed by food, the dog salivates again. **D)** This results in an effect of the bell ringing (now conditioned stimulus: CS) on salivation (now a conditioned response: CR). Adapted from (Hummel et al., 1991).*

Operant conditioning (also called instrumental conditioning) on the other hand corresponds to learning by associating behavior to consequences. Based on Thorndike's work, Skinner and his box are the first things we think of when we talk about operant conditioning. A skinner box or an operant conditioning chamber contains a lever on the side and when the animal moves around in the box, it knocks the lever. A food pellet is then presented in a box next to the lever (Fig.7). The animal would learn quickly the association between pressing the lever and

obtaining food. Thus he showed that positive reinforcement allows for a behavior to be repeated. This corresponds to positive reinforcement. Negative reinforcement can also allow the repetition of a behavior. Negative reinforcement corresponds to the removal of an unpleasant reinforce which would allow for the behavior to occur because it stops the unpleasant experience. Conversely, Skinner showed that negative consequences hinder the occurrence of a behavior (Camina & Güell, 2017; Skinner, 1938).

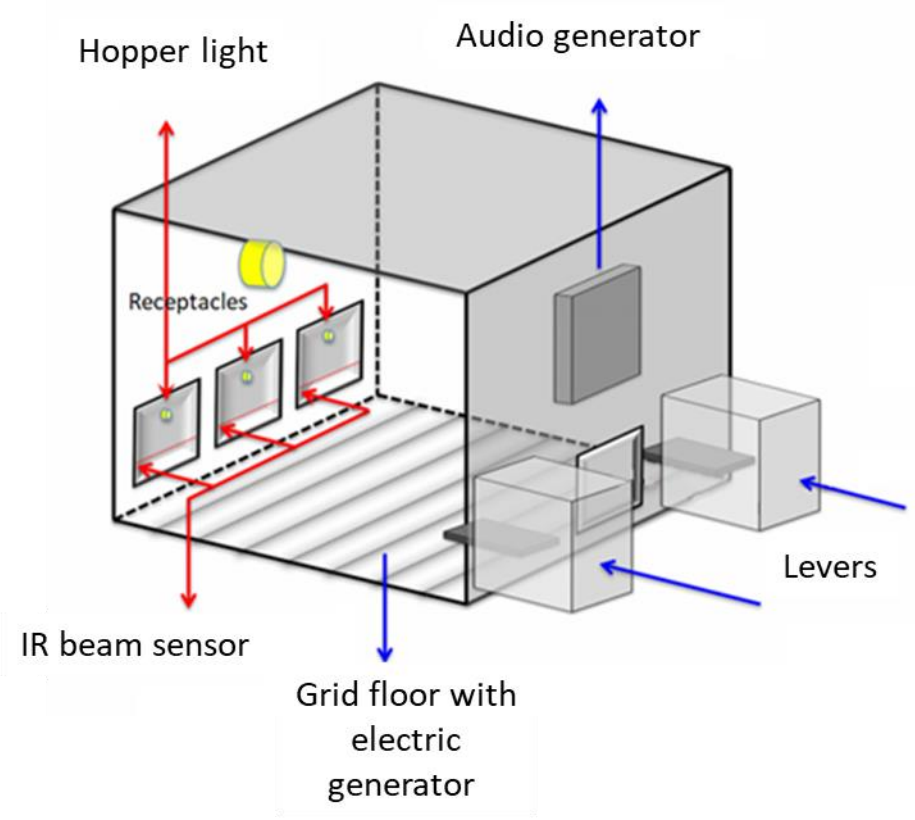

***Figure 7:* Experimental design of a Skinner box**. *For a positive reinforcement, the animal is given a reward through the food dispenser after pressing on a lever. For a negative reinforcement, the animal is electrically shocked until it presses the lever. For punishment, when the animal presses the lever, it gets an electrical shock. Adapted from* (Balcı & Freestone, 2020).

b- Non-associative memory

Non-associative learning is an implicit type of learning. Contrary to associative learning which is based on an association of two stimuli with the presence of reinforcement (positive or negative), non-associative learning takes place in the presence of one stimulus but without any reinforcement (Schausberger & Peneder, 2017). This single stimulus is presented repeatedly which leads to an attenuation of the behavioral response or an increase of this response. An attenuation of the behavioral response after the repetition of stimulus presentation is called habituation. An increase of the response is called sensitization (Poon &

Schmid, 2012). For example, having a new noise in our environment will draw our attention and may be distracting at first. But over time, we grow accustomed to the noise, and our attention towards it will decrease, we were habituated. If we hear a sudden noise, we are startled and if that noise is followed by a shock or something bigger, the next time we hear the noise our reaction is stronger. In that case we are describing sensitization. These two processes are adaptive mechanisms that give an evidence of neuronal plasticity.

Non-associative learning has been studied in a large variety of animals. Work on this type of memory earned Eric Kandel the Nobel Prize in Physiology and Medicine in 2000. Kandel and his team were able to establish a link between behavioral learning and synaptic plasticity by looking into the gill and siphon withdrawal reflex of the sea hare Aplysia (Poon & Schmid, 2012). This type of learning was later studied in other animals and their reflex pathways (response to odors in rats, proboscis extension reflex in bees and Drosophila, startle responses in rodents…).

c- Priming

Priming corresponds to the increased ability to identify and name an item after a second encounter. Priming is considered to be a part of perception and not an expression of memory *per se*. Interestingly, patients who suffered from memory dysfunctions did not have any trouble on tests of perception. When presented with a list of words and then cues of these words, they were able to complete the missing parts of the words (e.g. present brick and crate, and test bri--- and cra---) (for review see (Squire & Dede, 2015)). Electrophysiological studies showed signatures of priming occurring before the activity accompanying the recognition of an item or an event (Squire & Dede, 2015).

d- Procedural memory

Procedural memory is the memory of habits. It is the part of memory that allows for motor and executive skills that are necessary to perform certain tasks such as riding a bicycle, driving a car, chopping vegetables, playing a musical instrument... Procedural learning is acquired by repeating a task until this task becomes automatic. When a task is repeated, goals and intentions to perform the task become less and less influential and habit takes gradually over (Carden & Wood, 2018). Depending on the complexity of the task, reaching a habit will take

more or less time. Designing a behavioral test of this memory was therefore a little difficult at first. A type of learning we presented earlier, operant learning, fell into the category of a goal-directed behavior. Instrumental learning was first described as a stimulus-response (S-R) type of behavior which is strengthened by reinforcement (Hull, 1943; Thorndike, 1911). At this point, the effect of the outcome of a behavior was not taken into account. But studies have shown that animals are able to encode the relationship between an action and an outcome and can therefore control their actions based on these outcomes (reviewed in (H. H. Yin & Knowlton, 2006)). By taking into account these parameters, two types of assays to test goal-directed behaviors were put in place. One type of assays were based on the value of the outcome, others were based on the relationship between an action and an outcome, i.e. how much would an action affect the outcome. An action is considered a goal-directed action if it passes these two tests. In their review, Yin and Knowlton summarized the conditions that lead to habit formation. What they suggest is that with a 'ratio schedule', a similar response will always get a similar reward, and with more responses there are more rewards. In this case, we can speak of a goal-directed behavior. However, in an 'interval schedule', a delay is added between a response and the reward. Training under these conditions will result in a lesser sensitivity to the reward and will therefore lead to a S-R type of behavior or the formation of a habit. What was pointed out is that with an action-outcome (A-O) assay, early in training, the correlation between the response rate and the reward rate is high (when response rate varies, so does the reward rate), and with overtraining, this correlation is always high. On the contrary, with a S-R assay, this correlation is always low (Fig.8).

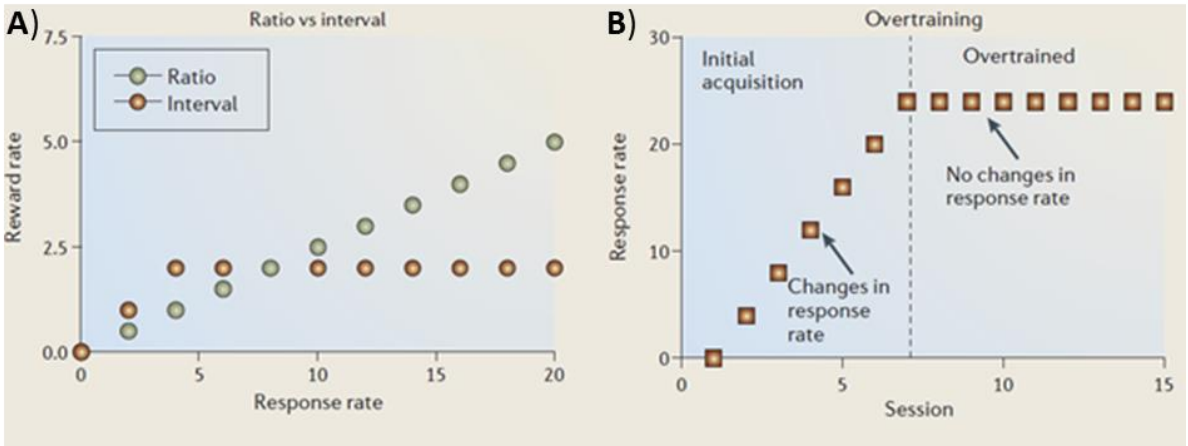

Figure 8: ***Defining an action as goal-directed and habit****. **A**) Following a ratio schedule where more responses give more rewards, leads to a goal-directed behavior. Following an interval schedule where a delay is added between the response and the reward leads to less sensitivity to the reward and to the formation of a habit. **B**) High correlation between response rate and reward rate in an action-outcome assay even with overtraining. From (H. H. Yin & Knowlton, 2006).*

Based on instrumental learning, the association between a consequence and a behavior, assays to study goal-directed behavior and habit formation were created.

One assay that allows the distinction between stimulus guided and response guided behaviors is one by Packard and McGaugh (M G Packard & McGaugh, 1996; Mark G. Packard, 2009). This test consists in a maze navigation in which animals are placed in one arm of the maze and are trained to get the food from another arm, on the left in Fig.9. Then the animal is placed in the opposing arm. If the animal goes to the same side as before (to its left), it is following a response strategy, whereas if the animal uses the cues to go where the food is placed, it is following a place strategy. Animals will initially start with a place strategy and then move to a response strategy when they received more training. Habits are considered to have been reached when animals perform a set of learned actions and not following a spatial cue.

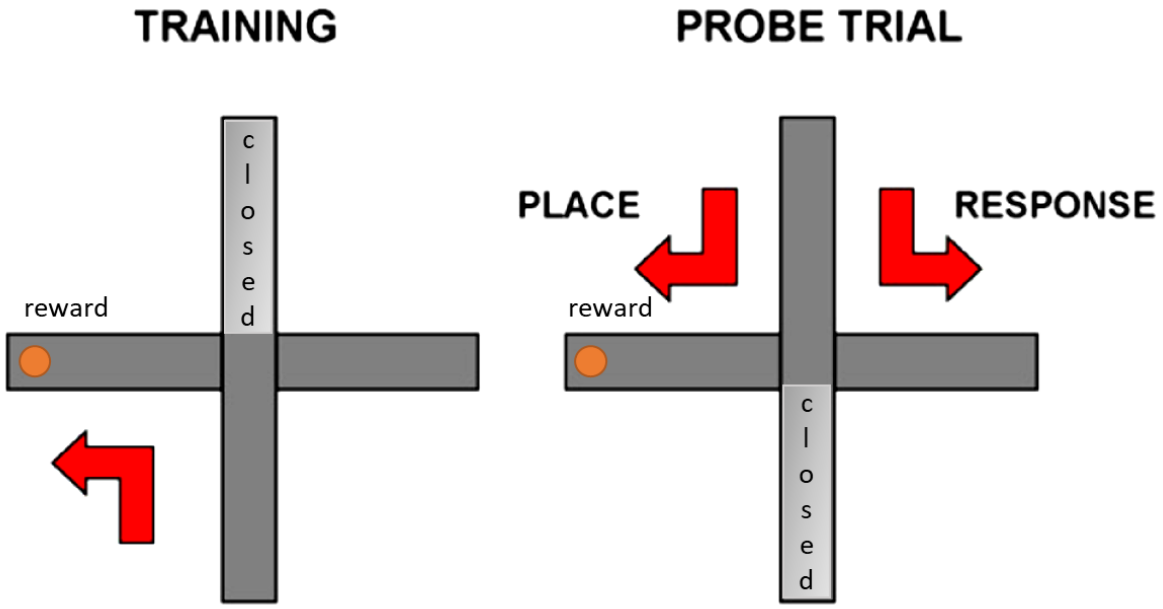

***Figure 9:* Place response task to test the formation of habits**. *Left: training of animals to go to the left on a plus-maze. Right: the animal is placed on the opposite side of the plus-maze and the chosen direction will correspond to a place strategy (if the animal goes to where the reward is) and a response strategy (if the animal goes to the side it was used to, on its left). Adapted from (Mark G. Packard, 2009).*

In order to determine the neural correlates that were responsible for the formation of habits, lesion studies were made in the late 90's. Packard and McGaugh used the plus-maze paradigm to test the involvement of the caudate nucleus (or dorsal striatum in rodents) in the formation of habit, i.e. animals adopting a response strategy. They made lesions with lidocaïne in the caudate nucleus or the hippocampus (Fig.10). Their experiments show that a lesion of the

striatum stops animals from choosing a response strategy whereas a lesion of the hippocampus stops animals from choosing a place strategy. This work shows that the striatum is indeed involved in the formation of a habit.

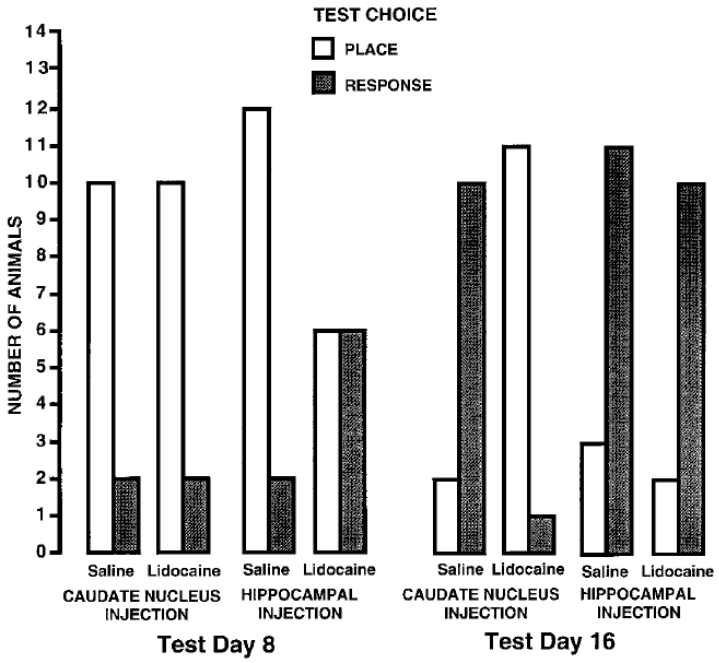

***Figure 10:* Involvement of the striatum in the formation of a habit with a place response task**. *After a lidocaine lesion of the striatum, animals do not follow a response strategy. When the hippocampus is injected with lidocaine, place strategy is avoided. From (M G Packard & McGaugh, 1996).*

Divac et al (Divac et al., 1967) were one of the firsts to show the role of the caudate nucleus in learning. They bilaterally ablated the caudate nucleus in monkeys by using electrodes to lesion the sites. Then they tested the monkeys with visual pattern discrimination, spatial delayed alternation and an object discrimination task. This study has demonstrated a dissociation of function between the different areas of the caudate nucleus based on the different behavioral tests that were used. More importantly, this study also showed that functions of the tail are similar to those of the cortex from which it receives projections. Indeed with this work, not only have they determined the role of the caudate in learning, but also that structures receiving projections from the cortex could have similar functions.

Several other studies using lesions (NMDA in (H. H. Yin & Knowlton, 2004), (McDonald & White, 1994) with radio-frequency or direct current, tetrodotoxine, (de Lorenzi et al., 1995), (Divac & Öberg, 1979)) demonstrated the role that the striatum plays in learning.

As described so far, these studies were shown mainly in the caudate nucleus or the whole striatum. But other studies showed the involvement of other structures and brain regions, such as other nuclei of the basal ganglia, in the formation of this memory and the different

parts of this memory. The role of the basal ganglia in learning will be described in more details in chapter IV.

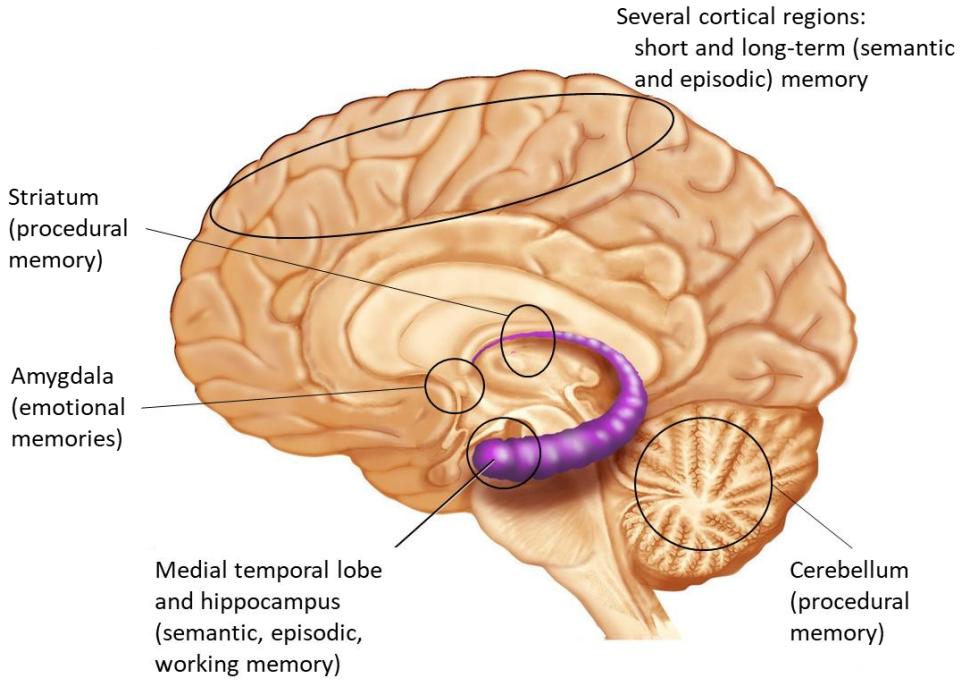

***Figure 11:* Summary of neural correlates for different memories.**

In this chapter, we described a historical overview of memory models. Memory is divided into short-term and long-term memory. Short-term memory is the memory we use every day. Long-term memory is divided into explicit memory and implicit memory. An event can become a long-term memory by repetition, with the presence of a reward or punishment, or thanks to its emotional weight. We also described the different brain structures that are involved in each of these memories (Fig.11). For the purpose of this work, only procedural memory will be discussed in the next chapters.

Dans ce chapitre, nous avons décrit comment les différents modèles de mémoire ont été établis et comment ils ont évolué au cours des années. La classification la plus récente des différents types de mémoire reconnaît deux grands types de mémoire : la mémoire à court-terme et la mémoire à long-terme. La mémoire à court-terme, comme son nom l'indique, est brève. Elle correspond à une mémoire que nous employons dans notre vie quotidienne. La mémoire à long-terme peut perdurer des heures, voire des années, et comprend deux principales catégories, la mémoire explicite qui est la mémoire classique de nos souvenirs et nos connaissances, et la mémoire implicite, qui est la mémoire de nos capacités motrices. Pour se former et perdurer, la mémoire à long-terme nécessite soit une répétition d'une tâche, d'une

information ou d'une histoire afin de la mémoriser, et ceci peut être fait en présence ou en absence de récompense. Nous avons décrit que les différentes formes de mémoire sont formées et stockées dans différentes structures cérébrales. Nous nous concentrerons dans ce travail sur la mémoire procédurale, un type de mémoire implicite qui permet la formation d'habitudes et nous permettant d'apprendre de nouvelles tâches. Grâce à des expériences de lésion ciblée, le striatum a été montré comme étant le principal acteur dans la formation de cette mémoire. L'implication du striatum et d'autres structures dans la formation de cette mémoire sera détaillée dans les prochains chapitres puisque c'est au centre de mon travail de thèse.

II- Anatomy and circuits of the basal ganglia

The basal ganglia (BG) are a group of bilateral structures known for so long for their involvement in motor control. They are the largest subcortical nuclei in the human brain. These nuclei are very well interconnected and form anatomical and functional loops, notably the cortico-basal ganglia-thalamo-cortical loops. When these circuits are altered, severe motor disorders occur such as Huntington's disease or Parkinson's disease for example, highlighting the strong involvement of these nuclei in motor control. However, more and more evidence shows the involvement of these structures in executive functions such as motor learning, behavioral control but also cognitive functions and emotion (H. H. Yin & Knowlton, 2006).

A) Historical overview of the basal ganglia

These structures were first identified in 1664 by Thomas Willis, an English anatomist in his text describing the central nervous system, *Cerebri Anatomie*. At that time, the BG were not named 'basal ganglia' yet and included only the striatum and the globus pallidus. It was suggested that they might have an important role since they were localized in the middle of the brain. From the 18th century until the end of 19th century and beginning of 20th century, the main focus of neurologists was the cortex that attracted them because of its fascinating organization and its implication in 'higher' functions. The term 'basal ganglia' was not introduced until 1876 by David Ferrier, a British neurologist. The interest in the basal ganglia started again after the discovery that lesions to these structures resulted in motor dysfunctions in humans. Indeed, the Lausanne stroke registry gathered all stroke incidents in the basal ganglia that resulted in motor dysfunctions, 38% corresponding to choreic movements (Ghika-Schmid et al., 1997). By the second half of the 20th century the BG were more and more studied ant other components were determined as being a part of the BG.

B) Basal ganglia anatomy

The BG are composed of several nuclei that are interconnected. This group of structures includes 4 nuclei: the striatum, the subthalamic nucleus (STN), the globus pallidus (external and internal parts), and substantia nigra (*pars reticulata and pars compacta*) (Fig.12). The

striatum constitutes the main input stage of the BG, receiving major inputs from the cerebral cortex with excitatory, glutamatergic projection neurons. In this chapter, I will describe the different components of the BG with special emphasis on the striatum.

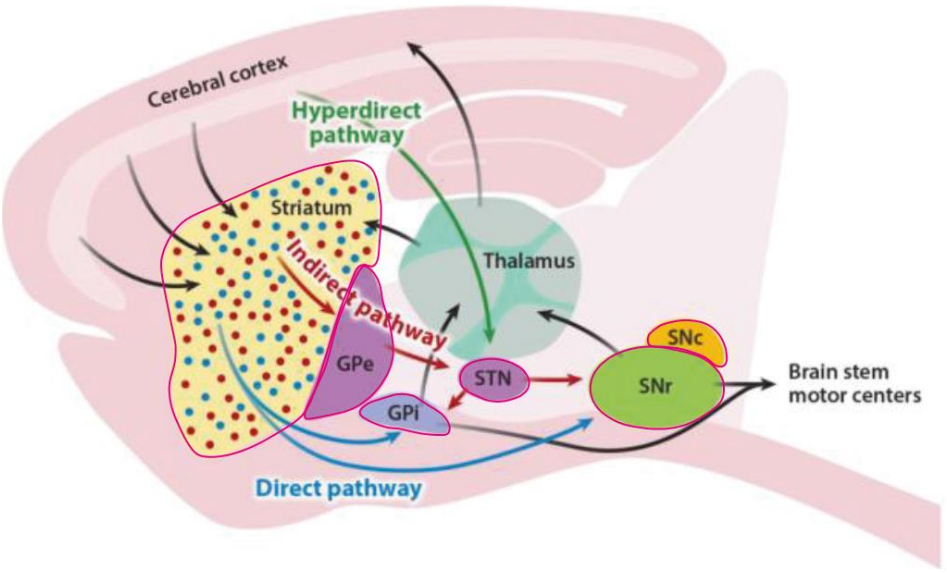

***Figure 12:* Basal ganglia pathways and nuclei.** *Schematic showing the different pathways connecting the basal ganglia nuclei and their connections to other structures, in a rodent brain with a sagittal view. The basal ganglia nuclei are circled in pink. The direct pathway is shown with blue arrows, the indirect pathway with red arrows, and the hyperdirect pathway with green arrows. Black arrows shows connections with external structures and different pathways. Adapted from (Nelson & Kreitzer, 2014).*

1) Nuclei of basal ganglia

a- Striatum

The term 'striatum' was first used in 1920 by Vogt and it corresponded to the caudate nucleus and putamen in the human brain (Vogt & Vogt, 1920). The striatum is the largest subcortical structure in the mammalian brain. The size of the striatum is around $10cm^3$ for humans (Schröder et al., 1975; D. Yin et al., 2009), $2cm^3$ for non-human primates (D. Yin et al., 2009) and varies between 20 and $37mm^3$ for mice (Rosen & Williams, 2001). In Humans, the caudate nucleus and putamen are two distinct gray matter masses that correspond to the dorsal striatum. These two parts of the dorsal striatum are separated during development due to the formation of fibers to and from the cortex. These fibers form an internal capsule that separates the caudate nucleus and putamen. And fibers connecting these two structures will go through the internal capsule. Due to these fibers and their organization, the structure was given the name striatum (or corpus striatum). When looking into rodents' brains for example, these two structures are not separated, but fibers still go through them and give a striated

aspect to the tissue. The striatum is the principal input nucleus to the BG. It receives major excitatory inputs directly from the cortex and also from the thalamus. Cortical inputs to the striatum allow for the emergence of two different pathways, called direct and indirect pathways, implicating different striatal neuronal subtypes (Fig.12) (see details in part 3 of chapter II and chapter III).

The striatum is a heterogeneous structure and can be divided into several parts. First, there is a dorso-ventral distinction with a dorsal and a ventral striatum. The dorsal striatum includes, as mentioned earlier, the caudate nucleus and the putamen, whereas the ventral striatum includes the medial and ventral part of the caudate/putamen, the nucleus accumbens. Additional heterogeneity has been described within the striatum. Since in my thesis most of the work is related to the dorsal striatum, I will detail dorsal striatum in part 3 of this chapter II, describing the anatomical and functional heterogeneity, the input/output structures and neuronal components.

b- The subthalamic nucleus

The subthalamic nucleus (STN) is a structure localized close to the striatum, present on the medial side of the internal capsule. It was discovered in 1865 by a French doctor Jules Bernard Luys, hence the name Luys Body. This structure is the only glutamatergic structure of the BG. It is also another entry structure to the BG (other than the striatum) since it receives direct inputs from the cortex, forming the hyperdirect pathway. The STN plays the role of a hub between the different BG structures. Receiving inputs from different structures in the BG, it is thus involved in the different pathways (hyperdirect and indirect, see chapter III) of the BG (Lanciego et al., 2012). Due to this particular position, the STN has been well known during the past years for being a target for deep-brain stimulation studies, especially ones involving degenerative disorders affecting the basal ganglia such as Parkinson's disease (for review see (Groiss et al., 2009)).

c- Globus pallidus

The globus pallidus (GP) is composed of GABAergic neurons. It is also situated close to the striatum, inserted between the putamen and the posterior part of the internal capsule. It receives glutamatergic projections from the STN and GABAergic projections from the striatum.

The GP is divided into three domains: the external GP (GPe), internal GP (GPi) and the ventral pallidum (VP). The boundary between the GPe and GPi is the medial medullarly lamina. These two domains share similar cytological features, they all express the calcium-binding protein, parvalbumin (Lanciego et al., 2012). The GPe receives GABAergic inputs from the striatum and then projects towards the STN, thus acting as a relay structure. The GPi on the other hand receives inputs from the striatum and projects to the thalamus, thus acting as an output structure of the BG (Lanciego et al., 2012).

d- The substantia nigra

The substantia nigra (SN) is a mesencephalic structure that runs throughout the midbrain. The SN is divided into two parts: SN *pars reticulata* (SNr) and SN *pars compacta* (SNc). The SNr is the ventral part of the SN and the SNc constitutes the dorsal part with a higher cell density. The SNc is mainly composed of dopaminergic neurons that exhibit a black pigmentation which earned the SNc the name 'locus niger'. The SNc neurons project mainly to the striatum, but also project to the STN and GP. The SNr on the other hand projects to the thalamus and other external structures, thus acting as an output structure of the BG. The SNr has a lower density of neurons that project to the thalamus and the brainstem and are characterized by their expression of GABA as a neurotransmitter. The SNr neurons are characterized by their tonic firing and high rate discharge which has an inhibitory effect on their output targets (Lanciego et al., 2012).

2) Cortico-basal ganglia-thalamocortical loops

The main inputs of the BG come from the cortex, with additional other inputs from thalamus and other nuclei. The BG form with the cortex and the thalamus loops of anatomical and functional organization. In this anatomical chapter of the thesis, we will be looking into the anatomical organization of these loops. The functional part will be discussed in the last chapter (chapter IV).

As previously shown, the striatum is the main input stage to the BG, while the GPi and SNr constitute the main output stage of the BG. The striatum receives glutamatergic inputs from different cortical areas. Both ipsi- and contralateral cortical areas project to the striatum in an asymmetric fashion, dividing the striatum into different compartments (see part 3 of chapter

II). Thus, these cortical projections seem to impose a certain organization on the striatum and this organization is maintained throughout the BG thus forming parallel functional loops. These loops are called the cortico-basal ganglia loops, or 'basal ganglia loops' for short. As mentioned, the cortex is not the only structure projecting to the striatum. The thalamus constitutes another important glutamatergic input to the striatum and receives inputs from output structures of the BG, the SNr and GPi, thus allowing the formation of these loops. This pathway was first described by (Vogt & Vogt, 1941), where the thalamus was added, forming the cortico-basal ganglia-thalamocortical loops.

a- Basal ganglia inputs

Inputs to the BG are mostly constituted by excitatory glutamatergic neurons in layer V (or II/III) of the cortex and from thalamic intralaminar nuclei, and by other inputs such as dopaminergic nigrostriatal projections (from the SNc). Other systems allow glutamatergic innervation of the striatum such as the amygdaloid complex projecting to the striosomes or the serotoninergic projections (Lanciego et al., 2012) but I will not discuss these further.
Since the striatum is the main input stage to the BG, the inputs to the BG I will describe in this part will relate to the striatum. I will discuss inputs from the cortex, the substantia nigra and other projections.

1. Cortico-striatal projections: funneling and parallel circuits

Several models of the basal ganglia loops were proposed. Originally, the BG models were created to understand the role of BG in motor function and how BG lesions could result in hyperkinetic our hypokinetic disorders (Mahlon R. DeLong, 1990; Shipp, 2017).
In 1944, Glees showed that there were cortico-striatal fibers coming from the different areas of the cortex. Cajal considered that these fibers were born from collaterals to projections for the lower centers. However, in the late 70's it was shown that these fibers were coming from different cells than the ones destined to be a part of the corticospinal and other motor systems (Coulter & Jones, 1977). Later, lesion studies of the different brain areas were performed in different species (Kemp & Powell, 1971) in order to understand the role of these areas in the striatal reconstruction. With these studies, they showed that there is a topographical organization of the cortical projections to the striatum. This organization was done on a

mediolateral and anteroposterior axis, i.e. the frontal areas project to the anterior parts of the striatum, and the occipital areas to the posterior part of the striatum; the medial part of the frontal lobe projects to dorsal striatum, the lateral part to the lateral striatum and the orbital part to the medial striatum. Kemp and Powell thus described that the cortico-striatal projections took advantage of their anatomical proximity, which Parent and Hazrati (A Parent & Hazrati, 1995) described as the cortico-striatal projections 'following a rule of proximity'. Kemp and Powell built a model based on this data (Fig.13) and proposed that the BG have the role of integrating the inputs of the different cortical areas before projecting to their outputs (Kemp & Powell, 1971) which gave rise to the 'information funneling hypothesis' (A Parent & Hazrati, 1995). Thus the BG are able to influence the motor cortex through sensory pathways but also the association cortex of the frontal and parietotemporal lobes. Due to this hypothesis, the BG were thought to participate in motor functions.

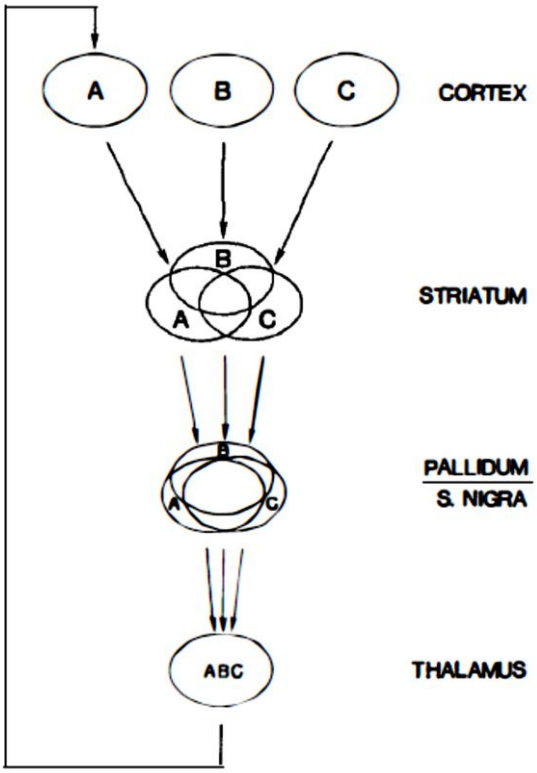

Figure 13: ***Model of the basal ganglia based on the information 'funneling' hypothesis****. From (G. E. Alexander et al., 1986).*

This funneling hypothesis was debated especially when other studies in the late 80's showed that the corticostriatal projections are topographically organized in a way that functionally related regions project to the same striatal sectors (A. W. Flaherty & Graybiel, 1991; Selemon & Goldman-Rakic, 1985). Also, it was shown that the BG not only project to motor areas, but to other regions as well. In the early 80's, DeLong and his group proposed a different model

of this topographical organization. They suggested that the topographic corticostriatal projections allow for a division of the striatum into functionally different subregions which in turn result in a topographic organization of the outputs through the GPi, SNr and thalamus going back until the cortex. In this case, they emitted a hypothesis of parallel circuits for information (M. R. DeLong et al., 1983). In this case, they proposed different functional loops in the BG: a motor loop with projections coming from the sensorimotor and premotor cortex to the putamen, and an 'association' loop with projections from the association areas to the caudate nucleus. The DeLong group later extended this model with five total loops (Fig.14): a motor loop, oculomotor loop, dorsolateral prefrontal cortex loop, a lateral orbitofrontal loop and an anterior cingulate loop. By proposing this model, Alexander et al. (G. E. Alexander et al., 1986) proposed a closed loop system for the functioning of the BG. In 1993, Hoover and Strick (Hoover & Strick, 1993) performed experiments using a neurotropic virus, a herpes virus that is transmitted transneuronally in a retrograde manner, to test the connectivity model that Delong and his group proposed. With these experiments, the basal ganglia were no longer considered as only involved in motor functions but also in cognitive processes such as learning and memory.

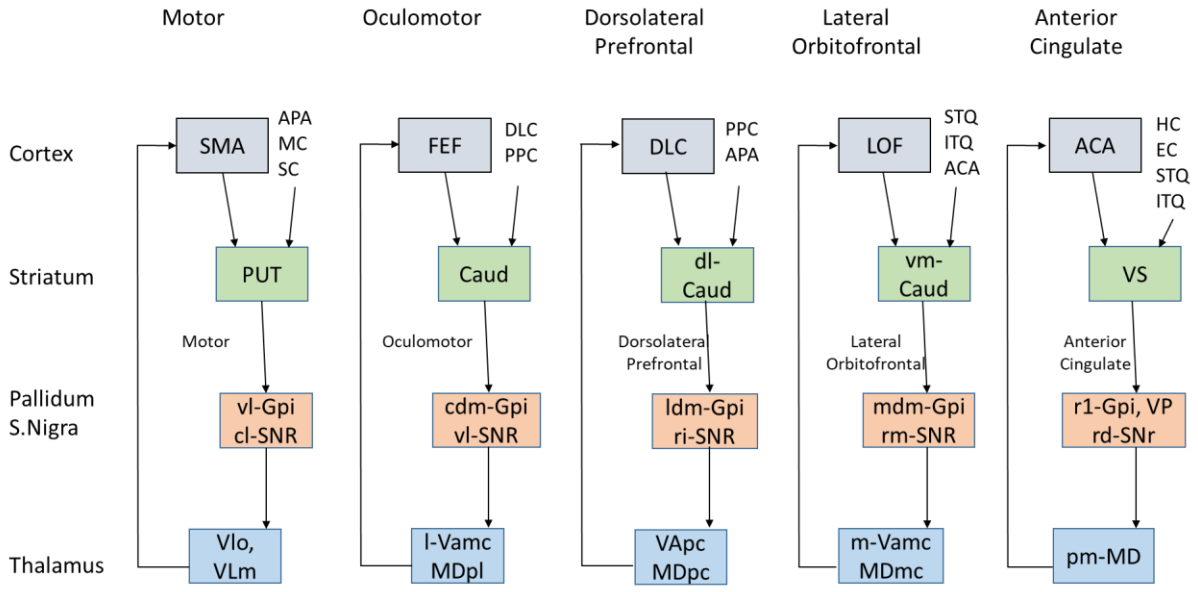

***Figure 14:* Parallel or segregated loops of the basal ganglia**. *Five circuits of BG-thalamocortical loops are proposed: each circuit with a corresponding cortical area. ACA: anterior cingulate area, APA: acute premotor area, Caud: caudate (body for the oculomotor and head for the dorsolateral prefrontal and lateral orbitofrontal circuits), DLC: dorsolateral prefrontal cortex, EC: entorhinal cortex, FEF: frontal eye fields, GPi: internal globus pallidus, HC: hippocampal cortex, ITG: inferior temporal gyrus, LOF: lateral orbitofrontal cortex, MC: motor cortex, MDpl: medialis dorsalis pars paralamellaris, MDmc: medialis dorsalis pars magnocellularis, MDpc: medialis dorsalis pars parvocellularis, PPC: posterior parietal cortex, PUT: putamen, SC: somatosensory cortex, SMA: supplementary motor area, SNs: substantia nigra pars reticulata, STG: superior temporal gyrus, Vmc: ventralis anterior pars magnocellularis, Vapc: ventralis anterior parvocellularis, VLm: ventralis lateralis pars medials, VLo: ventralis lateralis pars oralis, VP: ventral pallidum, VS: ventral striatum, cl: caudolateral, cdm: caudal dorsomedial, dl:*

dorsolateral, l: lateral; ldm: lateral dorsomedial; m: medial, mdm: medial dorsomedial, pm: posteromedial, rd: rostrodorsal, rl: rostrolateral, rm: rostromedial; vm: ventromedial, vl: ventrolateral. Based on the figure from (G. E. Alexander et al., 1986).

Other models were later proposed. In 1990, Parent proposed that the striatum could be divided into three functional areas: sensorimotor, associative and limbic (André Parent, 1990). The principle behind this models is based on the topographical organization of the corticostriatal projections. In primates, the motor striatum corresponds to the dorsolateral part of the caudate nucleus and the putamen, and it receives projections from the primary motor cortex, premotor cortex and supplementary motor area (Garrett E. Alexander & Crutcher, 1990; Garrett E Alexander et al., 1990; Selemon & Goldman-Rakic, 1985). This first loop presented by Parent corresponds to the motor loop presented in Figure 14. Concerning the associative striatum, it is formed by a large part of the putamen (in front of the anterior commissure) and most of the caudate nucleus, and it receives projections from associative areas of the cortex including the prefrontal cortex (areas 8, 9, 10 and 46) (André Parent, 1990). This associative loop corresponds to the dorsolateral prefrontal, orbitofrontal and oculomotor loops shown in Figure 14. The limbic loops include the ventral part of the striatum corresponding to the nucleus accumbens receiving projections from limbic structures (amygdala, hippocampus, prefrontal areas). This loop corresponds to the anterior cingulate, orbitofrontal loops in Figure 14. This model is still used until today (S. N. Haber & Calzavara, 2009; Joel & Weiner, 2000; A Parent & Hazrati, 1995; Postuma & Dagher, 2005; Sadikot & Rymar, 2009).

To summarize, several models were created to understand the functioning of the BG. These models were first based on anatomy alone, and later on functional aspects as well. We described here the funneling and parallel circuits that could explain how signals are transferred from one structure into another, while following a somatotopic scheme. Receiving inputs from the layers III and V of the motor, frontal and parietal lobes, the striatum acts as an important cog in the cortico-BG-thalamo-cortical machinery.

2. Nigrostriatal projections

The substantia nigra *pars compacta* is a part of the mesencephalic dopaminergic system. Dopaminergic neurons are organized in a way that gives an idea about their output targets. Ventral dopaminergic neurons in rats innervate one of the striatal compartments, the

striosomes, whereas dopaminergic neurons present on the dorsal part of the VTA and SNc will project to the matrix compartment of the striatum (C. R. Gerfen et al., 1987). As said earlier, the topographical organization of the basal ganglia is seen throughout the different components of the BG. This topographical organization is also visible in the SNs and VTA. The sensorimotor loops include dopaminergic inputs from the ventral SNc to the striatum, the limbic loops comprise projections from the VTA and dorsal SNc to the striatum, and finally the associative loops see projections from the ventral SNc to the striatum.

Five types of dopamine (DA) receptors were found (D1 to D5). In the striatum, MSNs will express either D1-like or D2-like receptors (Aizman et al., 2000) but also D3 receptors in the limbic striatum (Gurevich & Joyce, 1999). The D1-like receptors are mainly expressed in the direct pathway MSNs and are coupled to a Gi protein while the D2-like receptors are mainly expressed in the indirect pathway MSNs and are coupled to Go protein (Kebabian & Calne, 1979). The SNc and VTA have also been shown to project to the GPi and STN (Lanciego et al., 2012). Therefore, there is an important dopaminergic modulation mediated by SNc and VTA inside the BG.

3. Other projections to the striatum

Thalamostriatal projections represent another important glutamatergic striatal input (Berendse & Groenewegen, 1990) (Fig.15). The thalamostriatal projections come from thalamic intralaminar nuclei (parafascicular and centromedian nuclei). They seem to be ipsilateral (Y. Smith & Parent, 1986). These thalamic projections, along with projections from associative areas, are at the heart of motivation and integration processes. The difference between thalamic and cortical inputs can be seen by the type of glutamate transporter that is expressed. vGlut1 is expressed in the presence of corticostriatal projections whereas vGlut2 is expressed by the thalamostriatal projections (Fujiyama et al., 2004, 2006; Lanciego et al., 2012).

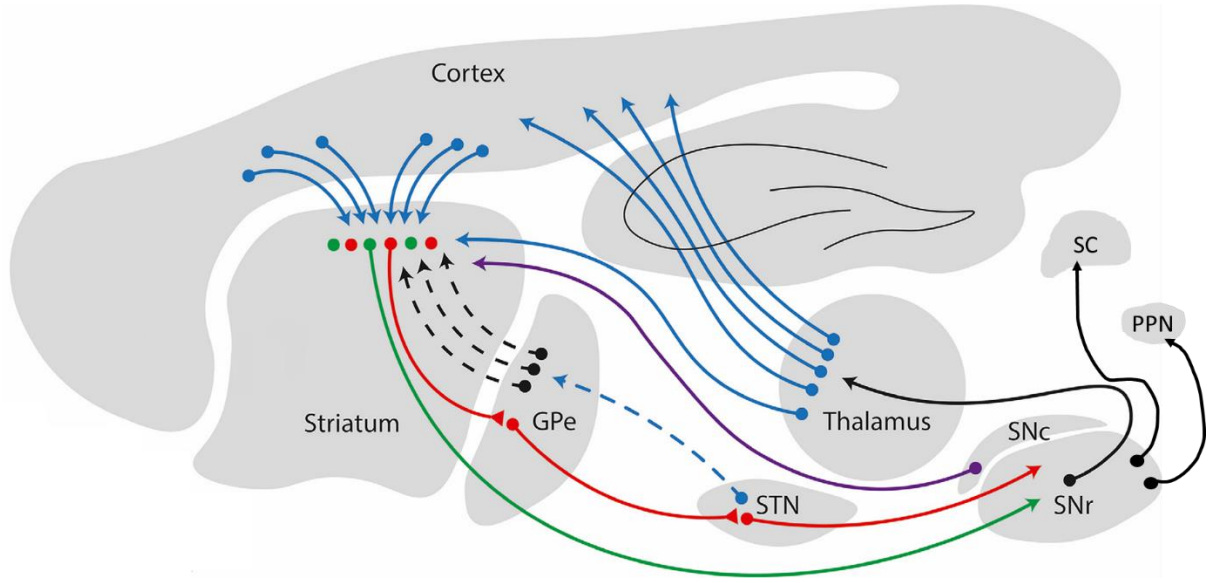

***Figure 15:* Input and output pathways of the basal ganglia on a sagittal view**. *Glutamatergic projections from the cortex to the striatum where two pathways are involved: direct (green line) and indirect (red line). Other projections towards the striatum include: glutamatergic (blue lines) projections from STN to the GPe and then GABAergic ones (black lines) from the GPe to the striatum; dopaminergic projections (purple line) from the SNc to the striatum; and glutamatergic inputs from the thalamus to the striatum. SNr sends inhibitory projections towards the SC (superior colliculus) and the PPN (pedunculopontine nucleus). Adapted from (Peak et al., 2019) with modifications based on* (Gittis et al., 2020).

b- Basal ganglia outputs

As previously mentioned, the GPi and SNr are the output nuclei of the BG. Both of these structures have GABAergic neurons with tonic and high discharge rate. The topographical and functional organization of the BG are kept throughout these nuclei. The projections coming from these two structures end up in the thalamus (S. Haber & McFarland, 2001; Watkins & Jenkinson, 2016). Pallido-thalamic projections are first separated into two fiber bundles or fascicles which are then merged, cross the internal capsule, and innervate the ventral anterior part of the thalamus and the ventral lateral (Nauta & Mehler, 1966). These two parts of the thalamus then project to the cortex. Another thalamic nucleus, the centromedian nucleus, receives the collaterals of the fascicles mentioned earlier and projects back to the striatum. The thalamic projections towards the cortex will target the motor, premotor areas of the cortex and the prefrontal cortex. Thus, by looking at the BG loops, we can see that although all the areas of the cortex innervate the striatum, the frontal cortex is the principal area to receive the output BG projections passing through the thalamus (Strick et al., 1995; Watkins & Jenkinson, 2016). Apart from the cortex and the thalamus, the brainstem is an important

output structure of the BG (Mana & Chevalier, 2001; McHaffie et al., 2005). Interestingly, the segregation of the BG into functional loops extends to the sensorimotor and motivational structures of the brainstem (superior colliculus, periaqueducal grey, pedunculopontine and parabrachial nuclei (for review see (McHaffie et al., 2005)).

To summarize, the different inputs and outputs of the BG and more specifically the striatum were described here. Inputs to the striatum are glutamatergic and dopaminergic. Depending on the different outputs of the striatum, different pathways are formed (direct, indirect and hyperdirect: please see detailed explanations in chapter III). Figure 15 summarizes the input and output pathways of the BG.

3) Anatomy of the striatum

a- The striatum on a cellular level

One of the first descriptions of striatal cells was made in the Golgi lab, using Golgi staining, or as it was called at the time, 'the black reaction' (Marchi, 1886). In this study, they showed that there were two types of neurons in the striatum, both types of Golgi cells (long axon type I and short axon type II neurons) (Fig.16). Striatal neurons were first described by Ramon y Cajal in 1895. He determined that there were 2 types of striatal neurons: giant, medium and small cells with short axons; and large cells with long axons. He later added in 1911 'dwarf or neurogliform neurons'. Later studies (Bielschowsky, 1919; Vogt & Vogt, 1920) only recognized two types of neurons in the striatum. The identification of the striatal cells took a small break after the 1920's and was carried out in 1957 by Namba, who decided to divide the striatum into cytoarchitectonic fields (based on the density of cells, and the density of each type of cells: alpha and beta). In 1971, Kemp and Powell published their study on the cat striatum which showed that the majority of striatal cells are 'medium size cells with dendrites densely covered with spines except for their proximal 20µm' (Kemp & Powell, 1971). In 1976, Difiglia, Pasik and Pasik revealed the presence of 6 types of striatal cells based on their size and their spine density: spiny I (medium size), spiny II (medium to large size), aspiny I (large), aspiny II (medium), aspiny III (small), and neurogliform (small) (Fig.16) (DiFiglia et al., 1976).
Different subtypes of striatal neurons were anatomically described in monkeys, cats and rodents, using Golgi staining of electron microscopy (Dimova et al., 1980; Kemp & Powell, 1971; Wilson & Groves, 1980). Nowadays, based on their projections targets and functions,

the different types of neurons found in the striatum can be classified as two main types of striatal neurons: the projection neurons (around 90% of striatal neurons) and the local interneurons (10% of striatal neurons).

A)

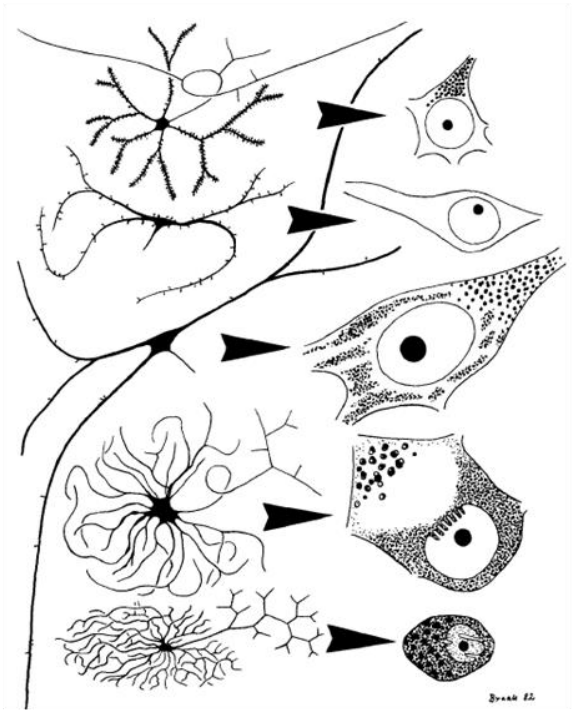

B)

Type	Size	Dendrites			Axon	
		Length	Spines	Varicosities	Length	Collaterals
Spiny I	medium	200	+++	0	long	+++
Spiny II	medium large	600	+	0	long	++
Aspiny I	medium	150	0	+++	short	arborization
Aspiny II	large	250	0	+++	short	arborization
Aspiny III	medium	150	rare	rare	short	arborization
Neurogliform	small	70	twigs	++	?	?

Length of dendrites in µm. Abundant, regular, sparse and absent indicated by +++, ++, + and 0 respectively.

Figure 16: ***Striatal neuronal types***. ***A****) Diagram of striatal neuronal types in humans. On the left, cells are recognizable thanks to their Golgi staining, and on the right a pigment-Nissl staining. From* (Braak & Braak, 1982). ***B****) Neuronal types in Monkey neostriatum. There are 6 types of striatal cells that are divided based on their size and their spine density. From (DiFiglia et al., 1976).*

1. Projection neurons or medium-sized spiny neurons

The striatal projection neurons (SPNs) have a soma of a medium size (12 to 20 µm). To the soma are attached in average 4 to 5 primary dendrites that have a high spine density (A Parent & Hazrati, 1995; Wilson & Groves, 1980). Thus, the name 'medium-sized spiny neurons' (MSNs) comes from the size and the spine density of these neurons. The dendritic arborization of the MSNs can reach up to 300µm. The axon, coming out of the soma, has several collaterals (Fig.17). These collaterals can either create local arborizations close to the cell body, which is the most common type of collaterals, or they can have larger arborizations that can extend away from the cell body and project out of the striatum (C. L. Gerfen, 2004; Yasuo Kawaguchi et al., 1990; A Parent & Hazrati, 1995).

Striatal medium spiny neurons are GABAergic neurons, i.e. they use GABA (gamma-aminobutyric acid) as their primary neurotransmitter (Oertel & Mugnaini, 1984; Ribak et al., 1979). However, they also co-express several other neuroactive peptides such as substance P, enkephalin, dynorphin and neurotensin. The expression of these peptides will depend on the cells subtypes (belonging to direct or indirect pathway, please see details in chapter III): D1-dopamine receptors, dynorphin and substance P are expressed by MSNs from the direct pathway, D2-dopamine receptors and enkephalin by MSNs of the indirect pathway.

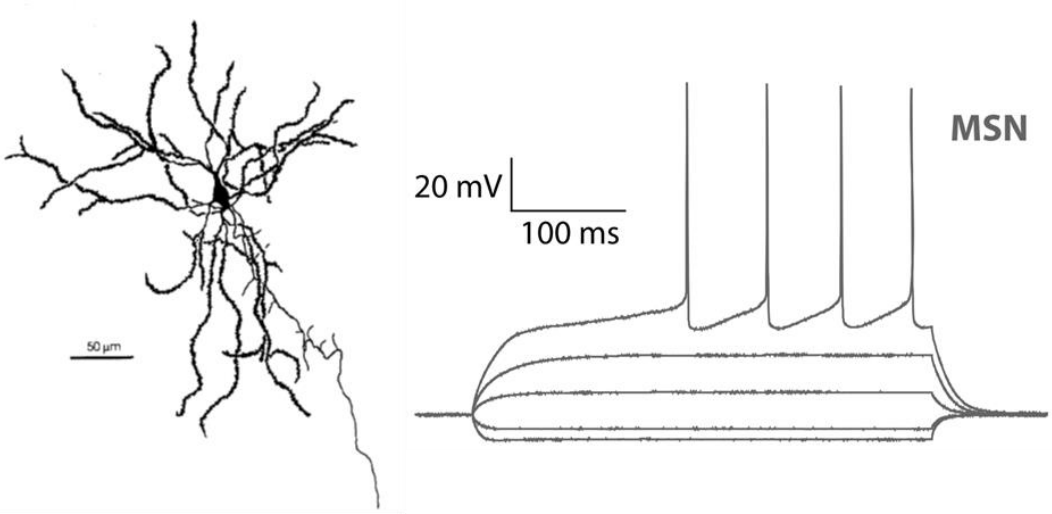

***Figure 17:* Representation of a medium spiny neuron and its electrical properties**. *Left: Drawing of a medium spiny neuron with its dendrites, axon and collaterals. The main axon is the long fine prolongation. From (Wilson & Groves, 1981). Right: firing properties of medium spiny neurons. From (Kreitzer, 2009).*

On an electrophysiological level, MSNs are characterized by a very hyperpolarized resting potential (< -75mV) and a relatively low input resistance (15-30 MOhm). Their membrane potential is not fixed *in vivo* since a fluctuation of the resting membrane potential has been described in MSNs. These fluctuations consist in transitions between two levels of

polarization: a depolarized state, called an 'up state' (around -55mV) and a more hyperpolarized level, the 'down state' which corresponds to the resting membrane potential (Wilson & Groves, 1981). The membrane potential and the input resistance of MSNs are dominated by a powerful voltage-dependent inwardly rectifying current (Wilson, 1993). Their hyperpolarization state results in quiescent cells which require huge excitatory inputs to spike. MSNs in the dorsal striatum receive mainly excitatory cortical (McGeorge & Faull, 1989) and thalamic inputs (Berendse & Groenewegen, 1990) but also dopaminergic inputs from the substantia nigra *pars compacta* (SNc) (Bentivoglio et al., 1979).

2. Interneurons

Based on the Golgi staining (Fig.16), three categories of aspiny neurons were identified (two medium sized neurons and one large), that were then grouped into two categories (the giant aspiny interneurons and the medium aspiny interneurons) (Y Kawaguchi et al., 1995). The aspiny neurons were then identified as interneurons in the striatum. In addition to their global anatomy, these interneurons can be divided based on what they express (GABA, acetylcholine esterase, NO-synthase…). They are outnumbered by the projection neurons or MSNs described earlier (Petryszyn et al., 2018). They represent around 20-25% of striatal neurons in primates (Graveland & Difiglia, 1985) but around 5% of striatal neurons in rodents (C R Gerfen & Bolam, 2010; Tepper et al., 2010).

There are two main groups of interneurons: the GABAergic interneurons with several subtypes, and the cholinergic interneurons (Fig.18). Figure 18 summarizes all the different types of interneurons and the percentage of striatal neurons they represent. I will focus on the few main GABAergic interneurons and the cholinergic interneurons in this paragraph.

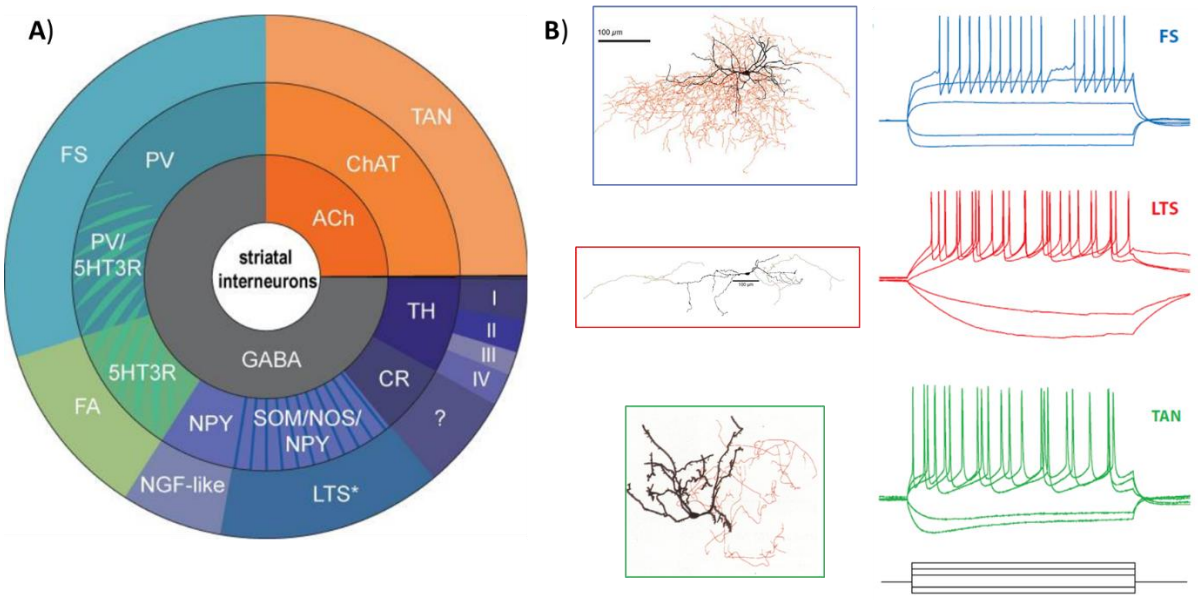

Figure 18:* Diversity of striatal interneurons**. ***A*) GABA and Ach are the two main groups of interneurons based on their neurotransmitter expression. Moving outwards, we have the different interneurons based on their molecular markers, and finally, based on their electrophysiological properties. From (Burke et al., 2017).* ***B****) Morphological (Tepper et al., 2010; Tepper & Bolam, 2004) and electrophysiological properties (Kreitzer, 2009) of different interneurons. Top: fast-spiking or FS interneurons. Middle: low-threshold spiking or LTS interneurons. Bottom: tonically active neuron or TAN.*

GABAergic interneurons

The GABAergic interneurons represent 1-2% of the striatal neuron population (Tepper et al., 2010). The main subtypes of GABAergic interneurons are: parvalbumin, somatostatin and calretinin-expressing interneurons, but there are also other subtypes that I will not detail here (Fig.18).

Parvalbumin interneurons

The first subtype of GABAergic interneurons is the most abundant type of striatal interneurons. They express parvalbumin, a calcium-binding protein, together with GABA. They are characterized by a spherical cell body of about 16µm. The axon of these interneurons is short and forms dense arborizations that are close to the cell body (Tepper et al., 2010). Their electrophysiological properties are characterized by a hyperpolarized resting potential and a very short duration of their action potential (around 1ms or shorter, compared to MSNs: around 1.5ms (Gage et al., 2010)). Notably, they are able to discharge with very high frequencies of action potentials, which gave them the name 'fast-spiking' interneurons (FSI) (Y Kawaguchi et al., 1995). These FSI fire phasically at high frequency in response to cortical stimulation (Kita et al., 1990).

Somatostatin interneurons

A second subtype of interneurons is the somatostatin/NPY (neuropeptide Y)/NOS (nitric oxide synthase) expressing interneurons. They have a small cell body (around 15µm) which emits 3 to 4 dendrites without spines. Their axon is short with an arborization that is not very dense. These neurons have a depolarized resting potential and very high input resistance and highly excitable. They fire for low inputs and can display a plateau of discharge, granting them the name of persistent and low threshold spiking (PLTS) interneurons (Y. Kawaguchi & Kubota, 1993).

Calretinin interneurons

Calretinin (CR) interneurons were first described in the beginning of the 90's when immunohistochemical mapping studies of the CR protein were more and more done (Bennett & Bolam, 1993; Jacobowitz & Winsky, 1991; Yasuo Kawaguchi, 1997). These interneurons are medium sized (12-20µm) with a not very dense dendritic arborization (Tepper et al., 2010). Little is known about their functional role.

Cholinergic interneurons

The second group corresponds to cholinergic interneurons which fall in the category of giant aspiny interneurons, and they represent around 1% of striatal neurons (Tepper et al., 2010). Their cell body is around 50µm. They have 3 to 6 dendrites without any spines, and long axons that can extend over an area of 2mm (Gittis et al., 2020). They are called cholinergic interneurons because of their expression of choline acetyltransferase (ChAT) (Bolam et al., 1984; Difiglia, 1987). These interneurons fire tonically and regularly at 2-10Hz, which gave them the name of Tonically-Active Neurons (TANs). Their resting potential is depolarized (-60mV), close to their spiking threshold and they have a high input resistance (Tepper & Bolam, 2004). Cholinergic modulation within the striatum is tightly linked to dopaminergic inputs from the SNc and they are also a preferential target of the thalamostriatal inputs (Tepper & Bolam, 2004).

Even though interneurons represent a small percentage of striatal neurons, each of them has the ability to play an important role in shaping the activity of the striatal networks (Tepper et al., 2010). GABAergic interneurons exert a powerful feedforward inhibition onto MSNs (Tepper et al., 2010), which modulate efficiently the excitability, activity and cortical integration of MSNs. The power of inhibition interneurons exert on the networks depends on their subtype, and on the territory where they are localized. Parvalbumin interneurons for

example, tend to be robustly connected to MSNs and other parvalbumin interneurons (Gittis et al., 2010; Szydlowski et al., 2013), but not so much to other interneurons. They can therefore have a strong inhibitory effect on their MSN targets. Somatostatin interneurons on the other hand, have weak and sparse outputs and have therefore a weaker synaptic weight on MSNs (Gittis et al., 2010). However, these roles are highly dependent and specific to the striatal territory. Indeed, a recent study showed a potent control of MSNs by parvalbumin interneurons in the dorsolateral part of the striatum, and by somatostatin interneurons in the dorsomedial part of the striatum (Fino et al., 2018). Cholinergic interneurons are also implicated in motor control by modulating activity of MSNs. These interneurons have been shown to synchronize the activity of MSNs during movement to suppress a movement and end it (Gritton et al., 2019).

Thus considering all the extrinsic and intrinsic inputs targeting the MSNs, the striatal circuitry is complex and MSNs express a variety of receptors allowing these inputs to strongly modulate MSN activity. They express AMPA/NMDA receptors (related to the cortical/thalamic inputs they receive), GABAergic receptors ($GABA_A$), cholinergic receptors (muscarinic) and dopaminergic receptors (related to the dopaminergic inputs) (Fig. 19).

There are different types of glutamatergic receptors: ionotropic receptors (NMDA, AMPA and kainate) and metabotropic receptors (mGluR). The striatum has a high density of glutamate receptors. AMPA receptors are composed of four units (GluR1 to GluR4). Only AMPAR without a GluR2 subunit are permeable to calcium. NMDA receptors are heterotetramers constituted of NR1 and NR2 subunits, and they are permeable to calcium. NMDAR are blocked by Mg2+ and their activation is facilitated by AMPA-R mediated depolarization of the membrane. Calculating an AMPA/NMDA ratio gives us an idea about the relative expression of these two receptors (Rao & Finkbeiner, 2007).

GABA receptors are composed of two classes of receptors: GABAA receptors that are ligand-gated ion channels, and GABAB receptors that are G protein-coupled receptors. GABAA receptors are constituted of several subunits. GABAA receptors subunits alpha 1 and 2 are present in dMSNs and iMSNs with more alpha 1 on iMSNs than dMSNs (Boccalaro et al., 2019). Muscarinic receptors are G-coupled protein receptors with a high sensitivity to muscarine. These receptors are activated by acetylcholine (Ach), thus earning them the name cholinergic receptors. Although Ach exerts its action via another type of receptors, the nicotinic receptors, muscarinic receptors are found on MSNs. Muscarinic receptors are divided into two groups:

group I (M1, M3, M5) which are coupled to the Gq protein thus giving them an activator status; group II (M2 and M4) are coupled to the Gi protein thus giving them an inhibitor status. M1 receptors are found in both dMSNs and iMSNs, M4 receptors are found in dMSNs (Abudukeyoumu et al., 2019; Kudlak & Tadi, 2020).

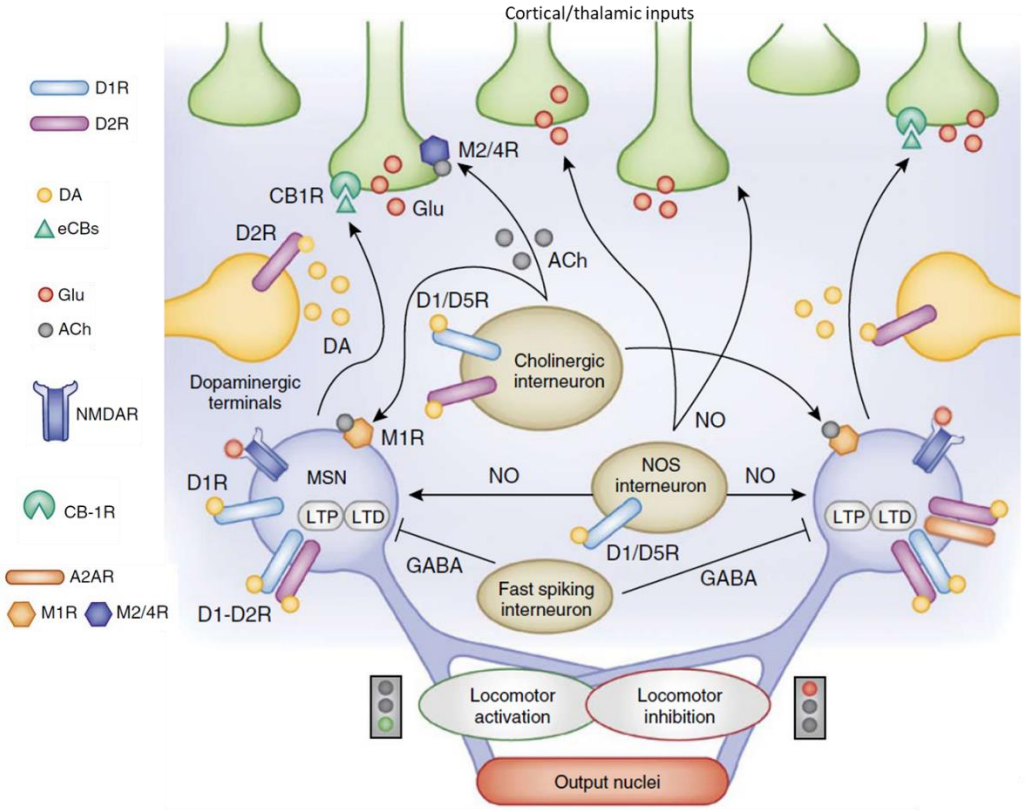

***Figure 19:* Striatal circuits**. *Glutamate inputs (thalamic and cortical) release glutamate onto striatal neurons. Glutamate goes to NMDA or AMPA receptors. Dopaminergic inputs from the SNc release dopamine onto striatal neurons: dopamine goes to D1R and D2R receptors. Striatal MSNs receive inputs from other striatal neurons, the interneurons: cholinergic neurons release ACh which goes to muscarinic receptors on the surface of MSNs, Fast-spiking interneurons release GABA which goes to GABA receptors. Adapted from* (Calabresi et al., 2014).

The dopaminergic receptors expressed by the striatal MSNs are of two kind: D1 and D2 receptors which allow the implication of these cells in two types of pathways (please see details in chapter III). Although electrophysiological membrane properties of these two subpopulations of neurons are quite similar, recently, a distinction based on their electrical properties was made possible. By using a transgenic mouse line where D2 and D1 MSNs are labeled, this study showed that D2 MSNs seem to have a higher excitability and stronger synaptic coupling with cortical neurons than the D1 counterparts (Cepeda et al., 2008; Planert et al., 2013).

To summarize, the striatum is a structure with an important cellular diversity. The MSNs constitute more than 90% of striatal neurons, and are divided into dMSNs and iMSNs, each involved in a different pathway. Although interneurons are outnumbered by MSNs, they play an important role in modulating the activity of the network via their effect on the MSNs. The role of each subtype seems to be dependent on the striatal territory and their intrinsic properties.

b- Striatum: a heterogeneous structure

1. Striosome / Matrix dichotomy

In many aspects, I have presented that the striatum is not a homogeneous structure. Another level of striatal heterogeneity comes from the segregation between two functional compartments, independent on the distribution of the cellular subtypes, dorso-ventral axis or cortical inputs. Using immunohistochemical markers, Graybiel and others revealed the presence of two compartments in the striatum: the striosomes (or patches) and the matrix (Crittenden & Graybiel, 2011; A. M. Graybiel & Ragsdale, 1978; A M Graybiel, 1995) (Fig.20). They used the acetylcholinesterase enzyme as a marker by looking at the intensity of the staining in cats and primates, but also at μ opiate receptors (Herkenham & Pert, 1981; Pert et al., 1976). Acetylcholinesterase is present in abundance in the matrix but absent in the striosomes or patches where the μ receptors with a high affinity to enkephalin are highly present.

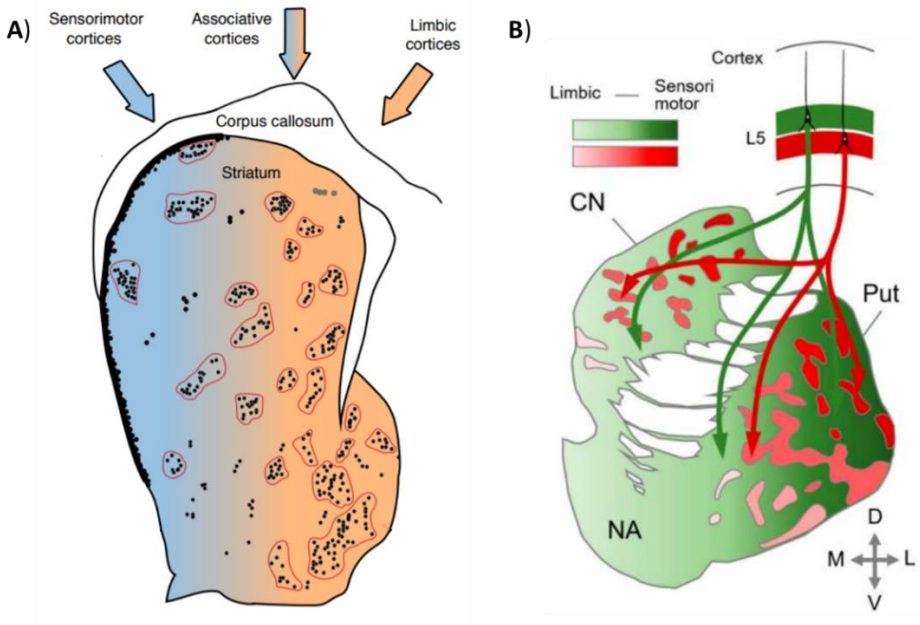

Figure 20: ***Segregation of the striatum into matrix and striosome compartments****. **A)** Compartmentalization of the striatum into matrix and striosomes (black dots). Dorsomedial striatum*

(orange) and dorsolateral striatum (blue) with their respective cortical inputs. Adapted from (Perrin & Venance, 2019). ***B****) Striosome compartment (red) receives inputs from deeper layer V (L5) of the cortex, and matrix (green) from upper layer 5. CN: caudate nucleus, Put: putamen, NA: nucleus accumbens. Gradient shows implication of the relative cortical inputs (limbic or sensorimotor). Light red and light green receive inputs from limbic areas. Dark red and dark green receive inputs from sensorimotor areas. From* (Hamasaki & Goto, 2019).

The striosomes occupy around 15% of the striatum (Johnston et al., 1990) and are enriched in μ receptors, enkephalin, neurotensin, GABA and substance P (Charles R. Gerfen, 1984; A. M. Graybiel et al., 1981). The matrix however, is enriched in parvalbumin and calbindin. The matrix itself is not completely homogeneous: striosome-like domains are present inside the matrix, they are thus called 'matrisomes' (Alice W. Flaherty & Graybiel, 1994). As shown earlier, MSNs can have large dense arborizations. However, all of their neurites remain in the designated compartment (Fujiyama et al., 2011; Y. Kawaguchi et al., 1989). One type of neurons was found to exist in between the matrix and striosomes (Aosaki et al., 1995), the cholinergic interneurons or tonically active interneurons. Given their localization, it is believed that they play a role in the interactions between these two compartments. Importantly, the functions of these two compartments are really different as indicated by the difference in their inputs and outputs. Indeed, matrix MSNs seem to project to the external and internal GP, and to the SNr, the 'regular' striatal output, but not the substantia nigra pars compacta (SNc) (Charles R. Gerfen, 1984; A. M. Graybiel et al., 1981). However the MSNs in the striosomes seem to project to the SNc with some collaterals to the globus pallidus and SNr (Fujiyama et al., 2011; Charles R. Gerfen, 1984). The inputs to these two compartments also allow this distinction: the striosomes are mainly innervated by the limbic areas of the cortex (layer III and deep layer V), when the matrix receives the majority of its projections which are topographically organized from sensorimotor and associative areas (upper layer V) ((Charles R. Gerfen, 1984; Selemon & Goldman-Rakic, 1985), and for review see (Crittenden & Graybiel, 2011)). In addition, it has been shown that MSNs in the matrix project more to direct and indirect pathways output nuclei (GPi, SNr and GPe) than the striosomes. If the striosomes are confirmed to be the only compartment with MSNs projecting to the SNc, the striosomes would have a functionally important role at the heart of the dopaminergic system. However, recently, these results were contradicted by showing that both compartments receive limbic and sensorimotor inputs, and even matrix neurons seem to project to the SNc (J. B. Smith et al., 2016). In addition, both compartments have been shown to respond similarly and to share common features in a conditioning task (Bloem et al., 2017). Even though it might seem like

the gap of differences is closing between these two compartments, striosomal neurons seem to encode more strongly reward prediction whereas matrix neurons encode strongly reward history (Bloem et al., 2017). Thanks to technological advances in two-photon microscopy, mouse lines generation, and tools targeting each compartment, more studies are examining the role of the striosomes and matrix compartments. Interestingly, specific lesions of the striosomal compartments in the dorsolateral striatum (using a dermorphin-saporin toxin) led to a disruption to the establishment of habitual behavior and an engagement of the dorsomedial striatum (Jenrette et al., 2019; Lawhorn et al., 2009). Altogether, these results show the role the matrix and striosomes could play in motor learning and conditioning.

2. DorsoMedial Striatum (DMS) and DorsoLateral Striatum (DLS)

The BG and the cortico-BG-thalamocortical loops are functionally divided, and the striatum follows this functional anatomy. Aside from the division of the striatum into a dorsal and ventral part, and the presence of striosome and matrix compartments, the striatum can be divided into 'sensorimotor', 'associative' and 'limbic' territories, sensorimotor and associative territories are localized in the dorsal striatum while the limbic one is integrated in the ventral striatum. I will be focusing here on the dorsal striatum.

The dorsal striatum can be divided into two territories: the caudate, equivalent of the associative territory in the dorsomedial striatum (DMS) in rodents and the putamen, the equivalent of the sensorimotor territory in the dorsolateral striatum (DLS) in rodents (H. H. Yin & Knowlton, 2006).

The DMS receives afferents from the associative areas of the cortex such as the prefrontal, temporal, posterior parietal, pre-occipital and oculomotor frontal cortex. The DLS receives afferents from the motor, premotor, supplementary and somatosensory cortex (Rüb et al., 2015).

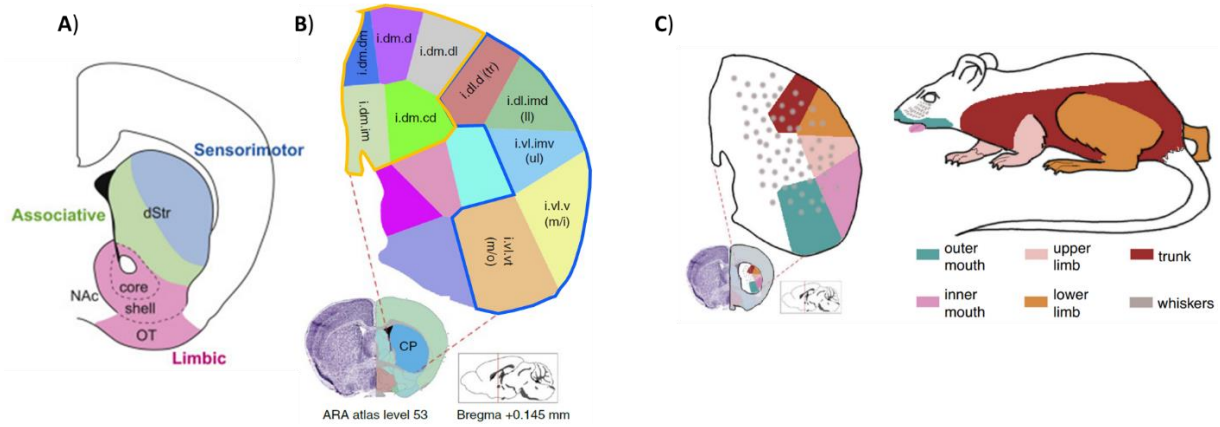

***Figure 21:* Striatal somatotopic map of a mouse body in the DLS but not the DMS**. ***A**: Segregation of the striatum into associative, sensorimotor and limbic parts. Adapted from* (Chuhma et al., 2017). ***B**: overview of striatum domains based on their connectivity. The DMS is divided into intermedial, dorsomedial, dorsal, centromedial and dorsolateral domains (delineated by orange line). The DLS is divided into dorsal and intermedial dorsal, and the ventrolateral striatum into intermedial ventral, ventral and ventrolateral (delineated by a blue line). The dorsolateral and ventrolateral parts both received inputs from somatic sensorimotor cortical areas. Adapted from (Hintiryan et al., 2016). **C**: somatotopic organization of the DLS. DLS divided into five domains. Mouse body parts color-coded based on the striatal body map. From (Robbe, 2018).*

The delineation of the different territories based on their cortical inputs was vague. A recent study realized a projectome of corticostriatal connections in mice and was able to divide the dorsal striatum into 29 regions based on their cortical inputs (Hintiryan et al., 2016). This study shows that the DLS receives inputs from all sensorimotor cortical areas which subdivides the DLS into five domains creating a somatotopic map of the mouse body (Fig.21). The DMS receives inputs from visual and auditory areas, but also from higher order associative areas such as the anterior cingulate cortex. The organization of the DMS however, did not allow for the construction of a topographical map. In their paper, Hintiryan et al. divide the DMS into five domains and each of them gets inputs from different cortical areas. The diversity of the cortical inputs for each of the DMS domains makes it difficult to allocate a role for each domain. This new detailed anatomical view of corticostriatal connections highlighted the complexity of the functional domains and the necessity to consider the different territories independently to understand their role in motor control and action selection.

To summarize, this chapter presented the BG and their anatomical organization. The BG are formed by a group of interconnected structures, including the striatum, the GPi, GPe, STN, SNr and SNc. Inputs to the BG correspond mainly to input to the striatum, which receives massive cortical inputs, but also thalamic inputs, and dopaminergic inputs from the SNc. I focused on the striatum which is at the center of my work and I described the anatomical composition of

this structure and the numerous aspects of its heterogeneity. Indeed, the striatum is heterogeneous whether we talk about its cellular composition (MSNs around 95%, GABAergic and cholinergic interneurons), its anatomical composition (striosome vs matrix) and its territories based on cortical connectivity (DMS vs DLS). This heterogeneity confers particular role to different part or constituents of the structure.

Dans ce chapitre j'ai décrit l'anatomie des ganglions de la base et des différentes structures qui les composent. Les ganglions de la base sont composés du striatum (qui correspond à la principale voie d'entrée des ganglions de la base), le globus pallidus (GPi et GPe), la substance noire (SNr et SNc), et le noyau sous-thalamique. Je me suis focalisée sur le striatum dorsal qui est au centre de mon projet. Cette structure est la principale structure d'entrée des ganglions de la base et reçoit majoritairement des entrées de l'ensemble du cortex cérébral, mais aussi thalamiques et dopaminergiques de la SNc. Le striatum est une structure très hétérogène à différents niveaux, au niveau cellulaire (composé de 95% de MSNs et d'environ 5% d'interneurones GABAergiques et cholinergiques), anatomique (matrice vs. striosomes), et fonctionnel par rapport à la connectivité corticale (striatum dorsomedial ou DMS et striatum dorsolateral ou DLS).

Le premier chapitre m'a permis d'introduire la mémoire procédurale, le second m'a permis de décrire l'organisation des ganglions de la base. Le prochain chapitre explorera le rôle des ganglions de la base dans le contrôle moteur et comment un dysfonctionnement au niveau de ces réseaux entrainera des désordres sévères, comme par exemple la maladie de Huntington.

III- Basal ganglia: role in motor control

BG have been known for a long time to be involved in motor control, which explains why this function has been the most studied. Based on the connections that are established between the different BG structures and output structures, several pathways were described. Simply put, one of the pathways will act as a facilitator of the targeted motor network whereas another will have an inhibitory role over thalamocortical and brainstem networks. In this chapter, I will describe the different pathways, the role they play in motor control and the pathologies that can occur when dysfunctions occur.

A) Pathways of the basal ganglia

On an anatomical level, the projections to the output structures of the BG can be divided into two pathways. Which pathway is employed will depend on the nuclei that are involved in the information transmission. Based on a model presented in 1989 (Albin et al., 1989), one of the pathways is called the direct pathway and the other is an indirect pathway.

The cortex projects to the striatum which in turn projects to the output nucleus, the GPi and SNr which project to the thalamus and the information goes back to the cortex. However, the striatum also projects towards the GPe which in turn projects to the STN which then projects to the GPi/SNr projecting to the thalamus which finally projects to the cortex (Fig.22). The direct pathway is called as such because it runs directly through the BG from the input (striatum) to the output (GPi and SNr), whereas two connections are added in the indirect pathway (the GPe and STN). A third pathway, the hyperdirect pathway, consists in cortical glutamatergic projections to the STN. By bypassing the striatum, the hyperdirect pathway projects excitatory stimuli from motor areas of the cortex to the STN in a shorter time frame than the direct or indirect pathways.

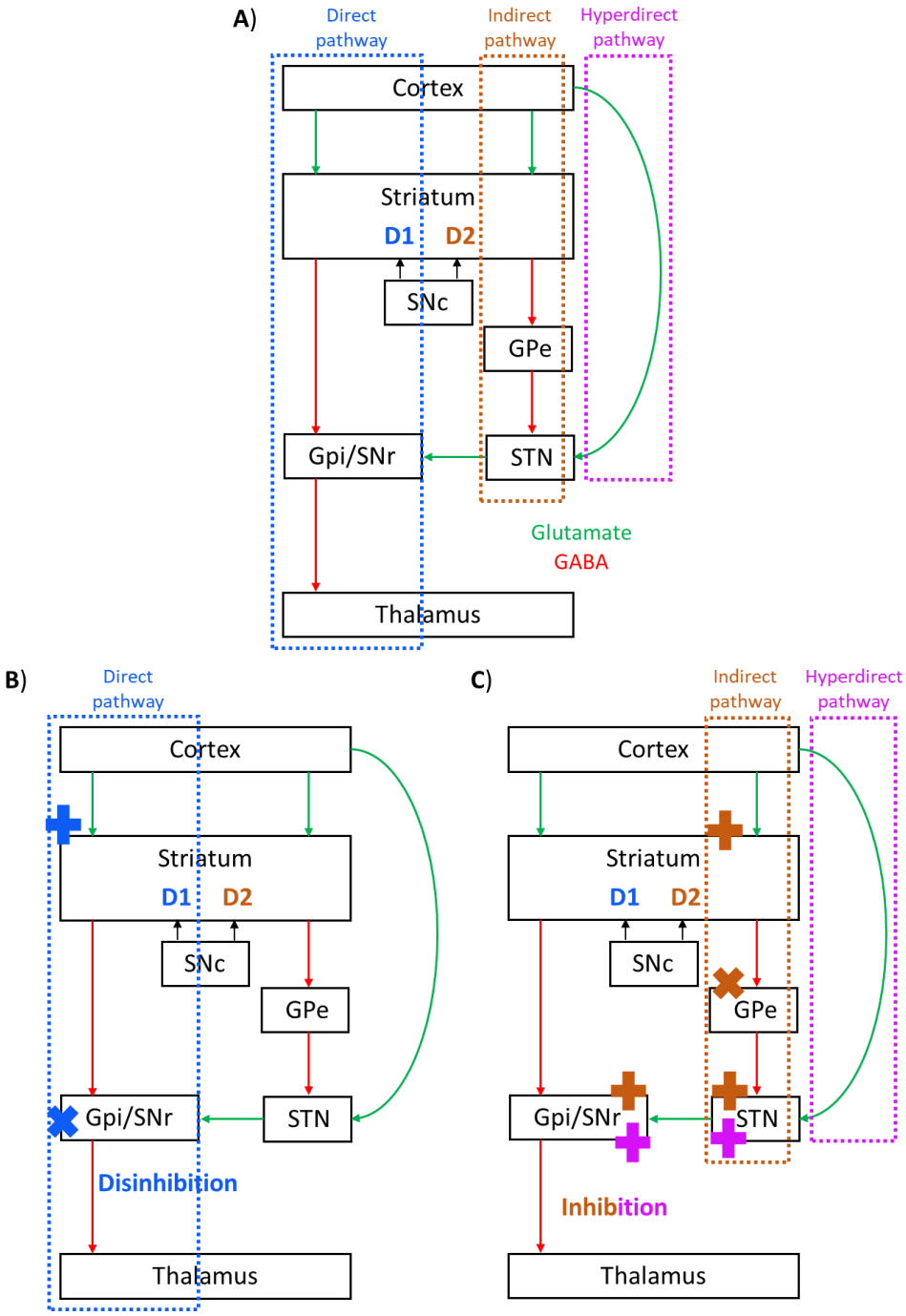

Figure 22:* Box and arrow model of the BG**. ***A*) model showing the three different pathways, direct (blue), indirect (brown) and hyperdirect (pink). Green arrows show glutamatergic excitatory projections. Red arrows show GABAergic inhibitory projections.* ***B****) model showing disinhibition in the case of the direct pathway. Cortical stimulations excite the striatum which inhibits the GPi, and the thalamus is not inhibited.* ***C****) model showing the inhibition of the thalamus in the indirect and hyperdirect pathways. In the indirect pathway, the striatum inhibits the GPe, the STN is not inhibited, and can stimulate the GPi which in turn inhibits the thalamus. In the hyperdirect pathway, STN is stimulated by the cortex, then STN stimulates the GPi/SNr which inhibit the thalamus. Based on models in* (Lanciego et al., 2012).

These three different pathways are presented as separated from each other: it is a simplified way of looking at the different actors of the BG and their involvement in these pathways. However, it is important to note that there is an interplay between these different pathways.

Seeing as the striatum projects towards two different structures involved in two different pathways, the idea of specific cell types involved in each of these pathways emerged. Indeed, it was shown that MSNs expressing D1 receptors and substance P project directly to the SNr and GPi and are thus involved in the direct pathway. Whereas MSNs expressing D2 receptors and enkephalin project to the GPe first and are therefore involved in the indirect pathway (Charles R. Gerfen et al., 1990; Watkins & Jenkinson, 2016). Both MSN types (D1 and D2 MSNs or dMSNs and iMSNs) are GABAergic neurons, but since they project either directly or via a relay to output structures, the overall results of these two will have opposite effects on the output structure, the thalamus. Indeed, through the direct pathway, the MSNs inhibit the cells in the GPi which then cannot inhibit the thalamus, and the thalamus will therefore excite the cortex, which acts as a 'go' signal, thus allowing for the initiation of an action (Fig.22). In the case of the indirect pathway, the striatum will inhibit the GPe which can no longer inhibit the STN, the STN will activate the GPi resulting in an inhibition of the thalamus and of the information transmission to the cortex. The indirect pathway acts therefore as a 'stop' or 'no-go' signal, thus inhibiting inappropriate actions. However, the image is not so simple, more evidence show there is not a strict dichotomy between these two pathways. Indeed, some anatomical bridges have been shown between the two pathways (Cazorla et al., 2014). In addition, the dopaminergic modulation of one pathway or the other is more complex. First, there is no clear restriction of the expression of D1 or D2 dopaminergic receptors in dMSNs or iMSNs but a difference in proportion (Aizman et al., 2000; Lester et al., 1993). Moreover, D1 receptors have been shown to have an excitatory effect whereas D2 receptors seem to have an inhibitory effect (Di Chiara et al., 1994). Therefore, the dopaminergic projections from the SNc to the striatum allow a certain balance between these two pathways.
We will describe in III-C how a dysfunction in these pathways can lead to movement disorders.

B) Role of direct and indirect pathways in motor control

Studying the role of the direct and indirect pathways in motor control was first based on electrophysiological studies. Differentiating dMSNs and iMSNs was based on morphological studies which took place *a posteriori*, once the recordings were made (Peak et al., 2019). However, recent advances in the field of transgenic mice and viral tools allowed for a live distinction between these two subpopulations. These novel techniques led to a better characterization of these two subpopulations and to a distinction based on their electrical

properties (Cepeda et al., 2008). These techniques associated to optogenetic tools allowed for a better understanding of the role of the different pathways in motor control, specifically striatal dMSNs and iMSNs (A. V. Kravitz & Kreitzer, 2012; Alexxai V. Kravitz et al., 2012). This first study used a specific optogenetic activation of dMSNs or iMSNs and confirmed that dMSNs activation triggered the mice to run while the activation of dMSNs exerted a brake (Alexxai V. Kravitz et al., 2012). Although these two subpopulations send 'go' or 'no-go' signals, an important cooperative work between them has been more recently described (Cui et al., 2013; Tecuapetla et al., 2014, 2016) thus allowing for a more controlled signal. Perhaps the best evidence of the cooperation between these two subpopulations of neurons comes from studies showing a simultaneous activation of both dMSNs and iMSNs. This is the case in several recent papers from the Costa lab (Cui et al., 2013; Jin et al., 2014; Tecuapetla et al., 2014, 2016). Calcium imaging in the dorsal striatum of mice performing an operant task showed an increased activity in both MSN populations before contraversive movements (Cui et al., 2013). Cui and colleagues also showed an inactivation of both pathways in the absence of movement, suggesting that a simultaneous activation of both groups is required to regulate action selection (Cui et al., 2013). Coactivation of dMSNs and iMSNs is also observed with different behavioral paradigms allowing for the observation of initiation of action (Jin et al., 2014; Sippy et al., 2015). Demonstrating the involvement of the striatal output pathways in motor control was made possible with studies manipulating MSNs. These studies explored the effect of MSN excitation or inhibition on movement, and they showed that triggering or inhibiting firing of MSNs leads to the initiation or termination of movement (Jin et al., 2014; Tecuapetla et al., 2016). The important part of this demonstration by optogenetics is that the duration of the stimulation matched with the affected movement (initiation or termination), showing the important role the different MSNs, and therefore the different pathways, play in motor control (for review see (Peak et al., 2019)).

To summarize this chapter, I described the inner workings of the BG and the different pathways that define them (direct, indirect and hyperdirect). The direct pathway is assimilated to the initiation of movement caused by a disinhibition of the thalamus. Whereas the indirect pathway is suggested to terminate a movement by inhibiting the thalamus. It has been recently shown that these two pathways do not work separately but cooperatively, thus refining the movement.

Pour résumer ce chapitre, j'ai présenté le fonctionnement des ganglions de la base et des différentes voies les constituant (directe, indirecte et hyperdirecte) et leur rôle dans le contrôle moteur. La voie directe a pour rôle l'initiation du mouvement grâce à une désinhibition du thalamus. La voie indirecte permettrait un arrêt du mouvement en inhibant le thalamus. Bien que ces deux voies aient été considérées comme ségrégées, il a été montré récemment qu'elles fonctionnement coopérativement permettant ainsi un raffinement du contrôle du mouvement.

IV- Procedural learning and Basal Ganglia circuits

A) Procedural learning: BG and striatal circuits

In chapter I, I defined procedural memory and detailed how it can be divided into 'goal-directed behavior' and 'habit'. In addition, I described evidence showing that the striatum is strongly involved in procedural learning. The striatum being a heterogeneous structure, with notably functional and anatomical division into two territories, the DMS and DLS, the question arose concerning the specialization of striatal territories in the learning process. Experiments done by Packard and McGaugh in the late 90's (M G Packard & McGaugh, 1996) show the involvement of the striatum, and particularly the DLS or dorsolateral caudate, in the formation of habit. Interestingly, what Packard and McGaugh tested was the role of the DLS once training was repeated several times. This would fall under the category of 'habit' in procedural learning. Indeed, later studies showed the involvement of the DLS in the late phase of procedural learning, once training has been repeated and learning established. The DMS, on the other hand, is involved in the first phase of learning, or 'goal-directed behavior' (Durieux et al., 2012; H. H. Yin et al., 2004, 2006; H. H. Yin, Ostlund, et al., 2005; H. H. Yin & Knowlton, 2006). Just like the approach followed to determine the role of the dorsal striatum in learning, the role of each of these dorsal territories was demonstrated with lesion and inactivation studies. For example, in one study where rats were required to push a lever when a cue is presented, an acquisition of stimulus-response associations was necessary for a good performance. When neurotoxic lesions of the DLS were made, the acquisition and retention of the task were impaired, even when motor requirements were not high (Gruber & McDonald, 2012). Yin and his collaborators examined the effects of excitotoxic lesions of the DLS in a lever press task with sucrose as reward. Sucrose was then devalued by inducing taste aversion. A reduction of sucrose consumption was observed with or without a lesion. During an extinction test in the instrumental chamber, only lesioned animals stopped pressing the lever when sucrose was not presented (H. H. Yin et al., 2004). Thus, it appears that when the networks involved in habit were affected, the goal-directed behavior system took over. These experiments were replicated in humans with a conditioning and devaluation paradigm (E. Tricomi et al., 2009; Valentin et al., 2007). Using fMRI, they were able to show a higher activity in the posterior DLS once behavior became habitual. The results from these experiments are consistent with the ones done in animal models. Similar experiments following a similar experimental paradigm were performed in the DMS to demonstrate the role of this territory

in goal-directed behavior. Lesions of the posterior DMS before and after training, and reversible inactivation after training reduced the performance of animals in a battery of behavioral tests established to detect action-outcome learning (H. H. Yin, Ostlund, et al., 2005). Also, blockade of NMDAR (necessary for LTP induction) specifically prevented the encoding of action-outcome (H. H. Yin, Knowlton, et al., 2005). The role of the DMS in goal-directed behavior was also shown in humans. Using fMRI techniques with monetary rewards and punishments, Tricomi et al. showed an activation of the caudate nucleus when individuals perceived the contingency between the button press and the outcome, thus showing the role of the caudate in reinforcement of action (E. M. Tricomi et al., 2004). Altogether, these results show the importance of the DMS in goal-directed behavior and the role of the DLS in habitual behavior (Fig.23).

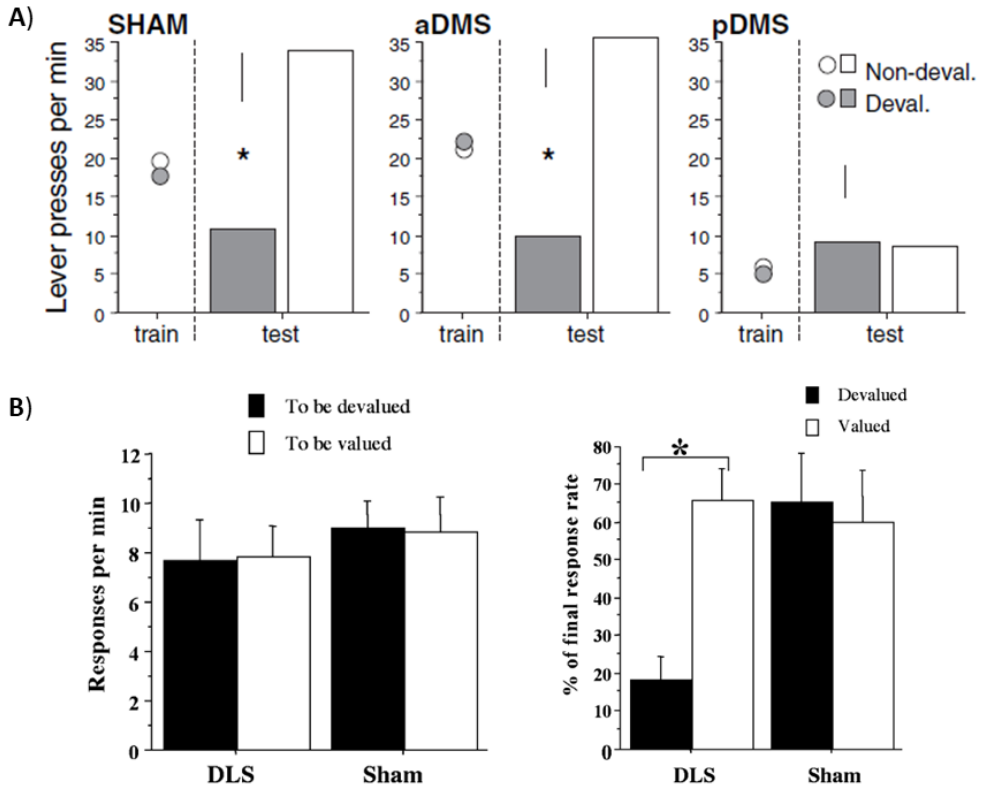

Figure 23: ***Involvement of the DMS and DLS in procedural learning based on lesion studies***. ***A)*** *Response rates on a lever press task in different conditions (sham, lesion of anterior DMS, aDMS, or posterior DMS, pDMS). Lesions of pDMS but not aDMS reduced instrumental performance (lower response rate on the lever press during training sessions). From* (H. H. Yin, Ostlund, et al., 2005). ***B)*** *Response rates on a lever press task in sham and animals with DLS lesions. Left: response rates on the last day of training on sucrose reinforcement and lever press. There was a similar response rates in sham and DLS-lesioned animals. Right: extinction test with LiCl injections. In the sham group, similar devaluation of sucrose with LiCl or saline injections. In the DLS-lesioned group, the effect of devaluation appeared after LiCl injection. Thus, lesions to the DLS resulted in a goal-directed behavior. From* (H. H. Yin et al., 2004).

The striatum is therefore a heterogeneous structure, divided into functional territories such as DMS and DLS, involved respectively in goal-directed behavior and habit formation. However the role of the striatum in behavior is anchored in the cortico-BG-thalamocortical loops. I described earlier the work of Alexander and colleagues showing the functional segregation of these circuits (G. E. Alexander et al., 1986). Five loops were described, but four of them are essential in procedural learning: motor, sensory, associative and limbic loops (Fig.24). It was suggested that there was a clear anatomical distinction between these loops, and more precisely the DMS and the DLS, the DLS receiving projections from sensory and motor cortex, and the DMS from limbic and associative cortex. But the segregation is not strict. An interplay between these different circuits occurs, leading to an interaction between the different circuits in a ventromedial to dorsolateral gradient, from the limbic through the associative to the motor circuit (Foerde & Shohamy, 2011).

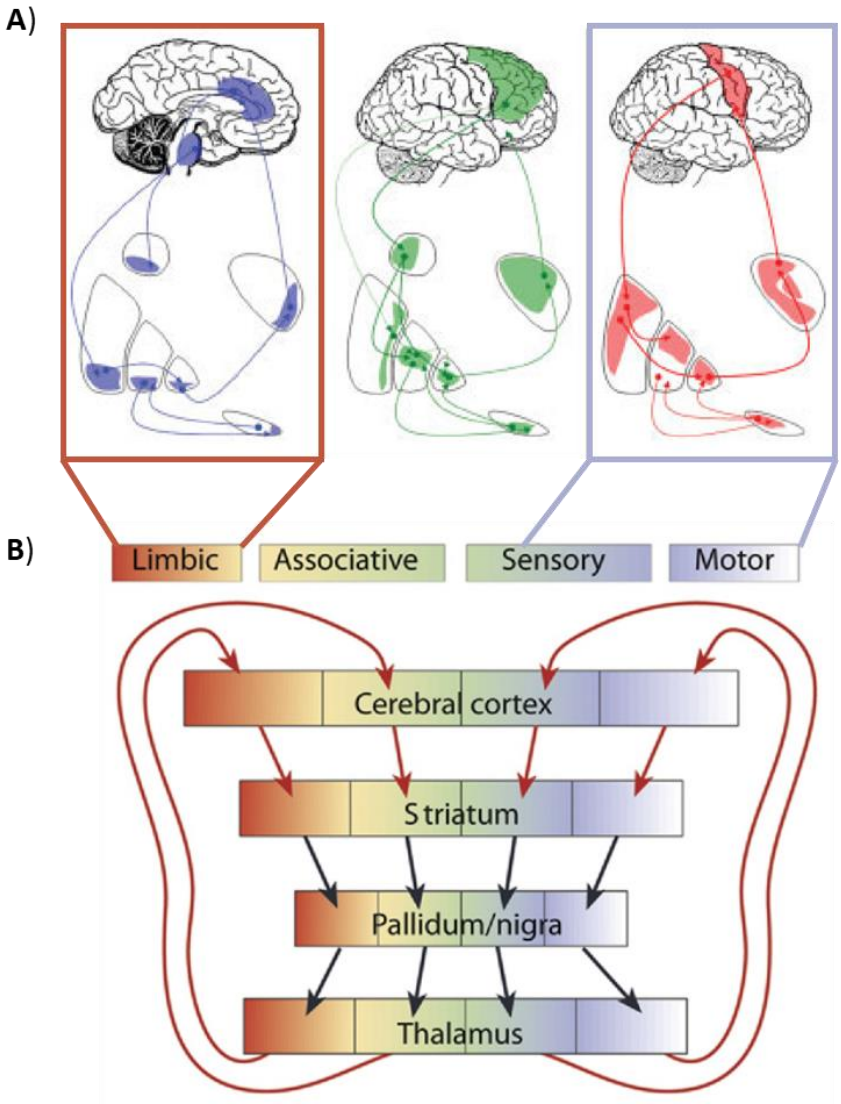

***Figure 24:* Functional segregation of the cortico-BG-thalamocortical loops in humans. A)** *Right: motor circuit; in red the motor cortical areas, posterolateral putamen, GPe and GPi, dorsolateral STN and ventrolateral thalamus. Middle: associative circuit. Left: limbic circuit. Adapted from (Obeso et al.,*

*2008). **B**) Loops divided into four circuits: limbic associative, sensory and motor. Limbic and associative loops are involved in goal-directed behavior. Sensory and motor loops are involved in habit. From (Redgrave et al., 2010).*

The roles of each of these territories is thus consistent with their connectivity. Indeed, the DMS receives input, not only from the cortex, but also from the thalamus, hippocampus, amygdala… For example, the connectivity between the DMS and the hippocampus allowed for a closer look on the role of the DMS in response flexibility (Peak et al., 2019; Ragozzino et al., 2002). With a variant of the water maze where the platform is moved every eight trials, normal rats find the platform in the first two trials, whereas rats with DMS lesions are impaired during the task but show within-session learning. When the lesion is in the hippocampus, rats do not show any improvement and are severely impaired. This suggests the important role the DMS plays in actions that are rapidly adaptable (Gruber & McDonald, 2012; Peak et al., 2019). These results are not surprising considering the activation of the DMS in the initial phase of learning a task, where an adaptation to the outcomes would be required. After the repetition of the task, and once habit is formed, this flexibility is not present anymore, the same behavior becomes independent of the outcome or the reward value (Ann M. Graybiel & Grafton, 2015; Gruber & McDonald, 2012).

In the late 50's, 'chunking' was proposed by George Miller as a tool allowing an association of several elements when there is a limited capacity in a memory system. This system was later proposed by Graybiel as a way of converting goal-directed behavior into habit (Ann M. Graybiel, 1998; Ann M. Graybiel & Grafton, 2015; Jin & Costa, 2015). Later, it was suggested that the BG and specifically the striatum played an important role in 'chunking' a task into several action sequences which, once unitized, will lose their flexibility (Barnes et al., 2011; Ann M. Graybiel, 1998; Hikosaka et al., 1998). Moving from a flexible process into a unitized one seems to follow an anterio-posterior axis in the striatum (first the anterior DMS is active, then the posterior DMS takes over) (Foerde & Shohamy, 2011; Peak et al., 2019). The T-maze was used to first demonstrate the chunking of actions by recording spiking activity in the DLS of rats learning to navigate the T-maze by following the cues to turn left or right. These studies showed that before learning started, neurons were active across the trial, however, once habit was formed, this activity was only expressed at the beginning and at the end of the trial (Barnes et al., 2005; Jog et al., 1999) (Fig.25). These experiments showed that the striatal networks were not only activated or inhibited based on learning, but that this activity was dynamic and divided into several sequences or 'chunks'.

I will describe in the next paragraph the evolution of the dynamics of the striatal networks during learning.

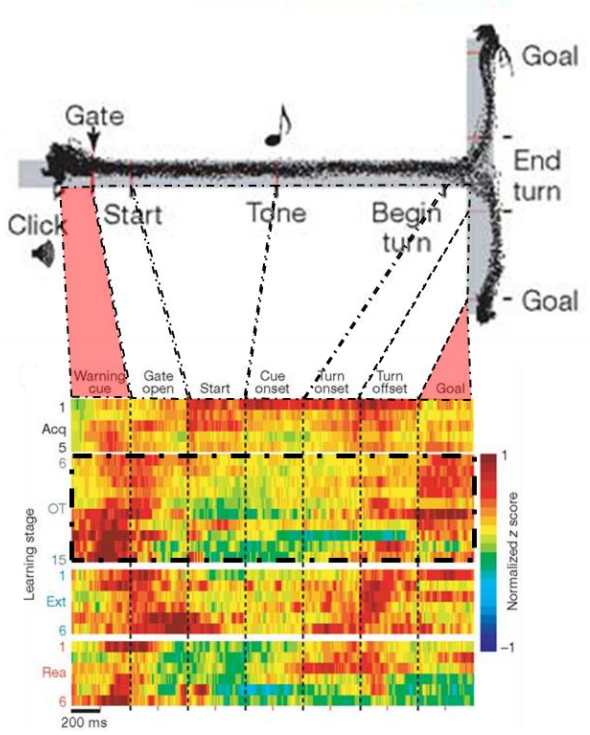

Figure 25: ***Chunking of DLS activity in a T-maze task.*** *Training of rats in a T-maze task. DLS activity increases across training during the acquisition phase. During overtraining, activity is high at the beginning and at the end of training, thus associating the different sequences during the task and separating them from the start-related activity. Activity related to each phase of the task separated by dotted lines. In transparent pink and dotted rectangle: high activity after overtraining. Adapted from* (Barnes et al., 2005).

B) Behavioral assays to test procedural memory

In order to study procedural memory and dissect the different structures that are involved and their relationship, one has to first form this memory. Several tests of procedural learning have been developed over the years. Depending on the question that one is asking, the test used won't be the same. Indeed it has been shown that depending on the test and the complexity of the test, habit could be reached more or less quickly, thus allowing for studying different phases of learning (Rossi & Yin, 2012). Therefore, not only is it important to choose the right test, but also the right parameters for the test.

A myriad of tests have been developed to test procedural learning and motor skill learning.

The two tests that have been mostly used are the T-maze and the accelerated rotarod. The T-maze is one of the most commonly used tests to form procedural memory (Barnes et al., 2005; H. H. Yin & Knowlton, 2006). This test allows for a separation of the different phases of

learning, and also allows for the study of action selection and decision making (Fig.26). I already described the principle of a T-maze test with the place-response task in chapter I. By taking into account the different steps in the test, different parts of memory can be accessed and studied (Fig.23). This test is based on giving a reward to train animals.

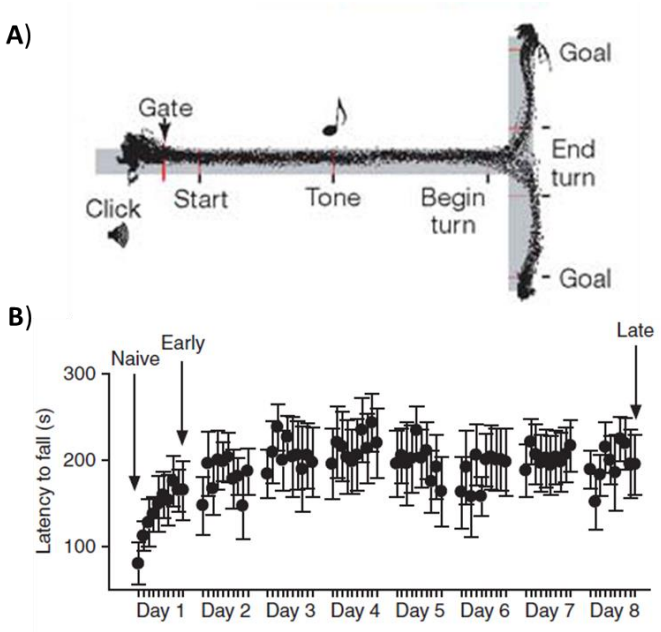

Figure 26: ***Behavioral tests for procedural memory****. **A**) T-maze test with run trajectories. The animal is placed at the beginning of the long arm of the maze before the gate. This test is based on an association between sounds and food. Once the animal has traveled halfway, a low or high tone will indicate if the reward is placed in the right or left arm of the maze. From* (Barnes et al., 2005)*. **B**) Learning curve on an accelerated rotarod. Test allowing the separation of different phases of motor skill learning (naïve, early and late). From* (H. H. Yin et al., 2009)

Another test, the accelerated rotarod paradigm, is a widely used test for motor skill learning and habit formation (Buitrago et al., 2004; Costa et al., 2004; Kupferschmidt et al., 2017; H. H. Yin et al., 2009). Animals are placed on the rotating rod that increases its rotation speed (Fig.26). The purpose of the test is to train animals to stay on the rotating wheel the longest. On the first day of training, animals start to learn and their performance gets better with every trial. On the second day we still observe an even better performance until the animals reach a plateau. This test does not use reward as a reinforcement. More importantly, it allows the study of different phases of procedural memory, from the beginning of the acquisition, until the formation of a habit. The first day of training corresponds to the early phase of motor skill learning. The test is repeated over 7 days, allowing the study of the late phase of motor skill learning.

In addition to these two tests, there are many others which would allow to evaluate different parameters of the procedural memory. Amongst these tests is the double H maze, which is

similar to the Morris water maze as a platform is submerged by water, and depending on the presence or absence of spatial cues, can be used to test spatial learning and procedural learning (Kirch et al., 2015). Also, the illuminated radial arm maze, or the win-stay version, is a test where animals have to rely on the association between light and food instead of spatial cues, thus allowing the study of procedural learning (McDonald & White, 1993; Xu et al., 2012). And finally there are tests such as the lever press test where animals have to learn a sequence of actions. Usually an operant chamber is used for this kind of test. The animal is placed in the chamber and trained to press a lever to get a reward and to associate the reward to either a light or a sound (see example in (Jin & Costa, 2010)).

C) Dynamics of striatal networks during procedural learning

I described in the previous section how the DMS is considered to support goal-directed behavior with flexible changes in choice outcomes, and is gradually replaced by the DLS when habit is formed and choice outcome becomes more predictable (Ann M. Graybiel & Grafton, 2015; Gruber & McDonald, 2012; Peak et al., 2019). This was shown with inactivation and lesion studies. Later, the activity of these two striatal territories was recorded. Simultaneous electrophysiological recordings in DMS and DLS while rats learned a T-maze task showed different dynamics of activity in DMS and DLS (Thorn et al., 2010). These results, along with other similar studies, show a higher activity of the DMS during early phases of learning (Costa et al., 2004; Thorn et al., 2010; H. H. Yin et al., 2009) and higher activity of the DLS once habit was formed (K. S. Smith & Graybiel, 2013; Thorn et al., 2010; H. H. Yin et al., 2009). Based on these results, a shift of activity from the associative to the sensorimotor part of the striatum was proposed. Indeed, studies with neural recordings in nonhuman primates, and later in humans, show a shift of activity between these two territories when learning a sequence of arm or finger movements (for review see (Ann M. Graybiel & Grafton, 2015)).

More recent studies show a simultaneous increase of the activity in the DLS and DMS during early learning. Once habit is formed, the activity of the DMS decreases but not the activity in the DLS (Kupferschmidt et al., 2017). I mentioned earlier the lesion studies in the DLS where goal-directed behavior takes over actions (H. H. Yin et al., 2006). This suggests that in the absence of DLS recruitment, nothing would be impeding the activity of the DMS, thus allowing for an improvement of the performance. This would correlate with the physiological dynamics during goal-directed behavior where the DLS starts getting activated along the DMS and

quickly takes over after training, leading the performance to a plateau. These results, along with similar studies showing habitual control of action after DMS inactivation (H. H. Yin, Ostlund, et al., 2005) suggest the competitive nature of the interaction between DLS and DMS circuits allowing for the formation of habits. The presence of these competing circuits was shown in rodent studies (Kupferschmidt et al., 2017; Thorn et al., 2010) and in human fMRI studies showing that individuals reducing activity in prefrontal regions earlier, learn faster (Bassett et al., 2015). Accumulating studies suggest the presence of a competitive relationship between goal-directed and habitual behaviors (Bergstrom et al., 2018; Bradfield & Balleine, 2013; Daw et al., 2005; K. S. Smith & Graybiel, 2013; Vicente et al., 2016). However, a coordination or cooperation between both circuits has been recently suggested (Robbins & Costa, 2017).

Thus, two models explaining the cooperative or competitive relationship between these two circuits are proposed: a sequential model where each territory is more involved in one part of learning; and a parallel model where both territories are active at all stages of learning (the DMS allowing for early learning while the DLS interferes, and both territories allow for late learning) (Bergstrom et al., 2018) (Fig.27). The sequential model corresponds to a cooperative relationship between goal-directed behavior and habits. Whereas the parallel model places both systems in a competing position for action control. The sequential model first proposed by Bergstrom et al. is refuted by the authors at the end of the paper based on their results. They showed that when the DLS was photosilenced, early learning was facilitated and the activity of the DMS (Arc expression) was reduced in later stages of learning (Bergstrom et al., 2018). Thus, the DMS seems to take over when the DLS is inactivated, adding evidence to the competing activity of both territories.

A recent study showed that although activity of DMS and DLS was similar in early learning, the activity of both territories becomes more similar after extended training (Vandaele et al., 2019). We could think that because of the DMS disengagement proposed by some studies (Kupferschmidt et al., 2017) but refuted by others (Vandaele et al., 2019), a cooperative relationship exists between both circuits. Moreover, I mentioned earlier ‘chunking’ of actions into different sequences. Based on the dynamics of activity of the DLS in a T-maze task, the pattern of activity of the DLS is considered to act as a ‘bracket’ for the task. Indeed, with training, the level of activity in the DLS becomes higher at the initiation and at the end of the task, and it can decrease to reach lower levels than the baseline (Ann M. Graybiel & Grafton, 2015; Jin et al., 2014; Jin & Costa, 2010; Jog et al., 1999; Lipton et al., 2019; K. S. Smith &

Graybiel, 2013; Thorn et al., 2010). This activity pattern seems to become stronger with over-training (Barnes et al., 2005; Jog et al., 1999; K. S. Smith & Graybiel, 2013; Thorn et al., 2010). We can see on Figure 26 that this is not the case for the DMS where activity is elevated consistently during the acquisition phase and it decreases as animals become trained, at which time 'task-bracketing' in the DLS takes place.

At this point one can wonder if chunking of actions into different sequences would involve the dynamics of activity mentioned earlier for each of the sequences. Thus explaining the concomitant activation of both territories. Also, this suggests that both competitive and cooperative relationships could be at play to allow the formation of habits. To give an example of how this could work: let us imagine a situation where we check the traffic reports before leaving the house in the morning or before leaving the work place. This act of checking the reports could be a habit, however looking for the right radio station, typing the information to look at it on the computer, or checking for the best route will be goal-directed behaviors. Thus two circuits will be working cooperatively.

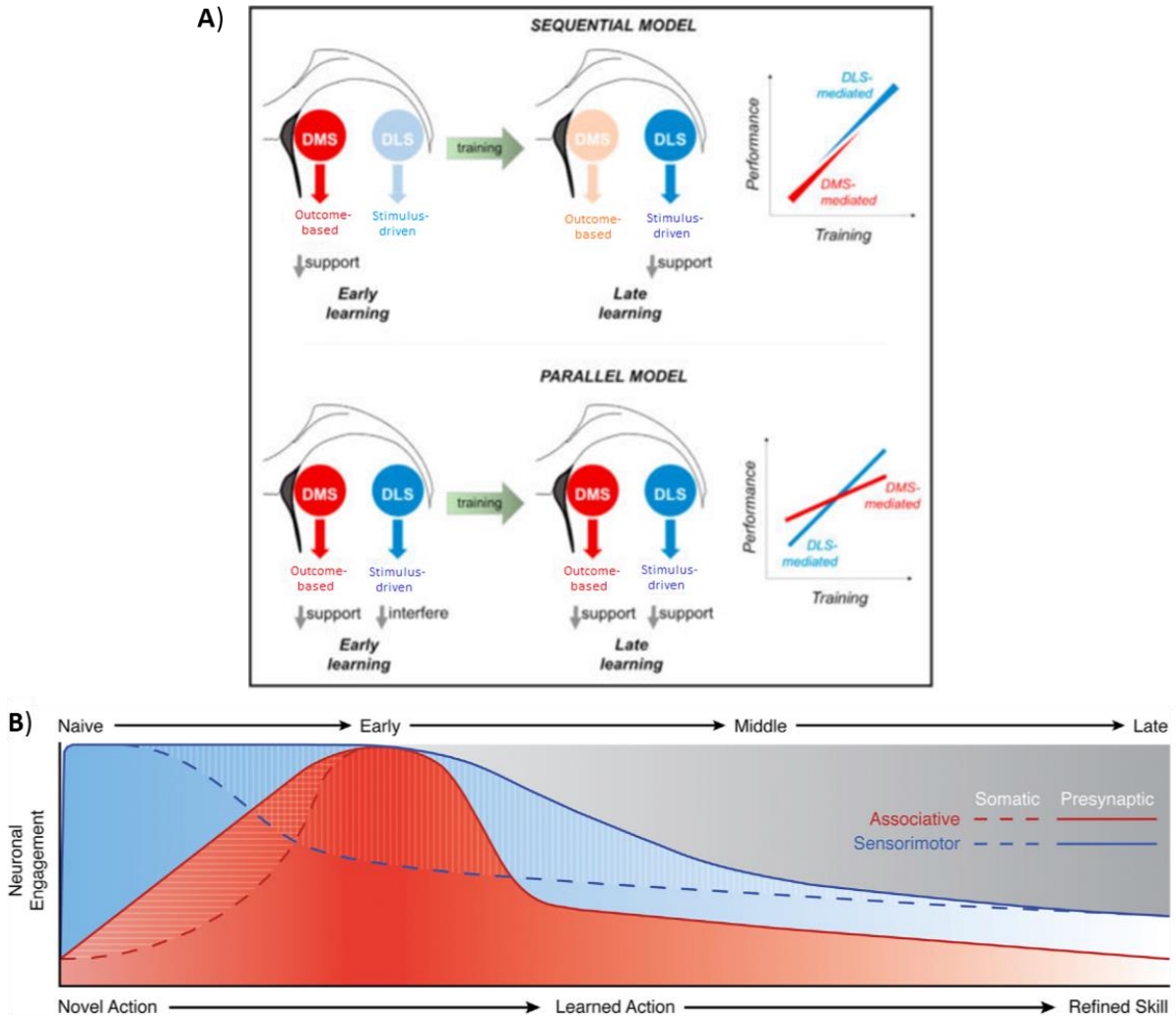

Figure 27: ***Models of associative and sensorimotor circuits during skill learning****. **A**) sequential and parallel models of associative and sensorimotor circuits showing competitive or cooperative*

contribution of DMS and DLS circuits in early and late learning. From (Bergstrom et al., 2018). ***B****) model of action learning with a transient activation of the DMS and progressive reduction of DLS inputs occur simultaneously. From* (Kupferschmidt et al., 2017)*.*

In conclusion, we described here the dynamics of the striatal circuits during learning. Each territory was first granted a role during learning: the DMS was linked to goal-directed behavior with a higher activity at this phase of learning, the DLS on the other hand was linked to habits. However, the role of each of these territories could not be strictly separated. Recent studies showed that both territories were active at the same time suggesting a competitive or cooperative relationship between the DMS and the DLS. Specific patterns of activation are observed in the DLS, suggesting a 'task-bracketing' role of the DLS. Ensembles of neurons that are active at the initiation and termination of an action suggest that storage of this memory is possible, at least in the DLS. We can thus wonder if there are neuronal substrates of skill learning and if they are located in the striatum (DMS or DLS).

Dans ce chapitre j'ai présenté les différents circuits impliqués dans la formation de la mémoire procédurale et dans l'apprentissage de nouvelles tâches. J'ai décrit les rôles spécifiques à chacun des territoires striataux : le DMS associé à la première phase d'apprentissage, et le DLS une fois l'habitude formée. Ces différents rôles sont basés sur une augmentation de l'activité dans ces territoires au cours de l'apprentissage. Cependant, la séparation n'est pas aussi stricte. En effet, des études récentes ont montré que les deux territoires sont actifs en même temps, mais avec des dynamiques différentes, soulignant une relation de compétition ou de coopération entre eux. Des patterns spécifiques d'activation sont observés dans le DLS, suggérant un rôle de 'task-bracket', délimitant les différentes parties de l'apprentissage d'une tâche, avec une activation d'un ensemble de neurones au moment de l'initiation du mouvement et au moment de l'arrêt. Ainsi, un groupe de neurones serait capable de stocker l'information correspondant à cet apprentissage. La question se pose donc s'il existe des substrats neuronaux pour l'apprentissage d'une tâche ou mémoire procédurale.

V- Dysfunctions in the BG pathways: example of Huntington's disease

I discussed the organization of the BG and the important role that they play in motor control and action selection. This role is also highlighted when dysfunctions occur on the level of the BG and lead to severe pathologies such as Parkinson's Disease, Tourette Syndrome, dystonia, or Huntington's Disease. Since the BG play such an important part in controlling movement, the common point of these pathologies are to be characterized by motor dysfunctions, even though there are more cognitive aspects involved as well. This correlation between motor and cognitive dysfunctions and BG-related pathologies was established in the first half of the 20th century (Yanagisawa, 2018), and I will describe here in more details the case of one disorder, Huntington's disease (HD).

A) Introducing Huntington's Disease

1) Genetic aspects

HD is an autosomal dominant neurodegenerative disorder known for the associated motor dysfunctions. The chorea in HD was first mistaken for the Saint-Guy or St Vitus' dance or Sydenham chorea (an infectious infantile disease that can be treated with penicillin). But in 1872, a 22 year-old doctor, George Huntington, separated these two diseases and described HD and the symptoms that were associated to it thoroughly. Although George Huntington was not the first to describe the disease, his name was associated to HD because he was the first to describe it with precision and in a concise manner and to report it to a wide medical community. Huntington's paper was a longitudinal study that was based on observations made during the beginning of his career but also by his father and grandfather before him. The three main points that he described in his paper were: the 'hereditary nature' of the disease, the emotional and psychiatric deficits that are observed ('a tendency to insanity and suicide'), and finally the age at which the disease appears and the progression of the disease ('manifesting itself as a grave disease only in adult life') (Huntington, 1872). The hereditary aspect of the disease (autosomal dominant) was described further once Mendel's laws came out at the beginning of the 19th century. The genetic mechanisms responsible for HD were left unknown for about a century until 1983, when the chromosome responsible for the disease was identified as a prolonged short arm of the chromosome 4, the protein coded by this gene was called Huntingtin or HTT (Gusella et al., 1983). The gene responsible for the disease is

discovered ten years later thanks to technological advancements in the genomics field. In 1993, it was discovered that HD was associated with an unstable expansion of a CAG (glutamine) repeat in the HTT gene (MacDonald et al., 1993). The group of scientists who identified this expansion of the gene showed that the variability of the expansion could explain the evolution of the disease and its manifestation. Individuals are considered healthy as long as they have less than 35 CAG repeats. The number of repetitions could be divided into 4 groups: normal, intermediate, reduced and full penetrance (Table 1).

CAG repeat length	10-26	27-35	36-39	40+
Penetrance	Normal	Intermediate	Reduced	Full

Table 1: *CAG repeat length and penetrance. Based on* (Kremer et al., 1994).

In normal conditions, the exon-1 of the HTT gene contains less than 26 CAG repeats (Kremer et al., 1994). The intermediate group will have between 27 and 35 CAG repeats. Reduced penetrance exists when there are less than 40 repeats. And the full penetrance corresponds to the group showing more than 40 CAG repeats. Individuals with more than 60 repeats show symptoms really early, they correspond to the juvenile and adolescent forms of the disease (Gencik et al., 2002). The length of the CAG repeats is therefore well correlated with the age onset of HD, however it is less correlated in the juvenile form of HD (Andresen et al., 2007). Not only is the length of the expansion directly correlated to the age of manifestation of the disease, but it is also correlated with the age of death onset which links the length of the expansion to the severity of the disease (Fig.28) (Keum et al., 2016).

It is important to note that even though individuals in the intermediate group might not show any symptoms, their descendants might develop the disease because of the instability and variability of the number of repeats (Ranen et al., 1995), the parents being more susceptible to depression and apathic behavior (Killoran et al., 2013).

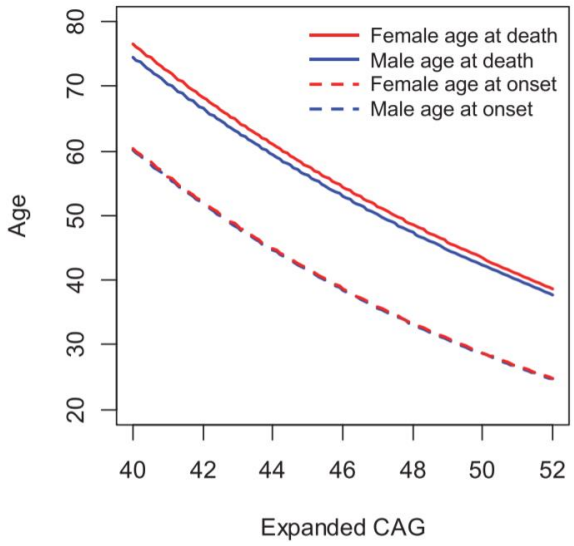

***Figure 28**: **Correlation between CAG repeats and age**. With a higher number of CAG repeats, the age at onset decreases, so does the age at death. From (Keum et al., 2016).*

The prevalence of HD is around 5 per 100,000 people. However this number changes depending on ethnicity. In Asia, the number of cases is much lower, but the number increases in Canada (around 14 per 100,000). In Latin America, this number increases significantly with clusters appearing across South America. This does not come as a shock since the gene of HTT was identified in patients from Maracaibo (Cardoso, 2017).

2) Triad of symptoms

Although HD is mostly known for motor impairments, it is actually characterized by a triad of symptoms: motor, cognitive and psychiatric. These symptoms are quantified with a scoring system, the Unified Huntington's Disease Rating Scale (UHDRS), which was developed in 1996 by the Huntington Study Group (HSG). This scaling system assesses four main points: 'motor function, cognitive function, behavioral abnormalities and functional capacity' (Kieburtz, 1996). These assessments were based on symptoms with rapid progression. The rating scale includes the following tests: motor assessment, cognitive assessment, a verbal fluency test, symbol digit modalities test, Stroop interference test, behavioral assessment (which includes a scoring system of mood, anxiety, irritability, delusions…), functional assessment, independence scale and functional capacity. With this scoring system, physicians are able to examine the three types of symptoms characterizing HD: motor, cognitive and psychiatric.
Clinically speaking, HD can be divided into 'premanifest' and 'manifest' periods (Fig.29). In the 'premanifest' period, a 'presymptomatic' phase corresponds to individuals who do not show

any symptoms which fades into a 'prodromal' phase where subtle motor, cognitive and behavioral changes occur. This brings the individual into the 'manifest' period, where all symptoms increase in a rapid manner. The subdivision of the 'manifest' period is characterized by a rapid development of all symptoms. As we can see on Figure 29, all symptoms are plotted in function of age and a CAP score (a calculated score of the number of CAG repeats).

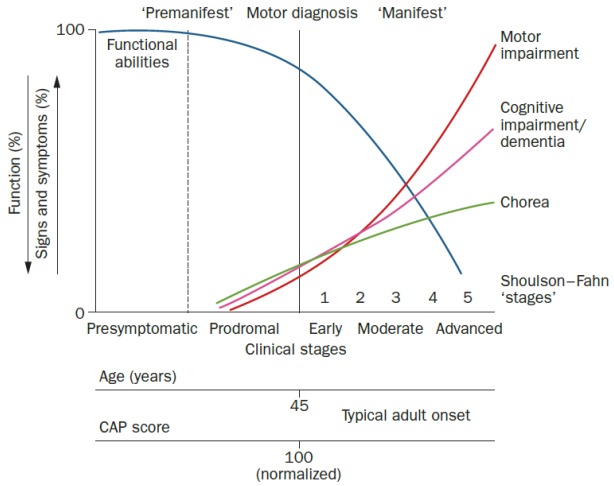

***Figure 29:* Symptom manifestation in relation to age and CAG repeats**. *The 'premanifest' period corresponds to the presymptomatic phase where no symptoms of the disease are visible, and the prodromal phase where subtle signs of HD appear. Cognitive symptoms are compared to a baseline, making the comparison easier. Once motor diagnosis is done, the 'manifest' period starts. The manifest period was divided into early, moderate and advanced clinical stages. During this period, motor and cognitive impairments progress slowly, chorea is predominant at first then reaches a plateau later. Motor and cognitive impairments progress more steadily. CAP: CAG age product. From (Ross et al., 2014).*

a- Motor symptoms

These symptoms consist in involuntary movements in the extremities, can affect facial muscles, and progressively spread to reach proximal muscles. Motor symptoms in the early phases of the disease consist in hyperkinesia and chorea which correspond to involuntary movements. When the late stages approach, hypokinesia, bradykinesia (slower movements) and dystonia (increased muscle tone with slower movements) predominate (Ajitkumar & De Jesus, 2020). Other symptoms include dysarthria, dysphagia and ataxia. In this second phase, patients show impairment of voluntary movements. These motor symptoms will progress over time and render the patients bedridden, unable to walk and completely dependent in their daily life. This impairment of voluntary movements correlate with functional disability whereas chorea does not (Ross et al., 2014). The motor assessment part of the UHDRS examines ocular pursuit, saccade initiation, saccade velocity, dysarthria, tongue protrusion,

maximal dystonia, maximal chorea, retropulsion pull test, finger tapping (used in the TRACK-HD study (Ross et al., 2014)), rigidity, bradykinesa, gait and tandem walking (Kieburtz, 1996). Patients are followed by their physician to study the progression and the severity of the disease in order to adjust the treatment. Tetrabenazine (TBZ), amantadine or riluzole are the only drugs recommended by the The American Academy of Neurology for managing chorea (Ajitkumar & De Jesus, 2020). TBZ inhibits a vesicular monoamine transporter (type 2) thus inhibiting the dopamine pathway. Another form of TBZ, deutetrabenazine was recently approved as a drug for chorea (Kumar et al., 2020). Other motor symptoms are treated with physiotherapy.

b- Psychiatric symptoms

Psychiatric symptoms appear very early in the disease, even before motor symptoms. These symptoms include apathy, depression, impulsivity, poor attention and irritability (Ajitkumar & De Jesus, 2020). Depression could be due to the disease or underlying neural pathology (Ajitkumar & De Jesus, 2020; Garcia-Gorro et al., 2017). Apathy seems to be the most associated to the progression of the disease (Ajitkumar & De Jesus, 2020), and the most common symptom in symptomatic and asymptomatic patients (28%) (Van Duijn et al., 2014). The behavioral and psychiatric assessment part of the UHDRS includes an examination of mood, irritability, compulsions, hallucinations, aggressive behavior, suicidal thoughts, a functional assessment and an independence scale (Kieburtz, 1996). Amongst the psychiatric symptoms in HD, depression and apathy are the ones physicians try to treat. Antidepressants such as selective serotonin reuptake inhibitors are commonly used in HD (Ajitkumar & De Jesus, 2020). However, when possible, environmental changes and therapy should be considered.

c- Cognitive symptoms

Cognitive symptoms are predominant in HD and they occur several years before motor symptoms. A deterioration of psychomotor speed and executive functions are the first signs of cognitive decline. Patients have difficulty in organizing, planning, attention, and in verbal fluency (Ajitkumar & De Jesus, 2020; Garcia-Gorro et al., 2017). These symptoms will progress and at late stages of the disease patients have dementia with global impairment of cognition

(Cardoso, 2017; Papoutsi et al., 2014). There is not a lot of evidence showing cognitive impairment more than 10 years before clinical diagnosis, but during the 10 years period before diagnosis, cognitive deficits and degeneration have been widely described (Biglan et al., 2016; Papoutsi et al., 2014). The deficits in executive functions of HD suggest alterations in the frontostriatal circuitry (Gray et al., 2013). However, visuospatial deficits and dysfunction of motor abilities implicate alterations in other regions such as the posterior occipital regions (Nopoulos et al., 2010) and somatosensory and motor (Bohanna et al., 2011; Burgold et al., 2019; Dumas et al., 2012) parts of the cortico-BG-thalamocortical loops.

The memory responsible for these motor abilities, procedural memory, seems to be affected in HD patients. Previous studies described deficits in declarative but not procedural memory in HD patients (Sprengelmeyer et al., 1995). However, studies from the same period (Bylsma et al., 1990) and more recent ones (Cayzac et al., 2011; Holtbernd et al., 2016; Kirch et al., 2013; Schneider et al., 2010) show the opposite in HD patients and in rodent models of HD. The paper by Bylsma et al. suggests the presence of subclasses of procedural memory that are independent: even though HD patients were able to learn a specific maze route like the control subjects, they were unable to apply these cognitive skills across mazes and when routes became unpredictable (Bylsma et al., 1990). More recently, Schneider et al. showed that in a serial reaction time task in manifest and premanifest HD patients, explicit, but not implicit sequence learning was affected (Schneider et al., 2010). Explicit learning implies an awareness and knowledge of the movements during the learning of a task, which turns after training into procedural learning. The shift from declarative to procedural control of movement is called *explicit motor learning* (Kal et al., 2016). Schneider et al. thus describe impairments in the first phase of procedural memory, before the task becomes automatic. Altogether, these studies showed an impairment of procedural learning in some animal models of HD and early in HD patients. The early expression of deficits in procedural learning makes it an interesting tool for early detection of HD. Combining the behavioral aspect of procedural learning to the activity of the underlying networks will result in a more robust early marker of the disease, thus responding to the necessity of developing reliable cognitive measures in HD.

3) Neurodegeneration in HD

a- Structure degeneration

HD is a neurodegenerative disorder and, although the mutant form of HTT is ubiquitous, the brain is the main organ to show degeneration. Post-mortem studies revealed a bilateral atrophy of the caudate and putamen (striatum), the GP and the cortex (Fig.30).

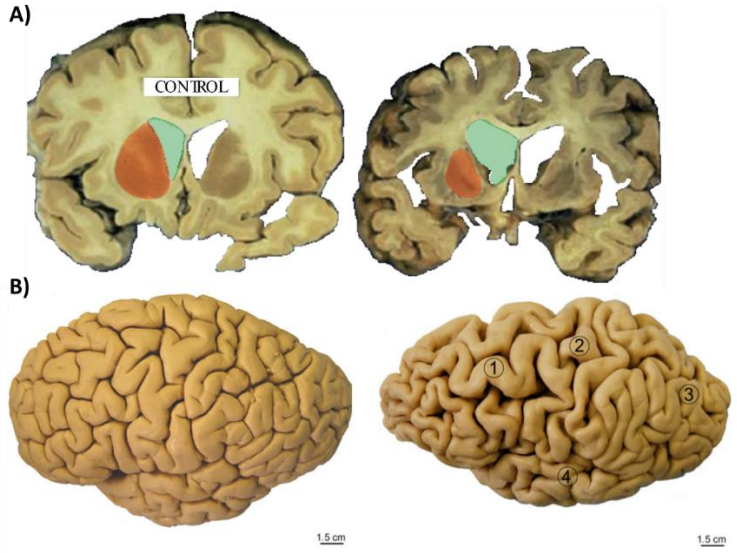

***Figure 30:* Normal vs HD brain**. *(A-B) Coronal sections (A) and cerebral hemisphere (B) of a normal (left) vs HD patient (right) brains. The basal ganglia (in red) as well as the rest of the cerebral tissue shrink in the HD condition, whereas the lateral ventricles (in green) are enlarged. There is also significant shrinkage of the cortex. 1: frontal lobe, 2: pericentral region, 3: occipital lobe, 4: temporal lobe. From (Rüb et al., 2015).*

The neuropathology of HD is based on post-mortem tissue and divides the disease into five different stages of severity (0-4). This grading system was developed by Vonsattel et al. (J. P. Vonsattel et al., 1985), which determines the stage of severity by looking at the level of degeneration in the brain (Fig.31).

- Grade 0: No gross or microscopic abnormalities related to HD
- Grade 1: No macroscopic alterations of the caudate, putamen and GP. However, on a microscopic level, a moderate fibrillary astrocytosis or astrogliosis was observed on the head of the caudate and the dorsal part of the putamen, but normal neuronal density
- Grade 2: Atrophy of the caudate (head) and the putamen (dorsal part) observed on a macroscopic level, and neuronal loss on a microscopic level. Lateral ventricle slightly enlarged.
- Grade 3: shrinkage of the caudate, putamen and GP with severe fibrillary astrocytosis in the GP
- Grade 4: severe atrophy of the caudate, putamen (up to 95% neuronal loss) and GP, smaller size of the nucleus accumbens, enlargement of the lateral ventricles

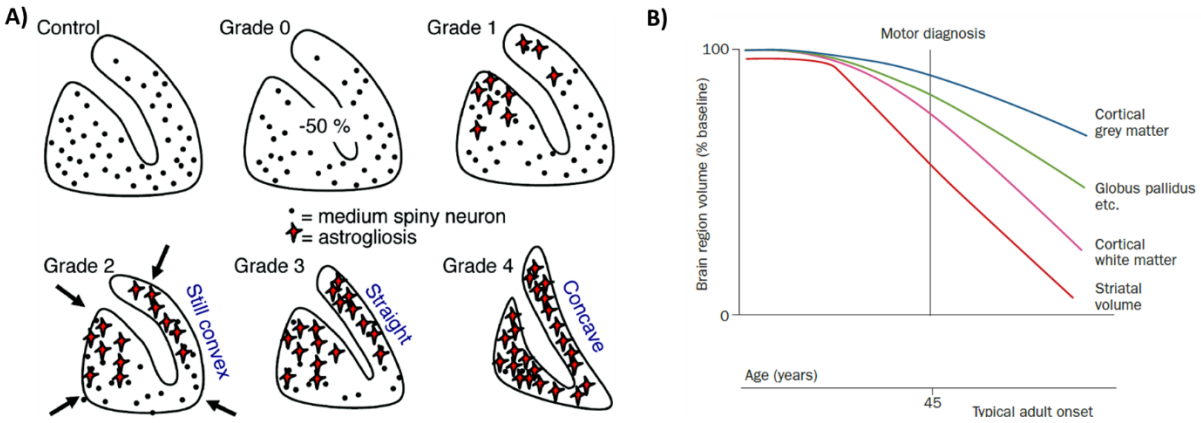

***Figure 31**: **Levels of severity of HD and affected structures**. **A**) Level of severity of HD and level of degeneration. Schematic showing the level of degeneration of the striatum in HD relative to the grade of severity (grades 0-4). Grade 0: no macroscopic changes; Grade 1: moderate astrogliosis affecting the head of the caudate nucleus and dorsal part of the putamen; Grade 2: atrophy at the head of the caudate that kept its convex shape, and the dorsal part of the putamen, astrogliosis; Grade 3: shrinkage of the caudate and putamen, with a loss of convexity of the caudate; Grade 4: the putamen and caudate are reduced to thin concave strips. Adapted from (Duyckaerts et al., 2014). **B**) Brain region volume decrease in HD in function of age. Degeneration occurs long before motor symptom onset. The striatum and cortical white matter are the fastest to degenerate followed by GP and cortical grey matter. Degeneration onset is marked by a dotted line. Adapted from (Ross et al., 2014).*

MRI studies allowed an *in vivo* quantification of the reduction volume at the intermediate stage of the disease: the volume of the putamen is reduced by 50-54% in HD patients, and the caudate by 28% (Harris et al., 1992, 1996). It was later shown that the atrophy and degeneration occur before the first symptoms of the disease appear, between 9 and 11 years before motor symptom onset (Aylward et al., 2004) (Fig.31).

As seen on Fig.29, several structures are affected by the degeneration during HD and this degeneration occurs in dorsomedial to ventrolateral direction (Reiner & Deng, 2018). Indeed, there is a generalized atrophy of the brain that can reduce brain size by up to 40% (Gil & Rego, 2008). The loss of neurons in the striatum is regarded as a hallmark of HD, and I will detail that in the following paragraph. But in addition, the cortex also suffers from neuronal loss during HD but at a slower pace than the striatum. The thinning and degeneration of the cortex affects all cerebral lobes and occurs mostly in pyramidal neurons from layers III, V and VI over grades 2 to 4 (Reiner & Deng, 2018; Waldvogel et al., 2014). Cortical degeneration occurs as mentioned earlier in the different lobes, however, it is localized in the following areas: visual are in the occipital lobe, primary somatosensory cortex, anterior cingulate cortex, posterior cingulate cortex, primary auditory cortex and insula and parahippocampal gyrus (Waldvogel et al., 2014). MRI studies have shown that the cortical volume is significantly reduced in HD patients even before motor symptoms occur (Rosas et al., 2006).

Other brain structures are affected by this neurodegeneration: GP, SNr and SNc, STN (Guo et al., 2012), select nuclei of the thalamus (motor ventrolateral nucleus, centromedian-parafascicular complex and mediodorsal nucleus), hypothalamus, hippocampus (reduction of volume in early patients (J. P. G. Vonsattel & DiFiglia, 1998), neuronal loss in the granule cell layer of the dentate gyrus and CA1, CA3 and CA4), the cerebellum and nuclei from the brainstem (Waldvogel et al., 2014), but we will not discuss them any further.

b- Cellular degeneration

Indeed, the striatum suffers from a dramatic neuronal loss mainly caused by the death of MSNs, the striatal output neurons. The loss of MSNs in the putamen of HD patients is significantly correlated to the observed motor impairments and to the increasing grade of severity (Guo et al., 2012). But the loss of MSNs does not seem to be correlated to the observed chorea (Guo et al., 2012). Both types of MSNs are affected. However, the iMSNs are more vulnerable than the dMSNs (Waldvogel et al., 2014). Thus, the inhibitory effect of the iMSNs is lifted, which would explain the motor impairments at the first symptomatic phase of HD. The subsequent loss of the dMSNs will account for the rigid ataxia towards the late phases of the disease. Amongst the dMSNs, one type of MSNs projecting to the SNr are more affected than the ones projecting to the GPi and SNc (Raymond et al., 2011). Although the reason of this difference is unknown, it could be explained by the progression of the disease on a dorsomedial axis first and then ventrolateral, the medial localization of dMSNs projecting to the SNr and lateral localization of dMSNs projecting to the GPi (Reiner & Deng, 2018).

The disparity in the vulnerability of dMSNs and iMSNs to HD could be explained by the higher probability of release of glutamate onto the iMSNs (Kreitzer & Malenka, 2009). Indeed, one of the hypotheses explaining the selective vulnerability of MSNs compared to other striatal neurons is excitotoxicity. Striatal neurons in general receive glutamatergic inputs from the cortex, but the MSNs receive more excitatory inputs making them more prone to excitotoxicity (Gil & Rego, 2008; Kreitzer & Malenka, 2009). Moreover, the types of expressed glutamate receptors should be taken into account. Most MSNs express high levels of NMDA receptors with the subunit NR2B (GluN2B), whereas unaffected interneurons express these receptors much less (Cepeda et al., 2007; Gil & Rego, 2008). An overactivation of NMDARs induces a higher calcium permeability and a slower deactivation, which increases the levels of intracellular calcium leading to the death of the cells by excitotoxicity. This mechanism was

shown using neuronal cultures and by crossing HD mouse models with mice overexpressing this subunit of the NMDARs (Sepers & Raymond, 2014). Interestingly, the iMSNs seem to express GluN2B at higher levels than dMSNs (Jocoy et al., 2011), making them more vulnerable to excitotoxicity. We presented here one of the theories that could explain neurodegeneration: excitotoxicity. But there are several others: Neuronal aggregates (mutant HTT would form aggregates inside the cell and accumulate which could lead to an impairment in several pathways), transcriptional dysregulation, mitochondrial dysfunction, alterations in axonal transport (Ajitkumar & De Jesus, 2020).

In addition to the MSNs, there are interneurons in the striatum which efficiently modulate the activity of striatal MSNs. It is therefore natural to wonder if the loss of their outputs to MSNs would contribute to the disease. Most of GABAergic interneurons and cholinergic interneurons seem to be intact in HD, even in the severe cases (Cicchetti et al., 2000; Waldvogel et al., 2014), however changes in their functionality and connectivity have been described (Reiner & Deng, 2018). Although calretinin interneurons were shown to be affected in HD (Petryszyn et al., 2018), one type of GABAergic interneurons has been the most described to be affected in HD, the parvalbumin-expressing interneurons. The loss of PV interneurons has been described in post-mortem HD brains at around 26% in the caudate and 20% in the putamen (Deng et al., 2013). Although loss of PV interneurons is not observed in HD mouse models (Reiner & Deng, 2018), a recent study using a transgenic non-human primate model of HD, confirms the loss of this type of interneurons and the progressive loss of neurons based on their subtype (Lallani et al., 2019). A loss of PV interneurons in the striatum raises the possibility of their implication in the motor impairments observed in HD. Interestingly, in a recent study, PV interneurons have been shown to exert a more powerful inhibition on dMSNs than iMSNs (Gittis et al., 2010). Since PV interneurons are not affected in the early stages of HD, the later degeneration of dMSNs could also be explained by a lack of inhibition of dMSNs and an imbalance of striatal outputs.

To summarize, the studies presented in this paragraph show that neurodegeneration occurs mostly in the striatum and specifically in the iMSNs first then the dMSNs, but other structures are affected afterwards. Notably, dysfunctions in the striatum and the cortex occur before degeneration.

4) Mouse models of HD

In order to study HD and to understand the mechanisms behind the disease, scientists turned to animal models. Before creating genetic models of the disease, lesions with neurotoxins were made in the striatum to mimic the observed striatal degeneration, for example kainate (a glutamate receptor agonist) to induce this lesion (Coyle & Schwarcz, 1976). After the discovery of the HTT gene in 1993, genetic models of the disease were developed to mimic appropriately the pathology.

There are three types of genetic rodent models of HD: truncated, full-length and knock-in models.

- Two truncated models of HD exist currently, and they both belong to the R6 mouse line: R6/1 and R6/2. The R6 mouse line, developed in 1996, contains around 1 kb of the 5' UTR, exon 1 with around 130 units and the first 262 base pairs of intron 1 of human HTT, with a human promoter (Mangiarini et al., 1996). The R6/1 mouse line has around 115 CAG repeats in exon 1, is characterized by a late age of onset and slow disease progression. These mice live for around 9 months, exhibit symptoms around 4.5 months of age. The R6/2 mouse line has around 150 CAG repeats and are characterized by a very early disease onset and a rapid progression of the disease. Their lifespan is very short (13-18 weeks) and they exhibit symptoms around 4-5 weeks of age (Mangiarini et al., 1996). Another truncated model of HD is the N171-82Q transgenic mouse model. This model expresses the first 171 amino-acids of HTT with 82 CAG repeats. These mice display abnormal motor behavior around 3 months of age (Schilling et al., 1999).
- The full length models of HD express the mutant HTT gene in full under a murine promoter. Two types of full-length models were generated: the BAC (bacterial artificial chromosome) and YAC (yeast artificial chromosome) mouse lines. YAC46, YAC72 and YAC128 are the most widely used. This model is characterized by a slow disease progression. The abnormal behavior is more severe and appears earlier when the number of repeats is more important (Cepeda et al., 2010; Rangel-Barajas & Rebec, 2018). The BAC model has around 97 CAG repeats with progressive late motor onset and cortico-striatal dysfunction (Cepeda et al., 2010; Rangel-Barajas & Rebec, 2018).
- Knock-in mouse models have the advantage of expressing mutant HTT in an endogenous form. Indeed, transgenic models with an exogenous promoter can

overexpress the gene in question. Murine exon 1 is replaced by human exon 1 with the CAG repeats (the physiological number of CAG repeats being 7) under an endogenous promoter. Thus, the human form of the disease can be reproduced with genetic mutation with high fidelity. Several knock-in mouse models of HD have been generated. The name of each model corresponds to 'Q' followed by the number of CAG repeats (from 48 to 400). Although at first these mice showed late onset of symptoms that were very mild, a detailed behavioral phenotype was later developed (Menalled et al., 2012). The mouse model we used in our project is the Q140 (or Hdh^{Q140}) mouse model, which displays a mild behavioral phenotype resembling the presymptomatic stage of HD (Hickey et al., 2008; Menalled et al., 2003).

When dysfunctions occur in the BG, motor disorders can occur, such as HD, a neurodegenerative disorder affecting the corticostriatal networks. It is characterized by a triad of symptoms: motor, psychiatric and cognitive. HD is caused by a mutation in a protein called huntingtin.

Degeneration of striatal neurons is a hallmark of HD. This degeneration starts before symptoms occur. What is particularly interesting is that there are dysfunctions in the striatal and corticostriatal networks that occur before this degeneration.

Several models of the disease were created in the past 30 years. In my project I will use the Hdh^{Q140} mouse model that will allow me to study the presymptomatic phase of the disease.

In this chapter, I described the role of the BG in motor control. In the next part, I describe how their involvement in motor control allows them to play an important role in procedural learning. I will also focus on the corticostriatal networks during learning.

Dans cette partie j'ai présenté des dysfonctionnements au niveau des ganglions de la base qui sont à la base de nombreux désordres moteurs. C'est le cas de la maladie de Huntington, une maladie neurodégénérative, caractérisée par une triade de symptômes : moteur, psychiatrique et cognitif. La maladie de Huntington est causée par une mutation d'une protéine, la huntingtine qui entraîne une augmentation du nombre de répétition de CAG. Cette répétition trop importante entraîne le déclenchement de la maladie, le développement de symptômes et une dégénérescence des neurones striataux, avant même l'apparition des symptômes moteurs. Il est à noter qu'un dysfonctionnement des réseaux striataux et cortico-striataux a lieu bien avant la dégénérescence.

Afin de mieux comprendre les mécanismes de mise en place de cette maladie et les dysfonctionnements qui ont lieu, plusieurs modèles de souris ont été développés pendant les 30 dernières années. Je m'intéresse dans mon travail à un modèle murin, les souris knock-in Hdh^{Q140} qui me permettront d'étudier les altérations des réseaux corticostriataux dans la phase présymptomatique de la maladie.

B) Dysfunction of cortico-striatal networks

HD is a neurodegenerative disorder characterized by impairments in motor control and a massive neuronal degeneration in the striatum and later in the cortex, two extensively connected structures (see chapter III).

Within the striatum, MSNs are the most vulnerable cells in the striatum: first iMSNs are affected in early HD, and then dMSNs in late HD (Fig.32).

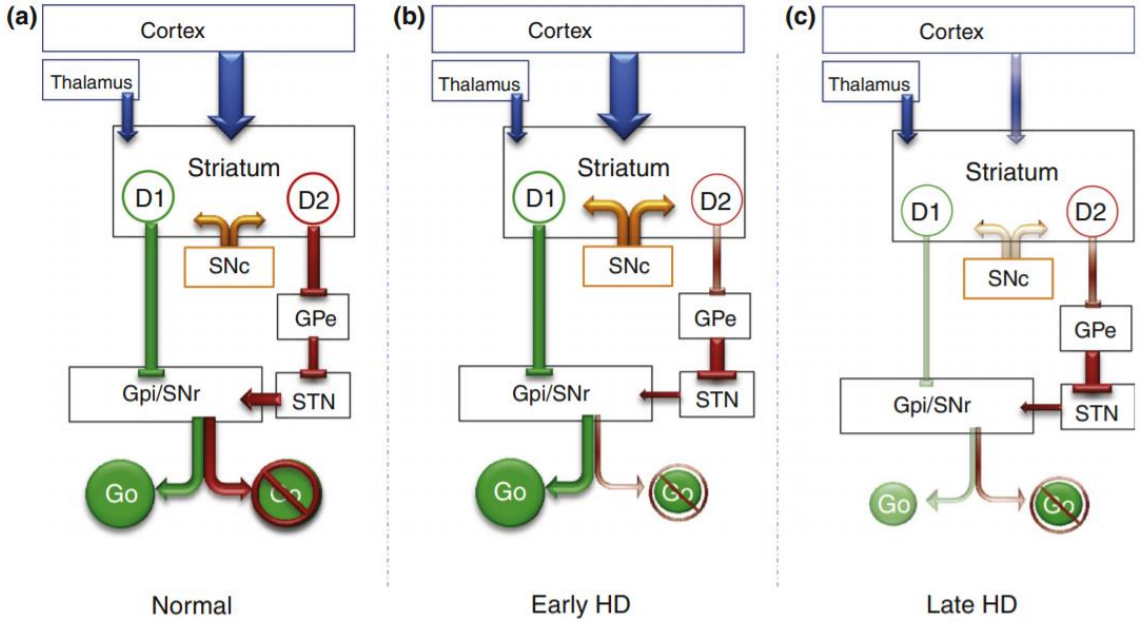

Figure 32: *Corticostriatal circuit in normal and HD conditions.* ***a****) Normal functioning of direct and indirect pathways. The direct pathway leads to a go signal and the indirect to a no-go signal.* ***b****) Early HD: a higher level of glutamate release from cortical inputs affects iMSNs (D2), thus affecting the indirect pathway and the following responses.* ***c****) Late HD: loss of cortical inputs, affecting dMSNs (D1) and thus the direct pathway. SNc is also affected. From (Sepers & Raymond, 2014).*

The cortex is composed of 80% of pyramidal glutamatergic neurons and 20% of GABAergic interneurons. Pyramidal neurons from layer III and V project to the striatum and layer VI to the thalamus (Huang, 2014). In the case of the cortex, pyramidal neurons are the most vulnerable. This degeneration occurs before the symptoms appear (see chapter III). Due to the vulnerability of both structures, the striatum and the cortex, it was proposed that HD is

caused by a dysfunction of the cortico-basal ganglia system and more specifically the cortico-striatal circuits. It was reported that 30% of pyramidal neurons from layer III, V and VI are lost in post-mortem tissue of HD patients (Bunner & Rebec, 2016). The loss of pyramidal neurons as well as dysfunctions in their firing properties could potentially underlie HD phenotypes. Dysfunctions in corticostriatal connections occur in two phases: increased glutamate release and MSN hyperexcitation in presymptomatic HD, and MSN silencing once the symptoms appear (Blumenstock & Dudanova, 2020; Cepeda et al., 2003). This elevated cortical activity in early HD leads to an increased glutamatergic release, activating extrasynaptic NMDA receptors constantly, which would lead to apoptosis of striatal neurons. The second phase where MSN silencing is observed could be due to the loss of cortical inputs. Indeed, a decrease of corticostriatal synaptic terminals has been described in symptomatic animals (Deng et al., 2013; Rebec, 2018). *In vivo* electrophysiological recordings in freely moving mice show altered synchrony between cortical and striatal networks in HD (Lee Hong & Rebec, 2012; Naze et al., 2018). In order to understand how dysfunctions in the cortex affect firing patterns in the striatum, studies are turning to *in vivo* imaging and using calcium imaging techniques in the cortex with multielectrode recordings in the dorsal striatum (Peters et al., 2019). These advances in imaging techniques paved the way for other calcium imaging studies in mouse models of HD. These studies showed an increased frequency of calcium transients in premanifest HD and at motor onset (Arnoux et al., 2018; Burgold et al., 2019; Donzis et al., 2020). These results concord with previous electrophysiological studies, showing that pyramidal neurons fire at a higher rate. Thus, results from *in vivo* studies in behaving animals show altered dynamics in cortical networks during the different stages of the disease. An *in vivo* longitudinal study of R6/2 mice showed that neurons in the primary motor cortex become more active before motor onset and remain high throughout disease progression (Burgold et al., 2019).

Even though the corticostriatal circuits and their communication have been extensively studied, they all rely on electrophysiological recordings in the striatum and the cortex. Calcium imaging studies that I mentioned were all done in the cortex. One of the studies mentioned in the previous paragraph recorded both structures, by recording calcium activity in the cortex and electrical activity in the striatum (Peters et al., 2019). By recording the activity in the sensorimotor striatum and the associated cortex, this study showed that striatal activity reflects cortical activity reliably. In the case of HD and animal models of HD, no such work has been done to my knowledge. Based on this study by Peters et al. and other studies in HD

recording cortical activity, we cannot conclude about the effects on dynamics of striatal activity *ex vivo* or *in vivo*. Indeed, in HD the corticostriatal connections are affected. Thus we can expect that striatal activity will not reflect cortical activity reliably. It is thus necessary to explore and record activity of individual striatal neurons which will enable us to understand precise alterations of the corticostriatal networks. In addition, since attention is towards the early cognitive symptoms in HD, understanding how corticostriatal networks function is extremely important because of their involvement in cognitive functions such as procedural learning.

Dans cette dernière partie j'ai présenté les dysfonctionnements qui sont observés dans le cas de la maladie de Huntington au niveau du cortex et du striatum. Ces dysfonctionnements, apparaissant avant toute apparition de symptômes moteurs et avant toute dégénérescence, pourraient être à la base des phénotypes observés dans la maladie de HD. Grâce à la technique d'imagerie calcique, des études récentes ont permis de montrer les dysfonctionnements au niveau du cortex in vivo. Il serait intéressant d'étudier la dynamique des réseaux corticostriataux en ayant une vue de l'activité de la population de neurones dans le striatum cette fois. Ceci nous permettra de mieux comprendre comment l'altération au niveau du cortex pourrait affecter l'activité individuelle au niveau du striatum.

Part II: Methods

In this part, I will describe the different techniques I used during my PhD and explain the principle of each technique and why it was used. The details of the methods (concentrations, volumes etc.) are detailed in the Materials and Methods sections of the articles in the Results part.

I- Experimental models

Animals used during my PhD were either C57Bl6J (for studies 1 and 2, see Part III: Results) or heterozygous Hdh^{Q140} mice with a C57Bl6J background (for study 3). Mice were between 1.5 and 4 months old and of both sexes. Animals were housed in a temperature-controlled room with 12 hours light/dark cycle and with food and water *ad libitum*.

II- Stereotaxic injections

I used stereotaxic injections to deliver either Adeno-associated viruses (AAVs of serotype 5 and 8) or tracers for anatomical studies such as CTB (Cholera Toxin B). Coordinates of the injection sites were based on the Franklin and Paxinos atlas (Franklin & Paxinos, 2008). Mice were anesthetized with isoflurane and placed in a stereotaxic frame (Kopf). Once the head was immobilized, the skull was exposed and the Bregma localized. The Bregma (intersection point of the coronal and sagittal sutures) was considered as the origin of an XYZ axis (Fig.33). Once the coordinate site was determined on the skull, a craniotomy was made with an electric drill at that spot. Then AAVs or CTB were injected through a pulled glass pipette using a nanoinjector. The pipette is lowered into the brain until reaching the wanted coordinate. After injection, the pipette is left in its place for a few minutes to avoid leakage in the cortex on the way out of the brain. Once the pipette pulled out, the incision is closed. Animals are placed on a heating pad and monitored for 1h before they were returned to their home cage. They were then monitored daily during the next 4-5 days.

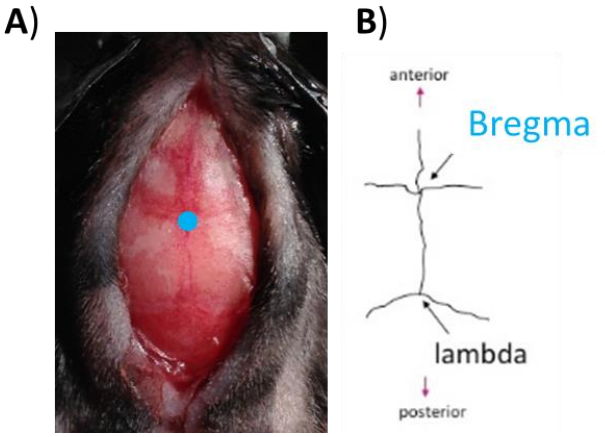

Figure 33:* Stereotaxic surgery**. ***A*) Exposed mouse skull. Blue dot represents the Bregma.* ***B****) Drawing of brain sutures. Intersection of the coronal and sagittal sutures: Bregma. And intersection of the sagittal and lambdoid sutures: Lambda. Adapted from* (Shimizu & Fukada, 2017).

III- Behavioral experiments

For all behavior experiments, mice were acclimated to the room and subjected to handling before the beginning of the experiment.

A) Accelerated rotarod

The accelerated rotarod is a behavioral paradigm used to study motor skill learning. Animals are placed on a rotating wheel with an increasing speed. Animals will have to adapt to the increase of speed, thus learning the task.

The rotation of the rod increased from 4 to 40 rotations per min over 300 sec. Each trial was ended when the animal fell or when 300 s elapsed. Animals were trained with 10 trials per day for either one day (early training) or 7 days every day (late training) (Fig.34).

In order to assess learning, we calculated a learning index which corresponds in early training to the difference between the first two trials and last two trials of the day ($T_{9,10} – T_{1,2}$), and in late training to the difference between day 7 and the first two trials of day 1 ($D7 – T_{1,2}$).

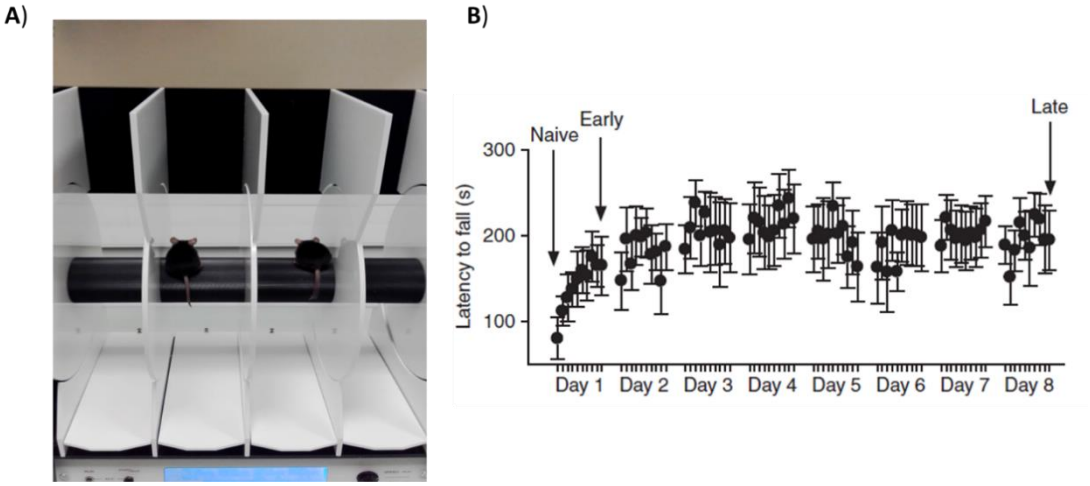

***Figure 34:* Rotarod and learning curve**. ***A**) Rotarod apparatus. Two mice are placed in different lanes on a rotating rod. **B**) Learning curve of animals during an accelerated rotarod task, at the beginning (naïve), after one day of training (early) and after 8 days of training (late). From* (H. H. Yin et al., 2009).

B) Fixed-speed rotarod

Here, the same apparatus as the accelerated rotarod was used. However, the rod rotates at a constant speed. This paradigm was used to test motor coordination in animals. Animals were placed on the rotating wheel and their latency to fall was measured. Low and high rotation speeds were tested, with 5 trials per speed separated by a 300 s resting period. When speeds were changed, a 600 s resting period was given to mice. This test was only used in study 3.

C) Open-field

The open-field test was performed to test locomotor activity. Mice were placed in the center of a square Plexigla open-field and their activity was recorded (Fig.35). Depending on the analyzed parameters, different aspects can be studied: the time spent in the center of the arena indicates the level of stress of the animals; the total traveled distance measures locomotor activity.

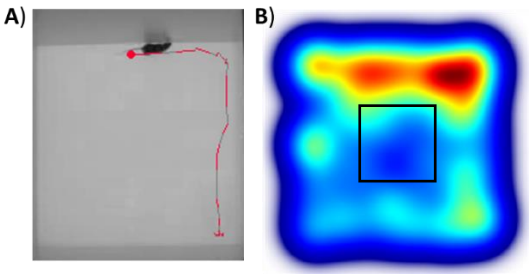

***Figure 35:* Open-field test**. ***A**) Tracking of a mouse in an open-field. **B**) Heatmap of the time spent in each area of the arena. Square representing the center of the arena.*

IV- Brain slices

In order to monitor calcium activity and perform electrophysiological studies of corticostriatal connections, in the different striatal territories, we needed brain slices preserving the corticostriatal projections of interest. This is possible with acute brain slices following a certain angle depending on the recorded territory (DMS or DLS) (Fino et al., 2018).

Mouse brain was quickly extracted after decapitation and placed in artificial cerebrospinal fluid (ACSF) at 4°C with constant bubbling with a mix of O_2/CO_2 (95% / 5%) to maintain the pH at 7.3. A vibratome (Leica VT1200S) was then used to get brain slices of 300µm. Depending on the recorded territory, slices were either sagittal (for DMS) or horizontal (for DLS) in order to keep the corticostriatal projections of interest intact (Fig.36). Slices were then transferred into a chamber at 34°C for 1 hour and then left at room temperature until the beginning of the recordings.

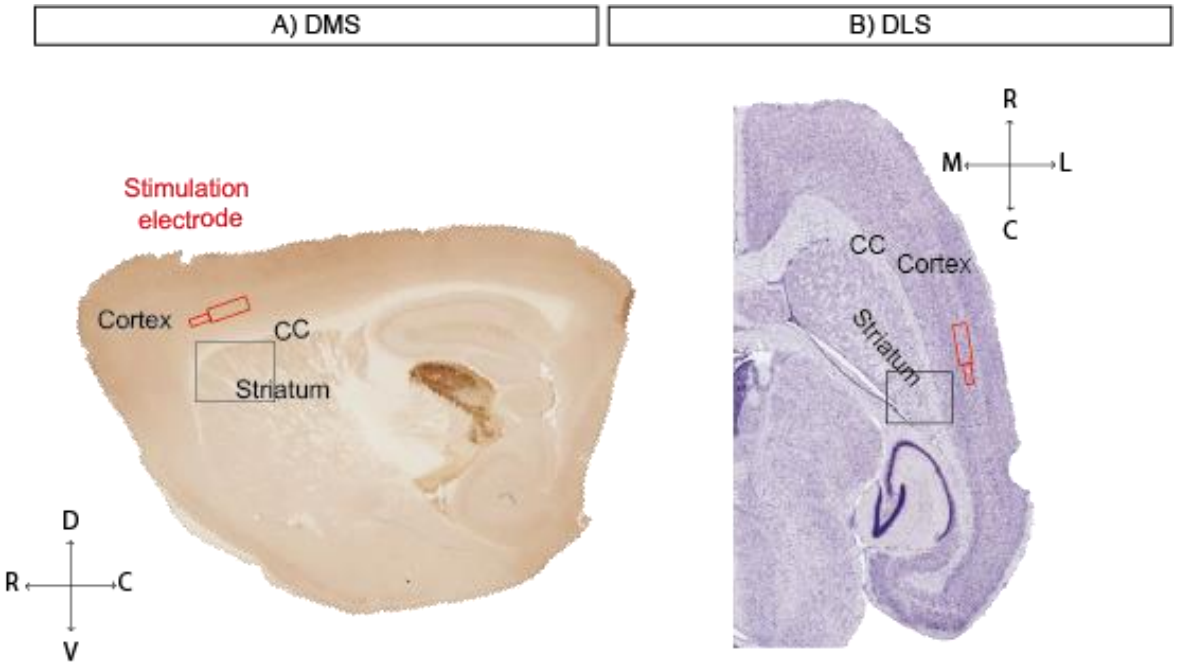

Figure 36:* Brain slices for DMS and DLS recordings**. ***A*) Sagittal mouse brain slice for recordings in the DMS. In red: stimulation electrode placed in layer V of the cortex. The rectangle represents the recording area of the striatum.* ***B****) Horizontal mouse brain slice for recordings in the DLS. CC: corpus callosum. R: rostral. C: caudal. D: dorsal. V: ventral. M: medial. L: lateral. Adapted from* (Franklin & Paxinos, 2008).

V- *Ex-vivo* two-photon imaging and mutli-patch-clamp recordings

A) Two-photon calcium imaging

Genetically-encoded calcium indicator GCaMP6f (Green fluorescent Calmodulin Protein) was used for calcium imaging of striatal cells. It was expressed in striatal cells thanks to the delivery of the AAV5-syn-GCaMP6f-WPRE-SV40 (purchased from UPennCore (PA, USA)). Two-photon imaging is performed at 940nm with a TRIMScope II system (LaVision Biotec, Germany) coupled to a Ti:Sapphire laser (Chameleon Vision II) and a 20x/1.0 water-immersion objective (Zeiss). A resonant scanner was used to allow fast acquisition (15.3 frames per second) and fluorescence was detected with a GaAsP detector (Hamamatsu H 7422-40). The frequency of the scanner and image acquisition were controlled with Imspector software (LaVision Biotec, Germany). Two-photon imaging enables us to do acquisitions between 50 and 150µm under the brain slice surface, thus avoiding dead cells on the surface. A field of acquisition was 392 µm x 392 µm.

We monitored the striatal network dynamics in response to cortical stimulations, realized in the cortex associated to the studied striatal territory (Fig.36). Slices were visualized with a 5x/0.15 objective for the placement of the stimulation electrode. The stimulation electrode delivered single cortical stimulations or trains of stimulation (5 consecutive stimulations at different frequencies).

In order to analyze these recordings, regions of interest (ROI) were drawn manually around each cell using the FIJI software. Then the mean grey value and the coordinates of each ROI were extracted. ΔF/F is obtained using $y(t) = (x(t) - x0) / x0$, where x0 is the mean value of the 50 % lowest values in the last 10 s. Recordings lasted around 1 min with an average of stimulations. Five of the seven responses were averaged as a mean effect per cell. A threshold to consider cells active was defined as Mean ± 2*SD (Fig.37).

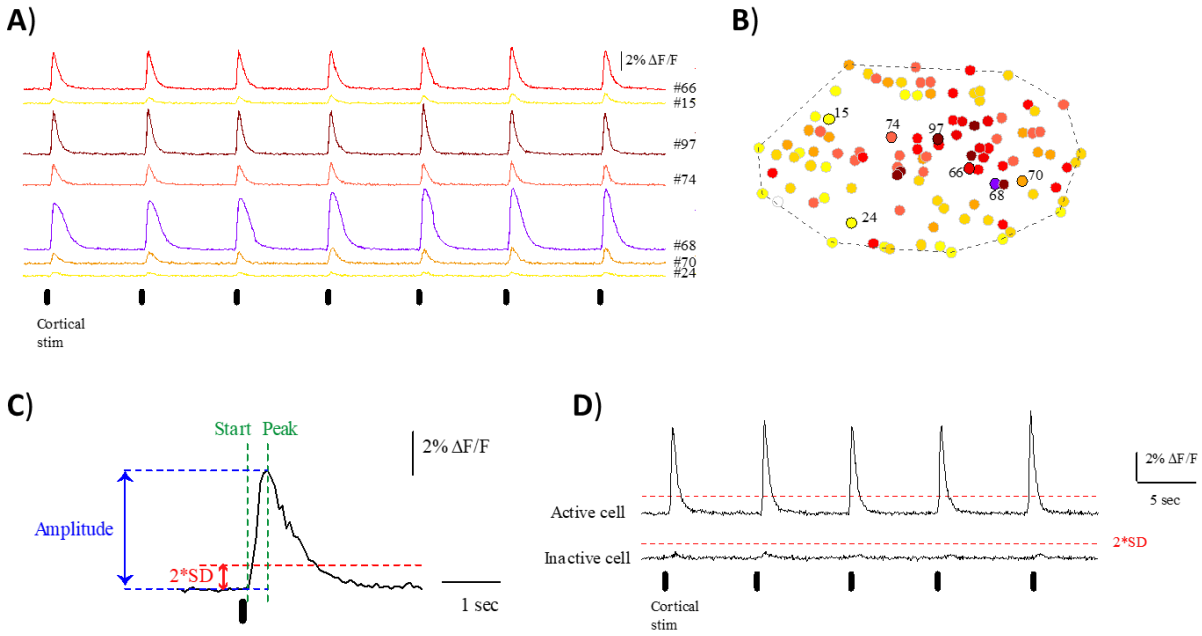

Figure 37:* Calcium imaging analysis**. ***A*) Representative calcium signals extracted for several cells.* ***B****) Functional map. Color code corresponds to the level of response. Calcium signals of cells from the map are represented in A.* ***C****) Analysis of a calcium signal: measure of amplitude of response in blue, definition of a threshold of response (2*SD) in red, start and peak of signal in green. Black lines: cortical stimulation.*

From these signals, functional maps representing the spatial organization of the cells with their level of activity were created (Fig. 37). We compared different parameters of calcium activity between the different training conditions. These parameters included the average amplitude of responses from all cells, the percentage, spatial and temporal organization of the most active cells in the fields. Extracting highly active cells relied on two methods: (1) a thresholding using the average of the mean amplitude in naive animals to normalize the activity throughout the training conditions or (2) a k-means analysis to perform amplitude clustering, each animal being considered independently. Thus, we extracted both the percentage of highly active cells and the clusters of high activity.

B) Whole cell patch-clamp recordings

Patch-clamp recordings were performed on the brain slices described in the previous paragraph. Recordings targeted MSNs, identified from their morphology and/or membrane properties (Tepper et al., 2010). A borosilicate glass pipette (pulled to have a resistance between 5 and 8 MΩ) filled with intracellular solution (containing in mM: 127 K-gluconate, 13 KCl, 10 HEPES, 10 phosphocreatine, 4 ATP-Mg, 0.3 GTP-Na, 0.3 EGTA (adjusted to pH 7.35 with

KOH)) was used for whole-cell patch-clamp recordings. Cells with a high access resistance were not considered for analysis.

The goal of patch-clamp recordings was to compare the intrinsic properties of MSNs and their cortical input integration properties to determine possible mechanisms of the networks reorganization. Concerning intrinsic electrophysiological properties, input resistance was measured by repeated current injections and frequency was measured for current steps +30 pA above AP threshold. Rheobase corresponds to the injected current necessary to reach AP threshold. AP threshold corresponds to the membrane potential right before the start of the spike (measured at the base of the spike). RMP was measured as the mean membrane potential without any injected current. For the cortical input integration, spiking probability was measured as the occurrence of a single action potential induced by a single cortical electrical stimulation, with a stimulation intensity giving around 50% spikes. MSNs were held at their holding membrane potential (around -78 mV). Spiking probability was measured by doing an input/output curve in response to a single cortical stimulation with increasing stimulation intensity. We also measured input/output curve of subthreshold EPSPs by measuring the amplitude of EPSPs with increasing stimulation intensity. We assessed short-term temporal dynamics of cortically-evoked EPSPs with trains of stimulation. We measured short-term temporal summation by measuring the total amplitude of each EPSP (from baseline to the peak of the response) and normalize it to the amplitude of the first EPSP. In a subset of experiments combining different frequencies, the normalized amplitude corresponded to the ratio between the fourth EPSP of the train compared to the first one (Fig.38). We compared the effect for each EPSP of the train and the fourth one was chosen as a representative. Data analysis was carried out in Fitmaster (HEKA Elektronik, Germany).

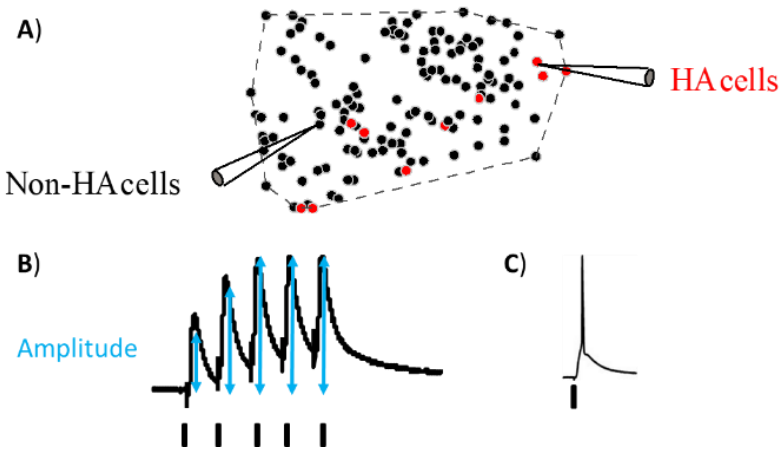

Figure 38:* Electrophysiological recordings and analysis**. ***A*) Patch-clamp protocol of HA and non-HA cells.* ***B****) Measurement of the amplitude of each EPSP after cortical stimulation (train).* ***C****) Single action potential after a single stimulation for the measurement of spiking probability. Black rectangle: cortical electrical stimulation.*

VI- Retrograde tracing with Cholera Toxin B (CTB)

In order to determine if the reorganization of the networks was due to anatomical modifications, such as a change in the number of cortical neurons projecting to the striatum. For this purpose I used a retrograde tracer, the Cholera toxin B (CTB) (Saleeba et al., 2019). The CTB enters in the neurons at the injection site. In my case, CTB was injected in the different striatal territories one day after training. CTB goes in striatal cells and is picked up by cortical projections until reaching the soma of cortical pyramidal cells. CTB is a static tracer, and thus will not jump synapses and pass from one neuron to the other.

Following the expression of CTB, animals were perfused, brains collected and sliced. Based on the acquired images, cortical cells that expressed CTB were counted in the different cortical layers. Density of neurons was normalized to the area of counting in the cortex (Fig.39).

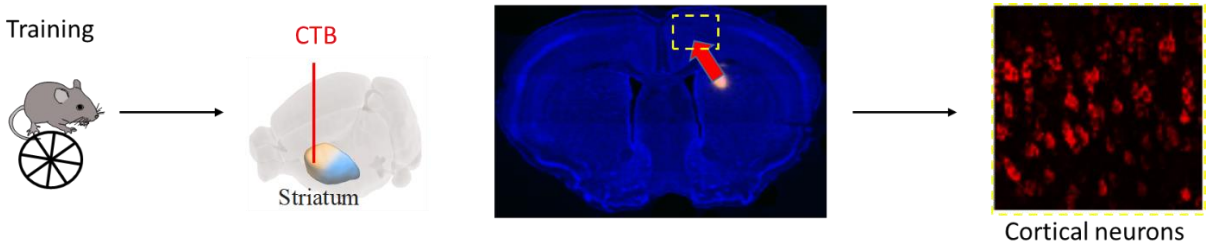

***Figure 39:* Retrograde tracing with CTB**. *After training, CTB is injected in the striatum. CTB goes into striatal neurons and cortical neurons that are projecting to the striatum. The number of labeled cortical cells is then counted in the cortex of interest.*

VII- cFos-TRAP experiments

I used a cFos TRAP strategy (Giannotti et al., 2019) to label and manipulate a subset of cells that were highly active. This strategy provides a cell- and time-specificity of gene of interest expression. The AAV used in this case contains a c-fos promoter (AAV8-cFos-ERT2-Cre-ERT2-PEST-no WPRE from Stanford Gene Vector and Virus Core (CA, USA)). This construct allowed me to specifically express the Cre recombinase in a subset of striatal neurons highly activated and with a high cFos expression. The presence of the Cre recombinase allows for the expression of a sequence with loxP sites on both ends (Fig. 40). The ERT2 part provides a time specificity of the expression of the gene since it will rely on the presence of 4-hydroxytamoxifen (4-OHT). I could therefore induce the expression of the gene right after the training of the animals to label highly active cells related to learning.

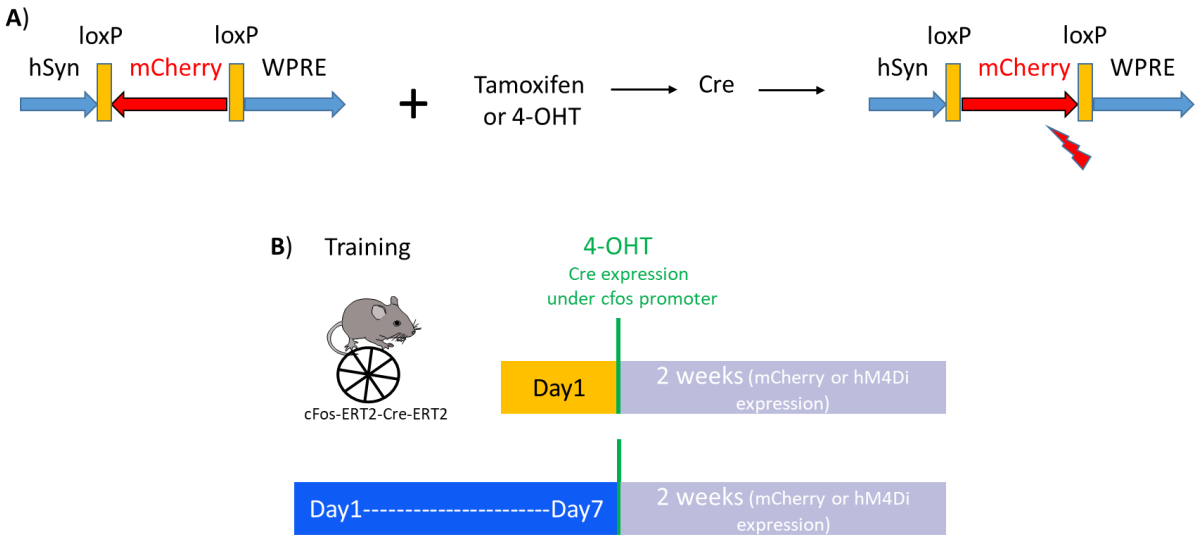

Figure 40:* Cre-lox system**. ***A*) The mCherry sequence is first inverted and cannot be expressed. In the presence of a Cre recombinase, the loxP sites are recognized, the mCherry sequence is inverted and can be expressed after the human synapsin promoter (hSyn) and label neurons.* ***B****) Experimental design for the cFos-TRAP experiments. Mice injected with the c-fos-ERT2-Cre-ERT2 virus are trained (for 1 or 7 days). At the end of training, an i.p. injection of 4-OHT is realized thus allowing the expression of Cre in cells expressing high levels of cfos. During the following 2 weeks, floxed AAVs are expressed.*

VIII- Chemogenetics experiments

I performed chemogenetics experiments using the DREADD system (Sharma & Pienaar, 2018) to manipulate the activity of MSNs during learning. For this I used AAV5-hSyn-DIO-hM4D(Gi)-mCherry, which expresses a modified inhibitory muscarinic receptor, which will be activated only in the presence of its ligand the CNO (clozapine-N-Oxide), with no effect by the endogenous ligand (Fig.41). I injected CNO intra-peritoneally. The control experiment consists in the expression of AAV5-hSyn-DIO-mCherry, which will not carry the hM4Di but only the fluorescent reporter mCherry. Thanks to the cFos strategy, I expressed hM4D(Gi)-mCherry or mCherry in highly active cells in DMS and DLS. I injected the CNO right before the training session to inhibit the highly active cells and evaluate the consequences on the performance of the animals.

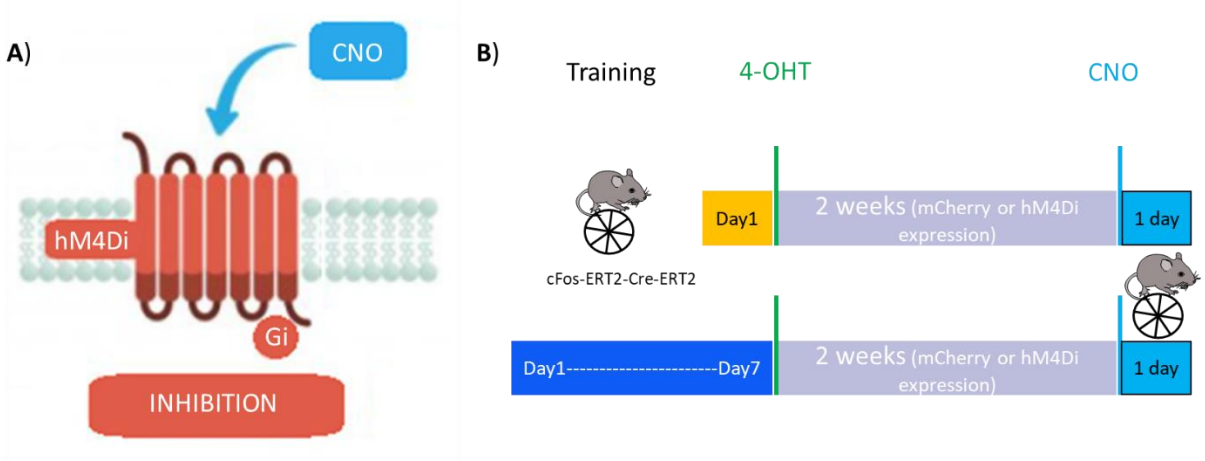

***Figure 41:* DREADD system**. ***A**) hM4Di is a modified muscarinic receptor which is activated by its ligand CNO. Since hM4Di is coupled to a Gi protein, activation of the receptor by CNO induces an inhibition. Adapted from* (Ju, 2018). ***B**) Experimental paradigm. Training followed by 4-OHT i.p. injections induces the expression of Cre in cfos positive cells. Thus a recombination of the floxed AAVs is possible: mCherry or hM4Di are expressed in cfos positive cells. Injection of CNO will inhibit cells expressing hM4Di but not ones expressing mCherry. Performance of animals is then tested on the accelerated rotarod.*

Part III: Results

I- Objectives

Procedural memory is formed thanks to the large contribution of the BG and the functional loops this group of structures forms with the cortex and thalamus. The networks formed by these different structures and the role they play in the formation of procedural memory has a long history. The striatum is at the center of these networks and has long been described as a focal point for the formation of this memory. Many studies were interested in the activity of the striatum and the structures that project to the striatum in the context of procedural learning. These studies showed the functional separation of the striatum into two territories (DMS and DLS) and the specificity of each of these territories to the different phases of learning (H. H. Yin et al., 2004; H. H. Yin, Ostlund, et al., 2005). More recent studies took advantage of the technical advances allowing them to directly correlate behavior to neuronal activity, thus opening the door for a more specific study of the networks and their dynamics. Indeed, it has been shown that the activity of the DMS increases in the early phases of learning and decreases in the late phase, whereas the activity in the DLS increases in the late phase of learning. Thus, the implication of both striatal territories in the different phases of learning were well described. However, the precise dynamics within corticostriatal networks allowing the encoding of procedural memory were unknown. In addition, the deficits in procedural memory in HD animal models was debated, and the dysfunctions of DMS and DLS networks in the pre-symptomatic phase of the disease were not described.

These questions form the two main objectives of my PhD work:

> **1/ Correlation between behavior and neuronal activity in each striatal territory have been described. Nevertheless, the cellular mechanisms responsible for procedural memory formation were unknown. We thus explored whether there could be neuronal substrates allowing for a long-term storage of this memory in a specific group of neurons.**

To answer this question, I studied how the network activity in DMS and DLS evolved during the different stages of motor skill learning. I trained animals to a procedural task. I then used two-photon calcium imaging in naïve and trained animals, to have an overall visualization of the striatal network activity, with single-cell resolution. I performed calcium imaging in each territory to distinguish their role in the different phases of learning. Spatial resolution and detailed analysis allowed us to determine neuronal substrates, with specific patterns in DMS

and DLS. The specific manipulation of these neurons with chemogenetics showed their direct implication in the development of motor skill learning.

These experiments correspond to the first part of the results that I will present. This first part will include a study currently in revision in which I am first author (Badreddine et al., in revision). In addition, we developed an analysis method to distinguish cell-specific calcium signals. This study is a conference paper published in 2019 in which I am second author (Becq et al., 2019).

- **2/ HD is characterized by motor, cognitive and psychiatric deficits, appearing along the disease progression. My aim here was to determine whether procedural memory was affected in a mouse model of HD and if and how the alterations of the networks can affect this learning process.**

We explored how striatal networks can be altered in HD, a neurodegenerative disorder mostly affecting the striatum. Interestingly, since the cognitive symptoms appear before the motor symptoms, we wondered whether alterations of procedural memory could be used as a pre-symptomatic indicator. I used an HD mouse model allowing to study early pre-symptomatic phase of the disease. I first characterized the DMS and DLS networks in naïve Hdh^{Q140} animals and report an alteration of the basal networks. In addition, I show that these animals have deficits in procedural memory formation, due to an absence of network reorganization upon training.

This pathological aspect of the project will be presented in the third part of the results in a study in preparation in which I am first author.

II- Study 1: Spatiotemporal reorganization of corticostriatal network dynamics encodes motor skill learning

The global dynamics of the striatal networks have previously been described allowing for a distinction of the role of each striatal territory. The aim of our study was to examine the dynamics of these networks with single-cell resolution and explore if specific neuronal substrates exist in corticostriatal networks in relation to procedural memory formation.

To form procedural memory, we used the accelerated rotarod behavioral paradigm which allows the distinction between the different phases of learning. Using two-photon calcium imaging, we studied overall neuronal activity of the different striatal territories, DMS and DLS, during the different phases of learning, and neuronal activity on a cellular level. With these recordings, we were able to extract patterns of activity specific to each territory. We explored the mechanisms responsible for the appearance of such patterns. We then used a cre-dependent method based on the expression of an immediate early gene to control these different patterns and see their effect on learning.

First I will present this first study corresponding to a paper that is currently in revision and of which I am co-first author.

Spatiotemporal reorganization of corticostriatal network dynamics encodes motor skill learning

Badreddine N*[1], Zalcman G*[1], Appaix F[1,], Becq G[2], Trembay N[2], Saudou F[1], Achard S[3] and Fino E[1#]

[1]Univ. Grenoble Alpes, INSERM U1216, CHU Grenoble Alpes, CNRS, Grenoble Institut Neurosciences, Grenoble, France

[2]Univ. Grenoble Alpes, Laboratoire Gipsa-Lab, UMR 5216 CNRS, Grenoble-INP, Grenoble, France

[3]Univ. Grenoble Alpes, Laboratoire Jean Kuntzmann, UMR 5224 CNRS, Grenoble, France

* These authors contributed equally to this work

[#]To whom correspondence should be addressed (corresponding author): Elodie Fino elodie.fino@gmail.com

Key words: striatum, motor skill learning, spatiotemporal dynamics, neural networks, plasticity.

ABSTRACT

Motor skill learning is a fundamental adaptive mechanism, characterized by an early phase of rapid improvement of the performance involving the dorsomedial striatum (DMS) and a late phase of motor skill maintenance within the dorsolateral striatum (DLS). Although the striatal sub-regions involved in these phases have been described, how neuronal substrates encode the acquisition and consolidation of motor skill learning remains unknown. Here, using *ex vivo* two-photon calcium imaging after motor skill learning, we find a spatiotemporal reorganization of corticostriatal networks that reveal the emergence of activity patterns specific to each territory at different stages of learning. During the early phase, the DMS overall activity transiently decreases, with few and sparsely distributed active hot spots remaining. In contrast, the DLS shows a gradual and long-lasting formation of clustered hot spots, stabilized long after training. We found that these two sequential phases of network reorganization arise from distinct levels of plasticity, with a transient reinforcement of synaptic connections from cingulate cortex on DMS hot spots, and long lasting anatomical rearrangements of somatosensory projections to the DLS. Using an AAV cFos-TRAP strategy coupled to chemogenetics during learning, we further demonstrate that silencing DMS and DLS hot spots strongly impairs motor learning, which highlights their sequential role in early acquisition and long-lasting retention of motor skill learning, respectively.

INTRODUCTION

Motor skill learning is a fundamental adaptive mechanism providing efficiency for common behaviors and setting cognitive resources free for other tasks. Mastering a new motor skill is a process that requires extensive practice leading to a motor command to be learned, automatized and stored, sometimes for a lifetime. This type of learning is characterized by an early phase of rapid improvement in performance that involves the exploration of a range of motor behaviors and the selection of those that yield a favorable outcome. This early phase is followed by a late and more moderate improvement of performance as the motor behavior is automatized and refined. One of the key brain structures for motor skill learning is the striatum, the main input nucleus to the basal ganglia [1,2]. The striatum is divided into several sub-regions mainly based on the existence of functional cortico-basal ganglia-thalamo-cortical loops [3,4]. These loops divide the basal ganglia into limbic, associative, sensory and motor regions, which receive inputs from different cortices. The dorsomedial striatum (DMS) receives inputs from the associative and limbic cortices and the dorsolateral striatum (DLS) receives inputs from the sensorimotor cortices.

The striatum plays a crucial role during the various phases of learning, from acquisition to automatism, with a preferential implication of DMS in the early phase and DLS in the late phase. This has been demonstrated with lesions and inactivation studies targeting either DMS or DLS [1,5-8]. Neural recordings further supported DMS and DLS involvement in the different phases of a procedural learning. Early phase of motor skill learning is associated with an increased activity in DMS [9-11], and/or enhanced synaptic inputs from frontal cortex to the DMS [12]. The late phase is associated with an enhanced activity in DLS [10,11,13]. However, these functional studies used field recordings in freely moving animals to monitor the overall

activity of striatal sub-regions, which did not allow exploring the spatiotemporal dynamics of striatal networks, with a single-cell resolution.

Here, we postulated that changes in DMS and DLS dynamics during learning might reveal specific neuronal substrates selectively encoding acquisition and consolidation at single cell level. Using *ex vivo* two-photon calcium imaging at different stages of motor learning (naive, early training and late training), we observed a strong and selective reorganization of striatal networks between DMS and DLS. In DMS the overall activity of striatal projection neurons (SPNs) transiently decreased during the early phase of training while few sparsely distributed neurons were highly active. In contrast, the DLS displayed progressive and long-lasting formation of spatially restricted clusters of highly active SPNs. We found that highly active cells in DMS were associated with an increase in synaptic weight from cingulate cortex inputs after early training. In contrast, clusters in the DLS were associated to anatomical rearrangements of somatosensory inputs after late training. Interestingly, the number of highly active SPNs emerging from the reorganization of DMS and DLS networks were correlated with the learning performance of the animal; we thus named these cells "learning-related activity", or LRA cells. Using an AAV cFos-TRAP strategy coupled to chemogenetics during learning, we showed that silencing the LRA cells in DMS during the early phase, or in DLS during the late phase, is sufficient to impair motor skill learning. These results demonstrate that selective reorganizations operate at the single cell level in the DMS and DLS to encode different stages of motor skill learning.

RESULTS

Specific spatiotemporal reorganization of DMS and DLS networks during motor skill learning

To form motor skill in mice, we used the accelerated rotarod task, a commonly used paradigm, known to induce modifications of the motor cortex and corticostriatal plasticity [9,10,12,14-16]. Accelerated rotarod learning involves two distinct stages, the early and late phases, respectively involving DMS and DLS, which thus appears as a suited procedure to study selective reorganization at a single cell resolution. As previously reported [9,10,17], we confirmed that the accelerated rotarod paradigm allowed strong and stable motor learning in mice (Fig. 1a-b). Mice performance was significantly increased between the first and tenth trial of early training (1 day) ($p < 0.0001$, n=21 mice, paired t-test) (Fig. 1b). Learning of motor skill was reinforced with late training (7 days) with a significant increase of performance between the first and last day ($p < 0.0001$, n=39 mice, paired t-test) (Fig. 1b).

To study neuronal dynamics associated with the different phases of learning, we used *ex vivo* two-photon calcium imaging to monitor neuronal activity in the DMS or the DLS of naive and trained mice. To do so, we injected AAV-GCaMP6f in DMS or DLS and mice were subjected to the accelerated rotarod paradigm at distinct stages of motor skill learning (naive, early and late phases) (Fig. 1c). To study corticostriatal dynamics and plasticity, we analyzed striatal projection neurons (SPNs) activity in response to cortical stimulations as previously described [18], and we built functional maps representing their amplitude of response (≈ 80-150 cells) in DMS and DLS (Fig. 1d and e).

In DMS, we observed a strong and transitory decrease of the overall activity of SPNs in early trained mice compared to naive and late trained animals ($p = 0.004$, One-way Anova) (Fig. 1d-

e). Notably, the overall decrease in amplitude led to the emergence of few highly activated SPNs, sparsely distributed throughout the field of acquisition (Fig. 1d). Indeed, the percentage of highly active cells (see details in material and methods) significantly decreased in early trained animals compared to naive and late trained mice (Naive, 44.2±5.2 %, n= 11 mice, Early, 27.9±5.2 %, n= 12 mice, Late, 53.8±7.0 %, n= 12 mice, p= 0.0057) (Fig. 1f). We next analyzed whether changes in corticostriatal network activity was linked to the animal's performance during motor learning by correlating the percentage of highly active cells with a learning index (see material and methods). We found that the number of highly active cells is inversely correlated to the motor performance of mice, only during early stages of learning (p= 0.0062) (Fig. 1g). These results demonstrate that the smaller the number of highly active cells is, the better the animals had learned the task. Based on these results, we extracted animals with 'good' performance (see details in material and methods) to perform in depth analysis of the network dynamics. Importantly, animals which did not learn the task did not show any specific network reorganization, confirming our hypothesis that this specific reorganization is tightly linked to the quality of learning. We next computed the mean distances between highly active cells at each stage of the training to explore potential spatial reorganization (Fig. 1h). We did not observe any significant changes in the distribution of distances, indicating that there is no specific spatial organization but instead sparse distribution of highly active cells after early training. We thus took the percentage of highly active cells as a marker of dynamic reorganization in DMS with a significant decrease of these cells in early condition (Naive, 44.2±5.2 %, n= 11, Early, 19.5±4.4 %, n= 9 and Late, 52.3±8.4 %, n= 10, p= 0.0054). Overall, our results showed that motor skill learning was associated with a transient decrease in the SPNs response after early training in the DMS. The reorganization of DMS network was marked by a transient emergence of sparse highly

active neurons, which strongly correlates with animal's performance during the early phase of training. We therefore named these highly active cells "learning-related activity" (LRA) cells.

We next assessed DLS dynamics during motor skill learning, using similar analysis. In contrast to DMS, we did not observe any change in amplitude ($p= 0.7936$, n=9 naive; n=9 early and n= 12 late) (Fig. 1i-j) or percentage of highly active SPNs throughout the different learning stages ($p= 0.5946$) (Fig. 1k). However we found a significant inverse correlation between the percentage of highly active cells and the learning index for late training ($p= 0.0063$) (Fig. 1l). This suggested that animals with a restricted number of highly active cells performed the best in the late phase of motor skill learning. Notably, we found that, in contrast to DMS, highly active SPNs of DLS were spatially redistributed, as shown by the significant decrease in highly active cells inter-distances in late trained animals (Fig. 1m). Using a k-means clustering analysis (see details in material and methods), we found a strong decrease of the cluster areas in late trained conditions, suggesting that highly active cells form clusters of active hot spots in the DLS (Cluster area in Naive, 55.6± 7.1%, Early, 22.7± 8.8%, Late, 9.0± 1.8%, $p<0.0001$) (Fig. 1m). In addition, we found an inverse correlation between cluster areas and quality of animal's performance after late training (Supplementary Fig. 1). These results therefore suggested a progressive formation of clusters of learning-related activity (LRA) cells from early to late phases in DLS, which correlates with individual learning performance.

Long-lasting reorganization in the DLS after motor learning

Because late training could be associated with long-lasting learning of motor skill, we next questioned whether network activity reorganization lasted for an extended period after training. To test this hypothesis, we trained animals for 7 days (late training, see Fig. 1) and

we evaluated the animal's motor skills 1-2 months after the first training. Notably, late trained animals performed well 1-2 months after the last day of training, as shown by a higher basal level than day 1 of training (pre-trained, p=0.0046 between Day 1 and Day 1', n=5 mice), and similar maximal performance level (p=0.3614 between Day 7 and Day 7') (Fig. 2a). We confirmed that this effect was not due to age by training animals of the same age that did not receive a first round of training (pre-naive, Day 1' to Day 7') (Fig. 2a). The learning curve of pre-naive animals was significantly different from pre-trained animals at the same age (p= 0.0006, Two-way Anova). These experiments therefore demonstrated that the learned motor skills were preserved in time. We next explored the DLS network dynamics in the pre-trained animals 1-2 months after the first round of training (at Day 1') (Fig. 2b). We observed that the amplitude of response was not significantly different between the pre-naive and pre-trained animals (Pre-naive, 2.0±0.1, n= 11, Pre-trained, 2.3±0.2, n= 9, p= 0.3287). However, by looking at LRA cells and using k-means clustering analysis as before, we observed a significant reduction of the cluster area in pre-trained animals compared to pre-naive mice (Pre-naive, 44.3±6.0 %, Pre-trained, 19.7±5.7 %, p= 0.0116). These results showed that progressive clustering during the initial period of training remained in the DLS network for months after the last day of training. Interestingly, the cluster area was also inversely correlated with the learning index of late trained animals (r^2= 0.48, p= 0.04). These results therefore demonstrated the long-lasting properties of the dynamic cluster reorganization observed during motor skill learning.

LRA cells have specific dynamic properties within the spatiotemporal reorganization of DMS and DLS

We next asked whether the spatially reorganized LRA cells were associated with specific properties within network activity, granting them a particular role in encoding motor skill. To reveal the dynamic properties of LRA cells within the networks, we decided to test their ability to develop plasticity. For this, we used cortical stimulation at increasing frequencies (5, 10, 20 and 50Hz), which mimicked various types of cortical activity patterns and built activity maps in response to these different frequencies. We analyzed the SPN responses to the different frequencies and extracted several parameters, such as the number of LRA cells, the amplitude of response and the correlation coefficient, mainly at low (5 Hz) and high (20 Hz) frequencies. Measuring a variation between these two frequencies allowed us to highlight how the network plasticity evolved with learning and how LRA cells behaved compared to non-LRA cells in the same trained animal, and compared to highly active (HA) cells observed in naive animals (Fig. 3 a-b).

In the DMS, we reported a globally lower percentage of LRA cells in early trained animals $p< 0.0001$) and higher in late trained animals ($p< 0.05$) as compared to highly active cells in naive mice for all frequencies (Supplementary Fig. 3a). Extracting the evolution between 5 and 20 Hz highlighted the fact that there was no change in the percentage of LRA cells for early trained mice ($p= 0.3750$) (Fig. 3c). In contrast, the percentage of highly active cells increased significantly from 5 to 20 Hz for naive and late trained animals ($p= 0.0137$ for naive and $p= 0.0091$ for late) (Fig. 3c). This observation suggested that after early training, DMS network may similarly respond to low and high frequency cortical inputs. This feature is illustrated by the progressive change of activity maps in naive but not early trained mice (Supplementary Fig. 2a). Importantly, in early condition, we observed that not only the percentage of LRA cells remains stable, but also, that the identity of the activated cells was the same for all stimulations (Supplementary Fig. 2b-d). Altogether, these observations

showed that the DMS spatiotemporal reorganization after early training allows a more efficient transmission of the cortical information. We next explored the plasticity in the amplitude of response. We found that the difference in amplitude between groups was preserved throughout frequencies stimulations with a significantly lower amplitude in early trained mice compared to naive and late trained mice ($p < 0.0001$) (Supplementary Fig. 3a-b). The interesting feature emerged when we explored independently the evolution of amplitude of response in LRA cells versus non-LRA cells. Similarly to the percentage of highly active cells, in naive mice, we observed an increase in the amplitude of response between 5 and 20Hz but with no significant difference between HA and non-HA cells (Fig. 3e). In contrast, after early and late training, we observed that the ratio between 5 and 20 Hz amplitude was significantly higher in non-LRA cells compared to LRA cells ($p < 0.01$ for early and $p < 0.01$ for late) (Fig. 3e).

In DLS, we observed that the percentage of HA area significantly increased between 5 and 20 Hz in naive animals ($p = 0.0066$), but not the percentage of LRA cluster area after early and late training ($p = 0.6451$ for early and $p = 0.5714$ for late) (Fig. 3d). This absence of difference between low and high frequency stimulation was illustrated on the activity maps of late trained mice, which showed a strong similarity of the LRA cell responses throughout the different frequencies (Supplementary Fig. 2e). In addition, the identity of LRA cells remained the same at all frequencies (Supplementary Fig. 2f-h). Importantly, while only about 30% of the common LRA cells were recruited for low frequencies in naive animals, already about 75% of these cells were activated in late trained animals (Supplementary Fig. 2h). As in DMS, we next explored the plasticity of amplitude of response. We found that in DLS the overall amplitude of SPN activity was not significantly different in naive, early and late trained animals (Supplementary Fig. 3c-d). Nevertheless, the evolution of amplitude responses to 5

and 20 Hz stimulations showed a significant increase in both HA active and non-HA cells for naive animals (p= 0.0111) (Fig. 3f). On the contrary, there was no change in LRA cell amplitude in early and late trained mice, while the non-LRA cells still displayed an increase in their response between 5 and 20 Hz after early and late training (Fig. 3f). Altogether, these results highlighted that DMS and DLS LRA cells have distinct plastic properties within the networks.

We next questioned whether large scale spatial reorganization of highly active SPNs in DMS and DLS was associated with temporal changes. We thus explored the timing of activation of SPNs in response to cortical activation by quantifying the percentage of co-active cells for each phase of learning (Fig. 3g-h). In DMS, we observed a clear and progressive shift of the proportion of co-active cells throughout training, showing that training led to a faster activation of most cells (Tau, p= 0.0293, One-way Anova) (Fig. 3g). In DLS, the shift in the proportion of co-active cells was significant only after late training (p= 0.02, One-way Anova) (Fig. 3h). This shows that learning induces a faster and more efficient recruitment of the network. We explored whether the shift in co-active cells proportion could be related to the correlation of activity of HA/LRA versus non-HA/non-LRA cells. For this purpose, we built correlation matrices of the network activity in the different conditions and extracted the mean of the correlation coefficient (Fig. 3i-j). In the DMS, we observed that LRA and HA cells have more correlated activity than non-LRA and non-HA cells in all the conditions but with a significant and less variable correlation coefficient for all frequencies in early and late conditions (Supplementary Fig. 3e). In the DLS, the correlation was significantly higher for LRA cells after early and late training (p=0.0182 for early and p=0.0128 for late at 20 Hz), compared to non-LRA cells. In contrast, in naive animals (p= 0.1266), there was no difference of correlation between HA and non-HA cells for all tested frequencies (Supplementary Fig.

3f). Therefore, the LRA cells have a significantly more correlated activity that would change the network response synchronization to cortical inputs.

Altogether these results indicate that LRA cells have specific dynamic properties within the network: they displayed less plasticity in term of number of cells and their amplitude of response and had more correlated activity compared to non-LRA cells. The radar charts highlighted the different parameters for different learning conditions in DMS and DLS (Fig. 3i-j). Altogether, these results indicated that LRA cells might form more stable neuronal ensemble arising at specific stages of the learning process.

DMS LRA cells display specific cortical input integration properties

We next investigated the mechanisms regulating early and late reorganization of DMS and DLS networks, respectively. Because specific properties of LRA cells could be due to intrinsic electrophysiological properties or to different integration properties of the cortical inputs, we performed double patch-clamp recordings of SPNs being part of the LRA cells, or not (non-LRA) in early DMS or late DLS networks. We first trained the animals according to the region of interest (early training for DMS and late training for DLS) and we then performed two-photon calcium imaging on acute brain slices at the end of the training session. The challenge here was to record LRA and non-LRA cells in the very same experiment to be able to compare their properties. We developed an online analysis protocol (using custom-made procedures in FIJI and RStudio software) to identify LRA cells right after the imaging acquisitions and we performed targeted patch clamp recordings of LRA or non-LRA SPNs (Fig. 4a). This experimental setup allowed us to compare the basic electrophysiological properties as well as the corticostriatal input connection properties of LRA and non-LRA SPNs, in the very same conditions.

283 We first compared the electrophysiological properties of LRA and non-LRA cells in DMS after
284 early training. We did not observe any significant difference in intrinsic properties between
285 the two subtypes (Fig. 4b). We next compared the integration properties of cortical inputs.
286 Using targeted cortical stimulation in cingulate cortex, we measured the spiking probability,
287 the input/output relationship of subthreshold cortically induced EPSPs and the short-term
288 plasticity of subthreshold EPSPs. We found that the spiking probability is significantly higher
289 for LRA cells compared to non-LRA cells ($p= 0.0038$, $n=8$ pairs, paired t-test) (Fig. 4d),
290 suggesting that they are more efficiently recruited by cortical afferents. The input/output
291 curve shows that the amplitude of EPSPs is significantly stronger in LRA cells compared to
292 non-LRA cells for different stimulation intensities ($p= 0.0232$), which corroborated their
293 higher spiking probability (Fig. 4e). We next evaluated the short-term plasticity of cortical
294 connections to LRA and non-LRA cells. To do so, we used trains of stimulations at various
295 frequencies and found that non-LRA cells displayed significant summation of the EPSPs for
296 most frequencies. This summation was also observed in naive animals (Supplementary Fig. 4)
297 and coherent with previous observations [18]. The striking observation was that LRA cells did
298 not display summation or even depression for low frequencies such as 5 Hz (Fig. 4f). These
299 observations suggested that the probability of release of cortical inputs to DMS might be
300 enhanced specifically on connections targeting the LRA cells.
301 Interestingly, we observed a striking difference in the DLS compared to DMS. When
302 analyzing intrinsic properties, we found a difference in the resting membrane potential of
303 LRA and non-LRA cells (Fig. 4c). In contrast, when studying cortical input integration
304 properties using targeted stimulation of somatosensory cortex, we did not observe any
305 significant difference between LRA and non-LRA cells neither for spiking probability ($p= 1.0$,
306 $n= 8$ pairs) (Fig. 4g) nor for input/output curves ($p= 0.4475$) (Fig. 4h). Finally, the short-term

plasticity developed at somatosensory inputs was not different between LRA and non-LRA cells (Fig. 4i).

Altogether, these results suggest that LRA cells in DMS receive stronger and more efficient connections from cingulate cortical cells while LRA cells in DLS receive somatosensory cortical connections with similar efficiency than other cells in the network.

Late DLS reorganization is associated with anatomical remodeling of cortical projections

Since the electrophysiological properties could not explain the reorganization induced by late training in the DLS, we explored whether anatomical plasticity also took place in cortical inputs. For this purpose, we performed tracing experiments using injections of the retrograde tracer, cholera toxin B (CTB) in DMS and DLS (Fig. 5a-b and Supplementary Fig. 5), to analyze anatomical rearrangement in the cingulate cortex and somatosensory cortex, respectively. CTB is captured by cortical terminals in DMS and DLS and is retrogradely transported to cortical cell somas as previously shown [19,20]. CTB-488 was injected in DLS and CTB-555 in DMS to simultaneously compare inputs from somatosensory and cingulate cortex in the same conditions. We counted the number of cortical cells from all layers projecting to DMS and DLS. We first explored the projections from cingulate cortex to DMS and we did not see any significant effect of training on the number of projecting cells for early or late trained animals compared to naive ones ($F_{2,117}$= 0.94, p= 0.3640, Two-way Anova) (Fig. 5d). In contrast, in the DLS, we observed a significant increase in the number of cortical somatosensory cells projecting to DLS in trained mice compared to naive mice ($F_{2,105}$= 8.12, p< 0.0001, Two-way Anova) (Fig. 5e). This increase was observed for the two main layers projecting to the striatum: layer 5 increased by +40 % (p< 0.01) after early training and +75 % (p< 0.001) after late training and layer 2/3 increased by +155 % (p< 0.05) after late

training. Layer 6 remained unchanged which is consistent to its projections mainly going to the thalamus [21].

These results therefore demonstrated that the dynamic reorganization of DLS after late training was supported by strong anatomical rearrangements of input projections from somatosensory cortex. This contrasts with the short-term changes in electrophysiological properties observed in DMS after early training.

Striatal LRA cells are necessary for motor skill learning

Because animal's performance correlated to spatiotemporal reorganization in both DMS and DLS networks and the emergence of LRA cells, we next questioned their direct implication in motor skill acquisition. Therefore, we investigated whether direct manipulation of LRA cells activity may affect motor skill formation, using a cFos-TRAP strategy [22-25]. We first asked whether cFos was efficiently induced in our training conditions. Using immunostainings of endogenous cFos, we found a significant increase in the number of cFos+ cells in DMS after early training, and in DLS after late training (Supplementary Fig. 6). We next used a cre-inducible virus under the control of cFos expression (AAV-cFos-ERT2-Cre-ERT2-PEST), co-injected with an AAV-DIO-mCherry reporter in DMS or DLS. We induced the activation of the cre-recombinase with 4-OH-Tamoxifen (4-OHT) injection immediately after the training session, which led to an efficient expression of mCherry in cFos expressing cells (Supplementary Fig. 7). Notably, we observed that the number of cFos-mCherry+ cells was similar to the number of LRA cells previously identified in the two-photon calcium imaging, in both territories (Fig. 1) ($p= 0.6538$ for DMS and $p= 0.6623$ for DLS) (Supplementary Fig. 8b). We also co-injected the AAV-GCaMP6f with AAV-cFos-ERT2-Cre-ERT2-PEST and AAV-DIO-mCherry to visualize both calcium-identified LRA cells and cFos expressing cells. We

found a high degree of overlap between LRA cells and cFos+ cells, both in DMS (78.9±10.0 %) and DLS (72.0±8.8 %) (Supplementary Fig. 8c). These experiments showed that the cFos TRAP strategy was suitable to selectively target and manipulate LRA cells in DMS and DLS during motor skill learning.

Mice were injected with AAV-cFos-ERT2-Cre-ERT2-PEST and either AAV-DIO-mCherry or AAV-DIO-hM4Di-mCherry and trained on the accelerated rotarod. Because LRA cells appear at its earliest after 1 day of training (early phase), we first trained the animals to allow the emergence of LRA cells before silencing. At the end of the training, we injected 4-OHT to allow the expression of either mCherry or hM4Di-mCherry proteins for a period of two weeks. This strategy led to an efficient expression in DMS and DLS (Fig. 6b and f and Supplementary Fig. 7). We then evaluated the performance of mice after silencing LRA cells either in DMS after early training or in DLS after late training.

For DMS manipulation, mice were trained for 1 day (10 trials) and were tested on Day 15 after 2 weeks of mCherry or hM4Di-mCherry expression (Fig. 6a). On Day 15, mice received CNO (a ligand of hM4Di) before testing motor skill retention. Importantly, on Day 1, control (mCherry) and hM4Di groups displayed similar training curves and learning index ($p=0.9571$, Two-way Anova), showing that mCherry or hM4Di-mCherry expression did not alter learning performance (Fig. 6c-d). On Day 15, the mCherry group displayed a significant increase in their performance between trial 1 and trial 10 ($p=0.0078$, paired t-test) (Fig. 6c-d). It should be noted that this increase was similar to what we observed on Day 2 of training (Supplementary Fig. 9a), indicating that the 2 weeks gap allowing viral expression did not affect the training curve. In contrast, the hM4Di group displayed an impaired learning curve compared to the control group ($p< 0.0001$, Two-way Anova) (Fig. 6c), with no improvement between Trial 1 and Trial 10 ($p= 0.4609$, paired t-test) (Fig. 6d). Interestingly, the learning

index was significantly lower compared to control mice (p= 0.0168, t-test). These experiments therefore highlighted the central role of LRA cells in DMS during the early phase of motor skill formation.

Given that silencing LRA cells of the DMS is sufficient to prevent learning acquisition after 1 day of training, we investigated whether silencing DLS LRA cells would have an effect on long-lasting retention. Indeed, we observed that LRA cells are still present few months after training (Fig. 2), targeting them could thus affect the retention of the motor skill. We repeated the previous cFos TRAP strategy in the DLS of mice trained for 7 days and we tested their performance on Day 21 (Fig. 6e). During the first week of training, the control (mCherry) group and the hM4Di group displayed similar performance (p=0.4623, Two-way Anova) (Fig. 6g-h). The learning index was not different between the two groups, showing that both groups learned similarly (Fig. 6h). On Day 21, we injected CNO before the first trial and we assessed the performance of the animals as before. The mCherry group displayed a significant increase in their performance between trial 1 and trial 10 on Day 21 (p= 0.0098) (Fig. 6h). The increase was similar to what we observed at Day 8 for the late training in wild-type mice (Supplementary Fig. 9b), which is coherent with our previous observations that skill acquisition is maintained over a long period (Fig. 2). In contrast, the hM4Di group showed strong impairments in their performance compared to the control group (p< 0.0001, Two-way Anova) (Fig. 6g). Indeed, we observed a decrease in their performance between Trial 1 and Trial 10 on Day 21, (Fig. 6h) as shown by the negative learning index compared to control group (p< 0.0001). These results therefore demonstrate that LRA cells formed after late training are determinant for long-lasting motor skill persistence.

DISCUSSION

In the present study, we show a strong spatiotemporal reorganization of striatal neuronal ensembles associated to specific phases of motor skill learning (Fig. 7). Early training leads to the transitory emergence of LRA cells in DMS and the start of a spatial restriction of the striatal cells recruited in DLS. After late training, DMS comes back to a basal-like state while, in DLS, the LRA cells appear and become more spatially restricted. These two sequential phases of network reorganization arise from distinct levels of plasticity: (i) transient reinforcement of synaptic connections from cingulate cortex onto DMS LRA cells and (ii) long lasting anatomical rearrangements of somatosensory projections in the DLS. Importantly, silencing these two types of LRA cells in DMS and DLS strongly impaired motor learning and highlighted that DMS transient LRA cells are sufficient for motor learning acquisition, while DLS LRA clusters allow long-term retention of the learning.

Sequence of striatal network reorganization in DMS and DLS

The striatum plays a crucial role during the different phases of learning, with a preferential implication of DMS in early phase and DLS in late phase. Lesions studies [1,5-7] have first highlighted the specificity of each territory. This has been confirmed with neural recordings of DMS or DLS ensembles during procedural task [9-11,26-28]. In the present study we also show a modification of DMS networks mainly during the early phase and more pronounced modifications in DLS at the end of the training. Nevertheless, as previously highlighted (for review see [2]), the scheme is not so simple as changes in neuronal activity patterns occur simultaneously in the associative and sensorimotor striatum, and, it would be more that as activity in the DMS starts to decline, activity in the DLS becomes stronger [11]. We also show

that reorganization of DLS networks is initiated at the early phase and strongly reinforced at the end; concerning the DMS, even though the network seems to go back to a naive level, we do observe that all network properties are not identical, for example the response stays more synchronized in the late training conditions. This highlights that there is a more prolonged change in the DMS dynamics. In addition, the cFos TRAP experiments were realized two weeks after training and the performance of animals was similar to a performance on a 2nd day of training, suggesting a persistence of the reorganization. Altogether, this suggests that the different corticostriatal loops can either compete or cooperate with one another during the learning process and subsequent performance [11,12]. A recent study showed that the intermingled activity of DMS and DLS during learning is even stronger if we consider the very long-term effects induced by extensive training [29]. All these evidence suggest that behavioral sequences may continue to engage both striatal regions long after initial acquisition, when skilled performance is consolidated.

Dynamic network reorganization in DMS and DLS

We studied the post-training effect of early and late motor skill learning in the network dynamics associated to the cingulate cortex-DMS pathway. We first reported that training to the rotarod task induced a transient decrease in the response of DMS neurons to cortical stimulation after early training. This observation is not totally in line with previous *in vivo* studies. Most of the rodent works which studied DMS neural activity during learning have been done *in vivo* and they show that DMS activity is increased during early phase of motor skill learning or goal-directed behaviors, such as the rotarod [10], the T-Maze [11,30] and operant conditioning tasks [31]. In these *in vivo* studies, recordings were done during the running period and by excluding the resting period. Our recordings are performed 24 hours after the

451 end of the training, they are therefore indicative of the plastic events that may be taking
452 place after the training has finished, this is, during the consolidation and not only the
453 acquisition of the motor skill. In addition, recent publications have also highlighted that
454 there is an inhibition in DMS during the early phase of operant conditioning, even during the
455 inter-trial period [29], and discrimination [32] tasks. Even though this could be interpreted as a
456 disengagement of DMS during early training, we do think that the global inhibition is a
457 mechanism revealing the LRA cells which could be determinant in the encoding of the early
458 phase of the motor skill acquisition. Nevertheless, further experiments should address if
459 local striatal modulations of the DMS SPNs activity are in play during early training, since
460 modulation of cortical synaptic weight may not be the only mechanism to induce a global
461 inhibition. In DLS, we did not observe a change neither in the mean amplitude of the
462 response nor in the percentage of highly active cells with early or extensive training.
463 Consistent with the role of DLS in habitual behavior, we showed an increase in the
464 synchronization of the response exclusively after late training and the progressive formation
465 of learning-related clusters whose mean amplitude was increased in trained animals and
466 whose size was negatively correlated with learning after late but not early training. This
467 could be coherent with previous reports of increased activity within DLS after late training
468 showing that training to motor skill, T-maze or instrumental conditioning task, is usually
469 associated with a progressive increase in DLS network activity as the behavior becomes
470 more habitual [10,11,30].
471 Importantly, a small percentage of DMS and DLS neurons, the LRA cells, remained highly
472 active after early and late training, respectively. The LRA cells also expressed cFos and the
473 percentage we observed is coherent with the ones describing modulation of early genes
474 such as cFos or Arc in striatum during a motor skill learning paradigm [26,33]. We demonstrated

that the LRA cells displayed different properties within the networks, notably on the plasticity they develop in response to increasing cortical stimulation. Indeed, the percentage of highly active cells in naive animals increases when the cortex is stimulated at higher frequencies. On the contrary, in DMS early trained and DLS late trained animals, the percentage of LRA cells is not significantly affected by the frequency of cortical stimulation. In addition, in DLS, we reported a difference in the percentage of co-active cells and the common LRA cells since only 30 % of the common cluster cells were recruited for low frequencies in naive animals, while already about 75 % of them were activated in late trained animals. The LRA cells activity also appears to be more synchronized than non-LRA cells for all frequencies after training. Altogether, these observations indicate that after training, early DMS and late DLS networks might be forming stable neuronal ensembles with a potentiated transmission, allowing them to relay information more efficiently, even for low cortical inputs.

Cortical inputs as determinant players in the reorganization

We explored the mechanisms that could be responsible for the emergence of LRA cells in DMS and DLS, and we focused on the cortical inputs to each territory. The modification of cortical inputs by motor learning have been highlighted by synaptic plasticity of corticostriatal connections related to learning [10,34-37]. Therefore, a first possible mechanism was a specific modification of synaptic weight onto the LRA cells compared to the other cells in the field. This hypothesis was validated for the DMS reorganization after early training, but not for DLS. A recent study also reported enhanced synaptic inputs from frontal cortex to the DMS during early training [12]. This could corroborate our description of stronger inputs to the LRA cells in DMS after early training, considering that *in vivo* fiber photometry used in

this study gives an averaged activity of presynaptic inputs without distinguishing different neuronal ensembles. These results are also coherent with an absence of postsynaptic modifications, such as NMDA/AMPA ratio, after early training in DMS [10]. Considering that the emergence of DMS LRA cells is only during the early phase and disappears after late training, the modifications of synaptic weight could therefore be coherent with this transitory state of the DMS LRA cells.

Contrary to DMS, in DLS we found no difference in the synaptic weight of cortical inputs onto LRA cells and non-LRA cells. Synaptic modifications have been evaluated in DLS after late training and the AMPA/NMDA receptor ratio is increased [10,34,35]. This would not be coherent with our observations. Nevertheless, we should be careful in the comparisons since in our experiments, we compare cortical connections to LRA and non-LRA cells after the end of the training. This does not exclude that other synaptic modifications took place earlier at the corticostriatal pathway but that we do not see at the time we perform our recordings.

Another plausible hypothesis was that anatomical plasticity could take place as an alternative mechanism for the modifications of corticostriatal networks. Most of the structural changes have been observed in spines and dendrites [38,39] but nothing was known about the potential existence and role of structural plasticity from the inputs. Using retrograde tracers we reported no difference in the cingulate cortical inputs to DMS but a gradual increase in the number of cortical somatosensory projections into DLS with learning. This is a remarkable result since most evidence for axonal growth in the brain comes from lesions on sensory periphery or brain damage studies [39]. Indeed, it has been shown in monkeys, that peripheral injury leads to large-scale sprouting of intercortical connections arising from somatosensory cortex [40]. However, axonal growth has also been suggested as a plausible mechanism for learning and memory formation [39,41]. Interestingly,

evidence for learning-induced axonal growth comes mainly from procedural or motor skill learning events. In humans for instance, novel juggling learning increases white matter structure in occipito-parietal regions involved in visual-motor coordination after 6 weeks of training [42]. In monkeys, intracortical collateral axonal sprouting and pruning was observed in primary visual cortex after 2 weeks of contour detection task training [43]. In mice, learning-induced axonal plasticity has been observed as early as 11 days after a single-pellet reaching task training in areas adjacent to motor cortex [44] and after 5 days of associative motor learning in the adult cerebellum (coming from basal pontine nuclei) [45]. Thus, there is growing evidence that axonal reorganization can be induced by motor and procedural learning, at time-scales as short as several days. Our results show that late training induced the appearance of clusters of highly active cells in DLS, thus one possible explanation for this phenomena could be that extensive learning induced new axonal branching or sprouting into the cells within the cluster. This could be corroborated by the strong convergence of the pyramidal cells to the striatum in the sensorimotor loops [46]. Interestingly, we see modifications of the number of somatosensory projecting cells originating from layer 5, which is the most known cortico-striatal pathway, with a significant increase of +75% of projecting layer 5 cells to the DLS. A more surprising observation was that the layer 2/3 projecting neurons are modified as well by learning, with a higher increase, more than +100%, after late training. The layer 2/3 projecting neurons have been shown to mainly connect other cortical areas but they also project to the dorsal striatum [47]. In addition, they display strong plasticity after motor skill learning [48]. Their stronger modifications with learning could indicate that these connections allow an improved transmission to the striatum but also to the cortical areas related to the behavioral tasks as well. The anatomical modifications are coherent with the maintenance of the motor skill. Indeed, once formed,

the motor skill is thought to be encoded within the sensorimotor loops, including the DLS, and therefore long-lasting anatomical modifications could be responsible for the maintenance of the skill encoding within striatal networks.

We chose to focus here on the cortical inputs from somatosensory cortex, which corresponds to the upper and lower limbs of the animal, directly implicated in the behavioral task, and we drove these inputs to assess the DLS network activity. There are other functional inputs to the DLS such as motor cortical inputs or thalamic inputs which could be involved also in the process and will need to be investigated. Indeed, recent studies highlighted that motor cortex is necessary for learning a motor task but not to execute the motor task [49]. Therefore further studies making a parallel between the various motor tasks used, the number of trials to form the skill and the network modifications will be needed to link altogether our observations with others.

LRA cells as striatal engram cells of motor skill

We demonstrated the emergence of LRA cells, in early DMS and late DLS, which are correlated to the quality of the performance, with a clustering of the activity for long-lasting retention of the motor skill within the DLS. Other studies performed in freely moving animals have also reported the formation of functional clusters in DLS and have attributed this activity to specific action, locomotion or movement-related events [50-52]. During learning-related tasks (like T- maze and lever-press tasks), activity in DLS has been related specifically to task bracketing motor patterns and not just movement [11,13,53]. Using fiber photometry Markowitz *et al.* demonstrated increases in DLS activity while mice explore an open field and concluded that DLS network dynamics encode the selection of specific concatenated actions [54]. Our present report of clustered active cells associated with motor learning is the first one

571 to show that LRA cells could be related to motor skill acquisition and retention. We thus
572 propose that LRA cells would be the striatal equivalent of engram cells described in
573 hippocampus, amygdala or cortex [55]. Indeed, engram cells have been defined as cells that
574 are (i) activated by a learning experience, (ii) physically or chemically modified by the
575 learning experience, and (iii) reactivated by subsequent presentation of the stimuli present
576 at the learning experience, resulting in memory retrieval [55]. The LRA cells observed both in
577 DMS and DLS comply with the definition of engram cells as we showed they were activated
578 by motor skill learning, they underwent either synaptic modifications or increased cortical
579 inputs, respectively, and we demonstrated through loss-of-function experiments that they
580 were necessary for proper memory retrieval. One interesting aspect of this striatal engram is
581 that in our study we found that the percentage of LRA cells in DMS and cluster area in DLS
582 are negatively correlated with behavioral performance after early and late training,
583 respectively. Thus, even if the size of the engram is quite stable in both cases, we did
584 observe that variability in size between animals correlated with performance. This could
585 mean that learning leads to a decrease of the noise in the network with a limitation of the
586 cells involved in motor learning. As the modulation of DLS activity has been correlated with
587 locomotion, movement in the selection of an action or concatenated actions [11,13,28,50,52-54],
588 we could imagine that the LRA cells described here could combine neurons involved in the
589 various parameters of the action and form a new heterogeneous ensemble which will
590 stabilize an optimized strategy and consolidate the neuronal substrate of the motor skill. Our
591 study opens new perspectives in the field of engram within striatal networks and further
592 studies will need to explore these hypotheses and characterize the properties of the striatal
593 engram cells in different behavioral contexts.
594

MATERIALS AND METHODS

EXPERIMENTAL MODELS

C57BL6 mice (*Mus musculus*) of 1.5 to 4 month-old of both sexes are used and housed in temperature-controlled rooms with standard 12 hours light/dark cycles and food and water were available *ad libitum*. Every precaution is taken to minimize stress and the number of animals used in each series of experiments. All experiments are performed in accordance with EU guidelines (directive 86/609/EEC) and in accordance with French national institutional animal care guidelines (protocol APAFIS#8241-2016092317163976 v2). No significant difference between males and females was observed (data not shown).

METHOD DETAILS

AAVs

Adeno-associated viruses (AAVs of serotype 5 and 8) were used to express different genes in striatal cells. AAV5-syn-GCaMP6f-WPRE-SV40 was purchased from UPennCore (PA, USA), the AAV8-cFos-ERT2-Cre-ERT2-PEST-no WPRE from Stanford Gene Vector and Virus Core (CA, USA) and AAV5-hSyn-DIO-hM4D(Gi)-mCherry or AAV5-hSyn-DIO-mCherry were purchased from Addgene (MA, USA).

Stereotaxic injections

Stereotaxic intracranial injections were used to deliver AAVs or CTB (Cholera Toxin B) in striatum. Mice are anesthetized with 2.5 % isoflurane and placed in a stereotaxic frame (Kopf). Under aseptic conditions, the skull is exposed and leveled and a craniotomy is made

619 with an electric drill. The viruses (serotype 5/8, ≈ 10^{12} genomic copies per mL) are injected
620 through a pulled glass pipette (pulled with a P-97 model Sutter Instrument Co. pipette
621 puller) using a nanoinjector (World Precision Instruments, Germany). The pulled glass
622 micropipette is slowly lowered into the brain and left 1 min in place before starting the
623 injection of the virus at an injection rate of 100 nL per min. A volume of 400 nL of the viruses
624 was enough to infect a large proportion of DMS or DLS. The injections targeted the DMS at
625 coordinates AP + 1.1mm, ML 1.2, DV - 1.9 and the DLS at AP - 0.3, ML 2.3, DV - 2.45.
626 Following injections, we wait 5 min before raising the pipette out of the brain. To minimize
627 dehydration during surgery mice received a subcutaneous injection of 1mL of sterile saline.
628 Postoperatively mice are monitored on a heating pad for 1 h before being returned to their
629 home cage. Mice are then monitored daily for 4-5 days. A period of 15 to 20 days after
630 injections was enough to allow for a good expression of AAVs (Fig. 1). We observe similar
631 expression of GCaMP6f in all striatal neurons in DMS or DLS in injected mice with viral
632 vectors.
633
634 **Retrograde tracing studies**
635 Retrograde tracer Cholera toxin subunit (CTB) pre-labelled with an Alexa-488 (CTB-488) or
636 Alexa-555 fluorophore (CTB-555) (0.25 µg/µl dissolved in saline; Thermo-Fisher Scientific) is
637 used to retrogradely label cortical neurons projecting to DMS or DLS. In order to study
638 learning-induced changes in the number of cortical neurons projecting to each striatal
639 territory, mice are injected in the left hemisphere with 400 nL of CTB-555 in DMS and 400 nL
640 of CTB-488 in DLS in naive animals or one day after early or late training. 5 days after
641 stereotaxic injections mice are perfused transcardially with PFA 4 % and brains are removed
642 and sliced as described in the immunohistochemistry section. Fifty micrometers coronal

643 slices are obtained using a cryostat (Microm HM 560, ThermoScientific). Coronal sections
644 spanning the whole striatum (1.70 mm to -2.18 mm AP from Bregma, according to Paxinos
645 Atlas) are incubated for 2 h with 1:4000 DAPI, then rinsed 3 times in PBS and mounted with
646 Dako fluorescent mounting medium (Agilent) on microscope slides.
647
648 **Behavioral training**
649 An accelerating rotarod is used as a motor skill learning paradigm. In the previous days of
650 the training, mice are acclimated to the room and to handling. For each trial the mouse is
651 placed on the still rotarod which is activated at that point. The rotation of the rod is
652 increasing from 4 to 40 rotations per min over 300 s [10,12]. Each trial is ended when the mouse
653 falls off the rotarod or when the 300 s have elapsed. There is a resting period of 300 s
654 between trials. Animals are trained with 10 trials per day for either 1 day (early training) or 7
655 days every day (late training). This training protocol was chosen since it was previously
656 described as a reliable test for motor skill learning or procedural learning [9,10,12,17].
657
658 **Tamoxifen induced expression**.
659 Mice are injected as previously described with AAV8-cFos-ERT2-Cre-ERT2-PEST and AAV-
660 hSyn-DIO-mCherry or AAV5-hSyn-DIO-hM4D(Gi)-mCherry. Two weeks later, mice are trained
661 on the accelerated rotarod (early or late training) and right after injected intraperitoneally
662 with 4-Hydroxytamoxifen (4-OHT; Sigma-Aldrich) (50 mg/kg) to induce recombination.
663 Expression of the floxed AAVs was allowed for 2 weeks and after this time mice are injected
664 with Clozapine-N-Oxide (CNO, 3 mg/kg) 30 minutes before training. Brains are extracted 2
665 hours after training for histological characterization.
666

667 ***Ex vivo* two-photon imaging and multi-patch-clamp recordings**

668

669 ***Brain slice preparation***. Two weeks after AAVs injections, and after rotarod training, brain
670 slices preserving DMS and DLS with their cortical inputs coming from sensory and cingulate
671 cortex respectively are prepared as previously described [18,56]. Animals are anesthetized with
672 isoflurane before extraction of the brains. We prepare brain slices (300 µm) using a vibrating
673 blade microtome (VT1200S, Leica Microsystems, Nussloch, Germany). Brains are sliced in a
674 95 % CO_2 and 5 % O_2-bubbled, ice-cold cutting solution containing (in mM) 125 NaCl, 2.5 KCl,
675 25 glucose, 25 $NaHCO_3$, 1.25 NaH_2PO_4, 2 $CaCl_2$, 1 $MgCl_2$, 1 pyruvic acid, and then transferred
676 into the same solution at 34°C for one hour and then moved to room temperature.

677 ***Two-photon calcium imaging***.

678 Genetically-encoded Ca^{2+} indicator GCaMP6f was used for calcium imaging of somas of
679 striatal cells. GCaMP6f is expressed with recombinant AAVs injected in DMS or DLS. Two-
680 photon calcium imaging is performed at 940nm with a TRiMScope II system (LaVision BioTec,
681 Germany) using a resonant scanner, equipped with a 20x/1.0 water-immersion objective
682 (Zeiss) and coupled to a Ti:Sapphire laser (Chameleon Vision II, Coherent, >3W, 140 fs pulses,
683 80MHz repetition rate). The average power of the laser emitted was set at ~40-50mW on
684 sample. Fluorescence is detected with a GaAsP detector (Hamamatsu H 7422-40). Scanning
685 and image acquisitions are controlled with Imspector software (LaVision BioTec, Germany)
686 (15.3 frames per second for 1024 x 1024 pixels, between 50 to 150 µm underneath the brain
687 slice surface, with no digital zoom). Typical images window for calcium imaging of wide field
688 is 392 µm x 392 µm.

Cortical stimulation protocols

Electrical stimulations were applied with a bipolar electrode (MicroProbes, USA) placed in the layer 5 of either the somatosensory or the cingulate cortex as previously described [18]. Electrical stimulations were monophasic at constant current (Iso-Flex, AMPI, Science Products). Single cortical stimulations or trains of stimulations are delivered; trains consist of 5 stimulations delivered at different frequencies (5, 10, 20, 50 Hz). Single or trains of stimulations are applied at 0.1 Hz, a frequency for which no short- or long-term changes are observed [56]. Single stimulation duration ranged from 0.1 to 1 ms, for subthreshold and suprathreshold activity.

Electrophysiological recordings.

Whole-cell patch-clamp recordings of SPNs are performed with borosilicate glass pipettes (5-8 MΩ) containing (mM): 127 K-gluconate, 13 KCl, 10 HEPES, 10 phosphocreatine, 4 ATP-Mg, 0.3 GTP-Na, 0.3 EGTA (adjusted to pH 7.35 with KOH). Slices are continuously superfused with the extracellular solution containing (mM): 125 NaCl, 2.5 KCl, 25 glucose, 25 $NaHCO_3$, 1.25 NaH_2PO_4, 2 $CaCl_2$, 1 $MgCl_2$, 10 µM pyruvic acid bubbled with 95% O_2 and 5% CO_2. Slices are visualized under a microscope (Slicescope Scientifica, London, UK) with a 5x/0.15 objective for the placement of the stimulating electrode and a 20x/1.0 water-immersion objective for localizing cells for whole-cell recordings. SPNs are distinguished from other striatal neurons such as interneurons based on morphology and/or passive and active membrane properties [57]. Signals are amplified using EPC10-2 amplifiers (HEKA Elektronik, Lambrecht, Germany). Current-clamp recordings are filtered at 2.5 kHz and sampled at 5 kHz and voltage-clamp recordings are filtered at 5 kHz and sampled at 10 kHz using the program Patchmaster v2x32 (HEKA Elektronik). Recordings are performed at 32-35°C to maintain physiological temperature conditions.

Immunohistochemistry

Quantification of cFos expressing striatal cells is done by immunohistochemistry targeting sFos. Two hours after the end of the training, mice are deeply anaesthetized with Dolethal (2 mL/kg) injected intraperitoneally, then transcardially perfused with first phosphate buffered saline (PBS) and finally 4 % paraformaldehyde (AntigenFix, Diapath). Following perfusion, brains are postfixed in 4 % paraformaldehyde for 24 hours at 4°C. Brains are washed with PBS 1X and then incubated in a 30 % (wt/vol) sucrose solution at 4°C until they sank. Brains are then placed in a mold with OCT and kept at -80 °C. Twenty-four hours before slicing, brains are placed at -20 °C. Forty micrometers coronal slices are obtained using a cryostat (Microm HM 560, ThermoScientific). Slices are kept in a cryoprotective solution at -20°C. Coronal sections are blocked with PBST (PBS with 0.3 % Triton X-100) with 5 % (vol/vol) normal goat serum for 1 h 30 and then incubated with the first primary antibody at 4 °C for 24 h (rabbit anti-c-Fos 1:500, Synaptic Systems #226003). The next day, slices undergo three wash steps for 10 min each in PBS. Slices are then incubated for 2 h with secondary antibodies (1:200 AlexaFluor 488 anti-rabbit, Invitrogen). Finally, slices undergo three more wash steps of 10 min each in PBS, followed by mounting and coverslipping with Dako fluorescent mounting medium (Agilent) on microscope slides.

Drugs

Clozapine-N-oxide (Bio –Techne SAS) is first dissolved in dimethylsulfoxide (DMSO, Sigma, final concentration 25 µg/µL), then aliquoted and stored at -20°C. For intraperitoneal injections, frozen aliquots are put at room temperature, and then further diluted in 0.9% sterile saline solution to a final concentration of 0.3 µg/µL. The solution is delivered

intraperitoneally (3 mg/kg) and, after the injection, the animals are placed back in the home cage for 30 min before the start of the experiment. 4-Hydroxytamoxifen (4-OHT) is dissolved by sonication for about 15 minutes (until total dissolution) in 10 % EtOH / 90 % corn oil at 40°C to get a final concentration of 5 mg/ml. Mice are injected with 50 mg/kg of 4-OHT (200 µL). 4-OHT is prepared on the same day of the experiment.

DATA ANALYSIS

Behavior

The time to fall (latency) from the accelerated rotarod is recorded to measure the level of the motor skill learning. In accordance with previous studies [10,17] trial 1 and 2 data are pooled as early trials and trial 9 and 10 data pooled as late trials for each day. We calculate a learning index by subtracting late trials from early trials for early training. For late training, learning index corresponds to a subtraction of the early trials of Day 1 from the average of Day 7. Animals with a learning index > 30 for DMS and > 50 for DLS were considered as good learners.

Immunohistochemistry

Images are acquired using a confocal microscope (LSM710, Zeiss, Germany). Z-stacks (20-30 µm) with 2 µm step size are acquired in DMS or DLS with a 20x/0.8 objective. Concerning the cFos immunostainings, we quantify the number of cFos expressing neurons in 3 mice per condition. For each mouse, we acquire Z-stacks on 2-3 different coronal slices on the anteroposterior axis per territory (DMS and DLS) in one or two hemispheres. Each Z-stack was first filtered using a White Top Hat Morphological filter (MorphoLibJ plugin, FIJI

761 software). Then, 3D object counter plugin was applied on the Z-stack obtained, with a
762 Threshold set to 20 and a size filter set to 200 to remove low signal and small objects. Finally,
763 one plane from the Z-stack was taken and 2 or 3 fields (400 x 400 µm) were selected to
764 determine the number of cells with high cFos expression. The quantification of mCherry+
765 and hM4Di-mCherry+ cells was done in fields of 400 x 400 µm to be compared with the
766 number of LRA cells we observed in DMS and DLS (Fig. 1 and Supplementary Fig. 6). We
767 quantified the number of cells with automatized detection using FIJI software in 2-5 mice per
768 condition (no tamoxifen, mCherry+ and hM4Di-mCherry+), in 2-3 different coronal slices on
769 the anteroposterior axis and within 2-3 fields of 400 x 400µm per slice.
770
771 **CTB quantification**
772 For the quantification of CTB-555+ cells in cingulate cortex (Cg->DMS projections) and CTB-
773 488+ cells in somatosensory cortex (S2-> DLS projections), 3 slices per region for each animal
774 are imaged with an Axioscan Z1 microscope (Zeiss, Germany) with a 20x /0.8 objective.
775 Analysis of the CTB-555+ cells in cingulate cortex is performed for slices spanning 1.2 mm to
776 0.2 mm AP from Bregma according to Paxinos Atlas, and for CTB-488+ cells in somatosensory
777 cortex from -0.1 mm to -1.1 mm. Quantification of striatal projecting neurons is performed
778 over all the cingulate and somatosensory cortex layers for each slice using the Cell Counter
779 plugin (FIJI software). DAPI staining is used to identify the layering in each cortical region and
780 the total number of neurons is then normalized to the area of the cortical layer in which it is
781 present and also to the area of the injection sites. To obtain the volume of the injection site
782 for each animal, all slices containing the injections are imaged with an AxioObserver7
783 microscope (Zeiss, Germany) with a 5x /0.15 objective. Then for each slice a region of
784 interest delineating the injection site was drawn and its area was measured ImageJ software.

The total volume of injection is calculated as the sum of the area measured per slice of all the slices.

Calcium imaging analysis

GCaMP6f fluorescence signals are analysed in R environment with custom-built procedures in R3.5.2 and RStudio. Cells outlines are drawn manually using FIJI software and we extract mean grey values and (x, y) coordinates of each ROI. Let x(t) be the averaged intensity values of pixels in the ROI at time t for one cell. ΔF/F is obtained using y(t) = (x(t) - x0) / x0, where x0 is the mean value of the 50 % lowest values in the last 10 s. ΔF/F is then filtered with a Savitsky-Golay filter of order 3 on sliding windows of 7 samples (0.458 s). Binarized data are obtained by using M±2 SD cut-off for each cell; a cell is defined active if its ΔF/F is above this threshold, with mean (M) and standard deviation (SD). Recordings are 700-1000 frames long (around 1 min) and included 6-9 stimulations of cortical afferents, 5 responses (stimulations #2 to #7) are averaged to have a mean effect per cell. We distinguish responses from SPNs and other cell types of striatal neurones thank to a method we previously developed [58]. We are thus confident that almost all the analyzed cells are SPNs. For DMS, the average amplitude of all cells in naive condition is taken as the threshold to determine the LRA cells population. Importantly, we tried other methods such as k-means algorithm to sort the highly active cells. The different methods gave similar results and since there was no clear spatial reorganization in DMS, it appeared more accurate to use a threshold than the k-mean analysis. For DLS, cells are clustered using a k-means algorithm. The optimal number of groups (k=3.3 ± 0.1) is defined using the 'elbow method', by visual inspection of the plot, of the function to compute total within-cluster sum of squares with k varying from 1 to 10 and determining the bend in the elbow. The group containing the cells with the maximal

amplitude is defined as the LRA cell and contains M ± SEM % of cells in the slice (field of the slice). The cluster area is computed using the convex hull formed by these cells and the percentage of cluster area is calculated based on the convex hull described by the active cells on the edges of the field of view. Pairwise correlations are computed using Pearson's correlation between signals extracted on windows of 40 samples (2.6 s) centered on the time of the first maximal amplitudes of ΔF/F (peaks) detected on cells after stimulus. Examples of correlation matrices for one slice, representing the pairwise correlations between cells in LRA and non- LRA cells are given in Fig.3 i and j, left and mid. Co-active cells were analyzed as followed. The response time of one cell to a stimulus was taken as the time of its peak. A normalized cumulative count of the responses times for all cells was fitted by an exponential model y(t) = 1 - exp(-t / Tau). The global response time for one mouse was obtained by averaging Tau fitted on all stimuli.

Electrophysiology

Whole cell recordings are not analyzed if the input resistance was varying more than 20 % throughout the recordings. Electrophysiological properties of striatal neurons are quantified as follows. Input resistance is measured by repeated current injections (-20 pA, 500 ms) and frequency is measured for current steps +30 pA above AP threshold. The spike probability is measured as the occurrence of a single action potential induced by a single electrical stimulation of the cerebral cortex. Cortically-evoked single EPSP amplitude ranged from 1 mV to 30 mV. SPNs are held at their physiological membrane potential, in average -78.2±0.3 mV (n= 41) and there is no statistical difference in the holding membrane potentials between the different experimental conditions. We assess short-term dynamics of cortically-evoked EPSPs with trains of stimulation. We measure short-term temporal summation by

measuring the total amplitude of each EPSP (from baseline to the peak of the response) and normalize it to the amplitude of the first EPSP. In a subset of experiments combining different frequencies, the normalized amplitude corresponds to the ratio between the fourth EPSP of the train compared to the first one. We compare the effect for each EPSP of the train and the fourth one was chosen as a representative. Data analysis is carried out in Fitmaster (HEKA Elektronik, Germany).

Statistical analysis

The data are presented and plotted as values ± SEM. p values are represented by symbols using the following code: * for $p< 0.05$, ** for $p< 0.01$, *** for $p< 0.001$. Exact p values and statistical tests are stated in the figure legends or in the core of the manuscript. Statistical analysis is performed using Prism 5.0 (GraphPad, San Diego, USA) or R environment. The sample size for the different sets of data is mentioned in the text or in the respective figure legends. Normality of each data set is checked using D'Agostino and Pearson's test. Unless otherwise stated, all data sets are reported as mean ± SEM, with SEM standard error of the mean, and statistical significance was assessed using Student's t-test or Mann-Whitney's U-test and Wilcoxon's signed rank test for unpaired and paired data, respectively. One-way Anova is used to compare all the effects together in DMS and DLS between the different training conditions. Pearson correlation was used for relationship between cluster size and learning index. Two-way Anova followed by Bonferroni *post-hoc* test was used to compare different parameters (calcium dynamics, anatomical modifications) evolving throughout the training conditions, electrophysiological I/O curves, short-term plasticity and learning curve in different treatment conditions.

FIGURES LEGENDS

Figure 1: Motor skill learning induces a strong and specific reorganization of striatal networks

(**a**) Behavioral paradigm used to induce motor skill learning. Accelerated rotarod was used to perform early training, 10 trials in one day, or late training, 10 trials a day for 7 days. (**b**) Early training led to a significant improvement in the performance of the animals between the first and last trials (mean latency to fall was 21.2±3.4 s for the trial#1 and 70.1±6.3 s for trial#10) ($p< 0.0001$, n= 21 mice, paired t-test). Similarly, after late training, animals displayed significant improvement on the motor skill between the first and last day of training (mean latency to fall was 53.5±2.5 s for Day 1 and 97.9±5.6 s for Day 7) ($p< 0.0001$, n= 39 mice, paired t-test). (**c**) Left, wide field image of a representative infection of the DMS with GCaMP6f (scale bar: 200 µm). Right, two-photon microscopy image of striatal neurons expressing GCaMP6f. Stereotaxic injections of AAV-Syn-GCaMP6f allowed a reliable expression of the genetically encoded calcium dye in both DMS and DLS (scale bar: 20 µm). (**d**) Representative functional maps of striatal networks in DMS for naive, early, or late trained animals. The color code corresponds to the amplitude of responses (ΔF/F) with yellow color for lower amplitude and red/purple/brown for the highest ones. (**e**) Distribution and averaged amplitudes of the responses of all the SPNs in the recording field in the different training conditions in DMS. Early training induces a significant decrease of the overall activity compared to naive and late conditions ($p= 0.004$, One-way Anova, Naive, grey, 3.3±0.2, n= 11, early, orange, 2.6±0.2, n= 12 and late, blue, 3.9±0.4, n= 12). (**f**) Percentage of cells with the highest amplitude in the three training conditions for DMS. The percentage is significantly lower in early trained animals (orange, n= 12) compared to naive

(grey, n= 11) and late trained ones (blue, n= 12) (p= 0.0057, One-way Anova). (**g**) Correlation between the percentage of highly active cells and the learning index of the animals after early training (orange) or late training (blue) in DMS. There is a significant correlation for the early trained mice in DMS (r^2= 0.58, p= 0.0062, Pearson correlation) while no correlation was found in the late condition (r^2= 0.02, p= 0.6689) (**h**) Left panel represents the distances between the highly active cells in the three conditions in DMS. The distribution was similar in all conditions (p= 0.1604, One-way Anova). This shows that no specific spatial organization of activity is displayed in DMS. We thus measured the percentage of highly active cells in DMS and observed that here is a strong transitory decrease of the percentage of highly active cells in early condition (p= 0.0054, One-way Anova). (**i**) Representative functional maps of striatal networks in DLS for naive, early, or late trained animals. The color code corresponds to the amplitude of responses (ΔF/F) with yellow color for lower amplitude and red/purple/brown for the highest ones. (**j**) Distribution and averaged amplitude of the responses of all the SPNs in the recording field in the different training conditions in DLS. The training conditions did not affect the amplitude of responses (p= 0.7936, One-way Anova, Naive, 2.9±0.2, n= 9, early, 2.7±0.4, n= 9 and late, 2.7±0.3, n= 12). (**k**) Percentage of cells with the highest amplitude in the three training conditions for DLS. In average there is no significant difference in the percentage of highly active cells in naive (n=9 mice), early (n= 9) or late (n= 12) conditions (p= 0.5946, One-way Anova). (**l**) Correlation between the percentage of highly active cells and the learning index of the animals after early training (orange) or late training (blue) in DLS. There is a significant correlation for the late trained mice (r^2= 0.54, p=0.0063) while no correlation was found in the early condition (r^2= 0.02, p= 0.6998). (**m**) Left panel represents the distances between the highly active cells in the three conditions in DLS. There was a significant decrease in the distances throughout the learning

process in DLS ($p< 0.0001$, One-way Anova). This shows that clusters of activity are forming in DLS. We thus measured the cluster area (k-means clustering, see methods) and observed a strong and progressive decrease in the area of activation through learning ($p< 0.0001$, One-way Anova). * $p< 0.05$, ** $p< 0.01$, *** $p< 0.001$.

Figure 2: Long-lasting learning and associated DLS reorganization

(**a**) Pre-trained animals (blue) followed a first late training and, after a gap of 1-2 months, they were subjected to late training again (n= 5 mice). The pre-naive animals were trained only once after the 1-2 month gap**.** The performance curve shows that after the 1-2 month gap, pre-trained animals start with a higher performance compared to the beginning of the first training. Pre-naive animals (grey) displayed a significantly different learning curve than pre-trained animals ($F_{1,36}$=21.42, p= 0.0006, Two-way Anova). Whisker-box plot shows that mice displayed a robust motor skill improvement between Day 1 and Day 7 (p= 0.0061). After the 1-2 months gap, the animals started with a significantly better performance at Day 1' compared to Day 1 (p= 0.0046) and rapidly reached, on Day 7', a similar level performance than at Day 7 (p= 0.6914). (**b**) Two-photon calcium imaging was performed in pre-trained animals 1-2 months after the first session of training to assess the network state a long time after the motor skill formation. Representative activity maps for one pre-naive and one pre-trained animal. Below, bar graphs represent the mean amplitude of response and the cluster area in the DLS in pre-naive (n= 11) and pre-trained (n= 7) animals. Mean amplitude of response was not significantly different between pre-naive and pre-trained animals (pre-naive, 1.9±0.1, n= 11, pre-trained, 2.3±0.2, n= 7). Cluster area was significantly smaller in

pre-trained (19.7±5.7 %) compared to pre-naive (44.3±6.0 %) animals (p= 0.0116, t-test). * p< 0.05, ** p< 0.01, *** p< 0.001.

Figure 3: LRA cells have specific dynamic properties within the networks during motor skill learning

(**a**) Representative maps illustrating the reorganization between naive and early trained mice in DMS: in naive mice there are highly active (HA) cells (red) distributed in the whole field while, after early training, sparse learning related highly active cells (LRA cells) appeared like hot spots. (**b**) Representative maps illustrating the reorganization between naive and late trained mice in DLS: in naive mice there are highly active (HA) cells (red) distributed within a large area of the field and, after late training, learning related highly active cells (LRA cells, red) formed small clusters. (**c**) Evolution of the percentage of LRA cells (for early and late) or HA cells (for naive) between 5 and 20 Hz frequency stimulation. This percentage is significantly increasing for naive (p= 0.0137, n= 11, paired t-test) and late (p= 0.0091, n= 10) animals, while it remains stable for early trained animals (p= 0.3750, n= 8). (**d**) Difference in percentage of cluster area between 5 and 20 Hz. The percentage of HA area is significantly increasing for naive animals (p= 0.0066, n= 9) while LRA cluster area remains stable for early (p= 0.6451, n= 6) and late (p= 0.5714, n= 8) trained animals. (**e**) Amplitude of response for HA or LRA cells (red) versus non-HA or non-LRA cells (black) between 5 and 20 Hz stimulation frequency in naive (grey), early (orange) or late (blue) trained animals. There is a significant increase in the amplitude between 5 and 20 Hz for all the conditions (HA, p< 0.0001 for naive, LRA, p< 0.0001 for early and p= 0.0001 for late; non-HA, p= 0.001 for naive, non-LRA, p= 0.0039 for early and p= 0.002 for late). Right panel, plot of the ratio between 20

and 5 Hz amplitudes for the LRA and non- LRA cells ($p < 0.0001$, One-way Anova). There is no significant difference between HA and non-HA cells amplitude ratio for naive animals while the ratio is significantly higher in non-LRA cells compared to LRA cells after early and late training. (**f**) Amplitude of response for HA cells or LRA cells (red) versus non-HA or non-LRA cells (black) between 5 and 20 Hz stimulation frequencies in naive (grey), early (orange) or late (blue) trained animals. There is a significant increase in the amplitude between 5 and 20 Hz only for HA cells in naive mice ($p = 0.0111$, $n = 9$), the amplitude stays stable after early ($p = 0.1139$, $n = 6$) and late training ($p = 0.2791$, $n = 8$). For non-HA and non-LRA cells, we observed in all conditions a significant increase of the amplitude with the frequency ($p = 0.0039$ for naive, $p = 0.0313$ for early and $p = 0.0078$ for late)). Right panel, plot of the ratio between 20 and 5 Hz amplitude for the LRA and non-LRA cells ($p = 0.004$, One-way Anova). There is no significant difference between LRA (or HA) and non-LRA (or non-HA) cells amplitude change in naive animals and early trained mice while the ratio is significantly higher in non-LRA cells compared to LRA cells after late training. (**g-h**) Percentage of co-active cells in naive (grey), early (orange) or late (blue) trained animals. Representative distribution of the co-active cells for the different conditions (left panel) and cumulative percentage (middle panel). Right panel represents the Tau of the cumulative percentage for each condition, extracted from an exponential fit $y(t) = 1 - \exp(-t / Tau)$. All these graphs are represented for DMS (g) and DLS (h). There is a significant shift in the Tau from naive to late trained animals in DMS ($p=0.0293$, One-way Anova, $n = 10$ naive, $n = 8$ early and $n = 10$ late) and for DLS ($p = 0.0200$, One-way Anova, $n = 8$ naive, $n = 6$ early, $n = 7$ late). (**i**) Left, representative correlation matrix in LRA and HA cells versus non-LRA or non-HA cells in DMS in naive and early trained mice respectively. Right, mean of correlation coefficient extracted from half of the matrices without the diagonal. The LRA cells have a significant higher correlation coefficient than non-

LRA cells (p=0.0009 for Naive and Early, p=0.0002 for Late, paired t-test). (**j**) Left, representative correlation matrix in LRA versus non-LRA cells in DLS in naive and late trained animals. Right, mean of correlation coefficient extracted from half of the matrices without the diagonal. The correlation coefficient is similar between HA and non-HA cells for naive animals (p=0.1266) while LRA cells have a significant higher correlation coefficient than non-LRA cells after early and late training (p= 0.0182 and p= 0.0128, respectively, paired t-test). (**k-l**) Radar charts summarizing the evolution of network dynamics in the different training conditions, naive (grey), early (orange) and late (blue) for DMS (k) and DLS (l). The different parameters represented are (1) the percentage of DMS LRA cells or DLS LRA cluster area, (2) the mean amplitude of response (Ampl), (3) the Tau of the cumulative curve of co-active cells (Tau), (4) the ratio of the number of LRA cells between 5 and 20 Hz, (5) the ratio of the correlation coefficient between LRA and non-LRA cells, (6) the ratio of amplitude between 5 and 20 Hz for LRA cells and (7) for non-LRA cells. * p< 0.05, ** p< 0.01, *** p< 0.001.

Figure 4: DMS LRA cells have specific cortical input integration properties

(**a**) Experimental design, mice were injected with AAV-Syn-GCaMP6f and trained with early (for DMS) or late (for DLS) training. Two-photon calcium imaging was performed and LRA cells were detected live with custom-made procedures using FIJI and R software. When identified, patch clamp recordings were performed, targeting either LRA cells or non-LRA cells to compare their electrophysiological and cortical input integration properties. (**b**) Intrinsic electrophysiological properties of SPNs from DMS for LRA (red) or non-LRA (black) cells. There was no significant difference in the various measured parameters: RMP (-77.9±0.6 mV, n=11 for LRA, -77.8±0.5 mV; n=12 for non-LRA, p= 0.8068), Ri (190.3±27.9 MΩ

997 for LRA, 175.5±20.8 MΩ for non-LRA, p= 0.6754), rheobase (135.5±19.9 pA for LRA,
998 131.7±15.5 pA for non-LRA, p= 0.8809), AP threshold (-43.3±1.7 mV for LRA, -44.2±1.3 mV
999 for non-LRA, p= 0.6686) or frequency (10.9±0.8 Hz for LRA, 11.7±0.5 Hz for non-LRA, p=
1000 0.4439). (**c**) Intrinsic electrophysiological properties of SPNs from DLS for LRA (red) or non-
1001 LRA (black) cells. There was no significant difference in the various measured parameters: Ri
1002 (157.2±12.6 MΩ, n=11 for LRA, 155.6±18.8 MΩ, n=8 for non-LRA, p= 0.9396), rheobase
1003 (136.0±17.1 pA for LRA, 148.6±15.3 pA for non-LRA, p= 0.6108), frequency (10.2±1.1 Hz for
1004 LRA, 11.3±1.0 Hz for non-LRA, p= 0.4884) or AP threshold (-46.3±2.0 mV for LRA, -46.9±2.7
1005 mV for non-LRA, p= 0.8487). There was a significant difference for RMP (-79.2±0.3 mV, n=11
1006 for LRA, -77.9±0.5 mV, n=8 for non-LRA, p= 0.0282). (**d**) Representative curves of the spiking
1007 probability for LRA and non-LRA cells in DMS. The quantification on the right shows that LRA
1008 cells have a significantly higher spiking probability than non-LRA cells (p= 0.0038, n= 7
1009 LRA/non-LRA pairs). (**e**) Representative curves of input/output subthreshold response of LRA
1010 and non-LRA cells in response to a single stimulation, with increasing stimulation intensity.
1011 Bar graph showing the paired EPSP amplitudes for LRA and non-LRA cells with the same
1012 intensity of stimulation. The amplitudes were higher in LRA cells compared to non-LRA cells
1013 (p= 0.0232, n= 8 pairs, paired t-test). (**f**) Top: representative 20 Hz trains of EPSPs recorded in
1014 non-LRA (black) or LRA cells (red). Bottom: temporal summations of EPSPs in SPNs after 20
1015 Hz cortical electrical stimulation in non-LRA cells (black) or LRA cells (red). In DMS, non-LRA
1016 cells display a significant summation during a 20Hz stimulation train while LRA cells do not
1017 ($F_{1,50}$=12.12, p= 0.0048, n= 8 pairs, Two-way Anova). Bottom right, summary of the temporal
1018 summation, ratio of the 4^{th} EPSP compared to the first one for the different frequencies. This
1019 absence of summation of cortical inputs in LRA cells is observed for different frequencies
1020 compared to non-LRA cells (p= 0.0033, n= 8 pairs, Two-way Anova). (**g**) Representative

curves of the spiking probability for LRA and non-LRA cells in DLS. The quantification on the right shows that there is no significant difference between LRA and non-LRA cells spiking probability (p= 1.0, n= 6 LRA/non-LRA pairs). (**h**) Representative curve of input/output response of LRA and non-LRA cells in response to a single stimulation, with increasing stimulation intensity. Bar graph showing the paired EPSP amplitudes for LRA and non-LRA cells with the same intensity of stimulation. The amplitudes were not significantly different for LRA and non-LRA cells (p= 0.4475, n= 8 pairs). (**i**) Top: representative 20 Hz trains of EPSPs recorded in non-LRA (black) or LRA cells (red). Bottom left: temporal summations of EPSPs in SPNs after 20 Hz cortical electrical stimulation in non-LRA cells (black) or LRA cells (red). Both LRA and non-LRA cells display a significant summation during a 20 Hz stimulation with no significant difference ($F_{1,69}$=0.00, p= 0.9611, n= 8 pairs, Two-way Anova). Bottom right: summary of the temporal summation, ratio of the 4th EPSP compared to the first one for the different frequencies. Similar summations between LRA and non-LRA cells were observed for different frequencies (p= 0.3537, Two-way Anova). * p< 0.05, ** p< 0.01, *** p< 0.001.

Figure 5: Motor skill learning induces anatomical plasticity of DLS corticostriatal projections

(**a**) Experimental design of the Cholera Toxin B (CTB) injections in the striatum. CTB-A_{555} was injected in DMS and CTB-A_{488} was injected in DLS. (**b**) Schematic localization and wide field representative images of the injection sites in DMS (top, red) and DLS (bottom, green). Blue is DAPI labelling (scale bars: 1 mm). Insets are the pictures shown in c. (**c**) Confocal images of neurons in cingulate cortex (red) and somatosensory cortex (green) labelled with CTB (scale bars: 20 µm). (**d**) Quantification of the density of labelled cortical neurons in the cingulate

cortex after injection of CTB-A_{555} in DMS. We quantified the total density of cortical cells in the whole cortical area per mm^2 (left) or considering the different layers independently (right) for naive (n= 4 mice), early (n= 5 mice) or late (n= 5 mice) trained animals, on 3 slices (200 µm apart) per animal. There is no significant difference in the number of cortical cells in the different training conditions, neither if we consider all the layers together (left, one-way Anova, p=0.8836) nor the different layers separately (right, $F_{2,117}$= 0.94, p= 0.3640, Two-way Anova). (**e**) Quantification of the density of labelled cortical neurons in the somatosensory cortex after injection of CTB-A_{488} in DLS. We quantified the total density of cortical cells in the whole cortical area per mm^2 (left) or considering the different layers independently (right) for naive (n= 5 mice), early (n= 4 mice) or late (n= 4 mice) trained animals. The training did not induce a significant effect on the total number of presynaptic cells overall (one-way Anova, p= 0.0625) but induced a significant increase of the neuronal density from somatosensory cortex projecting to DLS after late training (p< 0.05). Considering the layers independently, we observed a significant increase in the density of somatosensory cortical neurons after early and late training in layer 2/3 and layer 5 ($F_{2,105}$= 8.12, p< 0.0001, Two-way Anova, Bonferroni post-test). There is no effect of training on layer 6 projections and layer 4 is not represented since the number of labelled cells was negligible. * p< 0.05, ** p< 0.01, *** p< 0.001.

Figure 6: Silencing LRA cells impairs motor skill learning

(**a**) Experimental design, animals were injected with AAV-cfos-ERT2-Cre-ERT2-PEST with either AAV-DIO-mCherry for control animals or AAV-DIO-hM4Di-mCherry for silencing experiments in DMS. Tamoxifen was delivered right after early training (Day 1) and 2 weeks later CNO was injected at the beginning of the test Day 15. (**b**) Confocal images of the SPNs

1069 expressing either mCherry or hM4Di-mCherry two weeks after tamoxifen delivery (scale
1070 bars: 50 µm). (**c**) Training curves of control mice (mCherry, black, n= 8 mice) and tested
1071 animals (hM4Di, purple, n= 8 mice) for Day 1 training and Day 15 training. There is no
1072 significant difference between the two groups for Day 1 training ($F_{1,140}$= 0.04, p= 0.7699,
1073 Two-way Anova). On the contrary, on Day 15, the silencing of LRA cells triggers a strong
1074 decrease of the performance of the hM4Di group compared to the mCherry control group
1075 ($F_{1,133}$= 11.88, p< 0.0001, Two-way Anova). (**d**) Performance of the animals on Day 1 (top)
1076 and Day 15 (bottom) for mCherry (black) and hM4Di (purple) groups. On Day 1, there was a
1077 significant improvement in the performance between trial 1 and trial 10 for both groups (p=
1078 0.0007 for mCherry group and p= 0.0082 for hM4Di group, paired t-test). Right panel, the
1079 learning index was not different between the two groups (p= 0.9571, t-test). On Day 15, the
1080 mCherry group still shows significant improvements in their performance between trial 1
1081 and trial 10 (p= 0.0078, paired test) while the hM4Di group does not display any
1082 improvement (p= 0.4609, paired test). Right panel, the learning index is significantly
1083 different between the two groups (p= 0.0168, t-test). (**e**) Experimental design, animals were
1084 injected with AAV-cfos-ERT2-Cre-ERT2-PEST with either AAV-flex-mCherry for control
1085 animals or AAV-flex-hM4Di-mCherry for silencing experiments in DLS. Tamoxifen was
1086 delivered right after late training (From Day 1 to Day 7) and 2 weeks later CNO was injected
1087 at the beginning of test Day 21. (**f**) Confocal images of the SPNs expressing either mCherry or
1088 hM4Di-mCherry two weeks after tamoxifen delivery (scale bars: 50 µm). (**g**) Training curves
1089 of control mice (mCherry, black, n= 11) and tested animals (hM4Di, purple, n= 8) for Day 1 to
1090 Day7 training and Day 21 training. There was no significant difference between the two
1091 groups for the training on Days 1-7 ($F_{1,154}$= 0.25, p= 0.4623, Two-way Anova). On the
1092 contrary, on Day 21, the silencing of LRA cells triggers a strong decrease of the performance

of hM4Di group compared to mCherry one ($F_{1,165}$=15.57, p< 0.0001, Two-way Anova). (**h**) Performance of the animals for Day 1 to Day 7 (top) and Day 21 (bottom) for mCherry (black) and hM4Di (purple) groups. For Days 1-7, there was a significant improvement in the performance between Day 1 and Day 7 for both groups (p< 0.0001 for mCherry group and p< 0.0001 for hM4Di group). Right panel, the learning index was not different between the two groups (p= 0.4136). On Day 21, the mCherry group still shows significant increase of their performance between Day 1 and Day 7 (p= 0.0098, paired test) while hM4Di displays a significant decrease in their performance (p= 0.0049, paired test). Right panel, the learning index is significantly lower for hM4Di group compared to mCherry group (p< 0.0001, t-test). * p< 0.05, ** p< 0.01, *** p< 0.001.

Figure 7: Diagram of striatal reorganization during motor skill learning

In DMS, in naive condition, most of the striatal cells are activated by cingulate cortex inputs with similar synaptic weight. After early training, there is an emergence of LRA cells (red cells) which are more efficiently recruited by cortical inputs since they have a stronger synaptic weight compared to non-LRA cells (black). After silencing of LRA cells with CNO (purple crosses), mice are not able to learn the motor skill anymore. In DLS, in naive condition, most of the striatal cells are activated by somatosensory cortex inputs. After late training, spatially restricted LRA cells (red cells) appear. This is associated with a larger number of presynaptic cells in somatosensory cortex. One hypothesis is that these extra cortical cells would converge more on LRA cells than non-LRA cells (black).

ADDITIONAL INFORMATION SECTION

Competing interests:

The authors declare that they have no competing financial interest and conflict of interest.

Author contribution:

EF conceived the project; EF and SA supervised the study; EF, SA, NB, GZ and FA designed experiments; NB, GZ, FA and EF performed experiments; NB, GZ, FA, GB, NT and EF performed analysis; EF, FS and NT acquired funding; EF, NB and GZ wrote the manuscript; all authors read and edited the manuscript.

Acknowledgments:

The authors thank M. Albrieux, M. Cazorla, C. Kellendonk, A.S. Nicot and D. Robbe for careful reading of the manuscript and helpful comments. The authors would like to thank K. Deisseroth for making available the AAV-cFos-ERT2-Cre-ERT2-PEST-no WPRE virus, the Photonic Imaging Center, PIC-GIN facility (GIS-IBiSA ISdV, GIN) and Y. Saoudi for help with image acquisitions and the GIN animal facility for mouse care.

This work was supported by grants from Neuroglia (EF), University of Grenoble Alpes Data Institute (NT and EF), CNRS (EF, GB, SA, NT), University Grenoble Alpes (FA, GB, NT and SA), Agence Nationale de la Recherche: ANR-15-IDEX-02 NeuroCoG in the framework of the *investissements d'Avenir* program (PhD fellowship for N.B.; EF and SA) and ANR-18-CE16-

0009-01 AXYON (FS), Fondation pour la Recherche Médicale (FRM, DEI20151234418, FS), Fondation pour la Recherche sur le Cerveau (FRC, FS), Fondation Bettencourt Schueller (FS), and AGEMED program from INSERM (FS). The laboratory is member of the Grenoble Center of Excellence in Neurodegeneration (GREEN).

REFERENCES

1 Yin, H. H. & Knowlton, B. J. The role of the basal ganglia in habit formation. *Nat Rev Neurosci* **7**, 464-476, doi:10.1038/nrn1919 (2006).

2 Graybiel, A. M. & Grafton, S. T. The striatum: where skills and habits meet. *Cold Spring Harb Perspect Biol* **7**, a021691, doi:10.1101/cshperspect.a021691 (2015).

3 Redgrave, P., Vautrelle, N. & Reynolds, J. N. Functional properties of the basal ganglia's re-entrant loop architecture: selection and reinforcement. *Neuroscience* **198**, 138-151, doi:10.1016/j.neuroscience.2011.07.060 (2011).

4 Gruber, A. J. & McDonald, R. J. Context, emotion, and the strategic pursuit of goals: interactions among multiple brain systems controlling motivated behavior. *Front Behav Neurosci* **6**, 50, doi:10.3389/fnbeh.2012.00050 (2012).

5 Yin, H. H., Knowlton, B. J. & Balleine, B. W. Inactivation of dorsolateral striatum enhances sensitivity to changes in the action-outcome contingency in instrumental conditioning. *Behav Brain Res* **166**, 189-196, doi:10.1016/j.bbr.2005.07.012 (2006).

6 Packard, M. G. & McGaugh, J. L. Inactivation of hippocampus or caudate nucleus with lidocaine differentially affects expression of place and response learning. *Neurobiol Learn Mem* **65**, 65-72, doi:10.1006/nlme.1996.0007 (1996).

7 Yin, H. H., Knowlton, B. J. & Balleine, B. W. Lesions of dorsolateral striatum preserve outcome expectancy but disrupt habit formation in instrumental learning. *Eur J Neurosci* **19**, 181-189, doi:10.1111/j.1460-9568.2004.03095.x (2004).

8 Durieux, P. F., Schiffmann, S. N. & de Kerchove d'Exaerde, A. Differential regulation of motor control and response to dopaminergic drugs by D1R and D2R neurons in distinct dorsal striatum subregions. *EMBO J* **31**, 640-653, doi:10.1038/emboj.2011.400 (2012).

9 Costa, R. M., Cohen, D. & Nicolelis, M. A. Differential corticostriatal plasticity during fast and slow motor skill learning in mice. *Curr Biol* **14**, 1124-1134, doi:10.1016/j.cub.2004.06.053 (2004).

10 Yin, H. H. *et al.* Dynamic reorganization of striatal circuits during the acquisition and consolidation of a skill. *Nat Neurosci* **12**, 333-341, doi:10.1038/nn.2261 (2009).

11 Thorn, C. A., Atallah, H., Howe, M. & Graybiel, A. M. Differential dynamics of activity changes in dorsolateral and dorsomedial striatal loops during learning. *Neuron* **66**, 781-795, doi:10.1016/j.neuron.2010.04.036 (2010).

12 Kupferschmidt, D. A., Juczewski, K., Cui, G., Johnson, K. A. & Lovinger, D. M. Parallel, but Dissociable, Processing in Discrete Corticostriatal Inputs Encodes Skill Learning. *Neuron* **96**, 476-489 e475, doi:10.1016/j.neuron.2017.09.040 (2017).

13 Smith, K. S. & Graybiel, A. M. A dual operator view of habitual behavior reflecting cortical and striatal dynamics. *Neuron* **79**, 361-374, doi:10.1016/j.neuron.2013.05.038 (2013).

14 Yang, G., Pan, F. & Gan, W. B. Stably maintained dendritic spines are associated with lifelong memories. *Nature* **462**, 920-924, doi:10.1038/nature08577 (2009).

15 Cao, V. Y. *et al.* Motor Learning Consolidates Arc-Expressing Neuronal Ensembles in Secondary Motor Cortex. *Neuron* **86**, 1385-1392, doi:10.1016/j.neuron.2015.05.022 (2015).

16 Scholz, J., Niibori, Y., P, W. F. & J, P. L. Rotarod training in mice is associated with changes in brain structure observable with multimodal MRI. *Neuroimage* **107**, 182-189, doi:10.1016/j.neuroimage.2014.12.003 (2015).

17 Buitrago, M. M., Schulz, J. B., Dichgans, J. & Luft, A. R. Short and long-term motor skill learning in an accelerated rotarod training paradigm. *Neurobiol Learn Mem* **81**, 211-216, doi:10.1016/j.nlm.2004.01.001 (2004).

18 Fino, E., Vandecasteele, M., Perez, S., Saudou, F. & Venance, L. Region-specific and state-dependent action of striatal GABAergic interneurons. *Nat Commun* **9**, 3339, doi:10.1038/s41467-018-05847-5 (2018).

19 Melzer, S. *et al.* Distinct Corticostriatal GABAergic Neurons Modulate Striatal Output Neurons and Motor Activity. *Cell Rep* **19**, 1045-1055, doi:10.1016/j.celrep.2017.04.024 (2017).
20 Mandelbaum, G. *et al.* Distinct Cortical-Thalamic-Striatal Circuits through the Parafascicular Nucleus. *Neuron* **102**, 636-652 e637, doi:10.1016/j.neuron.2019.02.035 (2019).
21 Thomson, A. M. Neocortical layer 6, a review. *Front Neuroanat* **4**, 13, doi:10.3389/fnana.2010.00013 (2010).
22 Josselyn, S. A., Kohler, S. & Frankland, P. W. Finding the engram. *Nat Rev Neurosci* **16**, 521-534, doi:10.1038/nrn4000 (2015).
23 DeNardo, L. & Luo, L. Genetic strategies to access activated neurons. *Curr Opin Neurobiol* **45**, 121-129, doi:10.1016/j.conb.2017.05.014 (2017).
24 Tonegawa, S., Morrissey, M. D. & Kitamura, T. The role of engram cells in the systems consolidation of memory. *Nat Rev Neurosci* **19**, 485-498, doi:10.1038/s41583-018-0031-2 (2018).
25 Giannotti, G., Heinsbroek, J. A., Yue, A. J., Deisseroth, K. & Peters, J. Prefrontal cortex neuronal ensembles encoding fear drive fear expression during long-term memory retrieval. *Sci Rep* **9**, 10709, doi:10.1038/s41598-019-47095-7 (2019).
26 Bureau, G., Carrier, M., Lebel, M. & Cyr, M. Intrastriatal inhibition of extracellular signal-regulated kinases impaired the consolidation phase of motor skill learning. *Neurobiol Learn Mem* **94**, 107-115, doi:10.1016/j.nlm.2010.04.008 (2010).
27 Wachter, T., Lungu, O. V., Liu, T., Willingham, D. T. & Ashe, J. Differential effect of reward and punishment on procedural learning. *J Neurosci* **29**, 436-443, doi:10.1523/JNEUROSCI.4132-08.2009 (2009).
28 Gremel, C. M. & Costa, R. M. Orbitofrontal and striatal circuits dynamically encode the shift between goal-directed and habitual actions. *Nat Commun* **4**, 2264, doi:10.1038/ncomms3264 (2013).
29 Vandaele, Y. *et al.* Distinct recruitment of dorsomedial and dorsolateral striatum erodes with extended training. *Elife* **8**, doi:10.7554/eLife.49536 (2019).
30 Thorn, C. A. & Graybiel, A. M. Differential entrainment and learning-related dynamics of spike and local field potential activity in the sensorimotor and associative striatum. *J Neurosci* **34**, 2845-2859, doi:10.1523/JNEUROSCI.1782-13.2014 (2014).
31 Nonomura, S. *et al.* Monitoring and Updating of Action Selection for Goal-Directed Behavior through the Striatal Direct and Indirect Pathways. *Neuron* **99**, 1302-1314 e1305, doi:10.1016/j.neuron.2018.08.002 (2018).
32 Stubbendorff, C., Molano-Mazon, M., Young, A. M. J. & Gerdjikov, T. V. Synchronization in the prefrontal-striatal circuit tracks behavioural choice in a go-no-go task in rats. *Eur J Neurosci* **49**, 701-711, doi:10.1111/ejn.13905 (2019).
33 Gong, W. K., Ni, J., Yu, L. F., Wang, L. & Huang, Z. L. Temporal dynamics of Arc/Arg3.1 expression in the dorsal striatum during acquisition and consolidation of a motor skill in mice. *Neurobiol Learn Mem* **168**, 107156, doi:10.1016/j.nlm.2019.107156 (2020).
34 Koralek, A. C., Jin, X., Long, J. D., 2nd, Costa, R. M. & Carmena, J. M. Corticostriatal plasticity is necessary for learning intentional neuroprosthetic skills. *Nature* **483**, 331-335, doi:10.1038/nature10845 (2012).
35 Rothwell, P. E. *et al.* Input- and Output-Specific Regulation of Serial Order Performance by Corticostriatal Circuits. *Neuron* **88**, 345-356, doi:10.1016/j.neuron.2015.09.035 (2015).
36 Di Filippo, M. *et al.* Short-term and long-term plasticity at corticostriatal synapses: implications for learning and memory. *Behav Brain Res* **199**, 108-118, doi:10.1016/j.bbr.2008.09.025 (2009).
37 Lerner, T. N. & Kreitzer, A. C. Neuromodulatory control of striatal plasticity and behavior. *Curr Opin Neurobiol* **21**, 322-327, doi:10.1016/j.conb.2011.01.005 (2011).
38 Holtmaat, A. & Caroni, P. Functional and structural underpinnings of neuronal assembly formation in learning. *Nat Neurosci* **19**, 1553-1562, doi:10.1038/nn.4418 (2016).

39 Chklovskii, D. B., Mel, B. W. & Svoboda, K. Cortical rewiring and information storage. *Nature* **431**, 782-788, doi:10.1038/nature03012 (2004).

40 Florence, S. L., Taub, H. B. & Kaas, J. H. Large-scale sprouting of cortical connections after peripheral injury in adult macaque monkeys. *Science* **282**, 1117-1121, doi:10.1126/science.282.5391.1117 (1998).

41 Zatorre, R. J., Fields, R. D. & Johansen-Berg, H. Plasticity in gray and white: neuroimaging changes in brain structure during learning. *Nat Neurosci* **15**, 528-536, doi:10.1038/nn.3045 (2012).

42 Scholz, J., Klein, M. C., Behrens, T. E. & Johansen-Berg, H. Training induces changes in white-matter architecture. *Nat Neurosci* **12**, 1370-1371, doi:10.1038/nn.2412 (2009).

43 van Kerkoerle, T., Marik, S. A., Meyer Zum Alten Borgloh, S. & Gilbert, C. D. Axonal plasticity associated with perceptual learning in adult macaque primary visual cortex. *Proc Natl Acad Sci U S A* **115**, 10464-10469, doi:10.1073/pnas.1812932115 (2018).

44 Sampaio-Baptista, C. *et al.* Motor skill learning induces changes in white matter microstructure and myelination. *J Neurosci* **33**, 19499-19503, doi:10.1523/JNEUROSCI.3048-13.2013 (2013).

45 Boele, H. J., Koekkoek, S. K., De Zeeuw, C. I. & Ruigrok, T. J. Axonal sprouting and formation of terminals in the adult cerebellum during associative motor learning. *J Neurosci* **33**, 17897-17907, doi:10.1523/JNEUROSCI.0511-13.2013 (2013).

46 Hooks, B. M. *et al.* Topographic precision in sensory and motor corticostriatal projections varies across cell type and cortical area. *Nat Commun* **9**, 3549, doi:10.1038/s41467-018-05780-7 (2018).

47 Yamashita, T. *et al.* Diverse Long-Range Axonal Projections of Excitatory Layer 2/3 Neurons in Mouse Barrel Cortex. *Front Neuroanat* **12**, 33, doi:10.3389/fnana.2018.00033 (2018).

48 Hayashi-Takagi, A. *et al.* Labelling and optical erasure of synaptic memory traces in the motor cortex. *Nature* **525**, 333-338, doi:10.1038/nature15257 (2015).

49 Kawai, R. *et al.* Motor cortex is required for learning but not for executing a motor skill. *Neuron* **86**, 800-812, doi:10.1016/j.neuron.2015.03.024 (2015).

50 Klaus, A. *et al.* The Spatiotemporal Organization of the Striatum Encodes Action Space. *Neuron* **96**, 949, doi:10.1016/j.neuron.2017.10.031 (2017).

51 Barbera, G. *et al.* Spatially Compact Neural Clusters in the Dorsal Striatum Encode Locomotion Relevant Information. *Neuron* **92**, 202-213, doi:10.1016/j.neuron.2016.08.037 (2016).

52 Parker, J. G. *et al.* Diametric neural ensemble dynamics in parkinsonian and dyskinetic states. *Nature* **557**, 177-182, doi:10.1038/s41586-018-0090-6 (2018).

53 Jin, X. & Costa, R. M. Start/stop signals emerge in nigrostriatal circuits during sequence learning. *Nature* **466**, 457-462, doi:10.1038/nature09263 (2010).

54 Markowitz, J. E. *et al.* The Striatum Organizes 3D Behavior via Moment-to-Moment Action Selection. *Cell* **174**, 44-58 e17, doi:10.1016/j.cell.2018.04.019 (2018).

55 Josselyn, S. A. & Tonegawa, S. Memory engrams: Recalling the past and imagining the future. *Science* **367**, doi:10.1126/science.aaw4325 (2020).

56 Fino, E., Glowinski, J. & Venance, L. Bidirectional activity-dependent plasticity at corticostriatal synapses. *J Neurosci* **25**, 11279-11287, doi:10.1523/JNEUROSCI.4476-05.2005 (2005).

57 Fino, E. & Venance, L. Spike-timing dependent plasticity in striatal interneurons. *Neuropharmacology* **60**, 780-788, doi:10.1016/j.neuropharm.2011.01.023 (2011).

58 Becq G, B. N., Tremblay N, Appaix F, Zalcman G, Fino E and Achard S. Classification de types de neurones à partir de signaux calciques. *XXVIIème colloque du groupement de recherche en traitement du signal et de l'image (GRETSI)* (2019).

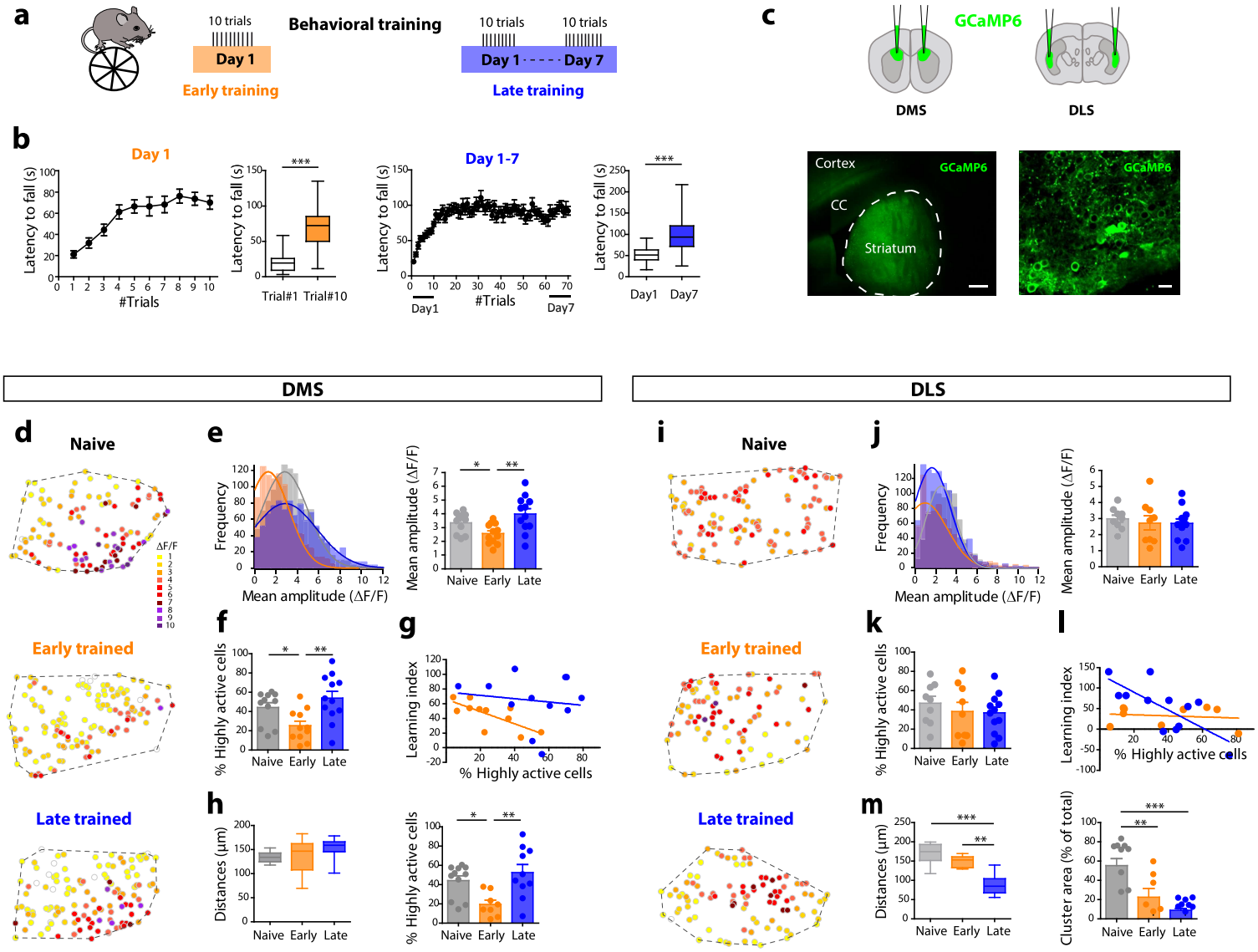
a
10 trials
Day 1
Early training
Behavioral training
10 trials
10 trials
Day 1 - - - - - Day 7
Late training
c
GCaMP6
DMS
DLS
b
Day 1
Latency to fall (s)
#Trials
Trial#1 Trial#10
***
Day 1-7
Day1
Day7
Cortex
GCaMP6
CC
Striatum
DMS
DLS
d
Naive
ΔF/F
Early trained
Late trained
e
Frequency
Mean amplitude (ΔF/F)
Naive Early Late
f
% Highly active cells
g
Learning index
% Highly active cells
h
Distances (μm)
i
j
k
l
m
Cluster area (% of total)

Figure2

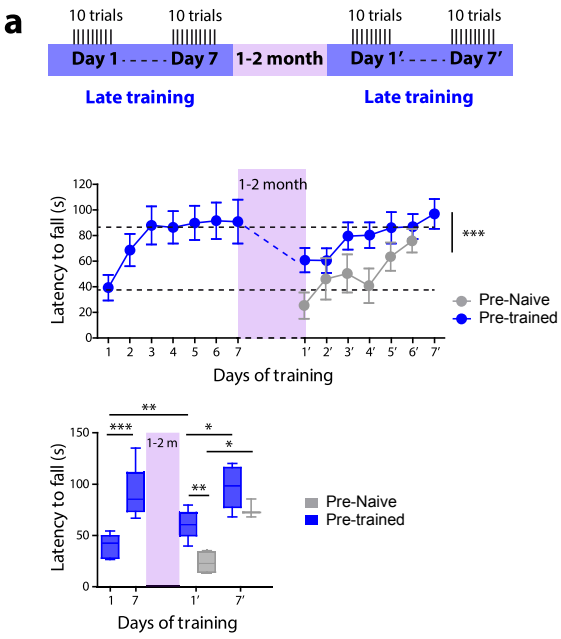
a
10 trials
10 trials
10 trials
10 trials
Day 1
Day 7
1-2 month
Day 1′
Day 7′
Late training
Late training
1-2 month
Latency to fall (s)
***
Pre-Naive
Pre-trained
Days of training
**
***
*
*
1-2 m
**
Latency to fall (s)
Pre-Naive
Pre-trained
Days of training

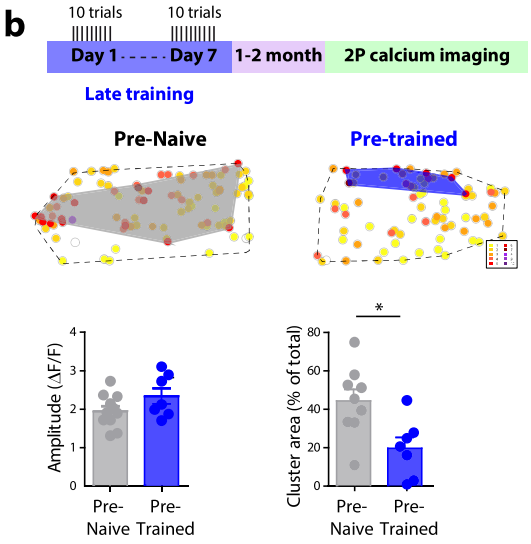
b
10 trials
10 trials
Day 1
Day 7
1-2 month
2P calcium imaging
Late training
Pre-Naive
Pre-trained
*
Amplitude (ΔF/F)
Cluster area (% of total)
Pre-
Naive
Pre-
Trained
Pre-
Naive
Pre-
Trained

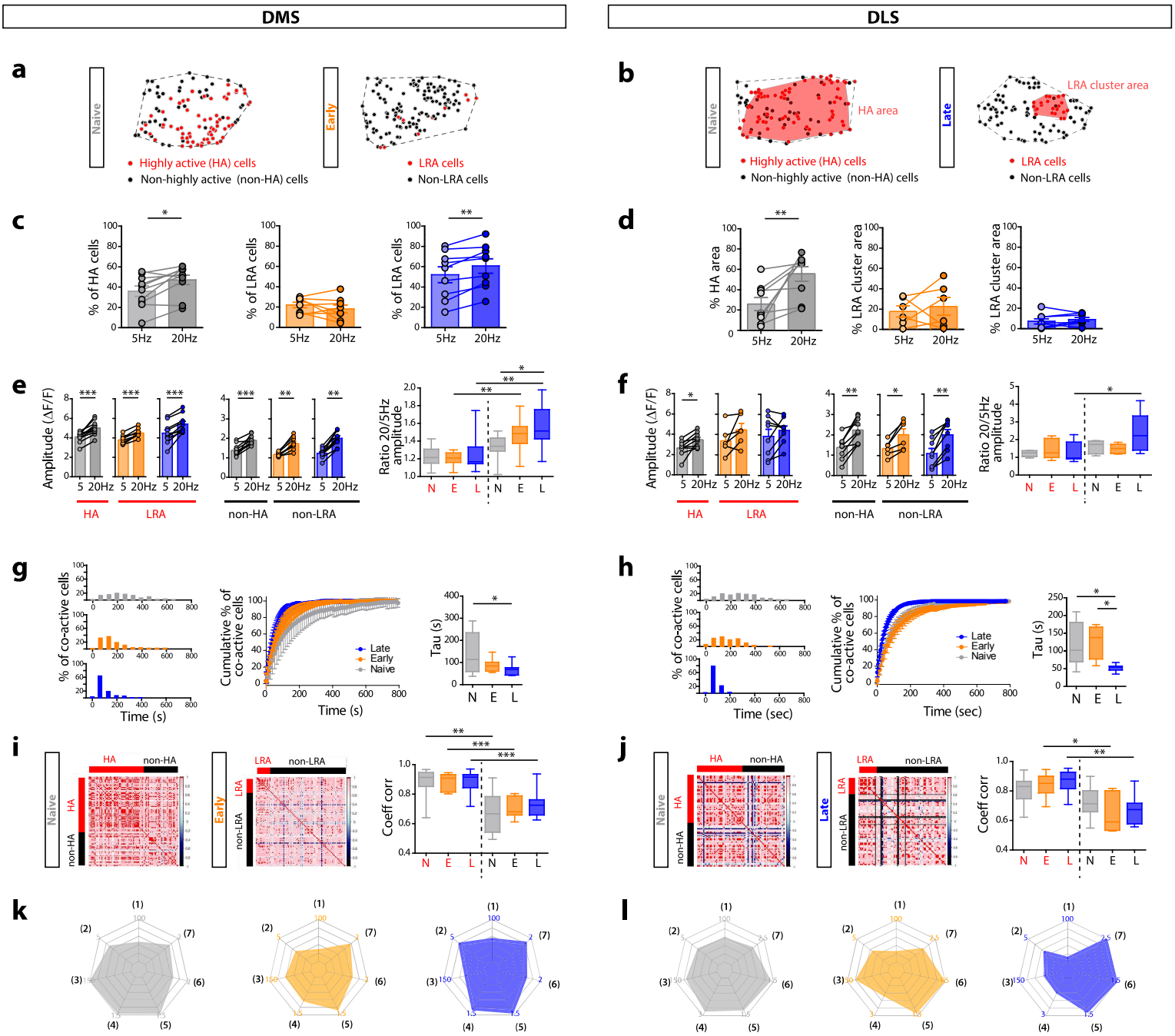
DMS
DLS
a
Naive
Early
Highly active (HA) cells
Non-highly active (non-HA) cells
LRA cells
Non-LRA cells
b
Naive
HA area
Late
LRA cluster area
Highly active (HA) cells
Non-highly active (non-HA) cells
LRA cells
Non-LRA cells
c
% of HA cells
% of LRA cells
% of LRA cells
5Hz
20Hz
d
% HA area
% LRA cluster area
% LRA cluster area
e
Amplitude (ΔF/F)
HA
LRA
non-HA
non-LRA
Ratio 20/5Hz amplitude
N E L N E L
f
Amplitude (ΔF/F)
Ratio 20/5Hz amplitude
g
% of co-active cells
Time (s)
Cumulative % of co-active cells
Late
Early
Naive
Tau (s)
h
% of co-active cells
Time (sec)
Cumulative % of co-active cells
Tau (s)
i
Naive
Early
HA
non-HA
LRA
non-LRA
Coeff corr
j
Naive
Late
Coeff corr
k
l

Figure 4

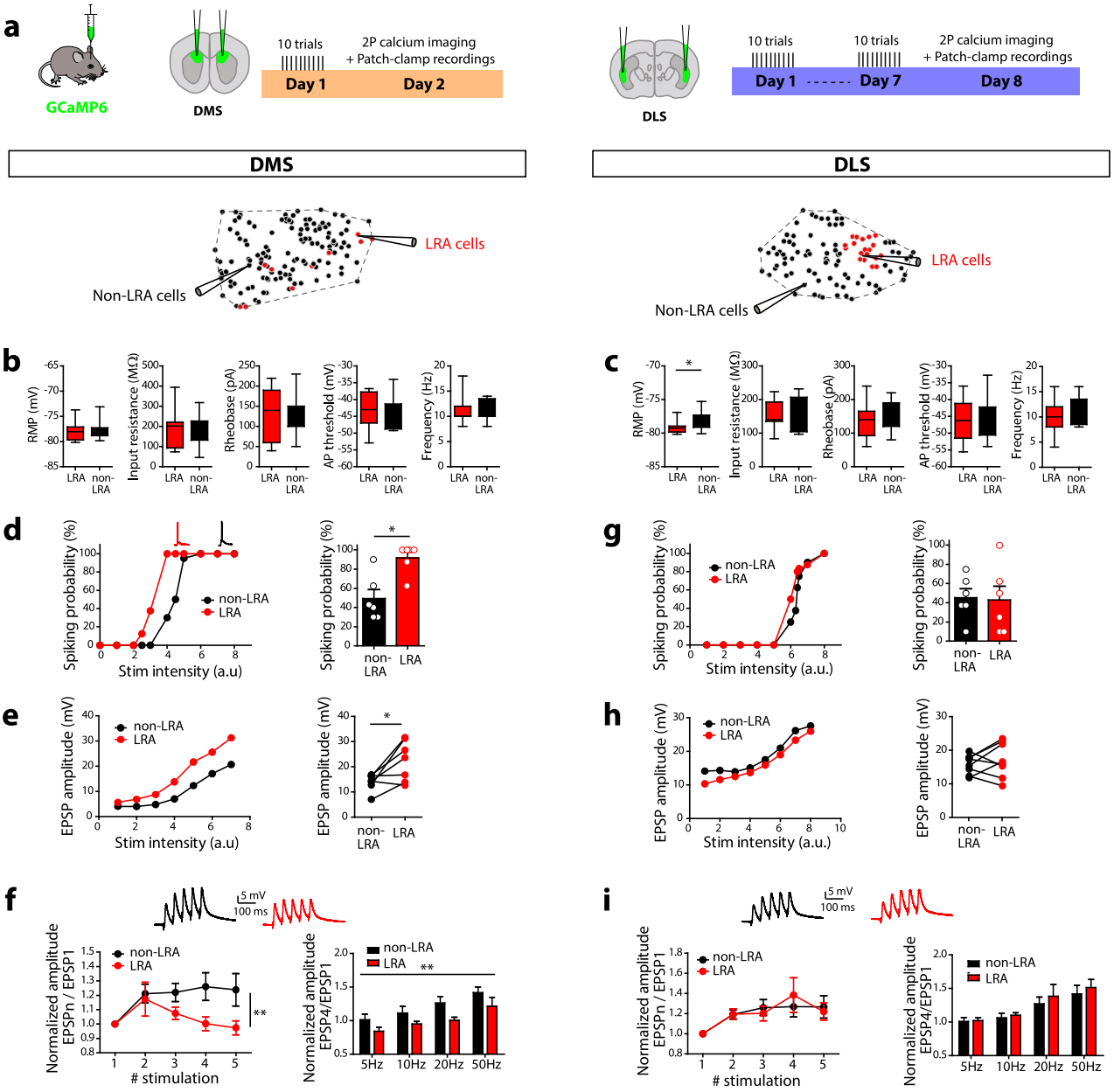
a
GCaMP6
DMS
10 trials
2P calcium imaging
+ Patch-clamp recordings
Day 1
Day 2
DLS
10 trials
10 trials
2P calcium imaging
+ Patch-clamp recordings
Day 1
Day 7
Day 8
DMS
DLS
LRA cells
Non-LRA cells
LRA cells
Non-LRA cells
b
c
RMP (mV)
Input resistance (MΩ)
Rheobase (pA)
AP threshold (mV)
Frequency (Hz)
LRA
non-LRA
d
g
Spiking probability (%)
Stim intensity (a.u)
non-LRA
LRA
e
h
EPSP amplitude (mV)
f
i
5 mV
100 ms
Normalized amplitude
EPSPn / EPSP1
stimulation
EPSP4/EPSP1
5Hz
10Hz
20Hz
50Hz

Figure 5

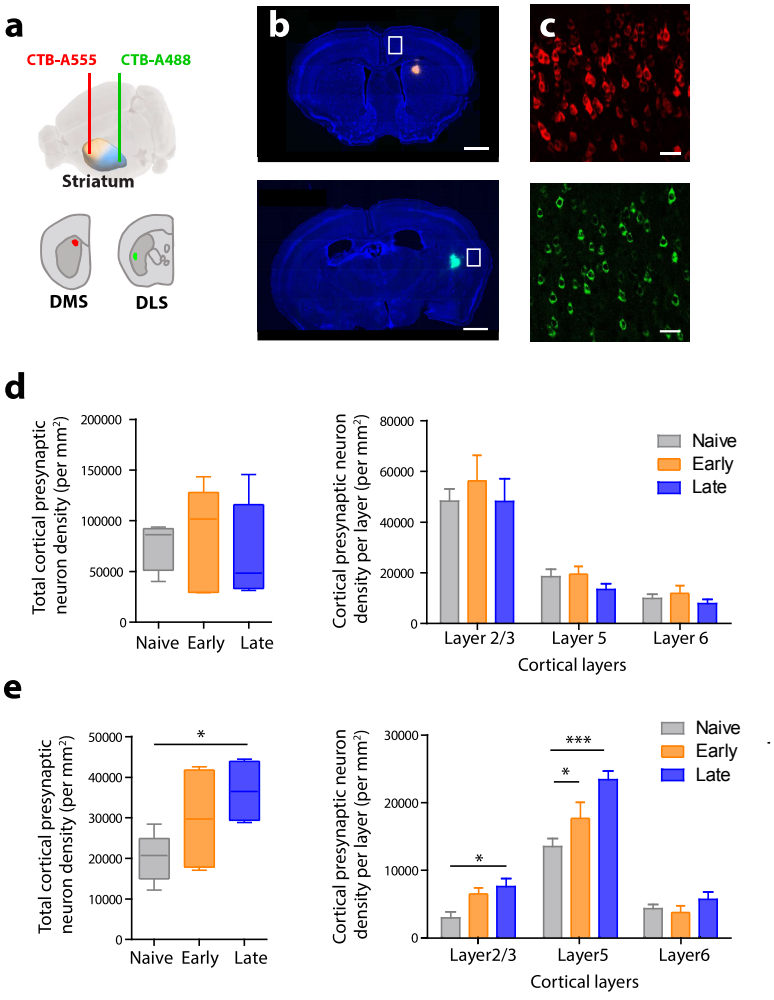
a
CTB-A555
CTB-A488
Striatum
DMS
DLS
b
c
d
Total cortical presynaptic neuron density (per mm²)
200000
150000
100000
50000
0
Naive Early Late
Cortical presynaptic neuron density per layer (per mm²)
80000
60000
40000
20000
0
Naive
Early
Late
Layer 2/3
Layer 5
Layer 6
Cortical layers
e
Total cortical presynaptic neuron density (per mm²)
50000
40000
30000
20000
10000
0
*
Naive Early Late
Cortical presynaptic neuron density per layer (per mm²)
30000
20000
10000
0
*
***
*
Naive
Early
Late
Layer2/3
Layer5
Layer6
Cortical layers

Figure 6

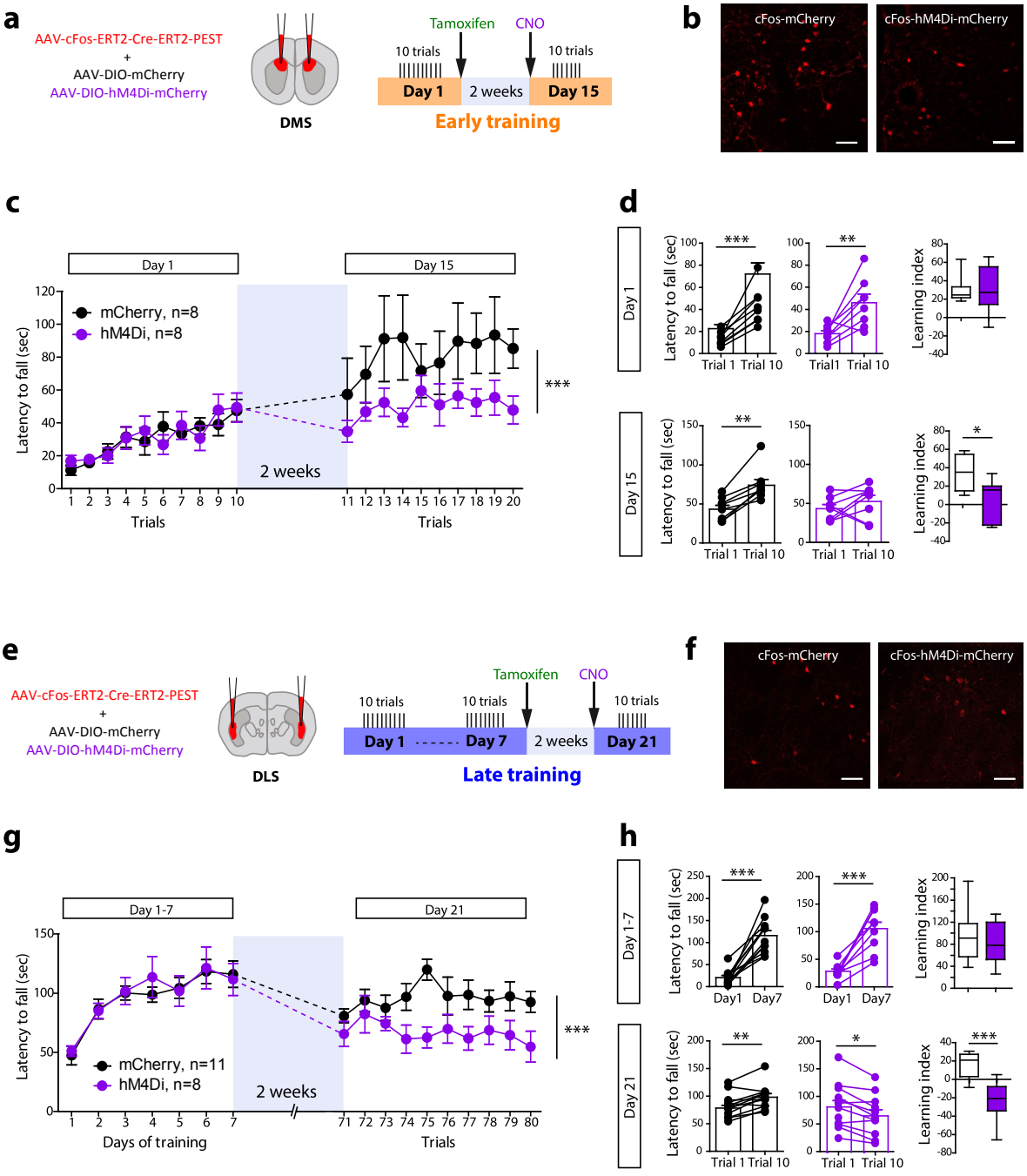
a
AAV-cFos-ERT2-Cre-ERT2-PEST
+
AAV-DIO-mCherry
AAV-DIO-hM4Di-mCherry
DMS
Tamoxifen
CNO
10 trials
10 trials
Day 1
2 weeks
Day 15
Early training
b
cFos-mCherry
cFos-hM4Di-mCherry
c
Day 1
Day 15
mCherry, n=8
hM4Di, n=8
Latency to fall (sec)
2 weeks
***
Trials
Trials
d
Day 1
Day 15
Latency to fall (sec)
Trial 1 Trial 10
Learning index
e
AAV-cFos-ERT2-Cre-ERT2-PEST
+
AAV-DIO-mCherry
AAV-DIO-hM4Di-mCherry
DLS
Tamoxifen
CNO
10 trials
10 trials
10 trials
Day 1
Day 7
2 weeks
Day 21
Late training
f
cFos-mCherry
cFos-hM4Di-mCherry
g
Day 1-7
Day 21
Latency to fall (sec)
mCherry, n=11
hM4Di, n=8
2 weeks
***
Days of training
Trials
h
Day 1-7
Day 21
Latency to fall (sec)
Day1 Day7
Learning index

Figure 7

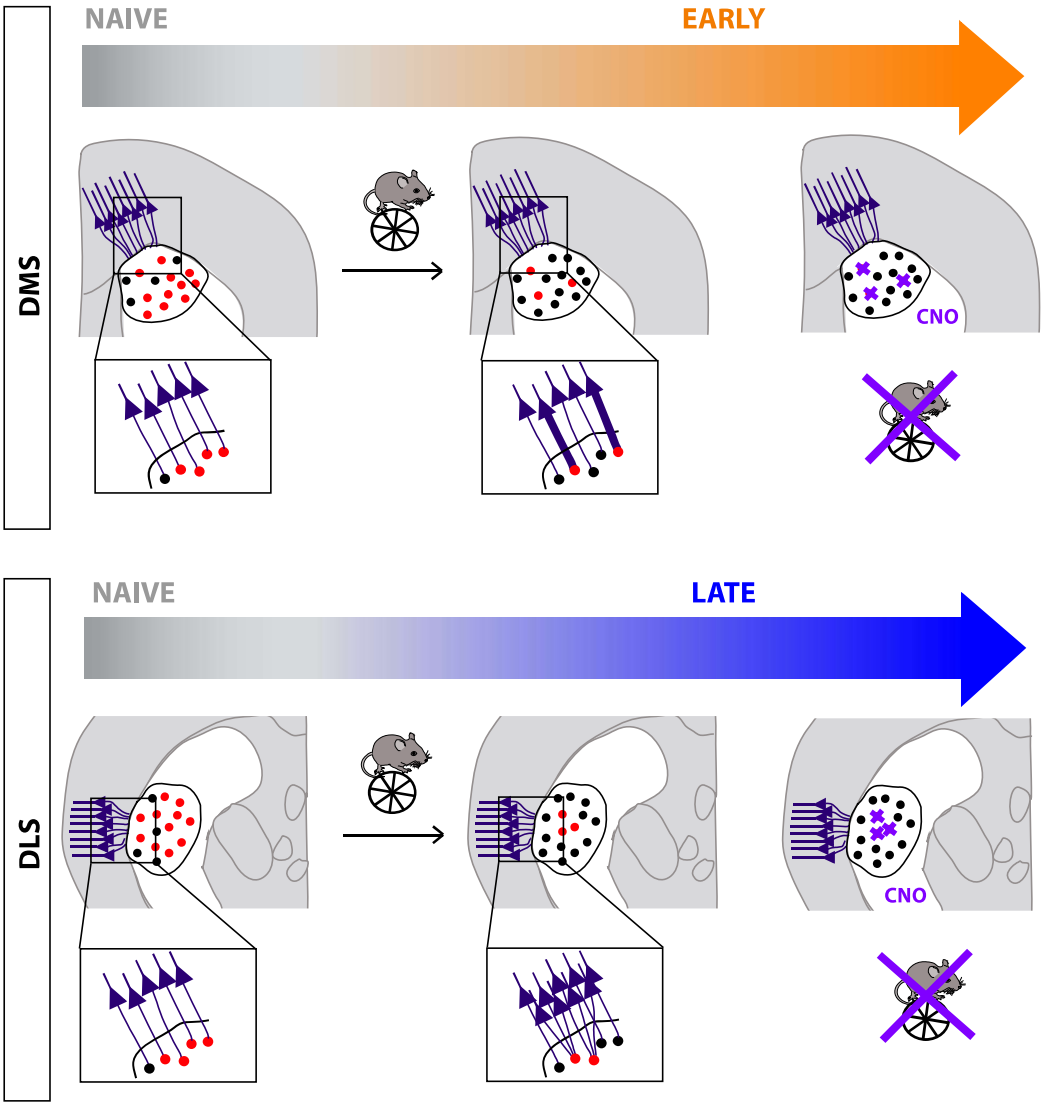

Supplementary Information

Spatiotemporal reorganization of corticostriatal network dynamics encodes motor skill learning

Badreddine N, Zalcman G, Appaix F, Becq G, Trembay N, Saudou F, Achard S and Fino E

Contents

Supplementary Figures 1-9

Supplementary Fig 1

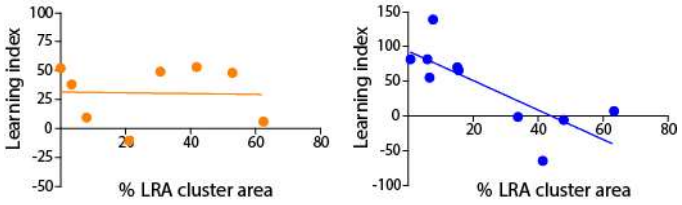

Supplementary Figure 1: Cluster area and performance in DLS

Correlation between the percentage of LRA cluster area and the learning index of the animals, after early training (orange) or late training (blue) in DLS. There is a significant correlation between these two parameters for late trained animals in DLS (r^2= 0.60, p= 0.0088, Pearson correlation) while no correlation was found when animals were early trained (r^2= 0.0009, p= 0.9414).

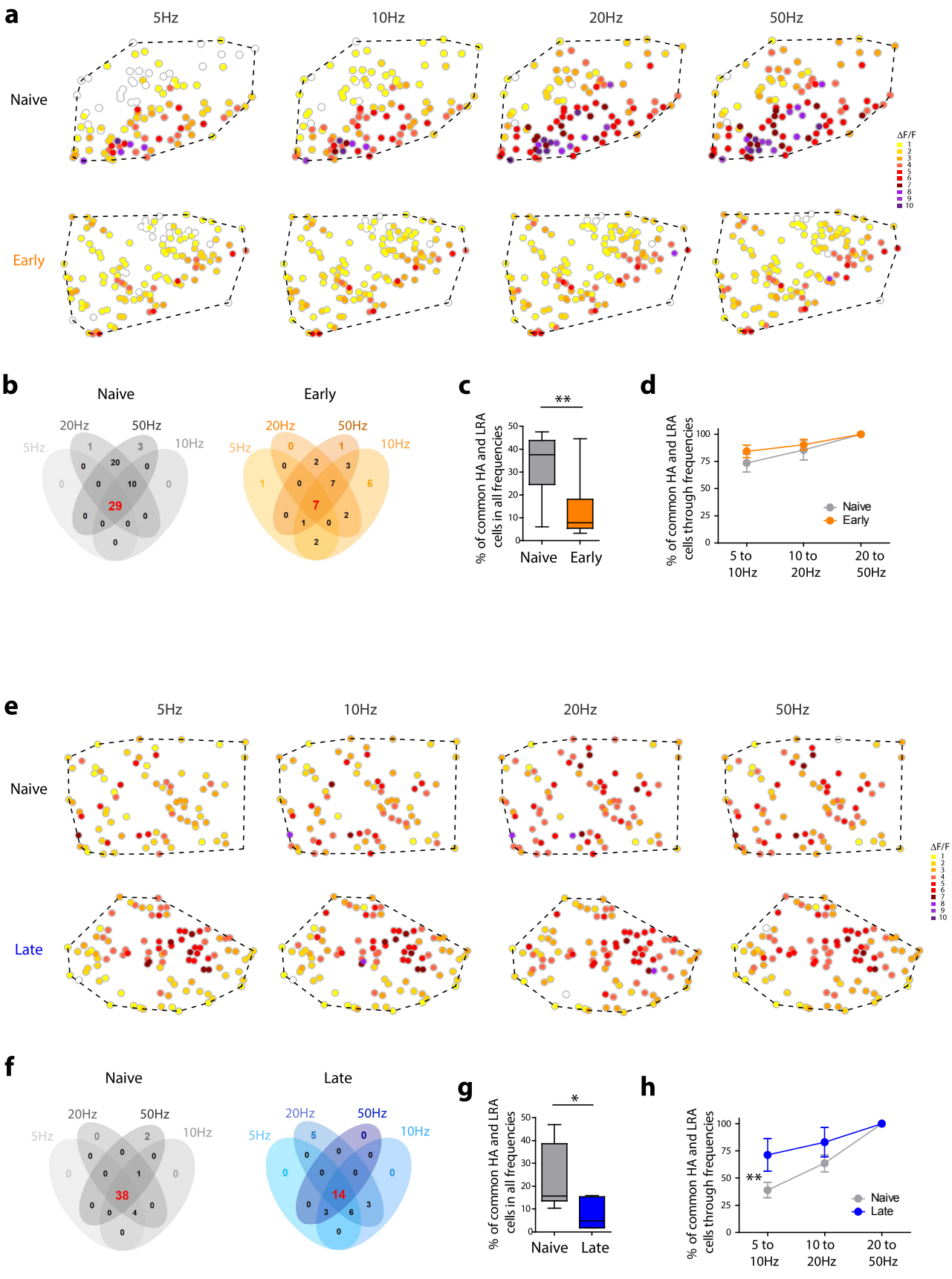
a
5Hz
10Hz
20Hz
50Hz
Naive
Early
ΔF/F
b
Naive
Early
20Hz
50Hz
5Hz
10Hz
29
7
c
**
% of common HA and LRA cells in all frequencies
Naive
Early
d
% of common HA and LRA cells through frequencies
Naive
Early
5 to 10Hz
10 to 20Hz
20 to 50Hz
e
5Hz
10Hz
20Hz
50Hz
Naive
Late
ΔF/F
f
Naive
Late
20Hz
50Hz
5Hz
10Hz
38
14
g
*
% of common HA and LRA cells in all frequencies
Naive
Late
h
**
% of common HA and LRA cells through frequencies
Naive
Late
5 to 10Hz
10 to 20Hz
20 to 50Hz

Supplementary Figure 2: Maintenance of functional maps throughout cortical stimulation frequencies

(**a**) Representative maps of DMS network activity for different frequencies of cortical activation in naive (top) or early (bottom) animals. (**b**) Venn diagram illustrating the percentage of common HA and LRA cells activated at different frequencies (5, 10, 20 and 50Hz) in a given DMS network. The two diagrams are for one representative naive (grey, for n= 104 total neurons in the field) and one representative early animals (orange, for n= 92 neurons). Each intersection has a black number corresponding to the number of identical cells between two or three frequencies. The red number indicates the total number of identical cells in the field at all frequencies. (**c**) The averaged total number of identical cells in the field is significantly higher in naive animals compared to early trained ones (p= 0.005, t-test). (**d**) Evolution of the percentage of common HA and LRA cells through the increase of the stimulation frequencies in DMS. For both naive and early trained groups, the common cells are recruited for low frequency (5Hz) and are maintained throughout the other frequencies ($F_{1,53}$=1.56, p= 0.3096, Two-way Anova). (**e**) Representative maps of DLS network activity for different frequencies of cortical activation in naive (top) or late trained (bottom) animals. (**f**) Venn diagram illustrating the percentage of common HA and LRA cells activated for different frequencies (5, 10, 20 and 50 Hz) in a given DLS network. The two diagrams are for one representative naive (grey, for n= 81 cells in the field) and one representative late trained animal (blue, for n= 97 cells in the field). Each intersection has a black number corresponding to the percentage of identical cells between two or three frequencies. The red number indicates the total percentage of identical cells in the field at all frequencies. (**g**) The averaged total number of identical cells in the field is significantly higher in naive animals compared to late trained ones (p= 0.0236, t-test). (**h**) Evolution of the percentage of

common HA and LRA cells through the increase of the activation frequencies in DLS. There is a significant difference between the naive and late trained group in the percentage of common cells throughout frequencies ($F_{1,27}$= 8.53, p= 0.0167, Two way Anova). For naive animals there is a progressive recruitment of identical cells through the increase of frequency while late training induces a rapid recruitment of common cells starting from the low frequency (5 Hz).

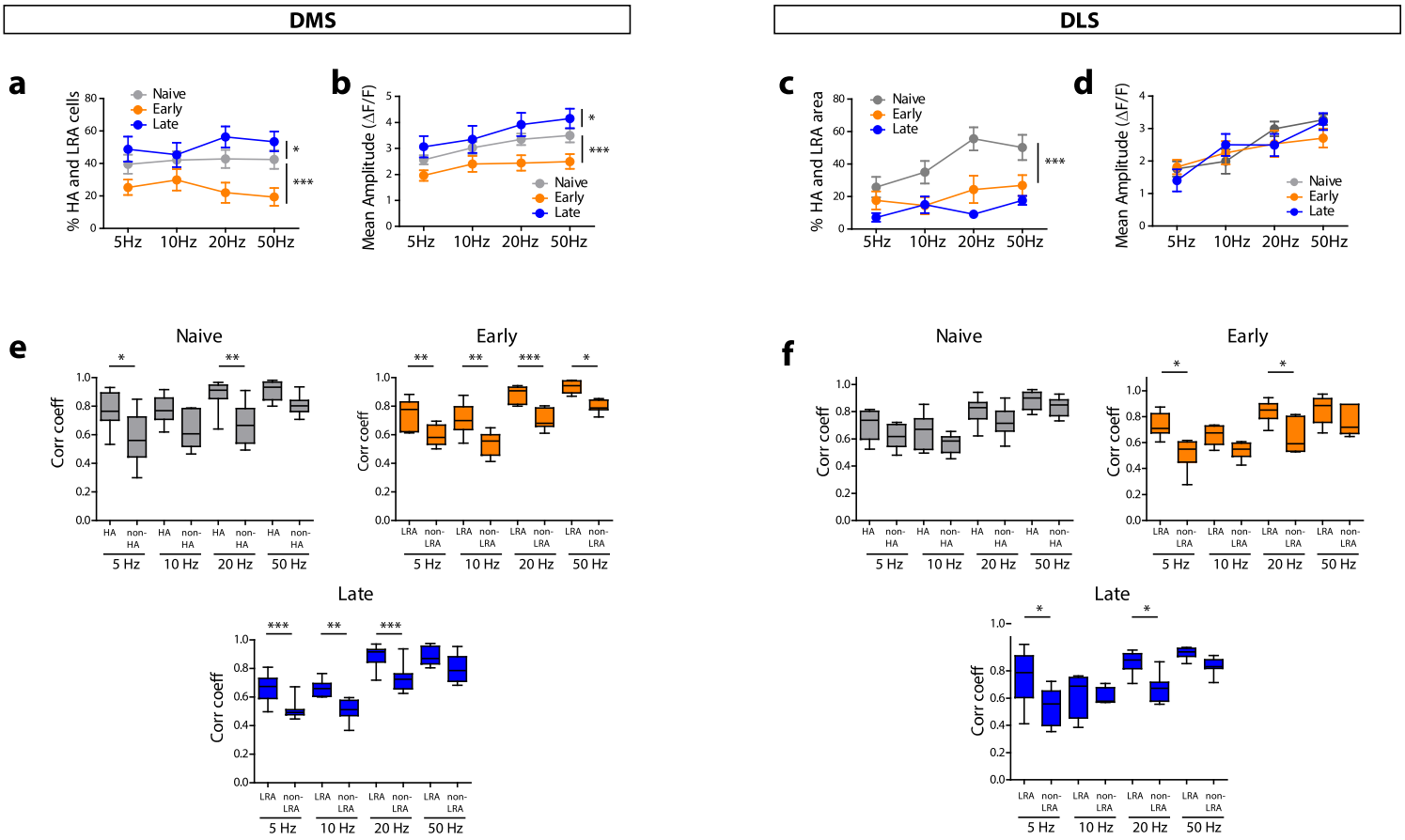
DMS
DLS
a
% HA and LRA cells
Naive
Early
Late
5Hz 10Hz 20Hz 50Hz
b
Mean Amplitude (ΔF/F)
c
% HA and LRA area
d
e
Naive
Early
Late
Corr coeff
HA non-HA
LRA non-LRA
5 Hz 10 Hz 20 Hz 50 Hz
f

Supplementary Figure 3: Correlation coefficient of HA/LRA cells and non-HA/non-LRA cells for all frequencies

(**a**) Evolution of the percentage of HA and LRA cells in DMS with the stimulation frequency of the cortical inputs. The percentage is significantly different between naive, early and late trained animals ($F_{2, 104}$= 24.41, p< 0.0001, Two-way Anova, n= 11 naive, n= 8 early and n= 10 late). (**b**) Evolution of the averaged amplitude of responses of all the cells in the recorded fields in DMS. In DMS, the amplitude is significantly different between the three training conditions ($F_{2,106}$= 20.47, p< 0.0001, Two-way Anova) and also increases with the different frequencies ($F_{3,106}$= 8.29, p= 0.0074, Two-way Anova). The amplitude is significantly lower in early trained animals compared to naive animals in all frequencies while it is higher in late trained animals. (**c**) Evolution of the percentage of HA and LRA area in DLS depending on the stimulation frequencies of the cortical inputs. The area is significantly different between naive, early and late trained ($F_{2,75}$= 34.02, p< 0.0001, Two-way Anova, n= 9 naive, n= 6 early and n= 8 late) animals and also significantly increasing with the frequencies ($F_{3,75}$= 7.57, p= 0.0119, Two-way Anova). (**d**) Evolution of the averaged amplitude of responses of all the cells in the recording fields in DLS. The mean amplitude is the same in the three different training conditions ($F_{2,74}$= 0.57, p= 0.7056, Two-way Anova) and increases significantly through frequencies ($F_{3,74}$= 31.10, p<0.0001, Two-way Anova). (**e**) Correlation coefficient of highly active (HA) and non-highly active (non-HA) for naive animals and LRA and non-LRA cells for early and late trained mice in DMS. In naive animals, there is a difference between HA and non-HA cells for 5 and 20 Hz (p< 0.05 for 5 Hz and p< 0.01 for 20 Hz, n= 11, One-way Anova, with Tukey post-hoc test). For early trained animals, the LRA cells have a significant higher correlation coefficient than non-LRA cells for all the frequencies (p< 0.01 for 5 Hz, p< 0.01 for 10 Hz, p<0.0001 for 20 Hz, p< 0.05 for 50 Hz, n= 8). For late trained animals, the LRA

cells have a significant higher correlation coefficient than non-LRA cells for 5, 10 and 20 Hz ($p< 0.001$ for 5 Hz, $p< 0.01$ for 10 Hz, $p< 0.001$ for 20Hz, n=9). (**f**) Correlation coefficient of highly active (HA) and non-highly active (non-HA) for naive animals and LRA and non-LRA cells for early and late trained mice in DLS. In naive animals, there is no difference between HA and non-HA cells for all frequencies. For early trained animals, the LRA cells have a significant higher coefficient of correlation than non-LRA cells for 5 and 20 Hz ($p< 0.05$ for 5 Hz and for 20 Hz, One-way Anova, with Tukey post-hoc test). For late trained animals, the LRA cells also have a significant higher coefficient of correlation than non-LRA cells for 5 and 20 Hz ($p< 0.05$ for 5 Hz and for 2 0Hz).

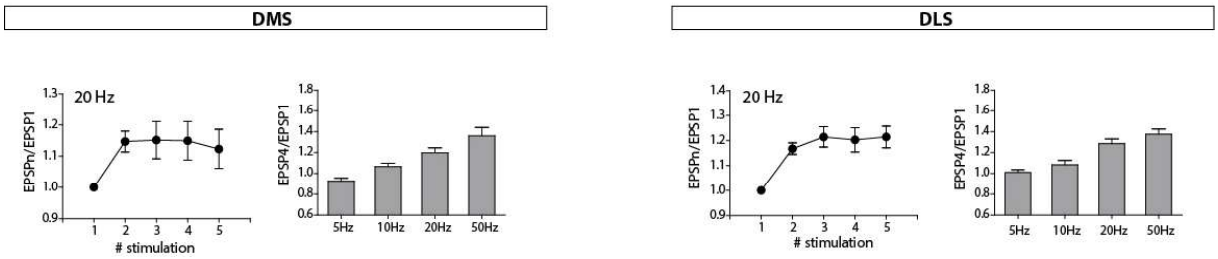

Supplementary Figure 4: Corticostriatal short-term dynamics in naive mice in DMS and DLS.

Summation properties in naive animals are similar to the ones in non-LRA cells after training. In both DMS and DLS, 20 Hz summation and average summation of the 4th EPSP compared to EPSP1 for 5, 10, 20 and 50 Hz cortical train stimulations.

Supplementary Fig 5

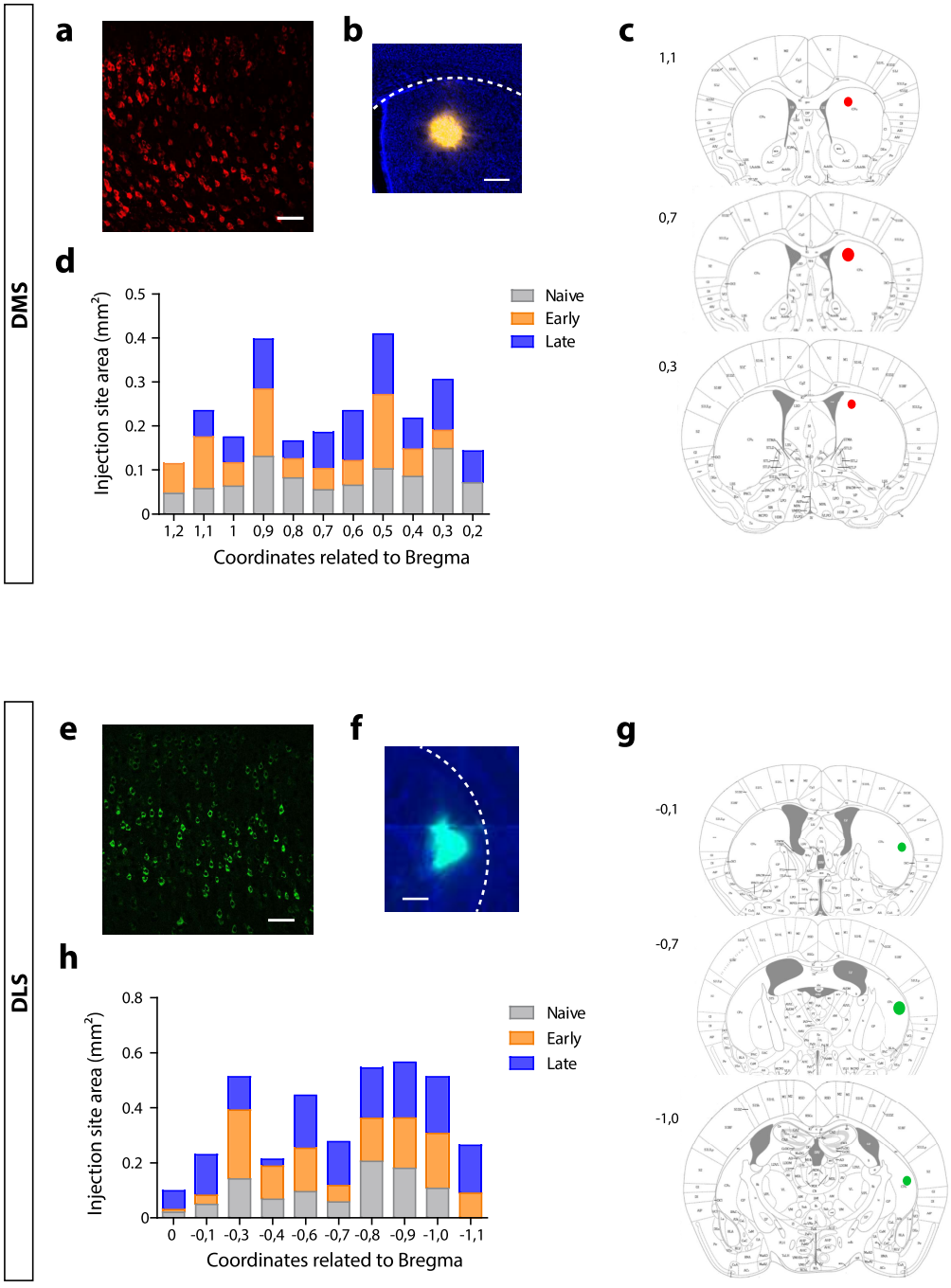

Supplementary Figure 5: Injection sites of CTB-555 and CTB-488 in DMS and DLS.

(**a**) Confocal images of the cingulate cortical cells labelled with CTB-555 after DMS injections (scale bar: 50 µm). (**b**) Injection site is shown in DMS (scale bar: 200 µm). (**c**) Representation of the injection site extent along the antero-posterior axis. The red dots indicate the sites on modified Paxinos slides, with the coordinates relative to Bregma indicated on the left of each slide (1.1, 0.7, 0.3). (**d**) Distribution of the area of the injection sites for Naïve (n= 4 mice), Early (n= 5 mice) and Late (n= 5 mice) trained mice along the antero-posterior axis. (**e**) Confocal images of the cingulate cortical cells labelled with CTB-488 after DLS injections (scale bar: 50 µm). (**f**) Injection site is shown in DLS (scale bar: 200 µm). (**g**) Representation of the injection site extent along the antero-posterior axis. The red dots indicate the sites on modified Paxinos slides, with the coordinates relative to Bregma indicated on the left of each slide (-0.1, -0.7, -1.1). (**h**) Distribution of the area of the injection sites for Naive (n= 5 mice), Early (n= 4 mice) and Late (n= 4 mice) trained mice along the antero-posterior axis.

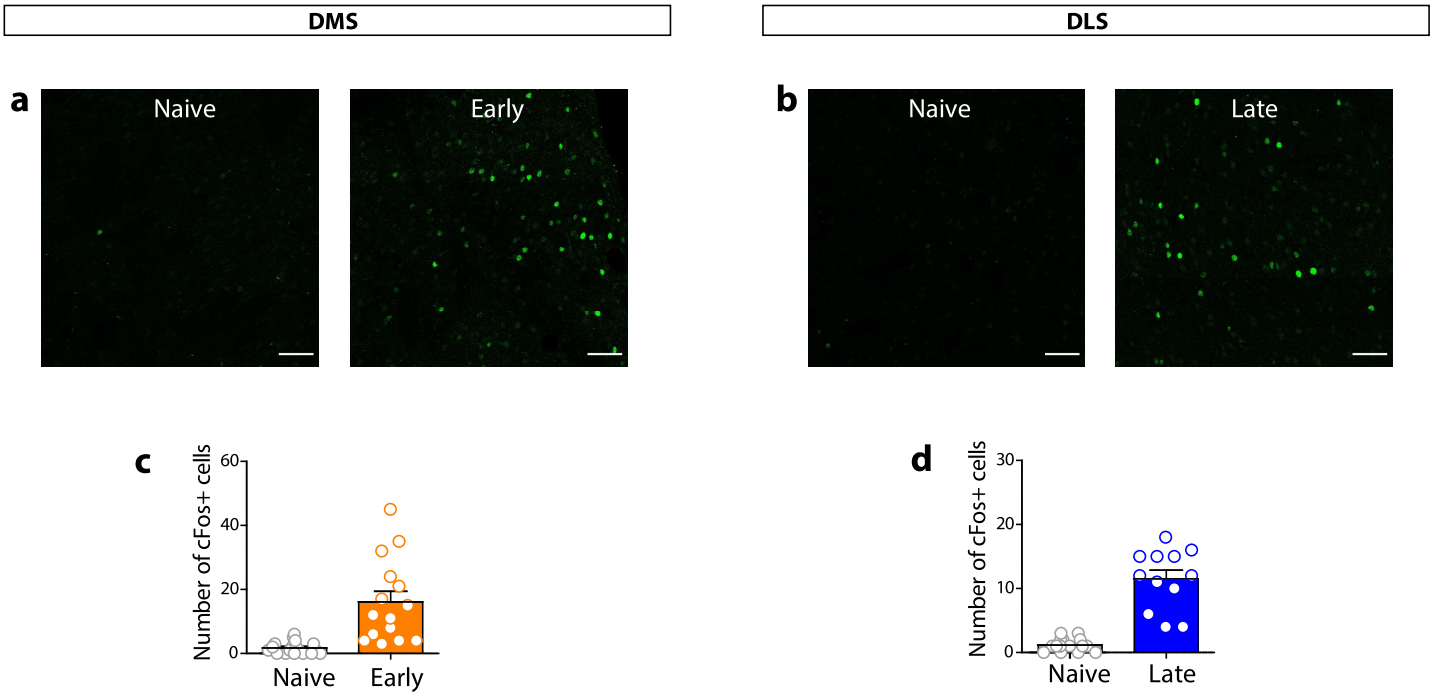
DMS
DLS
a
Naive
Early
b
Naive
Late
c
Number of cFos+ cells
60
40
20
0
Naive
Early
d
Number of cFos+ cells
30
20
10
0
Naive
Late

Supplementary Figure 6: Immunostainings of cFos in naive and trained mice.

(**a-b**) Confocal images of cFos expressing cells in naive and early trained mice in DMS (a) and in naive and late trained in DLS (b) (scale bar: 50 μm). (**c**) Bar graph of the number of cFos expressing cells in DMS in naive and early trained animals. The cFos expressing cells were significantly higher in early trained mice compared to naive ones (1.7±0.4 cells, n= 18 in naive and 16.1±3.3 cells, n= 15 in early trained mice, $p< 0.0001$, t-test). (**d**) Bar graph of the number of cFos expressing cells in DLS in naive and late trained animals. The number of cFos expressing cells was significantly higher in early trained mice compared to naive ones (1.2±0.2 cells, n= 18 for naive, 11.5±1.4 cells, n= 12 for late trained mice, $p< 0.0001$, t-test). In each territory, the number of cFos expressing cells was quantified in 3 different mice per training condition, with 5-6 fields of 400 x 400 μm quantified for each mouse on 2-3 different coronal slices on the anteroposterior axis.

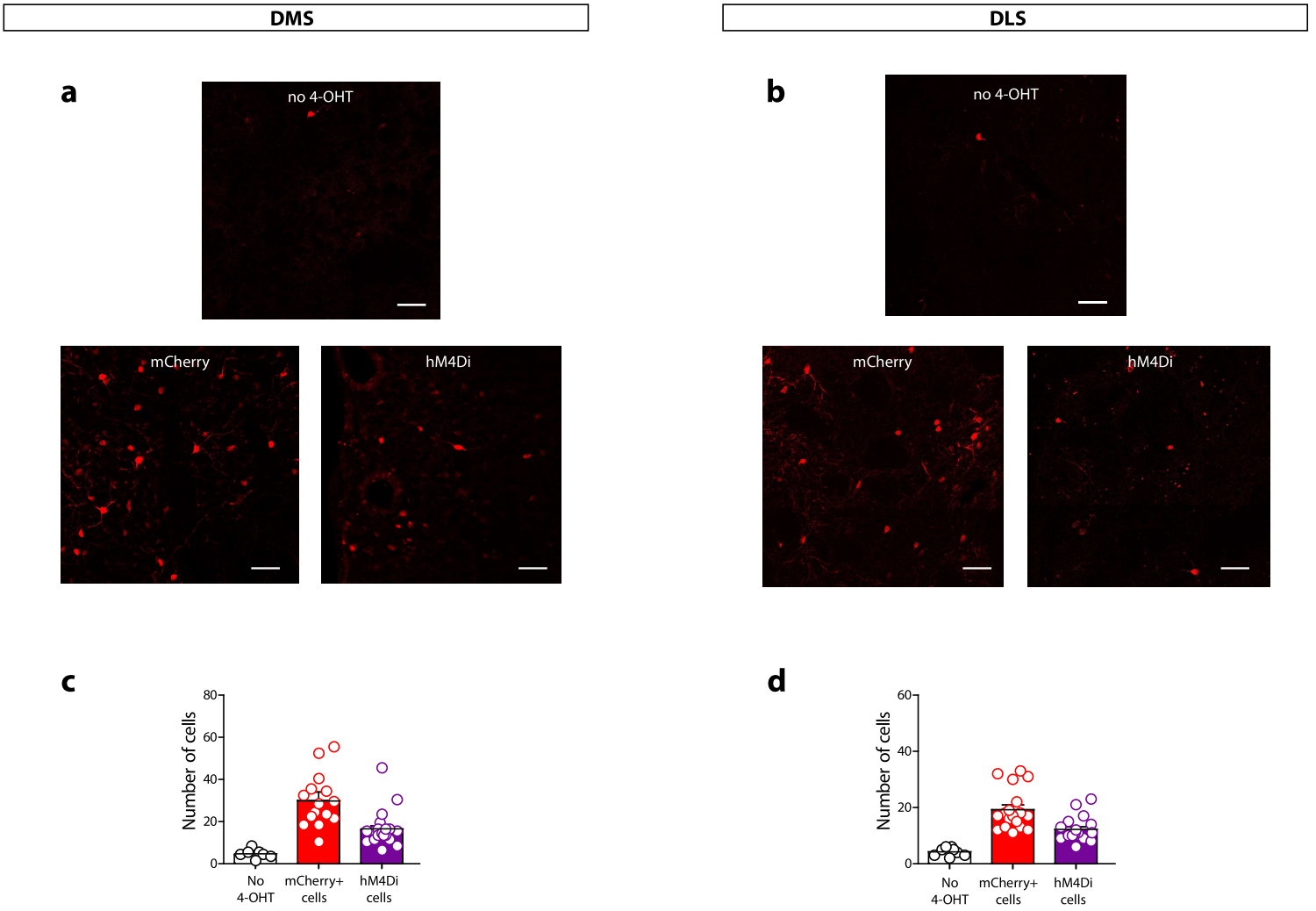
DMS
DLS
a
no 4-OHT
mCherry
hM4Di
b
no 4-OHT
mCherry
hM4Di
c
Number of cells
80
60
40
20
0
No 4-OHT
mCherry+ cells
hM4Di cells
d
Number of cells
60
40
20
0
No 4-OHT
mCherry+ cells
hM4Di cells

Supplementary Figure 7: 4-OH-Tamoxifen induces a specific and reliable expression of mCherry and hM4Di AAVs in LRA cells.

(**a-b**) Confocal images of c-fos-mCherry expressing cells, c-fos-hM4Di-mCehrry expressing cells in presence or in absence of intraperitoneal injection of 4OH-Tamoxifen within the DMS after early training (a) and in the DLS after late training (b). Scale bars: 50 µm. (**c**) The number of c-fos-mCherry+ cells or c-fos-hM4Di-mCherry+ cells was quantified in DMS with or without IP injection of 4OH-Tamoxifen. Without 4OH-Tamoxifen, there was very few expression of the AAVs and thus very few c-fos-mCherry cells (4.2±1.8 cells, n= 7). With 4OH-Tamoxifen, there was a significantly higher number of c-fos-mCherry+ cells (red, 23.1±3.9 cells, n= 12) and the number of hM4Di-mCherry+ cells (purple, 16.1±1.9 cells, n= 20) in DMS (p= 0.0012, One-way Anova, with no significant difference between mCherry+ cells and hM4Di-mCherry+ cells). (**d**) The number of c-fos-mCherry+ cells or c-fos-hM4Di-mCherry+ cells was quantified in DLS with or without IP injection of 4OH-Tamoxifen. Without 4OH-Tamoxifen, there was very few expression of the AAVs and thus very few c-fos-mCherry cells (4.3±0.5 cells, n= 8). With 4OH-Tamoxifen, there was a significantly higher number of c-fos-mCherry+ cells (red, 15.2±1.7 cells, n= 18) and the number of hM4Di-mCherry+ cells (purple, 12.2±1.0, n= 19) in DLS (p= 0.0001, One-way Anova, with no significant difference between mCherry+ cells and hM4Di-mCherry+ cells).

The quantification was done in 3-4 fields of 400 x 400 µm to be compared with the number of LRA cells we observed in DMS and DLS (Fig. 1 and Fig. 6). It should be noted that both mCherry+ cells and hM4Di-mCherry+ cells were not significantly different than the number of LRA cells in DMS (p= 0.2244, One-way Anova, 20.8±3.1 cells, n= 18 fields for LRA cells and 23.1±3.9 cells, n= 12 for mCherry+, 16.1±1.9 cells, n= 20 for hM4Di-mCherry+) or in DLS (p=

0.2737, One-way Anova, 14.3±1.3 cells, n=16 for LRA cells and 15.2±1.7 cells, n= 18 for mCherry+ cells, 12.2±1.0, n= 19 for hM4Di-mCherry+ cells).

Supplementary Figure 8

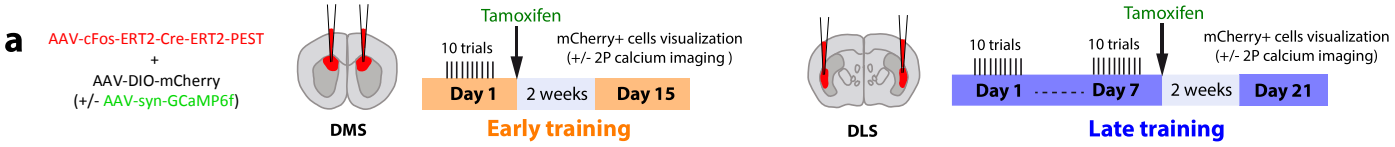

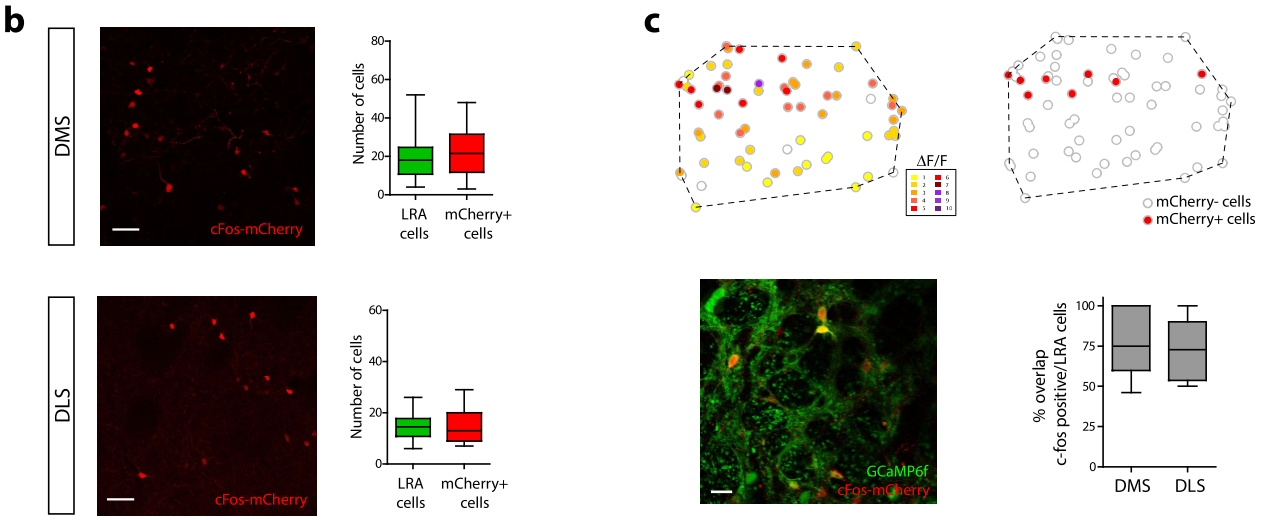

Supplementary Figure 8: LRA cells express cFos early gene

(**a**) Experimental design, mice were injected either with AAV-cFos-ERT2-Cre and AAV-flex-mCherry alone and trained for 1 day (for DMS) or 7 days (for DLS), or the injection was coupled to AAV-Syn-GCaMP6f. (**b**) Confocal images of cFos-mCherry expressing cells within the DMS and the DLS (scale bars: 50 µm). The number of cFos-mCherry+ cells was quantified in different fields of 400 µm x 400 µm to be compared with the number of LRA cells we observed in DMS and DLS (Fig. 1). There was no significant difference between the number of mCherry+ cells (red) and the number of LRA cells (green) in DMS ($p= 0.6538$, 20.8±3.1 cells, $n= 18$ for LRA cells and 23.1±3.9 cells, $n= 12$ for mCherry+ cells) and in DLS ($p= 0.6623$, 14.3±1.3 cells, $n= 16$ for LRA cells and 15.2±1.7 cells, $n= 18$ for mCherry+ cells). (**c**) Two-photon calcium imaging was performed on Day 15 or Day 21, coupled to imaging of the cFos positive cells. On top are shown a representative activity map in DLS and the associated distribution map of mCherry+ cells. Bottom: overlap of the two-photon microscopy images of GCaMP6f expressing cells (green) with the high activity cells and of the cFos-mCherry expressing cells (red) (scale bar: 20 µm). The quantification on the bottom right shows that there is a 78.9±10.0 % overlap in the DMS and 72.0±8.8 % overlap in the DLS. The overlap was not significantly different between the two territories ($p= 0.6180$, $n= 5$ for DMS and for DLS). * $p< 0.05$, ** $p< 0.01$, *** $p< 0.001$.

Supplementary Fig 9

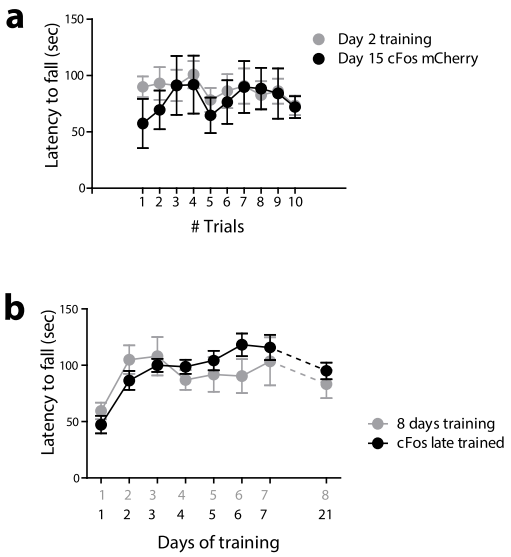

Supplementary Figure 9: Similar performance after 2 weeks expression of AAV-cFos-ERT2-Cre-ERT2.

(**a**) Learning curves of mice trained on Day 2 or on Day 15 after the 2 weeks delay for the expression of the virus. This delay does not affect the learning curve since the two groups do not show any differences in their learning curves ($F_{1,168}$= 0.84, p= 0.2260, n= 11 mice tested at Day 2 and n= 8 mice tested at Day 15). (**b**) Learning curves of mice trained on Day 8 or on Day 21 after the 2 weeks delay for the expression of the virus. This delay does not affect the learning curve since the two groups do not show any differences in their learning curves ($F_{1,126}$= 0.38, p= 0.4097, n=12 mice tested at Day 8 and n= 11 mice tested at Day 21).

III- Study 2: Classification of types of neurons from calcium imaging

Calcium imaging allows us to study activity of a network on a large scale with a cellular resolution allowing us to monitor the activity of individual neurons. Calcium imaging recordings were made possible with the development of calcium sensors allowing for a good temporal resolution and a higher sensitivity (Chen et al., 2013). The temporal resolution allows us to study the dynamics of the calcium signals. Interestingly, neurons can be differentiated based on their morphology and their electrophysiological properties. The striatum is constituted of different types of neurons: more than 90% of neurons are medium-spiny neurons and the rest is constituted of different subtypes of interneurons (A Parent & Hazrati, 1995; Tepper et al., 2010).

In study 1, we decided to focus on signals from MSNs, the striatal output neurons and for this, we needed to exclude all other neurons. Thus, without the possibility to label simultaneously all interneurons that we wanted to exclude, it was important to be able to differentiate MSNs from interneurons based on their calcium signals. To this end, we developed a tool which allows the classification of the different cell types in the striatum based on their calcium signals and their morphology with a high accuracy rate.

This classifier was the object of a published conference paper of which I am second author.

Classification of types of neurons from calcium imaging

Classification de types de neurones à partir de signaux calciques

Guillaume Becq 1 Nagham Badreddine 2 Nicolas Tremblay 1 Florence Appaix 2
Gisela Zalcman 2 Elodie Fino 2 Sophie Achard 1

1 – Univ. Grenoble Alpes, CNRS, Gipsa-lab, F-38000, Grenoble, France
2 – Univ. Grenoble Alpes, Inserm, U1216, Grenoble Institut Neurosciences,
GIN, F-38000 Grenoble, France

guillaume.becq@gipsa-lab.fr

1er septembre 2020

Chapter 2

English version – translation of the French article

Classification of types of neurons from calcium imaging

Abstract - Videos of calcium activities of mice striatum slices are recorded under stimulations by two-photon fluorescence microscopy. Neurons are selected by regions of interests (ROI) on the images and labeled into two classes: medium spiny neuron (MSN) and interneurons (IN). Each ROI enables to obtain a neural signal. Many features are extracted from both ROIs and the signals. In order to chose the most meaningful features for classification in two classes (IN vs MSN), a quadratic discriminant analysis is performed. It is shown that a realistic evaluation of the database leads to a classification with an accuracy of 75 % for IN and 90% for MSN.

2.1 Introduction

Calcium imaging has become a reference method to study neural networks dynamics [1]. It enables to obtain a high spatial resolution for the observation of the synchronous activity of a population of neurons and a temporal resolution that enables to evaluate the neural activity at the level of a single cell. It is nevertheless limited by low frequency components, uncalibrated measures and low signal to noise ratios. In order to compare measures, a relative fluorescence measure, usually written $\Delta F/F$, is retained by dividing the instantaneous fluorescence by a basal measure. This enables to highlight the diversity of answers of different sorts of neurons [1]. In this study, we focus on the striatum of the mouse, an area related to procedural memory [2, 3]. It is part of the thalamo-cortical loop and is involved in movement selection during specialised tasks. It contains only inhibitor neurons of different types that can be grouped into 95 % of medium spiny neurons (MSN) and 5 % of interneurons (IN) [4]. Mice brain slices are cut on selected areas from sacrificed animals following approved ethical protocols. Electrical stimulations are done in cortical areas that naturally stimulate the recorded striatum areas. The aim of this study is to evaluate the classification of the different types of neurons, MSN or IN, from features extracted on neural calcic activities observed during electrical stimulations. Quadratic discriminant classifiers are retained because they obtain decision boundaries appropriate to the problem, have few hyperparameters to tune, and are easy to evaluate [5, 6]. First, the creation of the features database is described from raw calcium images recorded during stimulation. Then, results with several supervised learning procedures are presented. Finally, results are discussed and directions are proposed.

2.2 Results

2.2.1 Image processing and features description

A sequence of 81 images of a square field of side 392.66 μm containing 1024 by 1024 pixels is presented in Fig. 2.1a. In this example, the lapse of time between images is set to 250 ms. For each slice recording, the original sequence contains 1000 images with a sampling rate of 15.3 Hz. The sequences of images are analysed using ImageJ [7] or Python using scikit-image [8]. An example of a time-average image is presented in Fig. 2.1b, c. This image highlights the biological structures

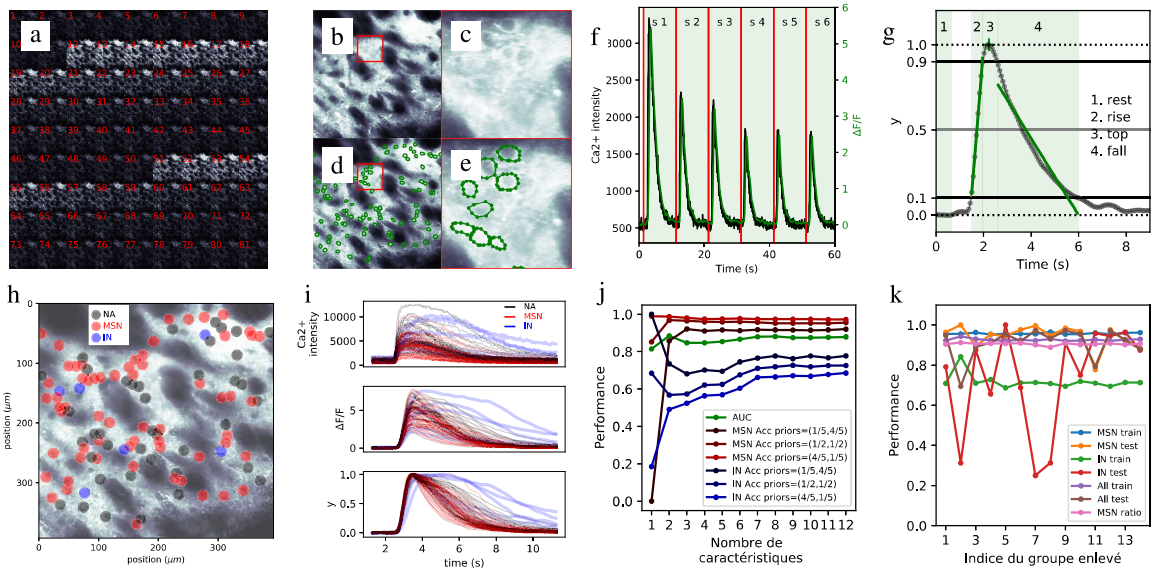

Figure 2.1 – Image processing, feature description and classification results. a) extract of a sequence of images. b-e) average image and selection of neurons. f) Stimulus answer of one neuron. g) Extraction of features. h) Expert labeling of neurons. i) Neural answers and normalisation. j) Evaluation of performances with AUC for the different features. k) Evaluation of performance using the accuracy, global or per class, using a leave-1-group-out procedure. A group is a recording of a slice available in the database.

that participate in the calcic activities of this slice, in particular neurons that can be detected visually. Neurons are delineated on the image with polygonal shapes to create regions of interests (ROI) (Fig. 2.1d, e). Dynamical measures and statistics are extracted from these ROIs leading to: 5 temporal series (MEAN, STDDEV, MODE, SKEW, KURT) and 11 static features related to shapes of ROI (AR, AREA, CIRC, FERET, FERET ANGLE, FERET MIN, FERET X, FERET Y, PERIM, ROUND, SOLIDITY). [1]. Samples of temporal series are computed using statistics made over the distribution of pixels intensity contained in ROIs. In the remainder of this paper, the signal of one neuron will refer to the temporal series obtained from the MEAN statistic. An example of one signal is presented in Fig.2.1f. Stimuli are represented by vertical lines. The intensity of Ca^{2+} corresponds to the intensity of the fluorescence of calcium ions. Variations of intensity can be observed after each stimulation. In order to normalise the data, signals are transformed by reference to the basal value of fluorescence F_0 and a new signal, noted $\Delta F/F$, is computed [9]: $\Delta F/F = (F - F_0)/F_0$ with $F_0 = \frac{1}{n_0} \sum_{i=1}^{n_0} F(i)$, with n_0 set to 10 samples in this study.

A low pass filter (< 1 Hz) is then used to eliminate noisy spurious frequencies (Butterworth filter: - 3 dB at 1 Hz, - 40 dB at 4 Hz, order 3). This leads to a signal noted x with an example presented in green in Fig2.1f. Beginnings and ends of stimulations are marked in order to study each stimulation and compute features. A zoom on one stimulation is given in Fig.2.1g. For each stimulation, several periods are selected and presented in Fig.2.1g. These periods are defined and used to compute some features as follows: • Computation of standard deviations on the signal x and on the raw signal STD and STD RAW • Search of the maximal value X MAX during the stimulation (peak), and its related raw value X MAX RAW • Search of the average basal value over the rest period (rest), X 0, defined on 10 samples: $x_0 = 1/10 \sum_{i=1}^{10} x(i)$ • Normalisation of data: $y = (x - x_0)/(x_{\max} - x_0)$. An example of this transformation is given in Fig. 2.1i. • Search of strong points of the rise period (rise), defined by the first sample < 0.9 and first sample < 0.1 on the left of the peak • Same operations for the fall (fall): first sample < 0.9 and first sample < 0.1 on the right of the peak. • Regression on samples during the rise time, with a linear model $y = a\,x + b$ to get the linear slope RISE LIN and a logarithmic regression with negative values clipped at 1e-5 to get the logarithmic slope RISE LOG • Same computations for values during the fall FALL LIN, FALL LOG • Computation of the time spent over 0.9 (top), T9 • Computation of the time spent over 0.1 (rise + top + fall) • Computation of the time spent over 0.5, T5 and duration of the time spent from top to 0.5 during fall, T5P • Computation of the mean values X KURT, X SKEW, X STDDEV and X MODE Finally, 29 features are retained, 12 from static shapes, 17 from temporal series.

In order to perform supervised learning, neurons are classified into 3 classes, not available (NA), MSN and IN according to the expertise of cells anatomy, chemical stainings and visual analysis of stimuli answers. An example of the spatial organisation of cells labelled by an expert is given in Fig.2.1h. The comparison of stimuli answers for the different classes of

1. (cf. `https://imagej.nih.gov/ij/docs/menus/analyze.html#set` for definition of these measures)

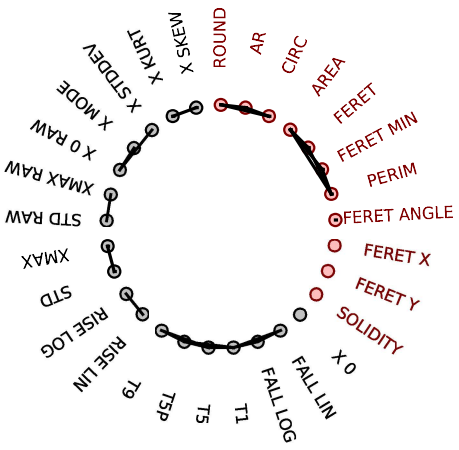

Figure 2.2 – Graph of correlation values between features. Colors correspond to features related to: the shape of neurons in red; dynamic of time series during stimulations in black.

cells for the slice given in example is proposed in Fig.2.1i, with answers of IN cells different than those of MSN cells.

2.2.2 Definition of the features database and classification using supervised learning

In this study, 14 brain slices considered as groups are used to generate data labelled MSN and IN. Proportions of cells population and n, the total number of cells in slices for each group are as follows, given in triplets (pMSN, pIN, n): (0.91, 0.09, 68), (0.56, 0.44, 18), (0.89, 0.11, 37), (0.86, 0.14, 56), (0.82, 0.18, 22), (0.80, 0.20, 40), (0.97, 0.03, 63), (0.98, 0.02, 178), (0.85, 0.15, 72), (0.95, 0.05, 74), (0.91, 0.09, 69), (0.87, 0.13, 71), (0.93, 0.07, 103), (0.89, 0.11, 90). For each group, 4 stimulations (s2 – s5), as presented in Fig. 2.1f, are retained for the extraction of features. The first stimulation is rejected because it presents singular behaviors. Finally, the database regroups 3844 cells corresponding to 3480 MSN and 364 IN. Several supervised learning procedures are evaluated on this database. Data processings are done in Python, principally using procedures of the scikit-learn package [10].

First, classification performances are evaluated on the whole dataset with features tested one after the other. In this procedure, a weighting according to the number of samples present in the group is used. The area under the curve (AUC) is retained as a performance criterion. It is computed from the estimation of sensitivity against one minus specificity curve [2], also called the receiver operating characteristic (ROC) [5, 6] and leads to the following sorting (AUC in parenthesis): FALL LOG (0.814), FALL LIN (0.807), T1 (0.791), X 0 (0.781), T5P (0.730), T5 (0.728), X SKEW (0.640), X 0 RAW (0.639), RISE LIN (0.636), T9 (0.632), RISE LOG (0.602), X STDDEV (0.595), FERET (0.583), ROUND (0.583), X KURT (0.581), CIRC (0.576), X MODE (0.575), AR (0.575), FERET ANGLE (0.569), XMAX RAW (0.569), FERET Y (0.564), PERIM (0.562), STD RAW (0.556), STD (0.553), FERET MIN (0.549), XMAX (0.548), FERET X (0.547), SOLIDITY (0.537), AREA (0.522).

The graph of correlation values between features i and j by taking $|C_{ij}| > 0.7$ is presented in Fig.2.2. Some features seem redundant and can be regrouped: (T9, T5P, T5, T1, FALL LOG*, FALL LIN), (X 0*), (X STDDEV, X 0 RAW*, X MODE), (RISE LIN*, RISE LOG), (X SKEW*, X KURT), (PERIM, FERET MIN, FERET*, AREA), (XMAX, STD*), (XMAX RAW*, STD RAW), (ROUND*, CIRC, AR), (SOLIDITY*), (FERET X*), (FERET ANGLE*). By retaining in each group the main feature, noted *, with the highest value of AUC, the set of features can be reduced to: FALL LOG, X 0, X 0 RAW, RISE LIN, X SKEW, FERET, STD, ... A quadratic classifier has been tested by grouping more and more features following a sequential forward selection (SFS) [5]: (FALL LOG), (FALL LOG, X 0), (FALL LOG, X 0, X 0 RAW), ... Performances of classification using AUC and accuracy (Acc) are proposed in Fig 2.1j in function of the number of selected features and classes priors [3]. After the selection of 2-3 features, improvements of the performances are attenuated, whatever classes priors. After the selection of 7 features, improvements are weak. This set of 7 features is retained for the remaining of this paper (FALL LOG, X 0, X 0 RAW, RISE LIN, X SKEW, FERET, STD).

The dataset being composed of 14 groups, cross-validation procedures by removing 1 group, 2 groups or 7 groups are evaluated to estimate generalisation performances. Fig. 2.1k. presents the results with 1 group out. The classification of IN is hard for 3 groups, the 3 test sets of the leave-1-group-out procedure. A comparison of the confusion matrices obtained with these procedures is given in Tab. 2.1b. by averaging the proportion of samples by groups and classes. The probability of test

2. for the problem of 2 classes: IN versus MSN
3. percentage of (MSN, IN)

Table 2.1 – Performances for leave-k-group-out (k-GO). a) Notations for confusion matrices. b) Mean values of the coefficients of the confusion matrices are reported with respect to weighted averaging by samples (global) or averaging by class (per class). Standard errors of the means (SEM) are represented by symbols according to values over 0.01 with the following notations: 0.01 < + < 0.05 < ++ < 0.1.

a)

	pred MSN	pred IN
true MSN	A	B
true IN	C	D

b)

		1-GO		2-GO		7-GO	
train	global	0.83	0.04	0.83	0.04	0.83	0.04
		0.04	0.09	0.04	0.09	0.03	0.10
train	per	0.96	0.04	0.96	0.04	0.96	0.04
	class	0.28+	0.72+	0.28+	0.72+	0.25	0.75
test	global	0.82++	0.05+	0.82+	0.05	0.80	0.07
		0.04++	0.09+	0.04+	0.09	0.04	0.09
test	per	0.94++	0.06++	0.94	0.06	0.92	0.08
	class	0.27++	0.73++	0.24++	0.76++	0.27	0.73

errors (test) tends to approximately 27 % for the classification of IN and 8 % for MSN. Variations of the mean values, in term of standard error of the mean (SEM), decrease with the number of tested groups and show a weak dispersion of performances with a leave-7-group-out procedure. For all procedures, the probability of training errors (train) are comparable to those obtained during test, and can be considered as generalisation performances.

2.3 Discussion

Performances can be presented in different ways, with unbalanced distributions and in fact few data for IN. A raw classification by taking only MSN would lead to an accuracy rate of 87 %, approximately the proportion of MSN in the database, but, taking into consideration the INs, the accuracy rate is only 73 %, indicating that the classification of IN is still difficult with the proposed features. In this study, only quadratic discriminant classifiers have been evaluated because they are simple, efficient, and the estimation of their parameters is fast, enabling to test several hypothesis. The use of others classifiers could probably lead to better performances at the cost of a fastidious hypertuning of parameters. As the number of data in the dataset is quite small, this hypertuning is hard to evaluate. For example, during the selection of the best features with SFS, as the number of IN is small as compared to the increasing dimension of the problem, the estimation of covariance matrices may be spurious after few iterations.

Concerning the choice of features, we have decided to evaluate features currently used by biologists in other studies [11]. Other features, such as those computed on spectral components, could enable to discriminate IN without having to proceed as proposed in this study. It would be interesting to try features obtained from different frequencies bands as those generally used in neurology [12], or try features associated with neural activities as those proposed in [13]. Another method could be to test procedures that work directly on the detection of neurons from videos [14].

In this paper, the primary selection of features has been performed by considering only the performance obtained with AUC leading to the selection of X 0 and X 0 MAX. But these features are dependent on the duration between stimulations and it was observed that some cells have not reached a resting state after 10 s, the time between two stimuli. If other parameters of stimulation are used, the procedure could probably not lead to the selection of these parameters.

2.4 Conclusion

The discrimination of neurons of type MSN and IN from calcium imaging is possible with the use of a quadratic discriminant classifier, leading to an error rate on IN classification of the order of 25 % and an error rate on MSN of the order of 10 %.

Bibliography

[1] C. Grienberger et A. Konnerth, *Imaging Calcium in Neurons*, Neuron, 73: 862–885, 2012.

[2] H. H. Yin, et B. J. Knowlton, *The role of the basal ganglia in habit formation*, Nat. Rev. Neurosci., 7: 464–476, 2006.

[3] P. Redgrave et al. *Goal directed and habitual control in the basal ganglia*, Nat. Rev. Neurosci., 11: 760–772, 2010.

[4] J. Tepper et al., *Heterogeneity and diversity of striatal GABAergic interneurons*, Front. Neuroanat., 4 (150): 1–18, 2018.

[5] A. Jain et al., *Statistical Pattern Recognition: A review*, IEEE Trans. Pattern Anal. Mach. Intell., 22: 4–37, 2000.

[6] T. Hastie et al., *The elements of statistical learning*, Springer, 2001.

[7] J. Schindelin et al., *Fiji: an open-source platform for biological-image analysis* Nat. Methods, 9(7): 676–682, 2012.

[8] S. van der Walt et al. *scikit-image: image processing in Python*, PeerJ, 2:e453, 2014.

[9] T. W. Chen et al., *Ultrasensitive fluorescent proteins for imaging neuronal activity*, Nature, 499: 295–302, 2013.

[10] F. Pedregosa et al., *Scikit-learn: Machine Learning in Python*, J. Mach. Learn. Res., 12: 2825–2830, 2011.

[11] T. P. Patel et al., *Automated quantification of neuronal networks and single-cell calcium dynamics using calcium imaging*, J. Neurosci. Meth., 243: 26–38, 2015.

[12] F. Varela et al., *The brainweb: phase synchronization and large-scale integration*, Nat. Rev. Neurosci., 2: 229–239, 2001.

[13] T. Deneux et al., *Accurate spike estimation from noisy calcium signals for ultrafast three-dimensional imaging of large neuronal populations in vivo*, Nat. Commun., 7: 12190, 2013.

[14] A. Petersen et al., *SCALPEL: Extracting neurons from calcium imaging data*, Ann. Appl. Stat., 12(4): 2430, 2018.

Discussion of Study 2

In study 1 we showed a reorganization of the networks and the networks activity in relation to the phase of procedural learning and to the striatal territory (DMS/DLS). We also showed the necessity of this reorganization in the different phases of learning.

In order to examine the reorganization of the networks and to determine the neuronal substrates that are responsible for the formation of this memory, we extracted signals from MSNs only, since they represent more than 90% of striatal neurons (A Parent & Hazrati, 1995). To be able to extract and analyze only calcium signals from MSNs, we developed a tool that is able to classify the different types of neurons based on their calcium signal.

In order to extract the calcium signals, each neuron was manually delineated and a region of interest (ROI) created. Firstly, once calcium signals of each neuron were extracted using ImageJ, each neuron of a set of slices was classified as being an MSN, an interneuron or IN (all types combined), or non-determined. The classification by an expert was based on labeling of different types of neurons, on the morphology of the neurons, or on the calcium signal. Since different neuronal subtypes have different electrophysiological and morphological properties (Tepper et al., 2010), we selected a set of parameters that would permit a classification of the different neurons in the field. Morphological properties were divided into 11 features (AR, AREA, CIRC, FERET, FERET ANGLE, FERET MIN, FERET X, FERET Y, PERIM, ROUND, SOLIDITY). Response properties of the neurons were divided into 5 temporal features (MEAN, STDDEV, MODE, SKEW, KURT).

A correlation between the different features is then estimated. Based on the results of MSNs and interneurons, supervised learning of the algorithm extracted 7 main features that allowed for the classification of neurons into these two groups. These features corresponded to response dynamics, temporal and morphological features (FALL LOG, X 0, X 0 RAW, RISE LIN, X SKEW, FERET, STD). These features correspond to ones that are used in the literature to study neuronal responses (Patel et al., 2015).

Thus, with this algorithm, we were able to differentiate MSN and interneuron responses in the recorded field. INs were not taken into account in study 1 in order to make sure that the observed dynamics are not due to the different intrinsic properties of different groups of neurons. This classifier is therefore important for that purpose. In addition, the striatal territories are composed of around 10% of INs which exert strong modulatory effects on the surrounding networks (Fino et al., 2018; Tepper et al., 2010). The classifier is therefore

important to separate the different groups of interneurons from MSNs and study the role interneurons play in the reorganization of the networks during learning. The accuracy of the classifier was around 87% for MSNs and 73% for interneurons. The lower accuracy rate of the interneurons could be due to the grouping of all types of interneurons in one group and to the lower number of interneurons (3840 MSNs vs 364 interneurons). Future work should label and record a higher number of striatal INs, allowing for a better classification of interneurons. This algorithm was limited to neurons from naïve animals since we did not know how the different phases of learning would affect the activity of the neurons and their response dynamics. Future work should increase the number of recorded cells, thus allowing for a better training of the classifier, and an increase in the accuracy rate. In addition, an increase of the number of samples for trained animals would allow a classification based on neuronal subtypes, but also based on the level of training.

Calcium signals based on the used calcium sensor (GCaMP6f) do not allow for a precise examination of the signals. Indeed, we do not know how many spikes are present in the recorded calcium signals. The stimulation protocol used in study 1 uses stimulation frequencies which do not allow for an individualization of the responses. It would be interesting to look at single stimulations in order to identify single spikes, thus having calcium dynamics closer to the electrophysiological dynamics. This can also be rectified by combining electrophysiological and calcium imaging experiments (Jouhanneau & Poulet, 2019).

IV- Study 3: Disruption of motor skill learning and associated striatal network activity in a Huntington's Disease mouse model

Dysfunctions in the BG can lead to the development of neurodegenerative disorders such as Huntington's disease (HD), a disease characterized by a triad of motor, cognitive and psychiatric symptoms. The discovery that cognitive deficits occur during the 10 years period before diagnosis of HD resulted in an increase of interest in the development of tests, tools and markers to examine these cognitive deficits, thus allowing an early detection of the disease. Degeneration mainly affects the striatum and the cortex, but before degeneration occurs, alterations in the corticostriatal projections have been described. Although alterations of cortical activity in relation to motor impairments have been well defined with electrophysiological and imaging studies, alterations in the striatum and of corticostriatal projections in the context of learning remain unclear.

Here, I used a mouse model of HD that expresses subtle motor deficits very late in the disease, the Hdh^{Q140} knock-in mouse model (Menalled et al., 2003). First I tested motor skill learning to determine if there were any early deficits in learning in this mouse model. Then I characterized the activity of the different striatal territories to determine if and how these networks would be affected in an early premotor symptomatic phase of HD. Our goal is to use these deficits and the alterations of the networks as an early marker of the disease.

Disruption of motor skill learning and associated striatal network activity in a Huntington's Disease mouse model

Badreddine N[1], Appaix F[1], Becq G[2], Tremblay N[2], Achard S[3], Saudou F[1] and Fino E[1#]

[1]Univ. Grenoble Alpes, INSERM U1216, CHU Grenoble Alpes, CNRS, Grenoble Institut Neurosciences, Grenoble, France

[2]Univ. Grenoble Alpes, Laboratoire Gipsa-Lab, UMR 5216 CNRS, Grenoble-INP, Grenoble, France

[3]Univ. Grenoble Alpes, Laboratoire Jean Kuntzmann, UMR 5224 CNRS, Grenoble, France

#To whom correspondence should be addressed (corresponding author): Elodie Fino: elodie.fino@inserm.fr

Key words: Striatum, Motor skill learning, Mice, Calcium Imaging, Spatiotemporal dynamics of neural networks, Huntington, Hdh^{Q140}.

INTRODUCTION

Huntington's disease (HD) is a neurodegenerative disorder characterized by a triad of symptoms: motor, cognitive and psychiatric, caused by an expansion of the CAG repeat in exon 1 of the huntingtin gene (MacDonald et al., 1993). The striatum is the most affected structure in HD, and the first one to start degenerating (Vonsattel et al., 1985). The cortex is also affected and suffers from degeneration in certain cortical areas. Degeneration in these brain structures has been linked to the characteristic motor deficits in HD. However, during the ten years period before motor symptoms appear, cognitive deficits have been widely described (Biglan et al., 2016; Papoutsi et al., 2014). A deterioration of executive functions and psychomotor speed are the first signs of cognitive decline. Patients have difficulty in organizing, planning, attention, and in verbal fluency (Ajitkumar & De Jesus, 2020; Garcia-Gorro et al., 2017). These symptoms will progress and at late stages of the disease patients have dementia with global impairment of cognition (Cardoso, 2017; Papoutsi et al., 2014). The examination of the speed of processing, initiation and attention measures seem to allow for a better diagnosis of HD and the onset of functional decline (Paulsen, 2011). Indeed, the PREDICT-HD study showed that prodromal HD patients suffer from a decline of the speed of thinking and motor skills, by using a speeded tapping test (Stout et al., 2011). One of these cognitive deficits was debated, the one concerning procedural memory. Only declarative

memory seemed to be affected by HD at first (Sprengelmeyer et al., 1995), but accumulating evidence shows that procedural memory is affected as well in HD patients (Bylsma et al., 1990; Holtbernd et al., 2016) and in HD animal models (Cayzac et al., 2011; Kirch et al., 2013). Since the tapping test showed promising results in detecting HD even in prodromal phases, motor skill learning seems to take a big part in HD detection in patients. Motor skill learning could therefore be a good parameter to detect HD early.

In order to understand the physiopathology behind the different deficits in HD, studies focused on the cortex and the striatum as the most affected structures during the progression of the disease. It was suggested that alterations and disturbances of the corticostriatal connections could precede the observed degeneration at late stages of the disease. Imaging and electrophysiological studies reported elevated cortical activity in premanifest HD (Arnoux et al., 2018; Burgold et al., 2019; Donzis et al., 2020) with an altered synchrony between cortical and striatal networks (Lee Hong & Rebec, 2012; Naze et al., 2018), thus confirming the occurrence of alterations in the networks before the start of degeneration. In an attempt to link dysfunctions in the cortex to the behavioral symptoms observed in premanifest HD, Deng et al. showed a significant reduction of the number of corticostriatal terminals in 12 month-old knock-in mouse model of HD, Hdh^{Q140}, but not earlier, thus involving cortical alterations in motor impairments (Deng et al., 2013). However, one can wonder what kind of alterations occur before motor dysfunctions appear and how specific it is to the functional corticostriatal networks involved. Indeed, corticostriatal connections are organized in functional territories, forming then cortico-basal ganglia-thalamocortical loops (Redgrave et al., 2010). Within the striatum, these loops are maintained and form two big functional territories, the dorsomedial striatum (DMS), involved in cognitive and associative loops, and dorsolateral striatum (DLS), included in the sensorimotor loops. Alterations of excitatory synaptic transmission from motor cortex to MSNs in the DLS were shown early in a YAC128 mouse model of HD with deficits in motor learning (Glangetas et al., 2020). In this study, they also showed the necessity of the plasticity from motor cortex to DLS for the consolidation of motor skill learning. Another recent study explored the territory-specificity of striatal activity and functional connectivity in the R6/1 mouse model of HD during learning of a striatum-dependent task (Cabanas et al., 2017). By measuring the level of c-fos expression in DMS and DLS (among others), they observed an increase of activity in the DMS of R6/1 mice at 2 months old and in the prefrontal cortex, but not in the DLS. Interestingly, the differential role of DMS and DLS territories has

been shown in striatal-dependent tasks involving procedural learning: the DMS would be more active in the first phase of learning, called goal-directed behavior, and the DLS would be more active once habit is formed (Costa et al., 2004; Kupferschmidt et al., 2017; Smith & Graybiel, 2013; Thorn et al., 2010; Yin et al., 2009).

Our aim here was thus to explore if deficits in motor skill learning occur early in a mouse model of HD with a long premotor symptomatic phase (Hdh^{Q140}) and if and how these deficits would be associated to detectable dysfunctions at the level of the corticostriatal networks. In order to characterize the full course of learning, we explored the contribution of two striatal functional territories, DMS and DLS, involved in the different phase of the motor skill formation.

We show an alteration of the performance of Hdh^{Q140} mice in a late phase of motor skill learning using the accelerated rotarod. Using *ex vivo* two-photon calcium recordings, we explored the activity of the DMS and DLS networks and we show alterations in the DMS and the DLS networks activity and an absence of a reorganization upon motor skill learning.

Our data show early deficits in motor skill learning, which were translated at the level of the networks. These alterations and deficits, occurring in an early premotor symptomatic phase, could be used as an early marker of the disease.

MATERIALS AND METHODS

EXPERIMENTAL MODELS

Hdh^{Q140} knock-in mice with a C57BL/6J background were used in this study. These mice express human HTT exon1 with 140 repeats of CAG. This HD model was chosen because Hdh^{Q140} develop motor symptoms after several months (Crook & Housman, 2011; Menalled et al., 2003), allowing us to study the pre-symptomatic phases. Mice used in this study were 1.5 month-old. Mice were housed in temperature-controlled rooms with standard 12 hours light/dark cycles and food and water were available *ad libitum*. Every precaution was taken to minimize stress and the number of animals used in each series of experiments. All experiments were performed in accordance with EU guidelines (directive 86/609/EEC) and in accordance with French national institutional animal care guidelines (protocol APAFIS#8241-2016092317163976 v2).

METHOD DETAILS

AAVs

An adeno-associated virus (AAV) of serotype of 5 was used to express a calcium indicator in striatal cells. AAV5-syn-GCaMP6f-WPRE-SV40 was purchased from UPennCore (PA, USA).

Stereotaxic injections

Stereotaxic intracranial injections were used to deliver the AAV in the striatum. Mice were anesthetized with 2.5 % isoflurane and placed in a stereotaxic frame (Kopf). Under aseptic conditions, the skull was exposed and leveled and a craniotomy was made with an electric drill. The viruses (serotype 5, ≈ 10^{12} genomic copies per mL) were injected through a pulled glass pipette (pulled with a P-97 model Sutter Instrument Co. pipette puller) using a nanoinjector (World Precision Instruments, Germany). The pulled glass micropipette was slowly lowered into the brain and left 1 min in place before starting the injection of the virus at an injection rate of 100 nL per min. A volume of 400 nL of the virus was enough to infect a large proportion of DMS or DLS. The injections targeted the DMS at coordinates AP + 1.1mm, ML 1.2, DV - 1.9 and the DLS at AP - 0.38, ML 2.3, DV - 2.45. Following injections, we waited 5 min before raising the pipette out of the brain. To minimize dehydration during surgery mice received a subcutaneous injection of 1mL of sterile saline. Postoperatively mice were monitored on a heating pad for 1 h before being returned to their home cage. Mice were then monitored daily for 4-5 days. A period of 15 to 20 days after injections was enough to allow for a good expression of AAVs. We observed similar expression of GCaMP6f in all striatal neurons in DMS or DLS in injected mice with viral vectors.

Behavioral training

Accelerated rotarod

An accelerating rotarod was used as a motor skill learning paradigm. In the previous days of the training, mice were acclimated to the room and to handling. For each trial the mouse was placed on the still rotarod which was activated at that point. The rotation of the rod increased from 4 to 40 rotations per min over 300 s. Each trial was ended when the mouse fell off the rotarod or when the 300 s had elapsed. There was a resting period of 300 s between trials. Animals were trained with 10 trials per day for either 1 day (early training) or 7 days every day

(late training). This training protocol was chosen since it was previously described as a reliable test for motor skill learning or procedural learning.

Open-field

The open-field test was performed during the light phase of the light cycle to test locomotor activity. Mice were placed in the center of a square Plexiglas open-field (50x50x50 cm) and their activity recorded with the Viewpoint VideoTrack system. Quantitative analysis of two behaviors was performed during the 60 minutes of recording: time spent by each mouse in the center to measure the level of stress, and total traveled distance to measure locomotor activity. Before each mouse was tested, the open-field was cleaned with ethanol.

Fixed-speed rotarod

To test motor balance of animals, a fixed-speed rotarod was used. The same apparatus was used. Four different speeds were tested: 4, 10, 20 and 30 rpm. Animals were placed on the rotating wheel and their latency to fall was measured. Five trials per speed were done, with a 300 s resting period between each trial. A resting period of 600 s was given to mice when there was a change in speed.

***Ex vivo* two-photon imaging**

Brain slice preparation.

Two weeks after AAVs injections and after rotarod training, brain slices preserving DMS and DLS with their cortical inputs coming from sensory and cingulate cortex respectively were prepared as previously described. Animals were anesthetized with isoflurane before extraction of the brains. We prepared brain slices (300 µm) using a vibrating blade microtome (VT1200S, Leica Microsystems, Nussloch, Germany). Brains are sliced in a 95 % CO_2 and 5 % O_2-bubbled, ice-cold cutting solution containing (in mM) 125 NaCl, 2.5 KCl, 25 glucose, 25 $NaHCO_3$, 1.25 NaH_2PO_4, 2 $CaCl_2$, 1 $MgCl_2$, 1 pyruvic acid, and then transferred into the same solution at 34°C for one hour and then moved to room temperature.

Two-photon calcium imaging.

Genetically-encoded Ca^{2+} indicator GCaMP6f was used for Ca2+ imaging of somas of striatal cells. GCaMP6f is expressed with recombinant AAVs injected in DMS or DLS. Two-photon calcium imaging was performed at 940nm with a TRiMScope II system (LaVision BioTec, Germany) using a resonant scanner, equipped with a 20x/1.0 water-immersion objective (Zeiss) and coupled to a Ti:Sapphire laser (Chameleon Vision II, Coherent, >3W, 140 fs pulses,

80MHz repetition rate). The average power of the laser emitted was set at ~40-50mW on sample. Fluorescence was detected with a GaAsP detector (Hamamatsu H 7422-40). Scanning and image acquisitions were controlled with Imspector software (LaVision BioTec, Germany) (15.3 frames per second for 1024 x 1024 pixels, between 50 to 150 µm underneath the brain slice surface, with no digital zoom). Typical images window for calcium imaging of wide field is 392 µmx392 µm.

Cortical stimulation protocols

Electrical stimulations were applied with a bipolar electrode (MicroProbes, USA) placed in the layer 5 of either the somatosensory or the cingulate cortex as previously described (Fino et al., 2018). Electrical stimulations were monophasic at constant current (Iso-Flex, AMPI, Science Products). Single cortical stimulations or trains of stimulations were delivered; trains consist of 5 stimulations (1 ms) delivered at different frequencies (5, 10, 20, 50 Hz). Single or trains of stimulations are applied at 0.1 Hz, a frequency for which no short- or long-term changes are observed.

DATA ANALYSIS

Behavior

Accelerated rotarod

The time to fall (latency) from the rod was measured to evaluate the performance in the motor skill learning. In accordance with previous studies trial 1 and 2 data were pooled as early trials and trial 9 and 10 data pooled as late trials for each day. We calculated a learning index by subtracting late trials from early trials for early training. For late training, learning index corresponded to a subtraction of the early trials of Day 1 from the late trials of Day 7.

Open-field

Total distance travelled during the 60 min recordings was averaged per animal. A central zone of 25x25 cm was drawn and the time spent in the center was averaged per animal.

Calcium imaging analysis

GCaMP6f fluorescence signals were analysed in R environment with custom-built procedures in R3.5.2 and RStudio. Cells outlines were drawn manually using FIJI software and we extracted mean grey values and (x, y) coordinates of each ROI. Let x(t) be the averaged intensity values of pixels in the ROI at time t for one cell. ΔF/F is obtained using y(t) = (x(t) - x0) / x0, where x0

is the mean value of the 50 % lowest values in the last 10 sec. ΔF/F is then filtered with a Savitsky-Golay filter of order 3 on sliding windows of 7 samples (0.458 s). Binarized data were obtained by using M±2 SD cut-off for each cell; a cell is defined active if its ΔF/F is above this threshold, with mean (M) and standard deviation (SD). Recordings were 700-1000 frames long (around 1 min) and included 6-9 stimulations of cortical afferents, 5 responses (stimulations #2 to #7) were averaged to have a mean effect per cell. We distinguished responses from SPNs and other cell types of striatal neurones thanks to a method we previously developed. We were thus confident that almost all the analyzed cells were SPNs. For DMS, the average amplitude of all cells in naive condition was taken as the threshold to determine the LRA cells population. Importantly, we tried other methods such as k-means algorithm to sort the highly active cells. The different methods gave similar results and since there was no clear spatial reorganization in DMS, it appeared more accurate to use a threshold than the k-mean analysis. For DLS, cells were clustered using a k-means algorithm. The optimal number of groups (k=3.3 ± 0.1) was defined using the 'elbow method', by visual inspection of the plot, of the function to compute total within-cluster sum of squares with k varying from 1 to 10 and determining the bend in the elbow. The group containing the cells with the maximal amplitude was defined as the LRA cell and contains M ± SEM % of cells in the slice (field of the slice). The cluster area was computed using the convex hull formed by these cells and the percentage of cluster area was calculated based on the convex hull described by the active cells on the edges of the field of view. Pairwise correlations were computed using Pearson's correlation between signals extracted on windows of 40 samples (2.6 s) centered on the time of the first maximal amplitudes of ΔF/F (peaks) detected on cells after stimulus.

Statistical analysis

The data are presented and plotted as values ± SEM. p values are represented by symbols using the following code: * for $p< 0.05$, ** for $p< 0.01$, *** for $p< 0.001$. Exact p values and statistical tests are stated in the figure legends or in the core of the manuscript. Statistical analysis was performed using Prism 7.0 (GraphPad, San Diego, USA) or R environment. The sample size for the different sets of data is mentioned in the respective figure legends. Normality of each data set was checked using D'Agostino and Pearson's test. Unless otherwise stated, all data sets are reported as mean ± SEM, with SEM standard error of the mean, and statistical significance was assessed using Student's t-test or Mann-Whitney's U-test and

Wilcoxon's signed rank test for unpaired and paired data, respectively. One-way Anova was used to compare all the effects together in DMS and DLS between the different training conditions. Pearson correlation was used for relationship between cluster size and learning index. Two-way Anova followed by Bonferroni *post-hoc* test was used to compare learning curves in WT and Hdh^{Q140} groups.

RESULTS

Early phase of motor skill learning is not affected in Hdh^{Q140} mice

To evaluate motor skill formation in mice, we used the accelerated rotarod paradigm. Accelerated rotarod learning involves two distinct stages, the early and late phases, respectively involving DMS and DLS, which thus appears as a suited procedure to evaluate the possible progressive alterations of performance in Hdh^{Q140} mice.

We first evaluated the performance of mice during the first stage of learning. This stage corresponds to early training, with 10 trials executed the same day (Day1) (Fig.1a). We trained two groups of mice, WT and Hdh^{Q140} mice and we compared their learning performance. We did not observe any difference in the learning curve between the two groups after early training ($p=0.4626$, $F_{(9,400)}=0.972$, two-way ANOVA) (Fig.1b). This result was confirmed by the measure of the learning index of mice (Fig.1b). The learning index is a measure of the level of learning of an animal, calculated by doing the difference between the beginning and end of training (last two trials – first two trials). We did not see any significant difference in the learning index between the two groups (unpaired t-test, $p=0.3776$). Therefore, there is no difference in early learning of the skill between these two groups.

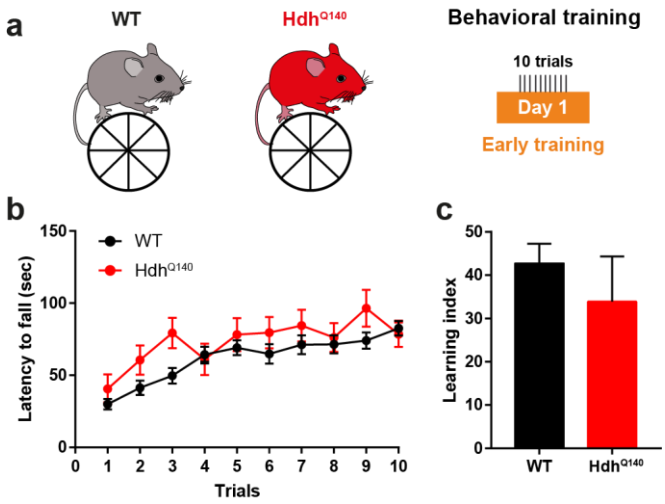

Figure 1: Similar learning curves during early training for WT and Hdh^{Q140} mice. **a**: Behavioral paradigm used to induce the first phase of learning. WT and Hdh^{Q140} mice are trained on an accelerated rotarod for 1 day with 10 trials, which corresponds to early training. **b**: learning curve of WT (n=27) vs Hdh^{Q140} (n=15) mice. No difference in performance was found between Hdh^{Q140} and WT mice (p=0.4626, $F_{(9,400)}$=0.972, two-way ANOVA). **c**: No difference in the learning index between WT and Hdh^{Q140} mice was observed (p=0.3776, unpaired t-test).

Dynamics of DMS networks are altered in Hdh^{Q140} mice

We showed in our previous study how neuronal dynamics are reorganized in DMS after early training. We described modifications in overall amplitude of responses and percentage of highly active cells (HA cells) between the different training conditions (Badreddine et al., in revision). Even though we did not observe a significant effect on the performance, we wondered if we could detect any alterations of the DMS dynamics in Hdh^{Q140} mice. To do so, a calcium sensor, GCAMP6f was injected in the DMS and mice were trained on the accelerated rotarod at two training stages (naïve or early). At the end of the training, as previously described (Badreddine et al., in revision), we recorded the network activity *ex vivo* for all animals using two-photon calcium imaging. Calcium signals were then extracted and measured in all medium spiny neurons (MSNs) which allowed us to build functional maps based on the amplitude of response (Fig.2a). In DMS of WT mice, we observed a strong decrease of the overall activity of MSNs in early-trained mice compared to naïve mice (p=0.0062, t-test) (Fig.2b). We observed a significantly lower response in naïve Hdh^{Q140} animals compared to naïve WT mice (p=0.0013, t-test). However, we did not observe any difference between naïve and early-trained Hdh^{Q140} mice (p=0.3519, t-test). Similar variations were observed for the percentage of highly active cells, or HA cells, between naïve and early-trained WT mice (p=0.0484, unpaired t-test) (Fig.2c). We next analyzed if changes in

corticostriatal network activity was linked to the animal's performance during motor learning by correlating the percentage of HA cells with the learning index measured earlier (Fig.2d). The number of HA cells is inversely correlated to the motor performance of WT early-trained (r^2=0.5189, p=0.0124) but not Hdh^{Q140} early-trained mice (r^2=0.01816, p=0.7733). These results show that, in WT mice, the smaller the number of HA cells, the better the animal learns the task, thus linking network reorganization and learning performance. This correlation does not exist in the case of Hdh^{Q140} animals.

It has been shown that most of HD mouse models exhibit alterations in cortical and striatal synaptic transmission and plasticity in presymptomatic animals (for review see (Raymond et al., 2011)). Thus, examining the plasticity properties of the corticostriatal networks could reveal specific characteristics of the networks in both mice groups which could explain the dysfunctions we observed in the DMS networks. To test plasticity, we used various stimulation frequencies and measured the evolution of the responses between different frequencies. We previously described that, in DMS, naïve mice display an increased response between low (5Hz) and high (20Hz) frequency cortical inputs while, after early training, DMS networks respond similarly (Badreddine et al., in revision). Thus, we wondered if the plasticity of the network (or lack of plasticity) could explain the alterations we observe in the DMS networks in Hdh^{Q140} mice. We first examined the evolution of the amplitude of response in function of the stimulation frequency (Fig.2e). We observed in both WT and Hdh^{Q140} groups an increase of the response with the increase of the stimulation frequency (WT p=0.0137, HD p=0.0025, paired t-test). However, after training, we observed no difference in the amplitude of response between 5 and 20Hz (WT p=0.0733, Hdh^{Q140} p=0.0964). By looking at the evolution of the percentage of HA cells between 5 and 20 Hz (low and high stimulation frequencies), we observe an increase in naïve conditions for both WT (p=0.0108) and Hdh^{Q140} mice (p=0.0097), but not for WT (p=0.4385) and Hdh^{Q140} (p=0.6550) early-trained mice (Fig.2f). The plastic behavior of the DMS networks does not seem to be affected in the Hdh^{Q140} mouse model. These results suggest that the alterations we observe in the DMS networks in Hdh^{Q140} mice are not due to the properties of these HA cells and the plasticity of the networks.

To sum up, we do not observe any major alterations of learning in Hdh^{Q140} mice in the early phase, but we do observe alterations of the dynamics of the DMS networks. We can hypothesize that the alterations we observe are not strong enough to have any effect on behavior in the early phase of training.

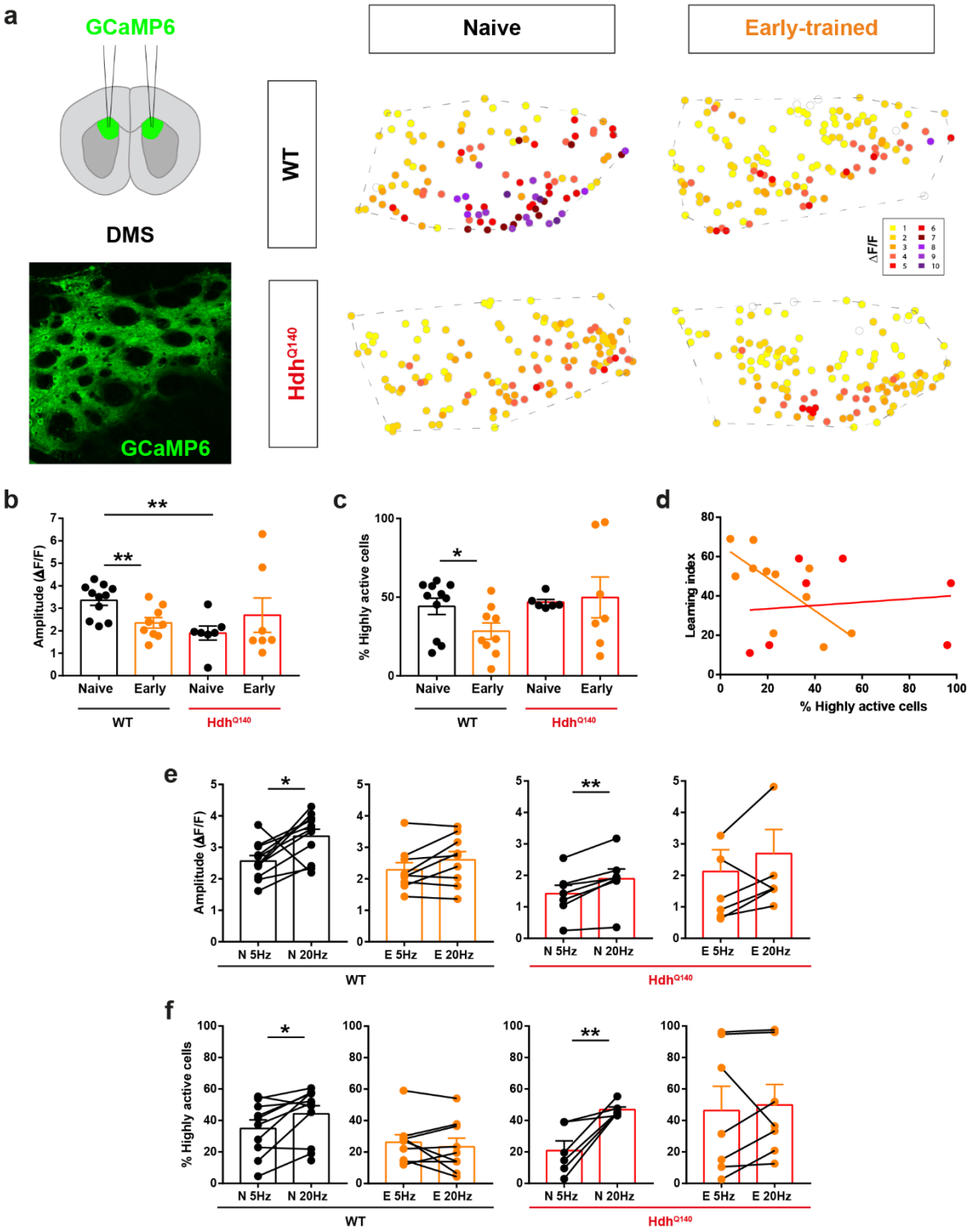

Figure 2: *DMS dynamics are altered in Hdh^{Q140} mice.* ***a****: Injection of calcium sensor GCaMP6f in the DMS and two-photon acquisition of a recording field of MSNs expressing GCaMP6 in the striatum. Representative functional maps of striatal networks in DMS for naïve and early-trained animals, in WT and Hdh^{Q140} conditions. The color code corresponds to the amplitude of response (ΔF/F) with yellow color for lower amplitude and red/purple/brown for the highest ones.* ***b****: Averaged amplitude of response of all MSNs in the recording field in the different training conditions (naïve, early) and different groups (WT, Hdh^{Q140}) in DMS. Significantly lower activity for naïve Hdh^{Q140} mice compared to WT (**p=0.0013, WT n=11, Hdh^{Q140} n=7, t-test). Decrease of overall activity in early conditions compared to naïve conditions in WT mice (**p=0.0062, t-test), but no difference between naïve and early-trained*

*Hdh^{Q140} mice (p=0.3519, t-test). **c**: Percentage of cells with the highest amplitude in naïve and early conditions in both mice groups, WT and Hdh^{Q140} in DMS. Similar percentage of cells with highest activity for naïve Hdh^{Q140} and WT mice (p=0.7234, WT n=11, Hdh^{Q140} n=7, t-test). Decrease of overall activity in early conditions compared to naïve conditions in WT mice (*p=0.0484), but no difference between naïve and early-trained Hdh^{Q140} mice (p=0.8353). **d**: Correlation between the percentage of highly active cells and the learning index of the animals after early training. WT mice: in orange, Hdh^{Q140} mice: in red. Significant correlation for the WT early-trained mice in DMS (r^2=0.52, p=0.0124, pearson correlation), but not for Hdh^{Q140} early-trained mice (r^2=0.02 p=0.773, pearson correlation). **e**: Evolution of the amplitude of response between 5 and 20Hz stimulation frequency. A significant increase of the amplitude between 5 and 20Hz for naïve WT mice (*p=0.0137, paired t-test) and Hdh^{Q140} mice (**p=0.0025, paired t-test), but not for early-trained WT (p=0.0733) and Hdh^{Q140} mice (p=0.0964). **f**: Evolution of the percentage of highly active cells between 5 and 20Hz stimulation frequency. This percentage significantly increases for naïve WT (*p=0.0108, paired t-test) and Hdh^{Q140} mice (**p=0.0097) but not for early-trained WT (p=0.4385) and Hdh^{Q140} mice (p=0.6550). N: naïve mice, E: early-trained mice, 5Hz and 20Hz refer to the stimulation frequency.*

The late phase of motor skill learning is strongly affected

We next examined the learning performance of Hdh^{Q140} mice after late training. This training corresponds to 7 days of training, with 10 trials a day, a protocol which allows a stable and long-lasting formation of the motor skill, as we and others previously described (Badreddine et al., in revision; Jin & Costa, 2015; Yin et al., 2009). We trained both groups of mice with late training and we evaluated the behavioral performance (Fig.3a). We observed that Hdh^{Q140} mice did not perform as well as WT mice since they have a significantly different learning curve (Fig.3b) (p=0.0131, $F_{(1,252)}$=6.247, two-way ANOVA). Moreover, we observe a significant decrease of the learning index of Hdh^{Q140} compared to WT mice (p=0.0052, unpaired t-test) (Fig.3c). Altogether we observed that motor skill formation was affected in Hdh^{Q140} mice compared to WT mice.

To verify that these changes in performance were not due to any motor deficits, we assessed motor behavior and motor coordination in both WT and Hdh^{Q140} mice using the open-field test (Fig.3d) and the fixed-speed rotarod (Fig.3e). Within the open-field, two measures are important, the total distance traveled in the field and the time spent in the center. The total distance gives a measure of the locomotor activity of the mice while the time spent in the center measures the level of stress of the animals. We first measured the distance traveled by WT and Hdh^{Q140} mice and we did not observe any difference between both groups (WT n=4, Hdh^{Q140} n=4, p=0.4465, unpaired t-test). When we measured the time spent in the center of the arena, again, we did not observe any difference between Hdh^{Q140} and WT mice (p=0.6209, unpaired t-test). We then tested the animals on the fixed-speed rotarod (10 rpm) paradigm to

have a more precise reading of motor coordination. We did not observe any difference between Hdh^{Q140} and WT mice on the fixed speed rotarod (p=0.5912, unpaired t-test). Thus, the changes we observed in Hdh^{Q140} mice after late training are not due to any motor activity or coordination deficits since they perform as well as WT mice.

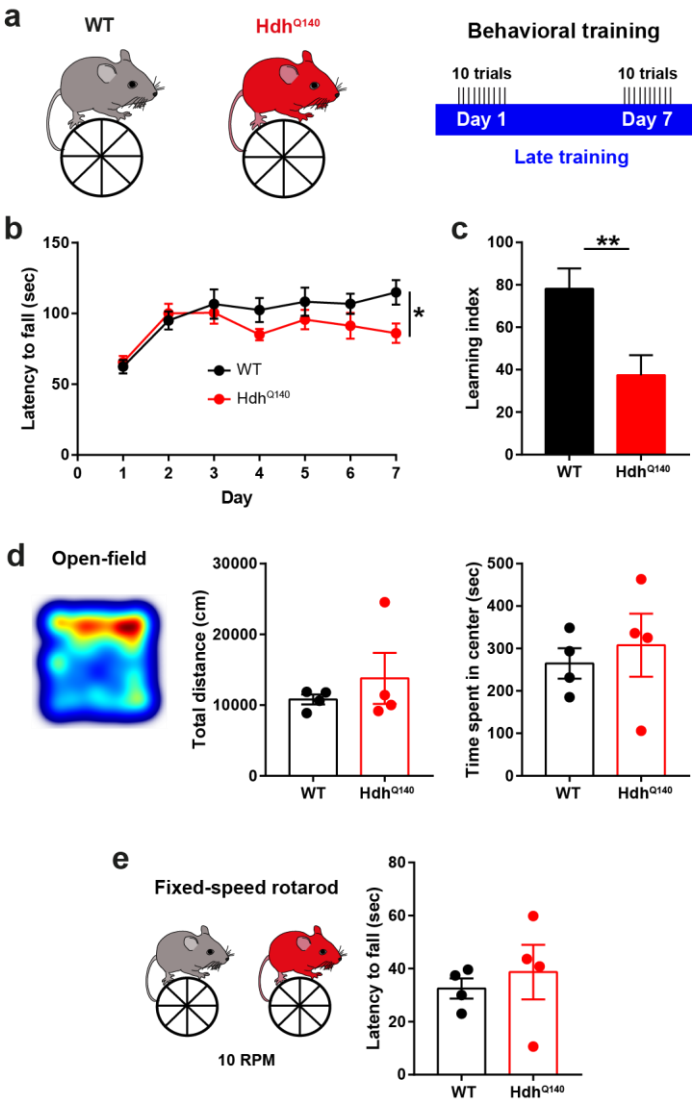

Figure 3: *Deficits in late phase of motor skill learning but not in motor activity in Hdh^{Q140} mice.* ***a****: Behavior paradigm used to induce the late phase of learning. WT and Hdh^{Q140} mice are trained on an accelerated rotarod for 7 days with 10 trials per day, which corresponds to late training.* ***b****: learning curve of WT (n=21) vs Hdh^{Q140} (n=17) mice. Hdh^{Q140} mice have a significantly lower performance compared to WT mice (*p=0.0131, $F_{(1,252)}$=6.247, two-way ANOVA).* ***c****: Learning index of Hdh^{Q140} mice is significantly lower compared to WT mice (**p=0.0052, unpaired t-test).* ***d****: Open-field test in which the total distance traveled and the time spent in the center were measured. Left: No difference in the total distance traveled between both groups (WT n=4, Hdh^{Q140} n=4, p=0.4465, unpaired t-test). Right: No difference in time spent in the center between both groups (p=0.6209, unpaired t-test).* ***e****: Fixed-speed rotarod was set at 10 rpm. Similar latencies were observed between WT and Hdh^{Q140} mice (p=0.5912, unpaired t-test).*

Learning deficits are associated to DLS network alterations

We then asked whether this deficit in learning performance of Hdh^{Q140} mice was associated to a modification of the DLS networks dynamics. For this purpose, we performed similar experiments and analysis than the one described for the DMS, but in DLS (Fig.4a). First we measured the averaged activity per field and we observed a clear and significantly lower amplitude of response in naïve Hdh^{Q140} mice compared to WT mice ($p=0.0022$, unpaired t-test) (Fig.4b). We did not observe any difference in the amplitude after late training for WT and Hdh^{Q140} mice. This would mean that Hdh^{Q140} mice start off with a lower activity than WT mice, but follow the same activity rules as in WT mice. We have shown previously that the DLS is characterized by the gradual formation of clusters of activity with learning (Badreddine et al., in revision). Thus, we decided to measure the area that is formed by the cells with highest activity based on a k-means cluster analysis. First we observed a significantly lower clustering area in Hdh^{Q140} mice compared to WT mice in naïve conditions ($p=0.0011$, unpaired t-test) (Fig.4c). When we looked at the effect of late training on the reorganization of the activity we observed a significant decrease of the area with the highest activity in WT mice after late training ($p>0.0001$, t-test), but this area remained the same in Hdh^{Q140} mice after late training ($p=0.9072$). Interestingly, late-trained WT mice had a smaller cluster area than Hdh^{Q140} mice ($p=0.0152$). These results show that Hdh^{Q140} mice start with a lower activity and a small clustering area which is not affected by training. We then wondered if these changes in the corticostriatal networks activity could be linked to the performance of the animals, so we correlated the clustering area and the learning index (Fig.4d). We observed an inverted correlation of these two parameters for WT mice ($r^2=0.5181$, $p=0.0083$) showing that the smaller the clustering area, the better the animal learns. On the contrary, we did not observe any correlation for Hdh^{Q140} mice ($r^2=0.2035$, $p=0.2619$).

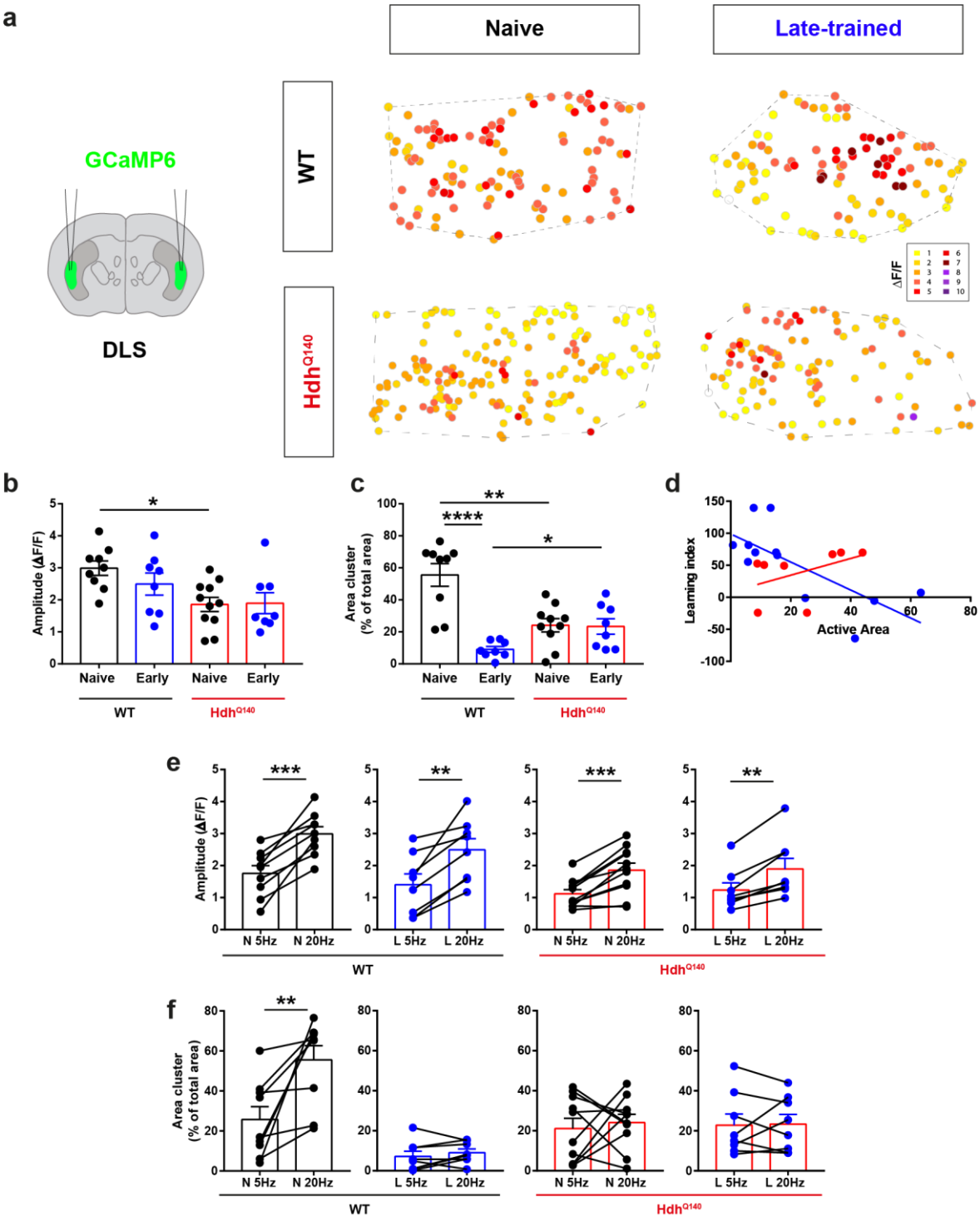

Figure 4: *Alterations in DLS networks activity in Hdh^{Q140} mice.* ***a****: Injection of calcium sensor GCaMP6f in the DLS. Representative functional maps of striatal networks in DLS for naïve and late-trained animals, in WT and Hdh^{Q140} conditions. The color code corresponds to the amplitude of response (ΔF/F) with yellow color for lower amplitude and red/purple/brown for the highest ones.* ***b****: Amplitude of response averaged from all MSNs in the field. No effect of training was observed in WT and Hdh^{Q140} mice (WT mice: p=0.2365, naïve n=9, late n=8; Hdh^{Q140} mice: p=0.9170, naïve n=11, late n=8, t-test). But naïve Hdh^{Q140} mice had a significantly lower amplitude of response compared to WT mice (**p=0.0022, t-test).* ***c****: Area formed by clusters of highest activity. Significantly smaller areas for naïve Hdh^{Q140} mice compared to naïve WT mice (**p=0.0011, t-test). The cluster area decreased significantly after late training for WT mice (****p<0.0001, t-test) but did not change for Hdh^{Q140} mice (p=0.9072).*

*The cluster area is bigger for late-trained Hdh^{Q140} mice than for WT mice (*p=0.0152). **d**: Correlation between the cluster area and the learning index of the animals after late training for WT mice (blue) and Hdh^{Q140} mice (red). There was a significant correlation for the WT late-trained mice in DLS (r^2=0.5181, p=0.0083, pearson correlation), but not for Hdh^{Q140} early-trained mice (r^2=0.2035, p=0.2619, pearson correlation). **e**: Evolution of the amplitude of response between 5 and 20Hz cortical stimulation frequency. A significant increase of the amplitude between 5 and 20Hz for naïve WT mice (***p=0.0003, paired t-test) and Hdh^{Q140} mice (***p=0.0003, paired t-test). An increase is present after late training for WT mice (**p=0.0016) and Hdh^{Q140}mice (**p=0.0011). **f**: Evolution of the percentage of clustering area between 5 and 20Hz stimulation frequency. This percentage significantly increases for WT naïve (**p=0.0081, paired t-test) but not for Hdh^{Q140} naïve (p=0.6696). After late training, clusters area does not increase between 5 and 20Hz for WT (p=0.3374) nor Hdh^{Q140} mice (p=0.8928). N: naïve mice, L: late-trained mice, 5 and 20Hz refer to the stimulation frequency.*

We can thus clearly state that the DLS networks are altered in the Hdh^{Q140} mouse model. And these alterations are reflected on behavior, where we can see learning deficits after late-training.

We then wondered if these alterations or non-reorganization can be explained by the plasticity or lack of plasticity in Hdh^{Q140} mice. Here, we decided to look at the evolution of the amplitudes of response (Fig.4e) and the clustering areas (Fig.4f) between high (20Hz) and low (5Hz) stimulation frequencies. We observed an increase of the amplitude of response for WT and Hdh^{Q140} mice, with an increase of the amplitude between 5 and 20Hz in naïve and late-trained mice (WT naïve p=0.0003, late-trained p=0.0016; Hdh^{Q140} naïve p=0.0003, late-trained p=0.0011). In concordance with the results described for clustering areas, we observed an increase of the clustering area between 5 and 20Hz in naïve WT mice but not Hdh^{Q140} mice (WT p=0.0081, paired t-test; Hdh^{Q140} p=0.6696). Training seemed to affect this evolution of the clustering area for WT, with similar clustering areas at 5 and 20Hz (p=0.0983). However, since in naïve Hdh^{Q140} mice there was no evolution between 5 and 20Hz, the results remained the same after late training, with a similar clustering area between 5 and 20Hz (p=0.8928).

Altogether these results show that DLS networks are altered in Hdh^{Q140} mice by not following the same reorganization as WT mice after training. These alterations could be explained by the lack of plasticity we observe in the corticostriatal inputs.

DISCUSSION

Here we showed deficits in the late, but not early, phase of motor skill learning in a mouse model of HD, Hdh^{Q140}. Although the early phase of learning was not affected, the activity of

the associated DMS network was altered in naïve animals and we did not observe any different in the DMS activity before and after training in Hdh^{Q140} mice. The late phase of motor skill learning was significantly affected in 2 month-old Hdh^{Q140} mice. The deficits in the performance of animals on the accelerated rotarod were here reflected by alterations in the DLS networks activity. Naïve Hdh^{Q140} mice had significantly lower activity than WT mice and training did not induce any reorganization of the network dynamics in Hdh^{Q140} mice.

In previous reports concerning Hdh^{Q140} mouse model, Rising et al. showed that deficits on the accelerated rotarod did not appear before 11 months (Rising et al., 2011). This study does not contradict what we observed in our work. Indeed, the accelerated rotarod paradigm was done over a period of 3 days with 4 trials per day. In our results, the first days of learning were comparable to those of WT mice, the deficits we observed were towards the last phase of motor skill learning. We showed that these deficits in the late phase of learning were not due to any motor deficits, concurring with other studies showing that motor deficits do not appear before 4 months in this mouse model of HD (Hickey et al., 2008).

We examined the activity of the DMS and DLS networks involved in each phase of learning. We showed that the DMS networks were altered in Hdh^{Q140} mice. They had a lower overall amplitude of response with a similar percentage of HA cells compared to naïve WT mice. After early training, this percentage was not affected, nor was the amplitude of response, thus showing a lack of reorganization of the networks after learning. These altered dynamics of the networks were not reflected by the behavior since Hdh^{Q140} mice were able to learn in a similar manner to WT mice. This would suggest that these alterations are not strong enough to affect behavior. Late phases of learning were affected in Hdh^{Q140} mice, and these deficits were translated at the level of the networks by a lower amplitude of response and a smaller clustering area which did not change after late training. Interestingly, the clustering area was smaller compared to naïve WT mice and bigger compared to late-trained WT mice. These results suggest not only a dysfunction in the DLS networks before training, but also highlight the inability of the DLS networks to reorganize in smaller clusters after training.

Only late phases of learning were affected in Hdh^{Q140} mice, but both DMS and DLS networks showed altered activity compared to WT mice. Interestingly, the first experiments showing the role of the different striatal territories in learning showed that an inactivation of the DMS forces a reliance on a habit strategy (Yin, Knowlton, et al., 2005; Yin, Ostlund, et al., 2005). We

could hypothesize that the alterations in the DMS networks we observed earlier could be pushing the networks towards a habit strategy. However, this is met by alterations in the DLS networks, thus affecting the late phase of motor skill learning. More importantly, studies examining the role of the DLS in learning showed that lesions in the DLS led to goal-directed behavior controlling action (Yin et al., 2004). This suggests that the alterations in the DLS networks would lead to a goal-directed behavior strategy, corresponding to the early phase of learning, which was not affected in Hdh^{Q140} mice. Thus, we can imagine a loop between these two striatal territories where one territory looks to the other to take over until a semblance of balance is found. These results would therefore add evidence to the cooperative/competitive relationship between the DMS and DLS (Bergstrom et al., 2018; Kupferschmidt et al., 2017; Thorn et al., 2010; Vandaele et al., 2019). The fact that one territory would take over the other in case of alterations or lesions suggests a cooperative behavior between these two territories. Confirming this hypothesis would require to study the DMS networks after late training and DLS networks after early training in future work.
If we assume that the alterations we observe in the DMS networks are not strong enough to result in any deficits in early learning, then the deficits in late training might not be a direct result of these alterations, but of the ones we observe in the DLS networks. Interestingly, the DLS has been shown to be involved in 'bracketing' by being active at the beginning and the end of a task, and a chunking of the sequences forming an action (Barnes et al., 2011; Graybiel, 1998; Graybiel & Grafton, 2015; Jin & Costa, 2010, 2015; Jog et al., 1999; Thorn et al., 2010). Since early learning is not affected in Hdh^{Q140} mice, one can wonder if the 'chunking' of actions is at the basis of the deficits in late learning.

We showed in a previous study that motor skill learning affects DMS and DLS networks differentially with the emergence of neuronal substrates during early phases of learning in the DMS and late phases of learning in the DLS (Badreddine et al., in revision). In order to explain this reorganization and the possible mechanisms behind it, we realized electrophysiological and tracing studies. We showed changes in corticostriatal synaptic input weight in DMS, and an increase in the number of somatosensory projections into DLS after late training. In HD, altered synchrony has been described between cortical and striatal networks (Lee Hong & Rebec, 2012; Naze et al., 2018). In addition, Deng et al. showed a decrease of the number of corticostriatal terminals in the DLS when mice were 12 month-old (Deng et al., 2013). An

elevated cortical activity has also been described early in the disease in animal models with imaging and electrophysiological studies (Arnoux et al., 2018; Burgold et al., 2019; Donzis et al., 2020). Based on these data, we could expect different mechanisms for the Hdh^{Q140} mice compared to WT mice we described earlier. Indeed, these results suggest alterations in the corticostriatal projections and a poorer synaptic plasticity. Thus, a modulation of these networks by training might not be possible. Interestingly, a recent study using optogenetics showed that a repetitive stimulation of the M2 to DLS projections not only reversed motor deficits in 12 month-old mice, but also increased synaptic plasticity (Fernández-García et al., 2020). We can thus wonder if repetitive training, stimulating these networks, might be able to restore the observed deficits in Hdh^{Q140} mice. Even though these mice reached a plateau in their performance after late training, we can wonder if longer training will allow Hdh^{Q140} mice to reach a similar level than WT mice. Indeed, since goal-directed behavior does not seem to be affected, an improvement in their performance might be possible.

Synaptic plasticity from the M2 onto the DLS is reduced in HD mouse models (Fernández-García et al., 2020; Hintiryan et al., 2016; Raymond et al., 2011). We explored the plasticity of the corticostriatal networks by examining the response at low and high frequencies (5 and 20Hz). At the level of the DMS and the associated corticostriatal networks, we observed an increase of the response and the percentage of HA cells in both WT and Hdh^{Q140} mice, suggesting no alterations in plasticity at this level. In addition, these results suggest that the alterations in the DMS networks might be due to alterations in local circuits. Interestingly, the reduction in the projections from the cortex to the striatum only concerned M2 to DLS projections (Hintiryan et al., 2016). These data corroborate with the absence of plasticity of the DLS networks where we observed a similar cluster areas at low and high stimulation frequencies, suggesting the corticostriatal dysfunctions might be responsible for the deficits in late learning. Previous studies focused mainly on the M2 to DLS projections because of the characteristic motor deficits in HD. However, future work should concentrate on exploring the different mechanisms behind the alterations in motor skill learning and the differential alterations we observed in both DMS and DLS networks.

Finally, in this study we tested motor skill learning on an accelerated rotarod and concluded that only the late phase of learning was affected. However, future work should examine learning using other behavioral tests to confirm our results. Indeed, if other tests confirm our

observations, the alteration of motor skill learning could be a potent early marker of the disease onset and could allow adjusting potential therapeutic targets for the patients.

REFERENCES

Ajitkumar, A., & De Jesus, O. (2020). *Huntington Disease.*

Arnoux, I., Willam, M., Griesche, N., Krummeich, J., Watari, H., Offermann, N., Weber, S., Dey, P. N., Chen, C., Monteiro, O., Buettner, S., Meyer, K., Bano, D., Radyushkin, K., Langston, R., Lambert, J. J., Wanker, E., Methner, A., Krauss, S., … Stroh, A. (2018). Metformin reverses early cortical network dysfunction and behavior changes in Huntington's disease. *ELife*, *7*. https://doi.org/10.7554/eLife.38744

Badreddine, N., Zalcman, G., Appaix, F., Becq, G., Trembay, N., Saudou, F., Achard, S., & Fino, E. (n.d.). Spatiotemporal reorganization of corticostriatal network dynamics encodes motor skill learning. *In Revision*.

Barnes, T. D., Mao, J. Bin, Hu, D., Kubota, Y., Dreyer, A. A., Stamoulis, C., Brown, E. N., & Graybiel, A. M. (2011). Advance cueing produces enhanced action-boundary patterns of spike activity in the sensorimotor striatum. *Journal of Neurophysiology*, *105*(4), 1861–1878. https://doi.org/10.1152/jn.00871.2010

Bergstrom, H. C., Lipkin, A. M., Lieberman, A. G., Pinard, C. R., Gunduz-Cinar, O., Brockway, E. T., Taylor, W. W., Nonaka, M., Bukalo, O., Wills, T. A., Rubio, F. J., Li, X., Pickens, C. L., Winder, D. G., & Holmes, A. (2018). Dorsolateral Striatum Engagement Interferes with Early Discrimination Learning. *Cell Reports*, *23*(8), 2264–2272. https://doi.org/10.1016/j.celrep.2018.04.081

Biglan, K. M., Shoulson, I., Kieburtz, K., Oakes, D., Kayson, E., Aileen Shinaman, M., Zhao, H., Romer, M., Young, A., Hersch, S., Penney, J., Marder, K., Paulsen, J., Quaid, K., Siemers, E., Tanner, C., Mallonee, W., Suter, G., Dubinsky, R., … Shults, C. (2016). Clinical-genetic associations in the Prospective Huntington at Risk Observational Study (PHAROS) implications for clinical trials. *JAMA Neurology*, *73*(1), 102–110. https://doi.org/10.1001/jamaneurol.2015.2736

Burgold, J., Schulz-Trieglaff, E. K., Voelkl, K., Gutiérrez-Ángel, S., Bader, J. M., Hosp, F., Mann, M., Arzberger, T., Klein, R., Liebscher, S., & Dudanova, I. (2019). Cortical circuit alterations precede motor impairments in Huntington's disease mice. *Scientific Reports*, *9*(1), 6634. https://doi.org/10.1038/s41598-019-43024-w

Bylsma, F. W., Brandt, J., & Strauss, M. E. (1990). Aspects of procedural memory are differentially impaired in Huntington's disease. *Archives of Clinical Neuropsychology : The Official Journal of the National Academy of Neuropsychologists*, *5*(3), 287–297.

Cabanas, M., Bassil, F., Mons, N., Garret, M., & Cho, Y. H. (2017). Changes in striatal activity and functional connectivity in a mouse model of Huntington's disease. *PLOS ONE*, *12*(9), e0184580. https://doi.org/10.1371/journal.pone.0184580

Cardoso, F. (2017). Nonmotor Symptoms in Huntington Disease. In *International Review of Neurobiology* (Vol. 134, pp. 1397–1408). Academic Press Inc. https://doi.org/10.1016/bs.irn.2017.05.004

Cayzac, S., Delcasso, S., Paz, V., Jeantet, Y., & Cho, Y. H. (2011). Changes in striatal procedural memory coding correlate with learning deficits in a mouse model of Huntington disease. *Proceedings of the National Academy of Sciences*, *108*(22), 9280–9285. https://doi.org/10.1073/pnas.1016190108

Costa, R. M., Cohen, D., & Nicolelis, M. A. L. (2004). Differential corticostriatal plasticity during fast and slow motor skill learning in mice. *Current Biology*, *14*(13), 1124–1134. https://doi.org/10.1016/j.cub.2004.06.053

Crook, Z. R., & Housman, D. (2011). Huntington's disease: can mice lead the way to treatment? *Neuron*, *69*(3), 423–435. https://doi.org/10.1016/j.neuron.2010.12.035

Deng, Y. P., Wong, T., Bricker-Anthony, C., Deng, B., & Reiner, A. (2013). Loss of corticostriatal and thalamostriatal synaptic terminals precedes striatal projection neuron pathology in heterozygous Q140 Huntington's disease mice. *Neurobiology of Disease*, *60*, 89–107. https://doi.org/10.1016/j.nbd.2013.08.009

Donzis, E. J., Estrada-Sánchez, A. M., Indersmitten, T., Oikonomou, K., Tran, C. H., Wang, C., Latifi, S., Golshani, P., Cepeda, C., & Levine, M. S. (2020). Cortical Network Dynamics Is Altered in Mouse Models of Huntington's Disease. *Cerebral Cortex*, *30*(4), 2372–2388. https://doi.org/10.1093/cercor/bhz245

Fernández-García, S., Conde-Berriozabal, S., García-García, E., Gort-Paniello, C., Bernal-Casas, D., García-Díaz Barriga, G., López-Gil, J., Muñoz-Moreno, E., Soria, G., Campa, L., Artigas, F., Rodríguez, M. J., Alberch, J., & Masana, M. (2020). M2 cortex-dorsolateral striatum stimulation reverses motor symptoms and synaptic deficits in Huntington's disease. *ELife*, *9*. https://doi.org/10.7554/eLife.57017

Fino, E., Vandecasteele, M., Perez, S., Saudou, F., & Venance, L. (2018). Region-specific and

state-dependent action of striatal GABAergic interneurons. *Nature Communications*, *9*(1). https://doi.org/10.1038/s41467-018-05847-5

Garcia-Gorro, C., Camara, E., & De Diego-Balaguer, R. (2017). Neuroimaging as a tool to study the sources of phenotypic heterogeneity in Huntington's disease. In *Current Opinion in Neurology* (Vol. 30, Issue 4, pp. 398–404). Lippincott Williams and Wilkins. https://doi.org/10.1097/WCO.0000000000000461

Glangetas, C., Espinosa, P., & Bellone, C. (2020). Deficit in motor skill consolidation-dependent synaptic plasticity at motor cortex to dorsolateral striatum synapses in a mouse model of huntington's disease. *ENeuro*, *7*(2). https://doi.org/10.1523/ENEURO.0297-19.2020

Graybiel, A. M. (1998). The basal ganglia and chunking of action repertoires. *Neurobiology of Learning and Memory*, *70*(1–2), 119–136. https://doi.org/10.1006/nlme.1998.3843

Graybiel, A. M., & Grafton, S. T. (2015). The striatum: Where skills and habits meet. *Cold Spring Harbor Perspectives in Biology*, *7*(8). https://doi.org/10.1101/cshperspect.a021691

Hickey, M. A., Kosmalska, A., Enayati, J., Cohen, R., Zeitlin, S., Levine, M. S., & Chesselet, M.-F. (2008). Extensive early motor and non-motor behavioral deficits are followed by striatal neuronal loss in knock-in Huntington's disease mice. *Neuroscience*, *157*(1), 280–295. https://doi.org/10.1016/j.neuroscience.2008.08.041

Hintiryan, H., Foster, N. N., Bowman, I., Bay, M., Song, M. Y., Gou, L., Yamashita, S., Bienkowski, M. S., Zingg, B., Zhu, M., Yang, X. W., Shih, J. C., Toga, A. W., & Dong, H. W. (2016). The mouse cortico-striatal projectome. *Nature Neuroscience*, *19*(8), 1100–1114. https://doi.org/10.1038/nn.4332

Holtbernd, F., Tang, C. C., Feigin, A., Dhawan, V., Ghilardi, M. F., Paulsen, J. S., Guttman, M., & Eidelberg, D. (2016). Longitudinal changes in the motor learning-related brain activation response in presymptomatic Huntington's disease. *PLoS ONE*, *11*(5). https://doi.org/10.1371/journal.pone.0154742

Jin, X., & Costa, R. M. (2010). Start/stop signals emerge in nigrostriatal circuits during sequence learning. *Nature*, *466*(7305), 457–462. https://doi.org/10.1038/nature09263

Jin, X., & Costa, R. M. (2015). Shaping action sequences in basal ganglia circuits. In *Current Opinion in Neurobiology* (Vol. 33, pp. 188–196). Elsevier Ltd. https://doi.org/10.1016/j.conb.2015.06.011

Jog, M. S., Kubota, Y., Connolly, C. I., & Graybiel, A. M. (1999). Building neural representations of habits. *Science*, *286*(5445), 1745–1749.

https://doi.org/10.1126/science.286.5445.1745

Kirch, R. D., Meyer, P. T., Geisler, S., Braun, F., Gehrig, S., Langen, K.-J., von Hörsten, S., Nikkhah, G., Cassel, J.-C., & Döbrössy, M. D. (2013). Early deficits in declarative and procedural memory dependent behavioral function in a transgenic rat model of Huntington's disease. *Behavioural Brain Research*, *239*, 15–26. https://doi.org/10.1016/j.bbr.2012.10.048

Kupferschmidt, D. A., Juczewski, K., Cui, G., Johnson, K. A., & Lovinger, D. M. (2017). Parallel, but Dissociable, Processing in Discrete Corticostriatal Inputs Encodes Skill Learning. *Neuron*, *96*(2), 476-489.e5. https://doi.org/10.1016/j.neuron.2017.09.040

Lee Hong, S., & Rebec, G. V. (2012). Biological sources of inflexibility in brain and behavior with aging and neurodegenerative diseases. In *Frontiers in Systems Neuroscience* (Vol. 6, Issue NOV). Front Syst Neurosci. https://doi.org/10.3389/fnsys.2012.00077

MacDonald, M. E., Ambrose, C. M., Duyao, M. P., Myers, R. H., Lin, C., Srinidhi, L., Barnes, G., Taylor, S. A., James, M., Groot, N., MacFarlane, H., Jenkins, B., Anderson, M. A., Wexler, N. S., Gusella, J. F., Bates, G. P., Baxendale, S., Hummerich, H., Kirby, S., … Harper, P. S. (1993). A novel gene containing a trinucleotide repeat that is expanded and unstable on Huntington's disease chromosomes. *Cell*, *72*(6), 971–983. https://doi.org/10.1016/0092-8674(93)90585-E

Menalled, L. B., Sison, J. D., Dragatsis, I., Zeitlin, S., & Chesselet, M.-F. (2003). Time course of early motor and neuropathological anomalies in a knock-in mouse model of Huntington's disease with 140 CAG repeats. *The Journal of Comparative Neurology*, *465*(1), 11–26. https://doi.org/10.1002/cne.10776

Naze, S., Humble, J., Zheng, P., Barton, S., Rangel-Barajas, C., Rebec, G. V., & Kozloski, J. R. (2018). Cortico-striatal cross-frequency coupling and gamma genesis disruptions in huntington's disease mouse and computational models. *ENeuro*, *5*(6). https://doi.org/10.1523/ENEURO.0210-18.2018

Papoutsi, M., Labuschagne, I., Tabrizi, S. J., & Stout, J. C. (2014). The cognitive burden in Huntington's disease: pathology, phenotype, and mechanisms of compensation. *Movement Disorders : Official Journal of the Movement Disorder Society*, *29*(5), 673–683. https://doi.org/10.1002/mds.25864

Paulsen, J. S. (2011). Cognitive impairment in Huntington disease: Diagnosis and treatment. *Current Neurology and Neuroscience Reports*, *11*(5), 474–483.

https://doi.org/10.1007/s11910-011-0215-x

Raymond, L. A., André, V. M., Cepeda, C., Gladding, C. M., Milnerwood, A. J., & Levine, M. S. (2011). Pathophysiology of Huntington's disease: time-dependent alterations in synaptic and receptor function. *Neuroscience*, *198*, 252–273. https://doi.org/10.1016/j.neuroscience.2011.08.052

Redgrave, P., Rodriguez, M., Smith, Y., Rodriguez-Oroz, M. C., Lehericy, S., Bergman, H., Agid, Y., Delong, M. R., & Obeso, J. A. (2010). Goal-directed and habitual control in the basal ganglia: Implications for Parkinson's disease. In *Nature Reviews Neuroscience* (Vol. 11, Issue 11, pp. 760–772). Nat Rev Neurosci. https://doi.org/10.1038/nrn2915

Rising, A. C., Xu, J., Napoli, V. V, Carlson, A., Denovan-Wright, E. M., & Mandel, R. J. (2011). Longitudinal Behavioral, Cross-sectional Transcriptional and Histopathological Characterization of a Knock-in Mouse Model of Huntington's Disease with 140 CAG Repeats. *Experimental Neurology*, *228*(2), 173–182. https://doi.org/10.1016/j.expneurol.2010.12.017

Smith, K. S., & Graybiel, A. M. (2013). A dual operator view of habitual behavior reflecting cortical and striatal dynamics. *Neuron*, *79*(2), 361–374. https://doi.org/10.1016/j.neuron.2013.05.038

Sprengelmeyer, R., Canavan, A. G. M., Lange, H. W., & Hömberg, V. (1995). Associative learning in degenerative neostriatal disorders: Contrasts in explicit and implicit remembering between Parkinson's and huntington's diseases. *Movement Disorders*, *10*(1), 51–65. https://doi.org/10.1002/mds.870100110

Stout, J. C., Paulsen, J. S., Queller, S., Solomon, A. C., Whitlock, K. B., Campbell, J. C., Carlozzi, N., Duff, K., Beglinger, L. J., Langbehn, D. R., Johnson, S. A., Biglan, K. M., & Aylward, E. H. (2011). Neurocognitive Signs in Prodromal Huntington Disease. *Neuropsychology*, *25*(1), 1–14. https://doi.org/10.1037/a0020937

Thorn, C. A., Atallah, H., Howe, M., & Graybiel, A. M. (2010). Differential Dynamics of Activity Changes in Dorsolateral and Dorsomedial Striatal Loops during Learning. *Neuron*, *66*(5), 781–795. https://doi.org/10.1016/j.neuron.2010.04.036

Vandaele, Y., Mahajan, N. R., Ottenheimer, D. J., Richard, J. M., Mysore, S. P., & Janak, P. H. (2019). Distinct recruitment of dorsomedial and dorsolateral striatum erodes with extended training. *ELife*, *8*. https://doi.org/10.7554/eLife.49536

Vonsattel, J. P., Myers, R. H., Stevens, T. J., Ferrante, R. J., Bird, E. D., & Richardson, E. P. (1985).

Neuropathological classification of huntington's disease. *Journal of Neuropathology and Experimental Neurology*, *44*(6), 559–577. https://doi.org/10.1097/00005072-198511000-00003

Yin, H. H., Knowlton, B. J., & Balleine, B. W. (2004). Lesions of dorsolateral striatum preserve outcome expectancy but disrupt habit formation in instrumental learning. *European Journal of Neuroscience*, *19*(1), 181–189. https://doi.org/10.1111/j.1460-9568.2004.03095.x

Yin, H. H., Knowlton, B. J., & Balleine, B. W. (2005). Blockade of NMDA receptors in the dorsomedial striatum prevents action-outcome learning in instrumental conditioning. *European Journal of Neuroscience*, *22*(2), 505–512. https://doi.org/10.1111/j.1460-9568.2005.04219.x

Yin, H. H., Mulcare, S. P., Hilário, M. R. F., Clouse, E., Holloway, T., Davis, M. I., Hansson, A. C., Lovinger, D. M., & Costa, R. M. (2009). Dynamic reorganization of striatal circuits during the acquisition and consolidation of a skill. *Nature Neuroscience*, *12*(3), 333–341. https://doi.org/10.1038/nn.2261

Yin, H. H., Ostlund, S. B., Knowlton, B. J., & Balleine, B. W. (2005). The role of the dorsomedial striatum in instrumental conditioning. *European Journal of Neuroscience*, *22*(2), 513–523. https://doi.org/10.1111/j.1460-9568.2005.04218.x

Part III: General discussion

During my thesis, I characterized the networks involved in the formation of procedural memory in physiological and pathological conditions.

First, we explored the reorganization of the networks during the different phases of learning in physiological conditions. We showed the existence of a strong reorganization of the corticostriatal networks specific to each striatal territory and each phase of learning. We showed that there is a decrease in the activity of the DMS in the first phase of learning, with the presence of spots of high activity (HA) in a small group of cells. The DLS starts to show spatial reorganization of activity in the first phase of learning: a group of cells with high activity that are spatially close to each other. Once habit is formed, activity in the DMS goes back to a basal level whereas activity in the DLS is spatially restricted to active clusters. In order to show the role of these HA cells and clusters in learning, we first show a strong correlation between them and the quality of learning animals. Finally, we used a Fos-TRAP strategy to manipulate their activity which allowed us to show their crucial role in learning. We thus proposed that the cells arising from network reorganization could constitute 'striatal engram cells' in the frame of procedural memory.

Second, we showed that this reorganization is strongly impaired in the pathological context of HD, with Hdh^{Q140} mice. These alterations of network dynamics are associated to deficits in late but not early phases of learning. These observations confirm the role of network reorganization in the formation of the memory. In addition, our approaches allowed us to show that the patterns of activity within DMS and DLS are severely affected early in pathological process in mouse model of HD, highlighting very early alterations in the corticostriatal networks in HD.

1) <u>Importance of striatal 'engram' cells</u>

The search for neural correlates of behavior started a while back. Interest increased when 'place cells' were discovered in the hippocampus, allowing for a correlation between the firing of the cells and the animal location. Then were discovered 'grid cells' in the medial entorhinal cortex, firing when the animal followed a grid-like pattern (for review see (Bush et al., 2014)). Thus the hippocampus and the associated cortex were at the center of the 'engram' world. Indeed, after the place or grid cells, engram cells within the hippocampus have been described as neuronal substrates of memory. An engram was thus defined as a neuronal trace of memory and would need to fulfill different requirements such as being: (i) activated by a

learning experience, (ii) physically or chemically modified by the learning experience, and (iii) reactivated by subsequent presentation of the stimuli present at the learning experience, resulting in memory retrieval. The development of new tools such as the use of immediate early genes allowed the identification of these engrams with immunohistochemistry and the specific manipulation of their activity (for review see Tonegawa et al., 2018) and the engram cells were validated in the hippocampus. Of course following the discovery of engram cells in the hippocampus, behavioral correlates in different structures started to emerge. During my thesis, I demonstrated the existence of groups of cells in early DMS and late DLS, which are correlated to the quality of the motor skill performance, with a clustering of the activity for long-lasting retention of the skill within DLS. Recent studies reported the formation of functional clusters in the DLS and linked them to a specific behavior (Barbera et al., 2016; Klaus et al., 2017; Parker et al., 2018). The DLS has also been shown to be involved in task 'bracketing' in T-maze learning task (Jin & Costa, 2010; K. S. Smith & Graybiel, 2013; Thorn et al., 2010), when the activity increases at the beginning and at the end of the task. My work would be a first evidence of clustered active cells related to motor skill acquisition and retention. C-fos labeling showed how these cells were activated by motor skill learning differentially in each territory, electrophysiological and tracing studies showed the physical and chemical changes of neurons after learning, and the time latency of the reorganization. As in hippocampus for example where they reported higher synaptic strength and spine density in engram cells compared to non-engram cells (Tonegawa et al., 2015). Therefore these HA cells comply with the definition of engram cells as they are activated by motor skill learning, there are either synaptic modifications or increased cortical inputs and a loss-of-function experiments show that they are necessary for proper memory retrieval. Thus proving that HA cells and cluster cells are the equivalent of engram cells in the hippocampus. While 'place' and 'grid cells' are spatially specific, the specificity of the reorganization to each striatal territory and each phase of learning shows that 'engram' cells in the striatum are time and action-specific.

We proposed mechanisms explaining the differential reorganization of the DMS and DLS networks and the emergence of these striatal 'engram cells'. However, different circuits and pathways should be taken into account. I will detail this idea in the next paragraphs.

2) Role of synaptic plasticity in learning

When memory is discussed, the plasticity of a network or a structure is mentioned immediately after to explain the mechanisms behind this memory. Activity-dependent synaptic plasticity is thought to be both necessary and sufficient for the establishment of a trace of memory and the encoding of memory (for review see (Takeuchi et al., 2014)). Four criteria are necessary in order to link synaptic plasticity and learning: 1/ changes in synaptic efficacy should be detected following learning, 2/ learning should be affected following the administration of a drug that affects plasticity, 3/ the administration of drugs or manipulations of synaptic plasticity after learning should affect the neural circuits and their ability to reconstruct the appropriate pattern, and finally 4/ if memory is encoded by a pattern of synaptic weights, a recreation of the pattern should create a false memory (Martin et al., 2000). The discovery of long-term potentiation (LTP: previously stimulated synapses are increasingly sensitive to stimulation), especially in a structure involved in memory (hippocampus) further linked synaptic plasticity and memory (Takeuchi et al., 2014).

Concerning motor learning, most of the different requirements announced by Martin et al. have been completed and the role of cortical inputs has been highlighted by synaptic plasticity of corticostriatal connections related to learning (Di Filippo et al., 2009; Fino & Venance, 2010, 2011; Koralek et al., 2012; Lerner & Kreitzer, 2011; Rothwell et al., 2015; H. H. Yin et al., 2009). Linking directly procedural memory to synaptic plasticity in the striatal networks was first reported by (H. H. Yin et al., 2009) who combined the analysis of *in vivo* firing rate and *ex vivo* NMDAR/AMPAR ratio after training on an accelerated rotarod. A more recent study also reported enhanced synaptic inputs from frontal cortex to the DMS during early training (Kupferschmidt et al., 2017). In accordance with these studies, one of the mechanisms we observed is an increase of the weight of associative cortical inputs onto cells highly active cells in the DMS, adding an evidence to the link between synaptic modifications and motor learning. After a T-maze task, the DMS was found to be involved in the early phase of learning by engaging LTP but not long-term depression (LTD), but after a late phase, when the activity in the DMS goes back to a naïve state, LTD was reported but not LTP (Hawes et al., 2015). Interestingly, the modifications we observed at the level of the DMS networks corresponded to a sparse high activity of cells with higher synaptic weights than other cells. We would therefore expect an overall reduced efficacy at synapses, i.e. the engagement of LTD, in DMS after early training, and not LTP. Confirming these results should rely on molecular and

structural studies associated with LTP. In DLS on the other hand, LTD is reported to be involved in the late phase of learning when habit is formed (Hawes et al., 2015). Interestingly, we did not observe synaptic modifications in cluster cells compared to non-cluster cells in DLS. This does not mean that no plasticity has occurred at the synapses during learning, since an enhanced AMPA/NMDA ratio was reported in DLS after late training (Yin et al., 2009). We observed a resulting synaptic state after the memory is formed. Thus it would be important to follow the synaptic plasticity all along memory formation to fully understand the mechanisms behind it.

Another aspect of plasticity far less studied is network plasticity. I tried to evaluate such plastic properties by comparing the network activity induced by different levels of cortical inputs (modifications of stimulation frequencies for example). We showed that an increase of the stimulation frequency allowed for an increase of the response in the late phase of learning and naïve conditions for DMS, and in naïve conditions for DLS. Training affected these networks by cancelling this plasticity of the response to cortical stimulation. This shows that learning allows the networks to respond in a similar manner independently of the intensity of cortical inputs. These results are interesting because they implicate the networks as a whole and shows the interaction between the structures and how they evolved during learning. Thus, future work should focus on simultaneous activity from both structures, allowing us to explore the corticostriatal networks at a larger scale.

In summary, synaptic plasticity plays an important role in memory and learning processes via the engagement of LTP and LTD to create patterns and encode memory. Nevertheless further studies will be necessary to explore different parameters such as the scale from the single neuron to the network, and the timing and conditions of occurrence of such plasticity all along memory formation.

3) Local inhibition as a mechanism of reorganization of striatal networks

I mentioned in the introduction that both territories, DMS and DLS, are simultaneously active during the first phase of learning. However, when training is repeated to form a habit, the DMS involvement is decreased while the DLS keeps a higher activity. We explored striatal extrinsic modifications, mainly coming from the cortical inputs. Notably, we described an increase of the synaptic weight in the associative/DMS part and an increased number of

projection cortical cells in the somatosensory/DLS part. However, since the reorganization we observe corresponds to a decrease of the activity in all but few neurons, a hypothesis of the role of local inhibition cannot be pushed aside. Indeed, interneurons exhibit an inhibitory effect on striatal MSNs and this inhibition could allow the reorganization and modulation of the networks. In fact, it has been shown that the majority of local inhibition in the striatum comes from GABAergic interneurons (Tepper et al., 2010) since their inhibitory weight is much stronger than the one coming from other MSNs (Planert et al., 2010). In a recent study the role of SST interneurons in goal-directed behaviors was revealed by using fiber photometry for *in vivo* calcium imaging (Holly et al., 2019). In this study they show a decrease of the activity of SST interneurons in the DMS during goal-directed behaviors. More importantly, they show that this decrease in the activity of SST interneurons is crucial for learning. The decrease of activity of SST interneurons in DMS suggests that they were spared in our first study (Badreddine et al., in revision) when we manipulated the activity of highly active cells with a Fos-TRAP strategy. By inhibiting these highly active cells we were able to affect learning. Since SST interneurons decrease their activity during goal-directed behavior, we can assume that 1/ neurons with a higher activity after training could be responsible for the inhibition that is observed over the rest of the neurons in the field, and that 2/ another subtype of GABAergic interneurons is also at play. Interestingly, SST interneurons are present in DMS and DLS at a similar density. However, another subtype of GABAergic interneurons, PV interneurons, are more present and have a stronger inhibitory weight in the DLS than in the DMS (Fino et al., 2018). A recent study using pharmacological and optogenetic manipulations of PV interneurons in the DLS showed that PV interneurons are more active during habitual behavior in the DLS than during goal-directed behavior. When they inhibited PV interneurons, the expression of habit was blocked (O'Hare et al., 2017). Another recent study showed similar results *in vivo*: when PV interneurons are inhibited, a disinhibition of MSN spiking occurs, and learning is impaired (Owen et al., 2018). Cortical inputs onto PV and other interneurons vary depending on the cortical region. It has been shown recently that PV interneurons receive their strongest inputs from somatosensory and primary motor cortex, and from the thalamic parafascicular nucleus while SST interneurons receive connections primarily from the contralateral primary motor cortex (Johansson & Silberberg, 2020)(Fig.42).

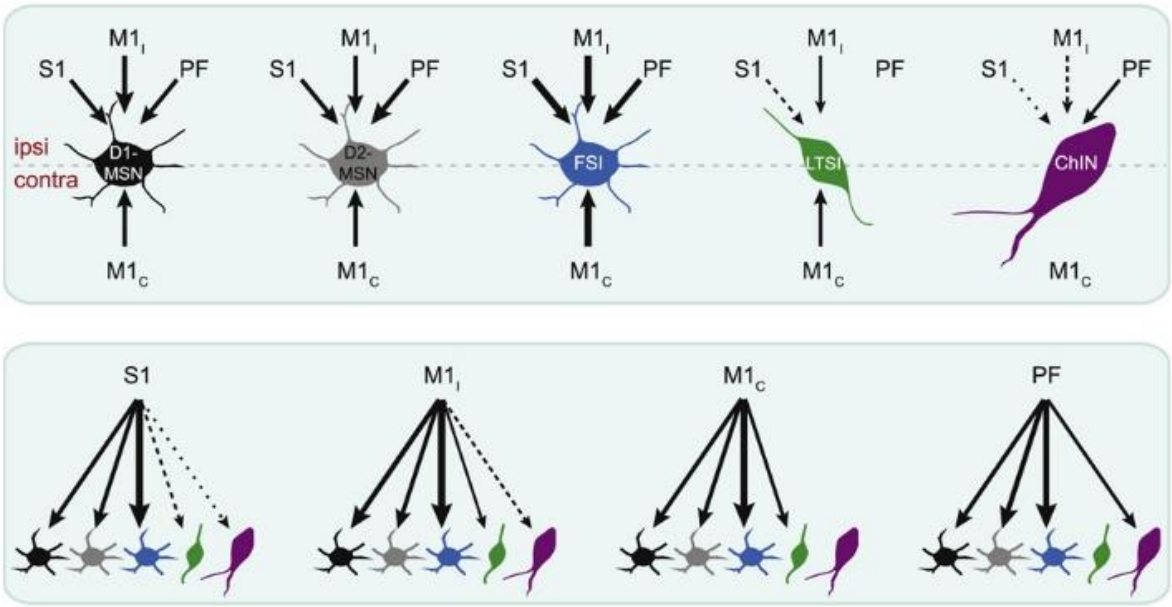

***Figure 42:* Cortical and thalamic inputs onto different striatal neurons**. *S1: somatosensory cortex; M1i: primary motor cortex with a stimulation of ipsilateral connections; M1c: primary motor cortex with a stimulation of contralateral connections; PF: parafascicular nucleus of the thalamus. Thickness of arrows corresponds to the strength of the inputs. Adapted from (Johansson & Silberberg, 2020).*

Interestingly, cortical inputs from the somatosensory cortex are stronger on PV interneurons than on MSNs, but are similar on both neuronal subtypes when inputs are from the primary motor cortex (C. R. Lee et al., 2019). The stronger somatosensory cortex inputs onto PV interneurons leads to behavioral inhibition. These results could explain the formation of clusters in the DLS after late training. Since in our study only MSNs activity was included in the analysis, future work should include interneurons and determine the position of interneurons in relation to the clusters of activity. In order to study the role of interneurons in the reorganization, the use of transgenic mouse lines will allow specific labeling of interneurons. We previously developed a cell-sorting classifier (Becq et al., 2019) allowing us to extract signals of only MSN responses. The accuracy of the classifier was based on calcium signals and *in vivo* labeling of different interneurons. So far, this classifier does not allow us to differentiate interneurons and groups all non-MSNs as interneurons because of the low number of analyzed interneurons. Labeling of interneurons will increase the precision of the classifier, thus allowing us to determine the role of interneurons in the reorganization of the networks and have a more comprehensive look on the corticostriatal networks and their role in learning.

From a pathophysiological aspect of HD, local inhibition would be interesting to dissect as well. PV interneurons have been reported to be the only interneurons (aside from calretinin

interneurons) to be affected in HD, in both humans and non-human primates (Deng et al., 2013; Lallani et al., 2019). Electrophysiological and intrinsic properties of PV interneurons were shown to be altered in a mouse model of HD (Holley et al., 2019). In this study they showed an increase of the excitability of PV interneurons with disease progression. More interestingly, they showed that SST interneurons were not affected in the early phases of the disease, but showed a higher excitability in later stages of the disease. Although it would be important to examine the role of the alterations of PV interneurons and their effect on the neighboring networks, it would be as important to examine the role of the other interneurons that do not seem to be affected by HD. Studying PV interneurons in HD could explain the motor deficits observed in the pathology. However, studying the other neuronal subtypes might reveal compensatory mechanisms that these interneurons go through, thus avoiding their degeneration. A combination of these ideas could open the door for novel therapeutic approaches targeting interneurons.

4) Dissecting functional heterogeneity of striatal networks in motor skill learning

a- Role of dMSNs vs iMSNs in learning

We mentioned in the introduction that striatal MSNs could be divided into two subtypes: dMSNs and iMSNs involved respectively in the direct and indirect pathways. Historically, dMSNs are involved in the initiation of movement and iMSNs in the termination of movement. It has been shown recently that both of these populations were simultaneously and similarly active allowing for a better control of signals and movement (Barbera et al., 2016; Cui et al., 2013). The study by Barbera et al. examined the presence of neural correlates of locomotion in the dorsal striatum by using a miniScope system. Even though the function of the two populations was recently grouped, the involvement of the dopaminergic system is different based on the phase of learning: goal-directed behavior requires the presence of a reward, when habitual behavior does not. In a study using two-photon calcium imaging in the DLS, it was shown that a faster activation of dMSNs relative to iMSNs occurs in habitual behavior, however iMSNs are activated first in goal-directed behavior (O'Hare et al., 2016). When habitual behavior was suppressed, dMSNs activity was suppressed as well, suggesting that decreased activity of dMSNs is sufficient to suppress habitual behavior (Fig.43). This is interesting considering the direct pathway, and by extension dMSNs, was thought to be solely responsible for the initiation of movement and concords with studies showing a stronger

synaptic coupling with cortical neurons than iMSNs (Cepeda et al., 2008; Planert et al., 2013). This also concords with the automatic aspect of habit, i.e. dMSNs will be active thus initiating movement 'automatically' and iMSNs will terminate their action, adding to the refinement of actions in habit. More importantly, these results indicate the specificity of each pathway in the different phases of learning, thus adding another modulatory parameter in the networks.

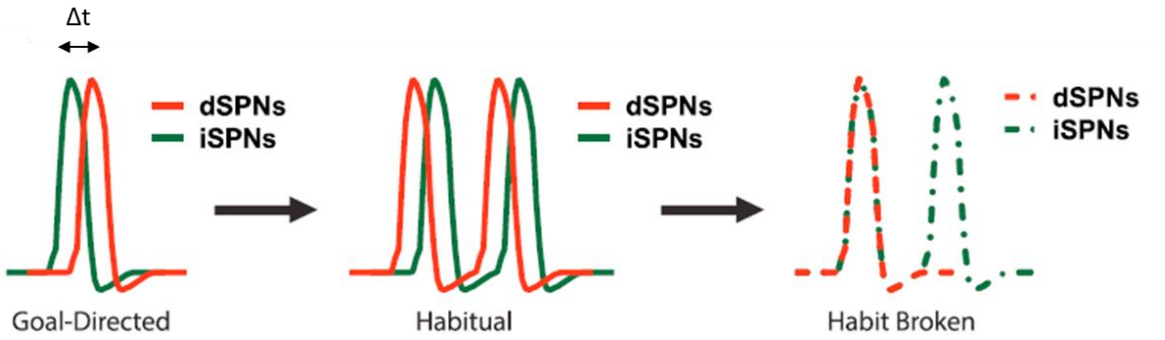

***Figure 43:* Plasticity of dMSNs and iMSNs during learning**. *Distinct plasticity mechanisms of dMSNs and iMSNs during goal-directed behavior and habitual behavior. A shift in relative timing between dMSNs and iMSNs: iMSNs first active in goal-directed behavior, dMSNs first when habitual behavior, decreased activity of dMSNs when habit is suppressed. Δt: delay of activation. Adapted from (O'Hare et al., 2016).*

A recent study characterized both MSNs populations during learning by using immunodetection of a transcriptional activation marker (Matamales et al., 2020). Both populations were active during goal-directed behavior as expected. However they showed that both populations compete in the striatum. A pharmacological overstimulation of iMSNs results in iMSNs active with a lower proportion of active dMSNs. An overstimulation of dMSNs, results in active dMSNs and a lower proportion of active iMSNs. However, when both populations are overstimulated, proportion of iMSNs is much more important than dMSNs (Matamales et al., 2020). This study suggests that iMSNs are responsible for 'updating' learning, i.e. they will limit outdated dMSNs function in the case of extinction of learning. In my thesis, MSNs in general were analyzed without distinguishing dMSNs and iMSNs. We can wonder how these two subpopulations of MSNs are involved in the process of learning. Thus could be addressed by labelling them during imaging experiments and determine the proportion of each subpopulation within the HA cells and if one subpopulation has a specific pattern regarding network dynamics. Another aspects is that dMSNs and iMSNs could be differentially affected by the interneuron inhibition. Indeed, PV interneurons showed a lower contribution after habit formation in DLS (K. Lee et al., 2017). Although PV interneurons were reported to preferentially target dMSNs via more connections (Gittis et al., 2010; Parthasarathy & Graybiel, 1997), another report showed similar connectivity and more

importantly similar dynamics of synaptic transmission on both dMSNs and iMSNs (Planert et al., 2010). Thus, the earlier activation of dMSNs might not be due to PV interneurons interference. It has been recently shown that the earlier activation of dMSNs might be a way of preventing action cancellation by avoiding stop-related SNr activity driven by iMSNs (Schmidt et al., 2013). Thus, based on the literature presented so far, we can expect a higher proportion of dMSNs to be highly active and to constitute the clusters of activity after late training, thus allowing for the initiation of the now automatic action.

In the pathological frame of HD, iMSNs were shown to be more vulnerable than dMSNs (Waldvogel et al., 2014). In study 3, we showed deficits in late but not early phases of learning. Based on the literature presented above, we can expect a decrease of the activity of both MSN populations, with a higher decrease in dMSNs thus affecting the late phases of learning. The higher decrease in dMSNs activity could be explained by the more important inhibition by the PV interneurons which would not be altered in the premotor symptomatic phase of the disease.

Thus, several local circuits are at play during learning: GABAergic circuits involving different interneurons, and MSNs circuits involving the direct and indirect pathways. The balance between these different circuits is necessary in learning, as it is exemplified by HD.

b- Role of matrix and striosomes in learning

The innervation of the striosomes by the limbic areas of the cortex and the matrix by the sensorimotor and associative areas infers a specific role to each of the striatal compartments (for review see (Crittenden & Graybiel, 2011)). In addition, each of these compartments projects to different structures: striosomes and matrix project to the GP and SNr, but only the striosomes were reported to project to the SNc (Charles R. Gerfen, 1984; A. M. Graybiel et al., 1981). Each compartment is thus implicated in different pathways and systems and infer different functions to each of them. Interesting recent studies showed that the striosomes in the DLS could play an important role in the formation of habitual behavior (Jenrette et al., 2019; Murray et al., 2014). After a lesion of the striosomes in the DLS, the stereotypy induced by methamphetamine was reduced and the animal was able to engage in non-repetitive behavior, suggesting a role of striosomes in repetitive inflexible behaviors (Murray et al., 2014). In addition, pharmacological ablation of striosomes in the DLS led to a decrease of the

activation of the DLS and sensorimotor cortex, but an increase of DMS and prefrontal cortex activity (Jenrette et al., 2019). These results are similar to the lesion studies used to demonstrate the role of the DLS in habit formation. We can thus wonder about the proportion of the role of the striosomes in habit compared to the matrix in DLS. The data I just presented are interesting since the striosomes receive inputs from the limbic areas of the cortex and amygdala. Thus we can imagine that the striosomes play a role in reward-based learning implicating the limbic system. The involvement of the DLS-striosomes in habit might play an important role in the shift of behavior from flexible goal-directed, to inflexible habit. We can wonder if the striosomes only play a role in the shift between both behaviors or if they have a role in the encoding of memory. In the frame of our results, it would be really interesting to distinguish between striosomes and matrix compartments. Since the proportion of striosomes compared to the matrix is low in DLS, we considered that all recorded activity was from the matrix. In addition, considering the reorganization of the network on a large scale in the striatum, the presence of HA cells and clusters in the matrix is more likely. Referring to the role of the DMS or the DLS in the literature corresponds to the role of the matrix in each territory. Interestingly, the DMS has been shown to have a larger proportion of striosomes than the DLS (Miyamoto et al., 2018). We can thus wonder how the presence of striosomes affects the reorganization after learning. Would they be responsible for the sparse localizations of HA cells we observed in DMS and their absence for the spatial organization we observed in DLS? Is the interaction between striosomes and matrix in DMS, and lesser interaction due to the lower proportion in DLS contributing to this reorganization? Thus, it would be important to evaluate how both matrix and striosomes interact for the formation of a memory. In addition, it has been shown that MSNs from both compartments do not interact, however cholinergic and SST interneurons residing at the interface between striosomes and matrix have been reported to mediate information transfer (for review see (Brimblecombe & Cragg, 2017)). This would thus implicate the interneurons at another level in striatal modulation.

5) Interaction of different brain structures during motor learning

Cortico-BG-thalamocortical loops are functionally segregated, and the different structures forming these loops follow a similar functional segregation. Thus, it would be interesting to see how the different systems and different circuits interact during learning. In my

experiments, I recorded striatal activity in response to cortical stimulation, focusing therefore my attention on the reorganization of the corticostriatal networks. We chose to characterize the corticostriatal networks first as the majority of glutamatergic inputs to the striatum emerge from the cortex. Nevertheless, there is another excitatory structure projecting to the striatum, the thalamus. Even though the anatomical contribution of the thalamus to glutamatergic inputs to the striatum have been known for a while, it is only recently that the role to the thalamostriatal circuitry has received attention (Cover et al., 2019; Parsons et al., 2007; Threlfell et al., 2012). In the dorsal striatum, thalamic glutamate release activates cholinergic interneurons which activate dopamine release by producing acetylcholine binding to nicotinic acetylcholine receptors on dopaminergic neurons axonal terminals (Cover et al., 2019; Threlfell et al., 2012). Thus, by inducing dopamine release, the thalamus plays a role in learning. Interestingly, a recent study where mice expressing channelrhodopsin-2 in the intralaminar thalamus and trained to an operant lever-press task started auto-stimulating after stimulation of thalamic terminals in the DMS (Johnson et al., 2020). These findings show that thalamostriatal transmission allows the reinforcement of an action.

A recent non-reviewed study aimed to 'elucidate how motor cortical and thalamic inputs to the striatum contribute to the acquisition and control of learned motor skills' (Wolff et al., 2019). They show that the DLS and motor cortex are essential for learning the presented behavioral task, and the thalamus essential to execute the learned motor sequences. In addition, the role of different thalamic nuclei in the different phases of procedural learning has been explored recently (Díaz-Hernández et al., 2018). The parafascicular nucleus seems to target the DMS when the ventral posterior nucleus, long thought to only act as a somatosensory relay, targets the DLS. More importantly, they showed that the thalamic nuclei play an important role in the initiation and execution of action. There is therefore an increasing interest for the thalamic inputs to the striatum and it will be determinant to integrate it in this framework to better understand the fine modulation of motor skill learning.

Finally, we have seen that forming motor learning is dependent on the BG, mostly the striatum, and cortico-BG-thalamocortical loops. However, interactions with other structures are also important for the motor learning, an important one being the cerebellum, a structure well known for its involvement in motor behavior (Anderson, 1993). Interestingly, a recent study showed that the cerebellum and the thalamus are connected differentially based on the targeted thalamic region (Gornati et al., 2018). Therefore, the functional loops between the cortex, BG and thalamus can be modulated by other brain regions. Interestingly, activation of

the cerebellar hemispheres has been reported in an early phase of learning (Hikosaka et al., 2002), thus following the same pattern as the DMS. The BG are segregated into functional loops. This functional connectivity spreads to the cerebellum and is enhanced during early learning (for review see (Bostan & Strick, 2018)). Studies using transcranial magnetic stimulation over the cerebellar cortex show an alteration in the speed of learning (Gheysen et al., 2017). Also, a decrease in the activity of the cerebellum was shown to follow the decrease seen in the DMS and enhanced connectivity to the putamen (or DLS in rodents) has been associated with improved learning in the late phases of learning (Bostan & Strick, 2018). These data show that the cerebellum follows similar dynamics than the different striatal territories during learning.

In summary, motor learning is mediated by multiple structures and the striatum is at the center of all of the activity. However, in order to better understand how memory is formed, it will be determinant to take into account all the different circuits involved in motor control. This is possible nowadays thanks to the development of small enough GRIN (Gradient-Index) lenses (continuous change of the refractive index within the lens material allows for the production of lenses with flat surfaces, to which optic fibers can be glued) and animal headsets, which allows multiregion investigation. These technical advances would allow us to dissect the contribution of the various brain structures in the different aspects of a motor behavior.

Conclusion

During my thesis, we employed a multiscale approach to study the dynamics of the corticostriatal networks involved in motor skill learning and to determine neuronal substrates of motor skill learning. Based on *ex vivo* two-photon calcium imaging, we showed the specific involvement and reorganization of the different corticostriatal networks in the different phases of learning. We identified the mechanisms responsible for the specific reorganization of the networks: changes in synaptic inputs weight during the early phase of learning, and more robust anatomical changes after the late phase of learning. Based on the reorganization of the networks, we then validated the role of the neural substrates of motor skill learning by using a Fos-TRAP strategy along with chemogenetics. Thus, we proved the necessity and the specificity of the neuronal substrates to each striatal territory. So far, we only explored the activity of one type of neurons in the striatum. This was possible when we developed a cell-sorting classifier allowing us to distinguish the different striatal neurons, and extracting the most abundant striatal populations. Finally, we explored if deficits in motor skill learning occur in a mouse model of Huntington's disease, and if and how these deficits could be associated to alterations in the corticostriatal networks. We showed that performance of mice in late phases of motor skill learning were altered. Using *ex vivo* calcium imaging we explored the activity of the different striatal territories and showed an absence of reorganization of the networks upon motor skill learning. The results from the different studies highlight the importance of the corticostriatal networks reorganization in motor skill learning.

References

Abudukeyoumu, N., Hernandez-Flores, T., Garcia-Munoz, M., & Arbuthnott, G. W. (2019). Cholinergic modulation of striatal microcircuits. In *European Journal of Neuroscience* (Vol. 49, Issue 5, pp. 604–622). Blackwell Publishing Ltd. https://doi.org/10.1111/ejn.13949

Aizman, O., Brismar, H., Uhlén, P., Zettergren, E., Levey, A. I., Forssberg, H., Greengard, P., & Aperia, A. (2000). Anatomical and physiological evidence for D1 and D2 dopamine receptor colocalization in neostriatal neurons. *Nature Neuroscience*, *3*(3), 226–230. https://doi.org/10.1038/72929

Ajitkumar, A., & De Jesus, O. (2020). *Huntington Disease.*

Albin, R. L., Young, A. B., & Penney, J. B. (1989). The functional anatomy of basal ganglia disorders. *Trends in Neurosciences*, *12*(10), 366–375. https://doi.org/10.1016/0166-2236(89)90074-X

Alexander, G. E., DeLong, M. R., & Strick, P. L. (1986). Parallel organization of functionally segregated circuits linking basal ganglia and cortex. *Annual Review of Neuroscience*, *VOL. 9*, 357–381. https://doi.org/10.1146/annurev.ne.09.030186.002041

Alexander, Garrett E., & Crutcher, M. D. (1990). Functional architecture of basal ganglia circuits: neural substrates of parallel processing. In *Trends in Neurosciences* (Vol. 13, Issue 7, pp. 266–271). Trends Neurosci. https://doi.org/10.1016/0166-2236(90)90107-L

Alexander, Garrett E, Crutcher, M. D., & Delong, M. R. (1990). Basal ganglia-thalamocortical circuits: Parallel substrates for motor, oculomotor, "prefrontal" and "limbic" functions. *Progress in Brain Research Elsevier Science Publishers B.V. (Biomedical Division)*, *85*, 119–149. http://ac.els-cdn.com/S0079612308626783/1-s2.0-S0079612308626783-main.pdf?_tid=a7e00e30-63f2-11e6-892a-00000aab0f27&acdnat=1471380633_ba838a2221d36104e74cd2cc84d54fd5

Amin, H. U., & Malik, A. S. (2014). Memory retention and recall process. In *EEG/ERP Analysis: Methods and Applications* (pp. 219–237). CRC Press. https://doi.org/10.1201/b17605-11

Anderson, M. E. (1993). The Role of the Cerebellum in Motor Control and Motor Learning. *Physical Medicine and Rehabilitation Clinics of North America*, *4*(4), 623–636. https://doi.org/10.1016/s1047-9651(18)30550-3

Andresen, J. M., Gayán, J., Djoussé, L., Roberts, S., Brocklebank, D., Cherny, S. S., Cardon, L. R., Gusella, J. F., MacDonald, M. E., Myers, R. H., Housman, D. E., & Wexler, N. S. (2007). The

Relationship Between CAG Repeat Length and Age of Onset Differs for Huntington's Disease Patients with Juvenile Onset or Adult Onset. *Annals of Human Genetics*, *71*(3), 295–301. https://doi.org/10.1111/j.1469-1809.2006.00335.x

Aosaki, T., Kimura, M., & Graybiel, A. M. (1995). Temporal and spatial characteristics of tonically active neurons of the primate's striatum. *Journal of Neurophysiology*, *73*(3), 1234–1252. https://doi.org/10.1152/jn.1995.73.3.1234

Arime, Y., & Akiyama, K. (2017). Abnormal neural activation patterns underlying working memory impairment in chronic phencyclidine-treated mice. *PLoS ONE*, *12*(12). https://doi.org/10.1371/journal.pone.0189287

Arnoux, I., Willam, M., Griesche, N., Krummeich, J., Watari, H., Offermann, N., Weber, S., Dey, P. N., Chen, C., Monteiro, O., Buettner, S., Meyer, K., Bano, D., Radyushkin, K., Langston, R., Lambert, J. J., Wanker, E., Methner, A., Krauss, S., … Stroh, A. (2018). Metformin reverses early cortical network dysfunction and behavior changes in Huntington's disease. *ELife*, *7*. https://doi.org/10.7554/eLife.38744

Atkinson, R. C., & Shiffrin, R. M. (1968). Human Memory: A Proposed System and its Control Processes. *Psychology of Learning and Motivation - Advances in Research and Theory*, *2*(C), 89–195. https://doi.org/10.1016/S0079-7421(08)60422-3

Axmacher, N., Mormann, F., Fernández, G., Cohen, M. X., Elger, C. E., & Fell, J. (2007). Sustained neural activity patterns during working memory in the human medial temporal lobe. *Journal of Neuroscience*, *27*(29), 7807–7816. https://doi.org/10.1523/JNEUROSCI.0962-07.2007

Aylward, E. H., Sparks, B. F., Field, K. M., Yallapragada, V., Shpritz, B. D., Rosenblatt, A., Brandt, J., Gourley, L. M., Liang, K., Zhou, H., Margolis, R. L., & Ross, C. A. (2004). Onset and rate of striatal atrophy in preclinical Huntington disease. *Neurology*, *63*(1), 66–72. https://doi.org/10.1212/01.WNL.0000132965.14653.D1

Baddeley, A. (2010). Working memory. In *Current Biology* (Vol. 20, Issue 4). Curr Biol. https://doi.org/10.1016/j.cub.2009.12.014

Baddeley, A. D., & Hitch, G. (1974). Working memory. *Psychology of Learning and Motivation - Advances in Research and Theory*, *8*(C), 47–89. https://doi.org/10.1016/S0079-7421(08)60452-1

Baddeley, A. D., & Hitch, G. J. (2000). Development of Working Memory: Should the Pascual-Leone and the Baddeley and Hitch Models Be Merged? *Journal of Experimental Child Psychology*, *77*(2), 128–137. https://doi.org/10.1006/jecp.2000.2592

Badreddine, N., Zalcman, G., Appaix, F., Becq, G., Trembay, N., Saudou, F., Achard, S., & Fino, E. (n.d.). Spatiotemporal reorganization of corticostriatal network dynamics encodes motor skill learning. *In Revision*.

Balcı, F., & Freestone, D. (2020). The Peak Interval Procedure in Rodents: A Tool for Studying the Neurobiological Basis of Interval Timing and Its Alterations in Models of Human Disease. *BIO-PROTOCOL*, *10*(17). https://doi.org/10.21769/BioProtoc.3735

Barbera, G., Liang, B., Zhang, L., Gerfen, C. R., Culurciello, E., Chen, R., Li, Y., & Lin, D.-T. (2016). Spatially Compact Neural Clusters in the Dorsal Striatum Encode Locomotion Relevant Information. *Neuron*, *92*(1), 202–213. https://doi.org/10.1016/j.neuron.2016.08.037

Barnes, T. D., Kubota, Y., Hu, D., Jin, D. Z., & Graybiel, A. M. (2005). Activity of striatal neurons reflects dynamic encoding and recoding of procedural memories. *Nature*, *437*(7062), 1158–1161. https://doi.org/10.1038/nature04053

Barnes, T. D., Mao, J. Bin, Hu, D., Kubota, Y., Dreyer, A. A., Stamoulis, C., Brown, E. N., & Graybiel, A. M. (2011). Advance cueing produces enhanced action-boundary patterns of spike activity in the sensorimotor striatum. *Journal of Neurophysiology*, *105*(4), 1861–1878. https://doi.org/10.1152/jn.00871.2010

Bassett, D. S., Yang, M., Wymbs, N. F., & Grafton, S. T. (2015). Learning-induced autonomy of sensorimotor systems. *Nature Neuroscience*, *18*(5), 744–751. https://doi.org/10.1038/nn.3993

Becq, G. J.-P. C., Badreddine, N., Tremblay, N., Appaix, F., Zalcman, G., Fino, E., & Achard, S. (2019). Classification de types de neurones à partir de signaux calciques. *Gretsi 2019*. https://hal.archives-ouvertes.fr/hal-02528364

Bennett, B. D., & Bolam, J. P. (1993). Characterization of calretinin-immunoreactive structures in the striatum of the rat. *Brain Research*, *609*(1–2), 137–148. https://doi.org/10.1016/0006-8993(93)90866-L

Bentivoglio, M., Van der Kooy, D., & Kuypers, H. G. J. M. (1979). The organization of the efferent projections of the substantia nigra in the rat. A retrograde fluorescent double labeling study. *Brain Research*, *174*(1), 1–17. https://doi.org/10.1016/0006-8993(79)90800-X

Berendse, H. W., & Groenewegen, H. J. (1990). Organization of the thalamostriatal projections in the rat, with special emphasis on the ventral striatum. *Journal of Comparative Neurology*, *299*(2), 187–228. https://doi.org/10.1002/cne.902990206

Bergstrom, H. C., Lipkin, A. M., Lieberman, A. G., Pinard, C. R., Gunduz-Cinar, O., Brockway, E.

T., Taylor, W. W., Nonaka, M., Bukalo, O., Wills, T. A., Rubio, F. J., Li, X., Pickens, C. L., Winder, D. G., & Holmes, A. (2018). Dorsolateral Striatum Engagement Interferes with Early Discrimination Learning. *Cell Reports*, *23*(8), 2264–2272. https://doi.org/10.1016/j.celrep.2018.04.081

Bielschowsky, M. (1919). Einige Bemerkungen zur normalen und pathologischen Histologie des Schweif-und Linsenkerns. *J. Psychol. Neurol.(Lpz.)*, *25*, 1–11.

Biglan, K. M., Shoulson, I., Kieburtz, K., Oakes, D., Kayson, E., Shinaman, M. A., Zhao, H., Romer, M., Young, A., & Hersch, S. (2016). Clinical-Genetic associations in the prospective Huntington at risk observational study (PHAROS): implications for clinical trials. *JAMA Neurology*, *73*(1), 102–110.

Bloem, B., Huda, R., Sur, M., & Graybiel, A. M. (2017). Two-photon imaging in mice shows striosomes and matrix have overlapping but differential reinforcement-related responses. *ELife*, *6*. https://doi.org/10.7554/eLife.32353

Blumenstock, S., & Dudanova, I. (2020). Cortical and Striatal Circuits in Huntington's Disease. In *Frontiers in Neuroscience* (Vol. 14). Frontiers Media S.A. https://doi.org/10.3389/fnins.2020.00082

Boccalaro, I. L., Cristiá-Lara, L., Schwerdel, C., Fritschy, J. M., & Rubi, L. (2019). Cell type-specific distribution of GABAA receptor subtypes in the mouse dorsal striatum. *Journal of Comparative Neurology*, *527*(12), 2030–2046. https://doi.org/10.1002/cne.24665

Bohanna, I., Georgiou-Karistianis, N., & Egan, G. F. (2011). Connectivity-based segmentation of the striatum in Huntington's disease: vulnerability of motor pathways. *Neurobiology of Disease*, *42*(3), 475–481. https://doi.org/10.1016/j.nbd.2011.02.010

Bolam, J. P., Wainer, B. H., & Smith, A. D. (1984). Characterization of cholinergic neurons in the rat neostriatum. A combination of choline acetyltransferase immunocytochemistry, Golgi-impregnation and electron microscopy. *Neuroscience*, *12*(3), 711–718. https://doi.org/10.1016/0306-4522(84)90165-9

Bostan, A. C., & Strick, P. L. (2018). The basal ganglia and the cerebellum: Nodes in an integrated network. In *Nature Reviews Neuroscience* (Vol. 19, Issue 6, pp. 338–350). Nature Publishing Group. https://doi.org/10.1038/s41583-018-0002-7

Braak, H., & Braak, E. (1982). Neuronal types in the striatum of man. *Cell and Tissue Research*, *227*(2), 319–342. https://doi.org/10.1007/BF00210889

Bradfield, L. A., & Balleine, B. W. (2013). Hierarchical and binary associations compete for behavioral control during instrumental biconditional discrimination. *Journal of*

Experimental Psychology: Animal Behavior Processes, *39*(1), 2–13. https://doi.org/10.1037/a0030941

Brimblecombe, K. R., & Cragg, S. J. (2017). The Striosome and Matrix Compartments of the Striatum: A Path through the Labyrinth from Neurochemistry toward Function. *ACS Chemical Neuroscience*, *8*(2), 235–242. https://doi.org/10.1021/acschemneuro.6b00333

Buitrago, M. M., Schulz, J. B., Dichgans, J., & Luft, A. R. (2004). Short and long-term motor skill learning in an accelerated rotarod training paradigm. *Neurobiology of Learning and Memory*, *81*(3), 211–216. https://doi.org/10.1016/j.nlm.2004.01.001

Bunner, K. D., & Rebec, G. V. (2016). Corticostriatal Dysfunction in Huntington's Disease: The Basics. *Frontiers in Human Neuroscience*, *10*, 317. https://doi.org/10.3389/fnhum.2016.00317

Burgold, J., Schulz-Trieglaff, E. K., Voelkl, K., Gutiérrez-Ángel, S., Bader, J. M., Hosp, F., Mann, M., Arzberger, T., Klein, R., Liebscher, S., & Dudanova, I. (2019). Cortical circuit alterations precede motor impairments in Huntington's disease mice. *Scientific Reports*, *9*(1), 6634. https://doi.org/10.1038/s41598-019-43024-w

Burianova, H., & Grady, C. L. (2007). Common and unique neural activations in autobiographical, episodic, and semantic retrieval. *Journal of Cognitive Neuroscience*, *19*(9), 1520–1534. https://doi.org/10.1162/jocn.2007.19.9.1520

Burke, D. A., Rotstein, H. G., & Alvarez, V. A. (2017). Striatal Local Circuitry: A New Framework for Lateral Inhibition. In *Neuron* (Vol. 96, Issue 2, pp. 267–284). Cell Press. https://doi.org/10.1016/j.neuron.2017.09.019

Bush, D., Barry, C., & Burgess, N. (2014). What do grid cells contribute to place cell firing? In *Trends in Neurosciences* (Vol. 37, Issue 3, pp. 136–145). Trends Neurosci. https://doi.org/10.1016/j.tins.2013.12.003

Bylsma, F. W., Brandt, J., & Strauss, M. E. (1990). Aspects of procedural memory are differentially impaired in Huntington's disease. *Archives of Clinical Neuropsychology : The Official Journal of the National Academy of Neuropsychologists*, *5*(3), 287–297.

Calabresi, P., Picconi, B., Tozzi, A., Ghiglieri, V., & Di Filippo, M. (2014). Direct and indirect pathways of basal ganglia: A critical reappraisal. In *Nature Neuroscience* (Vol. 17, Issue 8, pp. 1022–1030). Nature Publishing Group. https://doi.org/10.1038/nn.3743

Camina, E., & Güell, F. (2017). The neuroanatomical, neurophysiological and psychological basis of memory: Current models and their origins. In *Frontiers in Pharmacology* (Vol. 8, Issue JUN). Frontiers Media S.A. https://doi.org/10.3389/fphar.2017.00438

Carden, L., & Wood, W. (2018). Habit formation and change. In *Current Opinion in Behavioral Sciences* (Vol. 20, pp. 117–122). Elsevier Ltd. https://doi.org/10.1016/j.cobeha.2017.12.009

Cardoso, F. (2017). Nonmotor Symptoms in Huntington Disease. In *International Review of Neurobiology* (Vol. 134, pp. 1397–1408). Academic Press Inc. https://doi.org/10.1016/bs.irn.2017.05.004

Cascella, M., & Al Khalili, Y. (2019). *Short Term Memory Impairment*.

Cayzac, S., Delcasso, S., Paz, V., Jeantet, Y., & Cho, Y. H. (2011). Changes in striatal procedural memory coding correlate with learning deficits in a mouse model of Huntington disease. *Proceedings of the National Academy of Sciences of the United States of America*, *108*(22), 9280–9285. https://doi.org/10.1073/pnas.1016190108

Cazorla, M., deCarvalho, F. D., Chohan, M. O., Shegda, M., Chuhma, N., Rayport, S., Ahmari, S. E., Moore, H., & Kellendonk, C. (2014). Dopamine d2 receptors regulate the anatomical and functional balance of basal ganglia circuitry. *Neuron*, *81*(1), 153–164. https://doi.org/10.1016/j.neuron.2013.10.041

Cepeda, C., André, V. M., Yamazaki, I., Wu, N., Kleiman-Weiner, M., & Levine, M. S. (2008). Differential electrophysiological properties of dopamine D1 and D2 receptor-containing striatal medium-sized spiny neurons. *European Journal of Neuroscience*, *27*(3), 671–682. https://doi.org/10.1111/j.1460-9568.2008.06038.x

Cepeda, C., Cummings, D. M., André, V. M., Holley, S. M., & Levine, M. S. (2010). Genetic mouse models of Huntington's disease: focus on electrophysiological mechanisms. *ASN NEURO*, *2*(2). https://doi.org/10.1042/AN20090058

Cepeda, C., Hurst, R. S., Calvert, C. R., Hernández-Echeagaray, E., Nguyen, O. K., Jocoy, E., Christian, L. J., Ariano, M. A., & Levine, M. S. (2003). Transient and progressive electrophysiological alterations in the corticostriatal pathway in a mouse model of Huntington's disease. *Journal of Neuroscience*, *23*(3), 961–969. https://doi.org/10.1523/jneurosci.23-03-00961.2003

Cepeda, C., Wu, N., André, V. M., Cummings, D. M., & Levine, M. S. (2007). The Corticostriatal Pathway in Huntington's Disease. *Progress in Neurobiology*, *81*(5–6), 253–271. https://doi.org/10.1016/j.pneurobio.2006.11.001

Chen, T.-W., Wardill, T. J., Sun, Y., Pulver, S. R., Renninger, S. L., Baohan, A., Schreiter, E. R., Kerr, R. A., Orger, M. B., Jayaraman, V., Looger, L. L., Svoboda, K., & Kim, D. S. (2013). Ultra-sensitive fluorescent proteins for imaging neuronal activity. *Nature*, *499*(7458),

295–300. https://doi.org/10.1038/nature12354

Chuhma, N., Mingote, S., Kalmbach, A., Yetnikoff, L., & Rayport, S. (2017). Heterogeneity in Dopamine Neuron Synaptic Actions Across the Striatum and Its Relevance for Schizophrenia. In *Biological Psychiatry* (Vol. 81, Issue 1, pp. 43–51). Elsevier USA. https://doi.org/10.1016/j.biopsych.2016.07.002

Cicchetti, F., Prensa, L., Wu, Y., & Parent, A. (2000). Chemical anatomy of striatal interneurons in normal individuals and in patients with Huntington's disease. *Brain Research. Brain Research Reviews*, *34*(1–2), 80–101. http://www.ncbi.nlm.nih.gov/pubmed/11086188

Corkin, S. (2002). What's new with the amnesic patient H.M.? *Nature Reviews Neuroscience*, *3*(2), 153–160. https://doi.org/10.1038/nrn726

Costa, R. M., Cohen, D., & Nicolelis, M. A. L. (2004). Differential corticostriatal plasticity during fast and slow motor skill learning in mice. *Current Biology*, *14*(13), 1124–1134. https://doi.org/10.1016/j.cub.2004.06.053

Coulter, J. D., & Jones, E. G. (1977). Differential distribution of corticospinal projections from individual cytoarchitectonic fields in the monkey. *Brain Research*, *129*(2), 335–340. https://doi.org/10.1016/0006-8993(77)90012-9

Cover, K. K., Gyawali, U., Kerkhoff, W. G., Patton, M. H., Mu, C., White, M. G., Marquardt, A. E., Roberts, B. M., Cheer, J. F., & Mathur, B. N. (2019). Activation of the Rostral Intralaminar Thalamus Drives Reinforcement through Striatal Dopamine Release. *Cell Reports*, *26*(6), 1389-1398.e3. https://doi.org/10.1016/j.celrep.2019.01.044

Cowan, N. (2008). Chapter 20 What are the differences between long-term, short-term, and working memory? In *Progress in Brain Research* (Vol. 169, pp. 323–338). NIH Public Access. https://doi.org/10.1016/S0079-6123(07)00020-9

Cowan, N. (2015). George Miller's magical number of immediate memory in retrospect: Observations on the faltering progression of science. *Psychological Review*, *122*(3), 536–541. https://doi.org/10.1037/a0039035

Coyle, J. T., & Schwarcz, R. (1976). Lesion of striatal neurons with kainic acid provides a model for Huntington's chorea. *Nature*, *263*(5574), 244–246. https://doi.org/10.1038/263244a0

Crittenden, J. R., & Graybiel, A. M. (2011). Basal ganglia disorders associated with imbalances in the striatal striosome and matrix compartments. In *Frontiers in Neuroanatomy* (Vol. 5, Issue SEP). Front Neuroanat. https://doi.org/10.3389/fnana.2011.00059

Cui, G., Jun, S. B., Jin, X., Pham, M. D., Vogel, S. S., Lovinger, D. M., & Costa, R. M. (2013).

Concurrent activation of striatal direct and indirect pathways during action initiation. *Nature*, *494*(7436), 238–242. https://doi.org/10.1038/nature11846

Curtis, C. E., & D'Esposito, M. (2004). The effects of prefrontal lesions on working memory performance and theory. In *Cognitive, Affective and Behavioral Neuroscience* (Vol. 4, Issue 4, pp. 528–539). Psychonomic Society Inc. https://doi.org/10.3758/CABN.4.4.528

Daw, N. D., Niv, Y., & Dayan, P. (2005). Uncertainty-based competition between prefrontal and dorsolateral striatal systems for behavioral control. *Nature Neuroscience*, *8*(12), 1704–1711. https://doi.org/10.1038/nn1560

de Lorenzi, F. G., Bridal, T. R., & Spinelli, W. (1995). Voltage-dependent inhibition of the ATP-sensitive K+ current by the class Ia agent disopyramide in cat ventricular myocytes. *Journal of Pharmacology and Experimental Therapeutics*, *272*(2).

DeLong, M. R., Crutcher, M. D., & Georgopoulos, A. P. (1983). Relations between movement and single cell discharge in the substantia nigra of the behaving monkey. *Journal of Neuroscience*, *3*(8), 1599–1606. https://doi.org/10.1523/jneurosci.03-08-01599.1983

DeLong, Mahlon R. (1990). Primate models of movement disorders of basal ganglia origin. In *Trends in Neurosciences* (Vol. 13, Issue 7, pp. 281–285). Trends Neurosci. https://doi.org/10.1016/0166-2236(90)90110-V

Deng, Y. P., Wong, T., Bricker-Anthony, C., Deng, B., & Reiner, A. (2013). Loss of corticostriatal and thalamostriatal synaptic terminals precedes striatal projection neuron pathology in heterozygous Q140 Huntington's disease mice. *Neurobiology of Disease*, *60*, 89–107. https://doi.org/10.1016/j.nbd.2013.08.009

Di Chiara, G., Morelli, M., & Consolo, S. (1994). Modulatory functions of neurotransmitters in the striatum: ACh/dopamine/NMDA interactions. In *Trends in Neurosciences* (Vol. 17, Issue 6, pp. 228–233). Trends Neurosci. https://doi.org/10.1016/0166-2236(94)90005-1

Di Filippo, M., Picconi, B., Tantucci, M., Ghiglieri, V., Bagetta, V., Sgobio, C., Tozzi, A., Parnetti, L., & Calabresi, P. (2009). Short-term and long-term plasticity at corticostriatal synapses: Implications for learning and memory. In *Behavioural Brain Research* (Vol. 199, Issue 1, pp. 108–118). Behav Brain Res. https://doi.org/10.1016/j.bbr.2008.09.025

Díaz-Hernández, E., Contreras-López, R., Sánchez-Fuentes, A., Rodríguez-Sibrían, L., Ramírez-Jarquín, J. O., & Tecuapetla, F. (2018). The Thalamostriatal Projections Contribute to the Initiation and Execution of a Sequence of Movements. *Neuron*, *100*(3), 739-752.e5. https://doi.org/10.1016/j.neuron.2018.09.052

Dickerson, B. C., & Eichenbaum, H. (2010). The episodic memory system: Neurocircuitry and

disorders. In *Neuropsychopharmacology* (Vol. 35, Issue 1, pp. 86–104). Nature Publishing Group. https://doi.org/10.1038/npp.2009.126

Difiglia, M. (1987). Synaptic organization of cholinergic neurons in the monkey neostriatum. *Journal of Comparative Neurology*, *255*(2), 245–258. https://doi.org/10.1002/cne.902550208

DiFiglia, M., Pasik, P., & Pasik, T. (1976). A Golgi study of neuronal types in the neostriatum of monkeys. *Brain Research*, *114*(2), 245–256. https://doi.org/10.1016/0006-8993(76)90669-7

Dimova, R., Vuillet, J., & Seite, R. (1980). Study of the rat neostriatum using a combined Golgi-electron microscope technique and serial sections. *Neuroscience*, *5*(9), 1581–1596. https://doi.org/10.1016/0306-4522(80)90022-6

Divac, I., & Öberg, R. G. E. (1979). Current Conceptions of Neostriatal Functions History and an Evaluation. In *The Neostriatum* (pp. 215–230). Elsevier. https://doi.org/10.1016/b978-0-08-023174-7.50019-9

Divac, I., Rosvold, H. E., & Szwarcbart, M. K. (1967). Behavioral effects of selective ablation of the caudate nucleus. *Journal of Comparative and Physiological Psychology*, *63*(2), 184–190. https://doi.org/10.1037/h0024348

Donzis, E. J., Estrada-Sánchez, A. M., Indersmitten, T., Oikonomou, K., Tran, C. H., Wang, C., Latifi, S., Golshani, P., Cepeda, C., & Levine, M. S. (2020). Cortical Network Dynamics Is Altered in Mouse Models of Huntington's Disease. *Cerebral Cortex*, *30*(4), 2372–2388. https://doi.org/10.1093/cercor/bhz245

Dudchenko, P. A. (2004). An overview of the tasks used to test working memory in rodents. *Neuroscience and Biobehavioral Reviews*, *28*(7), 699–709. https://doi.org/10.1016/j.neubiorev.2004.09.002

Dumas, E. M., van den Bogaard, S. J. A., Ruber, M. E., Reilman, R. R., Stout, J. C., Craufurd, D., Hicks, S. L., Kennard, C., Tabrizi, S. J., van Buchem, M. A., van der Grond, J., & Roos, R. A. C. (2012). Early changes in white matter pathways of the sensorimotor cortex in premanifest Huntington's disease. *Human Brain Mapping*, *33*(1), 203–212. https://doi.org/10.1002/hbm.21205

Durieux, P. F., Schiffmann, S. N., & De Kerchove D'Exaerde, A. (2012). Differential regulation of motor control and response to dopaminergic drugs by D1R and D2R neurons in distinct dorsal striatum subregions. *EMBO Journal*, *31*(3), 640–653. https://doi.org/10.1038/emboj.2011.400

Duyckaerts, C., Joyon, N., & Dürr, A. (2014). Neurodegenerative diseases linked to trinucleotide repeats. In G. G. Kovacs (Ed.), *Neuropathology of Neurodegenerative Diseases: A Practical Guide* (pp. 195–208). Cambridge University Press. https://doi.org/DOI: 10.1017/CBO9781107588660.011

Eichenbaum, H. (2014). Time cells in the hippocampus: A new dimension for mapping memories. In *Nature Reviews Neuroscience* (Vol. 15, Issue 11, pp. 732–744). Nature Publishing Group. https://doi.org/10.1038/nrn3827

Fino, E., Vandecasteele, M., Perez, S., Saudou, F., & Venance, L. (2018). Region-specific and state-dependent action of striatal GABAergic interneurons. *Nature Communications*, *9*(1). https://doi.org/10.1038/s41467-018-05847-5

Fino, E., & Venance, L. (2010). Spike-timing dependent plasticity in the striatum. In *Frontiers in Synaptic Neuroscience* (Vol. 2, Issue JUN). Front Synaptic Neurosci. https://doi.org/10.3389/fnsyn.2010.00006

Fino, E., & Venance, L. (2011). Spike-timing dependent plasticity in striatal interneurons. *Neuropharmacology*, *60*(5), 780–788. https://doi.org/10.1016/j.neuropharm.2011.01.023

Flaherty, A. W., & Graybiel, A. M. (1991). Corticostriatal transformations in the primate somatosensory system. Projections from physiologically mapped body-part representations. *Journal of Neurophysiology*, *66*(4), 1249–1263. https://doi.org/10.1152/jn.1991.66.4.1249

Flaherty, Alice W., & Graybiel, A. M. (1994). Input-output organization of the sensorimotor striatum in the squirrel monkey. *Journal of Neuroscience*, *14*(2), 599–610. https://doi.org/10.1523/jneurosci.14-02-00599.1994

Foerde, K., & Shohamy, D. (2011). The role of the basal ganglia in learning and memory: Insight from Parkinson's disease. In *Neurobiology of Learning and Memory* (Vol. 96, Issue 4, pp. 624–636). NIH Public Access. https://doi.org/10.1016/j.nlm.2011.08.006

Franklin, K. B. J., & Paxinos, G. (2008). *The mouse brain in stereotaxic coordinates* (Issue Sirsi) i9780123694607).

Fujiyama, F., Kuramoto, E., Okamoto, K., Hioki, H., Furuta, T., Zhou, L., Nomura, S., & Kaneko, T. (2004). Presynaptic localization of an AMPA-type glutamate receptor in corticostriatal and thalamostriatal axon terminals. *European Journal of Neuroscience*, *20*(12), 3322–3330. https://doi.org/10.1111/j.1460-9568.2004.03807.x

Fujiyama, F., Sohn, J., Nakano, T., Furuta, T., Nakamura, K. C., Matsuda, W., & Kaneko, T.

(2011). Exclusive and common targets of neostriatofugal projections of rat striosome neurons: A single neuron-tracing study using a viral vector. *European Journal of Neuroscience*, *33*(4), 668–677. https://doi.org/10.1111/j.1460-9568.2010.07564.x

Fujiyama, F., Unzai, T., Nakamura, K., Nomura, S., & Kaneko, T. (2006). Difference in organization of corticostriatal and thalamostriatal synapses between patch and matrix compartments of rat neostriatum. *European Journal of Neuroscience*, *24*(10), 2813–2824. https://doi.org/10.1111/j.1460-9568.2006.05177.x

Funahashi, S. (2013). Space representation in the prefrontal cortex. In *Progress in Neurobiology* (Vol. 103, pp. 131–155). Prog Neurobiol. https://doi.org/10.1016/j.pneurobio.2012.04.002

Funahashi, S. (2017). Working memory in the prefrontal cortex. In *Brain Sciences* (Vol. 7, Issue 5). MDPI AG. https://doi.org/10.3390/brainsci7050049

Funahashi, S., Chafee, M. V., & Goldman-Rakic, P. S. (1993). Prefrontal neuronal activity in rhesus monkeys performing a delayed anti-saccade task. *Nature*, *365*(6448), 753–756. https://doi.org/10.1038/365753a0

Fuster, J. M. (2008). The Prefrontal Cortex. In *The Prefrontal Cortex*. Elsevier Ltd. https://doi.org/10.1016/B978-0-12-373644-4.X0001-1

Gage, G. J., Stoetzner, C. R., Wiltschko, A. B., & Berke, J. D. (2010). Selective Activation of Striatal Fast-Spiking Interneurons during Choice Execution. *Neuron*, *67*(3), 466–479. https://doi.org/10.1016/j.neuron.2010.06.034

Garcia-Gorro, C., Camara, E., & De Diego-Balaguer, R. (2017). Neuroimaging as a tool to study the sources of phenotypic heterogeneity in Huntington's disease. In *Current Opinion in Neurology* (Vol. 30, Issue 4, pp. 398–404). Lippincott Williams and Wilkins. https://doi.org/10.1097/WCO.0000000000000461

Gencik, M., Hammans, C., Strehl, H., Wagner, N., & Epplen, J. T. (2002). Chorea huntington: A rare case with childhood onset. *Neuropediatrics*, *33*(2), 90–92. https://doi.org/10.1055/s-2002-32367

Gerfen, C. L. (2004). Basal Ganglia. In *The Rat Nervous System* (pp. 455–508). Academic Press. https://doi.org/10.1016/B978-012547638-6/50019-5

Gerfen, C. R., Herkenham, M., & Thibault, J. (1987). The neostriatal mosaic: II. Patch- and matrix-directed mesostriatal dopaminergic and non-dopaminergic systems. *Journal of Neuroscience*, *7*(12), 3915–3934. https://doi.org/10.1523/jneurosci.07-12-03915.1987

Gerfen, C R, & Bolam, J. P. (2010). *Handbook of Basal Ganglia Structure and Function (eds.*

Steiner, H. & Tseng, KY) 3–28. Elsevier/Academic Press, Amsterdam.

Gerfen, Charles R. (1984). The neostriatal mosaic: Compartmentalization of corticostriatal input and striatonigral output systems. *Nature*, *311*(5985), 461–464. https://doi.org/10.1038/311461a0

Gerfen, Charles R., Engber, T. M., Mahan, L. C., Susel, Z., Chase, T. N., Monsma, F. J., & Sibley, D. R. (1990). D1 and D2 dopamine receptor-regulated gene expression of striatonigral and striatopallidal neurons. *Science*, *250*(4986), 1429–1432. https://doi.org/10.1126/science.2147780

Gheysen, F., Lasne, G., Pélégrini-Issac, M., Albouy, G., Meunier, S., Benali, H., Doyon, J., & Popa, T. (2017). Taking the brakes off the learning curve. *Human Brain Mapping*, *38*(3), 1676–1691. https://doi.org/10.1002/hbm.23489

Ghika-Schmid, F., Ghika, J., Regli, F., & Bogousslavsky, J. (1997). Hyperkinetic movement disorders during and after acute stroke: The Lausanne Stroke Registry. *Journal of the Neurological Sciences*, *146*(2), 109–116. https://doi.org/10.1016/S0022-510X(96)00290-0

Giannotti, G., Heinsbroek, J. A., Yue, A. J., Deisseroth, K., & Peters, J. (2019). Prefrontal cortex neuronal ensembles encoding fear drive fear expression during long-term memory retrieval. *Scientific Reports*, *9*(1). https://doi.org/10.1038/s41598-019-47095-7

Gil, J. M., & Rego, A. C. (2008). Mechanisms of neurodegeneration in Huntington's disease. In *European Journal of Neuroscience* (Vol. 27, Issue 11, pp. 2803–2820). Eur J Neurosci. https://doi.org/10.1111/j.1460-9568.2008.06310.x

Gittis, A. H., Hooks, B. M., & Gerfen, C. R. (2020). Basal ganglia circuits. In *Neural Circuit and Cognitive Development* (pp. 221–242). Elsevier. https://doi.org/10.1016/b978-0-12-814411-4.00010-x

Gittis, A. H., Nelson, A. B., Thwin, M. T., Palop, J. J., & Kreitzer, A. C. (2010). Distinct Roles of GABAergic Interneurons in the Regulation of Striatal Output Pathways. *Journal of Neuroscience*, *30*(6), 2223–2234. https://doi.org/10.1523/JNEUROSCI.4870-09.2010

Gornati, S. V., Schäfer, C. B., Eelkman Rooda, O. H. J., Nigg, A. L., De Zeeuw, C. I., & Hoebeek, F. E. (2018). Differentiating Cerebellar Impact on Thalamic Nuclei. *Cell Reports*, *23*(9), 2690–2704. https://doi.org/10.1016/j.celrep.2018.04.098

Graveland, G. A., & Difiglia, M. (1985). The frequency and distribution of medium-sized neurons with indented nuclei in the primate and rodent neostriatum. *Brain Research*, *327*(1–2), 307–311. https://doi.org/10.1016/0006-8993(85)91524-0

Gray, M. A., Egan, G. F., Ando, A., Churchyard, A., Chua, P., Stout, J. C., & Georgiou-Karistianis, N. (2013). Prefrontal activity in Huntington's disease reflects cognitive and neuropsychiatric disturbances: the IMAGE-HD study. *Experimental Neurology*, *239*, 218–228. https://doi.org/10.1016/j.expneurol.2012.10.020

Graybiel, A. M., & Ragsdale, C. W. (1978). Histochemically distinct compartments in the striatum of human, monkey, and cat demonstrated by acetylthiocholinesterase staining. *Proceedings of the National Academy of Sciences of the United States of America*, *75*(11), 5723–5726. https://doi.org/10.1073/pnas.75.11.5723

Graybiel, A. M., Ragsdale, C. W., Yoneoka, E. S., & Elde, R. P. (1981). An immunohistochemical study of enkephalins and other neuropeptides in the striatum of the cat with evidence that the opiate peptides are arranged to form mosaic patterns in register with the striosomal compartments visible by acetylcholinesterase staining. *Neuroscience*, *6*(3). https://doi.org/10.1016/0306-4522(81)90131-7

Graybiel, A M. (1995). The basal ganglia. *Trends in Neurosciences*, *18*(2), 60–62. http://www.ncbi.nlm.nih.gov/pubmed/7537409

Graybiel, Ann M. (1998). The basal ganglia and chunking of action repertoires. *Neurobiology of Learning and Memory*, *70*(1–2), 119–136. https://doi.org/10.1006/nlme.1998.3843

Graybiel, Ann M., & Grafton, S. T. (2015). The striatum: Where skills and habits meet. *Cold Spring Harbor Perspectives in Biology*, *7*(8). https://doi.org/10.1101/cshperspect.a021691

Gritton, H. J., Howe, W. M., Romano, M. F., DiFeliceantonio, A. G., Kramer, M. A., Saligrama, V., Bucklin, M. E., Zemel, D., & Han, X. (2019). Unique contributions of parvalbumin and cholinergic interneurons in organizing striatal networks during movement. *Nature Neuroscience*, *22*(4), 586–597. https://doi.org/10.1038/s41593-019-0341-3

Groiss, S. J., Wojtecki, L., Sudmeyer, M., & Schnitzler, A. (2009). Deep brain stimulation in Parkinson-s disease. In *Therapeutic Advances in Neurological Disorders* (Vol. 2, Issue 6, pp. 379–391). SAGE Publications. https://doi.org/10.1177/1756285609339382

Gruber, A. J., & McDonald, R. J. (2012). Context, emotion, and the strategic pursuit of goals: Interactions among multiple brain systems controlling motivated behavior. In *Frontiers in Behavioral Neuroscience* (Vol. 6, Issue AUGUST). Front Behav Neurosci. https://doi.org/10.3389/fnbeh.2012.00050

Guo, Z., Rudow, G., Pletnikova, O., Codispoti, K. E., Orr, B. A., Crain, B. J., Duan, W., Margolis, R. L., Rosenblatt, A., Ross, C. A., & Troncoso, J. C. (2012). Striatal neuronal loss correlates

with clinical motor impairment in Huntington's disease. *Movement Disorders*, *27*(11), 1379–1386. https://doi.org/10.1002/mds.25159

Gurevich, E. V., & Joyce, J. N. (1999). Distribution of dopamine D3 receptor expressing neurons in the human forebrain comparison with D2 receptor expressing neurons. *Neuropsychopharmacology*, *20*(1), 60–80. https://doi.org/10.1016/S0893-133X(98)00066-9

Gusella, J. F., Wexler, N. S., Conneally, P. M., Naylor, S. L., Anderson, M. A., Tanzi, R. E., Watkins, P. C., Ottina, K., Wallace, M. R., Sakaguchi, A. Y., Young, A. B., Shoulson, I., Bonilla, E., & Martin, J. B. (1983). A polymorphic DNA marker genetically linked to Huntington's disease. *Nature*, *306*(5940), 234–238. https://doi.org/10.1038/306234a0

Haber, S., & McFarland, N. R. (2001). The place of the thalamus in frontal cortical-basal ganglia circuits. In *Neuroscientist* (Vol. 7, Issue 4, pp. 315–324). SAGE Publications Inc. https://doi.org/10.1177/107385840100700408

Haber, S. N., & Calzavara, R. (2009). The cortico-basal ganglia integrative network: The role of the thalamus. In *Brain Research Bulletin* (Vol. 78, Issues 2–3, pp. 69–74). Brain Res Bull. https://doi.org/10.1016/j.brainresbull.2008.09.013

Hamasaki, T., & Goto, S. (2019). Parallel emergence of a compartmentalized striatum with the phylogenetic development of the cerebral cortex. In *Brain Sciences* (Vol. 9, Issue 4). MDPI AG. https://doi.org/10.3390/brainsci9040090

Harris, G. J., Aylward, E. H., Peyser, C. E., Pearlson, G. D., Brandt, J., Roberts-Twillie, J. V., Barta, P. E., & Folstein, S. E. (1996). Single photon emission computed tomographic blood flow and magnetic resonance volume imaging of basal ganglia in Huntington's disease. *Archives of Neurology*, *53*(4), 316–324. https://doi.org/10.1001/archneur.1996.00550040044013

Harris, G. J., Pearlson, G. D., Peyser, C. E., Aylward, E. H., Roberts, J., Barta, P. E., Chase, G. A., & Folstein, S. E. (1992). Putamen volume reduction on magnetic resonance imaging exceeds caudate changes in mild Huntington's disease. *Annals of Neurology*, *31*(1), 69–75. https://doi.org/10.1002/ana.410310113

Hawes, S. L., Evans, R. C., Unruh, B. A., Benkert, E. E., Gillani, F., Dumas, T. C., & Blackwell, K. T. (2015). Multimodal plasticity in dorsal striatum while learning a lateralized navigation task. *Journal of Neuroscience*, *35*(29), 10535–10549. https://doi.org/10.1523/JNEUROSCI.4415-14.2015

Herkenham, M., & Pert, C. B. (1981). Mosaic distribution of opiate receptors, parafascicular

projections and acetylcholinesterase in rat striatum. *Nature*, *291*(5814), 415–418. https://doi.org/10.1038/291415a0

Hickey, M. A., Kosmalska, A., Enayati, J., Cohen, R., Zeitlin, S., Levine, M. S., & Chesselet, M.-F. (2008). Extensive early motor and non-motor behavioral deficits are followed by striatal neuronal loss in knock-in Huntington's disease mice. *Neuroscience*, *157*(1), 280–295. https://doi.org/10.1016/j.neuroscience.2008.08.041

Hikosaka, O., Miyashita, K., Miyachi, S., Sakai, K., & Lu, X. (1998). Differential roles of the frontal cortex, basal ganglia, and cerebellum in visuomotor sequence learning. *Neurobiology of Learning and Memory*, *70*(1–2), 137–149. https://doi.org/10.1006/nlme.1998.3844

Hikosaka, O., Nakamura, K., Sakai, K., & Nakahara, H. (2002). Central mechanisms of motor skill learning. In *Current Opinion in Neurobiology* (Vol. 12, Issue 2, pp. 217–222). Elsevier Ltd. https://doi.org/10.1016/S0959-4388(02)00307-0

Hintiryan, H., Foster, N. N., Bowman, I., Bay, M., Song, M. Y., Gou, L., Yamashita, S., Bienkowski, M. S., Zingg, B., Zhu, M., Yang, X. W., Shih, J. C., Toga, A. W., & Dong, H. W. (2016). The mouse cortico-striatal projectome. *Nature Neuroscience*, *19*(8), 1100–1114. https://doi.org/10.1038/nn.4332

Holley, S. M., Galvan, L., Kamdjou, T., Cepeda, C., & Levine, M. S. (2019). Striatal GABAergic interneuron dysfunction in the Q175 mouse model of Huntington's disease. *European Journal of Neuroscience*, *49*(1), 79–93. https://doi.org/10.1111/ejn.14283

Holly, E. N., Davatolhagh, M. F., Choi, K., Alabi, O. O., Vargas Cifuentes, L., & Fuccillo, M. V. (2019). Striatal Low-Threshold Spiking Interneurons Regulate Goal-Directed Learning. *Neuron*, *103*(1), 92-101.e6. https://doi.org/10.1016/j.neuron.2019.04.016

Holtbernd, F., Tang, C. C., Feigin, A., Dhawan, V., Ghilardi, M. F., Paulsen, J. S., Guttman, M., & Eidelberg, D. (2016). Longitudinal changes in the motor learning-related brain activation response in presymptomatic Huntington's disease. *PLoS ONE*, *11*(5). https://doi.org/10.1371/journal.pone.0154742

Hoover, J. E., & Strick, P. L. (1993). Multiple output channels in the basal ganglia. *Science*, *259*(5096), 819–821. https://doi.org/10.1126/science.7679223

Howard, M. W., & Eichenbaum, H. (2015). Time and space in the hippocampus. *Brain Research*, *1621*, 345–354. https://doi.org/10.1016/j.brainres.2014.10.069

Huang, Z. J. (2014). Toward a genetic dissection of cortical circuits in the mouse. In *Neuron* (Vol. 83, Issue 6, pp. 1284–1302). Cell Press.

https://doi.org/10.1016/j.neuron.2014.08.041

Hull, C. L. (1943). *Principles of Behavior - an introduction to behavior theory*. https://www.passeidireto.com/arquivo/6707483/hull-c-l-1943-principles-of-behavior-an-introduction-to-behavior-theory

Hummel, J. H., Abercrombie, C., & Koepsel, P. (1991). Teaching Students to Analyze Examples of Classical Conditioning. *The Behavior Analyst*, *14*(2), 241–246. https://doi.org/10.1007/bf03392579

Huntington, G. (1872). On Chorea. *The Medical and Surgical Reporter: A Weekly Journal*, *26*(15), 317–321.

Jacobowitz, D. M., & Winsky, L. (1991). Immunocytochemical localization of calretinin in the forebrain of the rat. *Journal of Comparative Neurology*, *304*(2), 198–218. https://doi.org/10.1002/cne.903040205

Jacobsen, C. F. (1935). Functions of frontal association area in primates. *Archives of Neurology And Psychiatry*, *33*(3), 558–569. https://doi.org/10.1001/archneurpsyc.1935.02250150108009

Jenrette, T. A., Logue, J. B., & Horner, K. A. (2019). Lesions of the Patch Compartment of Dorsolateral Striatum Disrupt Stimulus–Response Learning. *Neuroscience*, *415*, 161–172. https://doi.org/10.1016/j.neuroscience.2019.07.033

Jin, X., & Costa, R. M. (2010). Start/stop signals emerge in nigrostriatal circuits during sequence learning. *Nature*, *466*(7305), 457–462. https://doi.org/10.1038/nature09263

Jin, X., & Costa, R. M. (2015). Shaping action sequences in basal ganglia circuits. In *Current Opinion in Neurobiology* (Vol. 33, pp. 188–196). Elsevier Ltd. https://doi.org/10.1016/j.conb.2015.06.011

Jin, X., Tecuapetla, F., & Costa, R. M. (2014). Basal ganglia subcircuits distinctively encode the parsing and concatenation of action sequences. *Nature Neuroscience*, *17*(3), 423–430. https://doi.org/10.1038/nn.3632

Jocoy, E. L., André, V. M., Cummings, D. M., Rao, S. P., Wu, N., Ramsey, A. J., Caron, M. G., Cepeda, C., & Levine, M. S. (2011). Dissecting the contribution of individual receptor subunits to the enhancement of N-methyl-d-aspartate currents by dopamine D1 receptor activation in striatum. *Frontiers in Systems Neuroscience*, *5*(MAY 2011). https://doi.org/10.3389/fnsys.2011.00028

Joel, D., & Weiner, I. (2000). The connections of the dopaminergic system with the striatum in rats and primates: An analysis with respect to the functional and compartmental

organization of the striatum. In *Neuroscience* (Vol. 96, Issue 3, pp. 451–474). Neuroscience. https://doi.org/10.1016/S0306-4522(99)00575-8

Jog, M. S., Kubota, Y., Connolly, C. I., & Graybiel, A. M. (1999). Building neural representations of habits. *Science*, *286*(5445), 1745–1749. https://doi.org/10.1126/science.286.5445.1745

Johansson, Y., & Silberberg, G. (2020). The Functional Organization of Cortical and Thalamic Inputs onto Five Types of Striatal Neurons Is Determined by Source and Target Cell Identities. *Cell Reports*, *30*(4), 1178-1194.e3. https://doi.org/10.1016/j.celrep.2019.12.095

Johnson, K. A., Voyvodic, L., Loewinger, G. C., Mateo, Y., & Lovinger, D. M. (2020). Operant self-stimulation of thalamic terminals in the dorsomedial striatum is constrained by metabotropic glutamate receptor 2. *Neuropsychopharmacology*, *45*(9), 1454–1462. https://doi.org/10.1038/s41386-020-0626-y

Johnston, J. G., Gerfen, C. R., Haber, S. N., & van der Kooy, D. (1990). Mechanisms of striatal pattern formation: conservation of mammalian compartmentalization. *Developmental Brain Research*, *57*(1), 93–102. https://doi.org/10.1016/0165-3806(90)90189-6

Jonides, J., Lewis, R. L., Nee, D. E., Lustig, C. A., Berman, M. G., & Moore, K. S. (2008). The mind and brain of short-term memory. *Annual Review of Psychology*, *59*, 193–224. https://doi.org/10.1146/annurev.psych.59.103006.093615

Jouhanneau, J. S., & Poulet, J. F. A. (2019). Multiple Two-Photon Targeted Whole-Cell Patch-Clamp Recordings from Monosynaptically Connected Neurons in vivo. *Frontiers in Synaptic Neuroscience*, *11*(MAY), 15. https://doi.org/10.3389/fnsyn.2019.00015

Ju, W. (2018). Chemogenetic Methods to Examine the Brain and Behaviour. In S. L. Georgia Bains, Ingrid Barany, Maksym Shcherbina (Ed.), *Neuroscience: Canadian 1st Edition*. https://openlibrary-repo.ecampusontario.ca/jspui/handle/123456789/546

Kal, E., Winters, M., Van Kamp, J. Der, Houdijk, H., Groet, E., Bennekom, C., & Scherder, E. (2016). Is implicit motor learning preserved after stroke? A systematic review with meta-analysis. *PLoS ONE*, *11*(12). https://doi.org/10.1371/journal.pone.0166376

Kalonaris, S. (2018). Satisficing goals and methods in human-machine music improvisations: Experiments with Dory. *Journal of Creative Music Systems*, *2*(2). https://doi.org/10.5920/jcms.2018.03

Kawaguchi, Y., & Kubota, Y. (1993). Correlation of physiological subgroupings of nonpyramidal cells with parvalbumin- and calbindin(D28k)-immunoreactive neurons in layer V of rat

frontal cortex. *Journal of Neurophysiology*, *70*(1), 387–396. https://doi.org/10.1152/jn.1993.70.1.387

Kawaguchi, Y., Wilson, C. J., & Emson, P. C. (1989). Intracellular recording of identified neostriatal patch and matrix spiny cells in a slice preparation preserving cortical inputs. *Journal of Neurophysiology*, *62*(5), 1052–1068. https://doi.org/10.1152/jn.1989.62.5.1052

Kawaguchi, Y, Wilson, C. J., Augood, S. J., & Emson, P. C. (1995). Striatal interneurones: chemical, physiological and morphological characterization. *Trends in Neurosciences*, *18*(12), 527–535. http://www.ncbi.nlm.nih.gov/pubmed/8638293

Kawaguchi, Yasuo. (1997). Neostriatal cell subtypes and their functional roles. *Neuroscience Research*, *27*(1), 1–8. https://doi.org/10.1016/S0168-0102(96)01134-0

Kawaguchi, Yasuo, Wilson, C. J., & Emson, P. C. (1990). Projection subtypes of rat neostriatal matrix cells revealed by intracellular injection of biocytin. *Journal of Neuroscience*, *10*(10), 3421–3438. https://doi.org/10.1523/jneurosci.10-10-03421.1990

Kebabian, J. W., & Calne, D. B. (1979). Multiple receptors for dopamine. *Nature*, *277*(5692), 93–96. https://doi.org/10.1038/277093a0

Kemp, J. M., & Powell, T. P. (1971). The connexions of the striatum and globus pallidus: synthesis and speculation. *Philosophical Transactions of the Royal Society of London. Series B, Biological Sciences*, *262*(845), 441–457. https://doi.org/10.1098/rstb.1971.0106

Keum, J. W., Shin, A., Gillis, T., Mysore, J. S., Abu Elneel, K., Lucente, D., Hadzi, T., Holmans, P., Jones, L., Orth, M., Kwak, S., Macdonald, M. E., Gusella, J. F., & Lee, J. M. (2016). The HTT CAG-Expansion Mutation Determines Age at Death but Not Disease Duration in Huntington Disease. *American Journal of Human Genetics*, *98*(2), 287–298. https://doi.org/10.1016/j.ajhg.2015.12.018

Kieburtz, K. (1996). Unified Huntington's disease rating scale: Reliability and consistency. *Movement Disorders*, *11*(2), 136–142. https://doi.org/10.1002/mds.870110204

Killoran, A., Biglan, K. M., Jankovic, J., Eberly, S., Kayson, E., Oakes, D., Young, A. B., & Shoulson, I. (2013). Characterization of the Huntington intermediate CAG repeat expansion phenotype in PHAROS. *Neurology*, *80*(22), 2022–2027. https://doi.org/10.1212/WNL.0b013e318294b304

Kirch, R. D., Meyer, P. T., Geisler, S., Braun, F., Gehrig, S., Langen, K.-J., von Hörsten, S., Nikkhah, G., Cassel, J.-C., & Döbrössy, M. D. (2013). Early deficits in declarative and procedural memory dependent behavioral function in a transgenic rat model of

Huntington's disease. *Behavioural Brain Research*, *239*, 15–26. https://doi.org/10.1016/j.bbr.2012.10.048

Kirch, R. D., Pinnell, R. C., Hofmann, U. G., & Cassel, J. C. (2015). The double-h maze: A robust behavioral test for learning and memory in rodents. *Journal of Visualized Experiments*, *2015*(101), 1–19. https://doi.org/10.3791/52667

Kita, H., Kosaka, T., & Heizmann, C. W. (1990). Parvalbumin-immunoreactive neurons in the rat neostriatum: a light and electron microscopic study. *Brain Research*, *536*(1–2), 1–15. https://doi.org/10.1016/0006-8993(90)90002-S

Klaus, A., Martins, G. J., Paixao, V. B., Zhou, P., Paninski, L., & Costa, R. M. (2017). The Spatiotemporal Organization of the Striatum Encodes Action Space. *Neuron*, *95*(5), 1171-1180.e7. https://doi.org/10.1016/j.neuron.2017.08.015

Koralek, A. C., Jin, X., Long, J. D., Costa, R. M., & Carmena, J. M. (2012). Corticostriatal plasticity is necessary for learning intentional neuroprosthetic skills. *Nature*, *483*(7389), 331–335. https://doi.org/10.1038/nature10845

Kravitz, A. V., & Kreitzer, A. C. (2012). Striatal Mechanisms Underlying Movement, Reinforcement, and Punishment. *Physiology*, *27*(3), 167–177. https://doi.org/10.1152/physiol.00004.2012

Kravitz, Alexxai V., Tye, L. D., & Kreitzer, A. C. (2012). Distinct roles for direct and indirect pathway striatal neurons in reinforcement. *Nature Neuroscience*, *15*(6), 816–818. https://doi.org/10.1038/nn.3100

Kreitzer, A. C. (2009). Physiology and pharmacology of striatal neurons. In *Annual Review of Neuroscience* (Vol. 32, pp. 127–147). Annu Rev Neurosci. https://doi.org/10.1146/annurev.neuro.051508.135422

Kreitzer, A. C., & Malenka, R. C. (2009). Striatal Plasticity and Basal Ganglia Circuit Function. In *Neuron* (Vol. 60, Issue 4, pp. 543–554). Neuron. https://doi.org/10.1016/j.neuron.2008.11.005

Kremer, B., Goldberg, P., Andrew, S. E., Theilmann, J., Telenius, H., Zeisler, J., Squitieri, F., Lin, B., Bassett, A., Almqvist, E., Bird, T. D., & Hayden, M. R. (1994). A worldwide study of the huntington's disease mutation: The sensitivity and specificity of measuring CAG repeats. *New England Journal of Medicine*, *330*(20), 1401–1406. https://doi.org/10.1056/NEJM199405193302001

Kudlak, M., & Tadi, P. (2020). Physiology, Muscarinic Receptor. In *StatPearls*. StatPearls Publishing. http://www.ncbi.nlm.nih.gov/pubmed/32310369

Kumar, A., Kumar, V., Singh, K., Kumar, S., Kim, Y. S., Lee, Y. M., & Kim, J. J. (2020). Therapeutic advances for huntington's disease. In *Brain Sciences* (Vol. 10, Issue 1). MDPI AG. https://doi.org/10.3390/brainsci10010043

Kumaran, D. (2008). Short-term memory and the human hippocampus. In *Journal of Neuroscience* (Vol. 28, Issue 15, pp. 3837–3838). Society for Neuroscience. https://doi.org/10.1523/JNEUROSCI.0046-08.2008

Kupferschmidt, D. A., Juczewski, K., Cui, G., Johnson, K. A., & Lovinger, D. M. (2017). Parallel, but Dissociable, Processing in Discrete Corticostriatal Inputs Encodes Skill Learning. *Neuron*, *96*(2), 476-489.e5. https://doi.org/10.1016/j.neuron.2017.09.040

Lallani, S. B., Villalba, R. M., Chen, Y., Smith, Y., & Chan, A. W. S. (2019). Striatal Interneurons in Transgenic Nonhuman Primate Model of Huntington's Disease. *Scientific Reports*, *9*(1), 1–9. https://doi.org/10.1038/s41598-019-40165-w

Lanciego, J. L., Luquin, N., & Obeso, J. A. (2012). Functional neuroanatomy of the basal ganglia. *Cold Spring Harbor Perspectives in Medicine*, *2*(12). https://doi.org/10.1101/cshperspect.a009621

Lawhorn, C., Smith, D. M., & Brown, L. L. (2009). Partial ablation of mu-opioid receptor rich striosomes produces deficits on a motor-skill learning task. *Neuroscience*, *163*(1), 109–119. https://doi.org/10.1016/j.neuroscience.2009.05.021

Lee, C. R., Yonk, A. J., Wiskerke, J., Paradiso, K. G., Tepper, J. M., & Margolis, D. J. (2019). Opposing Influence of Sensory and Motor Cortical Input on Striatal Circuitry and Choice Behavior. *Current Biology*, *29*(8), 1313-1323.e5. https://doi.org/10.1016/j.cub.2019.03.028

Lee Hong, S., & Rebec, G. V. (2012). Biological sources of inflexibility in brain and behavior with aging and neurodegenerative diseases. In *Frontiers in Systems Neuroscience* (Vol. 6, Issue NOV). Front Syst Neurosci. https://doi.org/10.3389/fnsys.2012.00077

Lee, K., Holley, S. M., Shobe, J. L., Chong, N. C., Cepeda, C., Levine, M. S., & Masmanidis, S. C. (2017). Parvalbumin Interneurons Modulate Striatal Output and Enhance Performance during Associative Learning. *Neuron*, *93*(6). https://doi.org/10.1016/j.neuron.2017.02.033

Lerner, T. N., & Kreitzer, A. C. (2011). Neuromodulatory control of striatal plasticity and behavior. In *Current Opinion in Neurobiology* (Vol. 21, Issue 2, pp. 322–327). Curr Opin Neurobiol. https://doi.org/10.1016/j.conb.2011.01.005

Lester, J., Fink, S., Aronin, N., & DiFiglia, M. (1993). Colocalization of D1 and D2 dopamine

receptor mRNAs in striatal neurons. *Brain Research*, *621*(1), 106–110. https://doi.org/10.1016/0006-8993(93)90303-5

Levy, R., & Goldman-Rakic, P. S. (2000). Segregation of working memory functions within the dorsolateral prefrontal cortex. In *Experimental Brain Research* (Vol. 133, Issue 1, pp. 23–32). Springer Verlag. https://doi.org/10.1007/s002210000397

Lipton, D. M., Gonzales, B. J., & Citri, A. (2019). Dorsal striatal circuits for habits, compulsions and addictions. In *Frontiers in Systems Neuroscience* (Vol. 13). Frontiers Media S.A. https://doi.org/10.3389/fnsys.2019.00028

MacDonald, M. E., Ambrose, C. M., Duyao, M. P., Myers, R. H., Lin, C., Srinidhi, L., Barnes, G., Taylor, S. A., James, M., Groot, N., MacFarlane, H., Jenkins, B., Anderson, M. A., Wexler, N. S., Gusella, J. F., Bates, G. P., Baxendale, S., Hummerich, H., Kirby, S., … Harper, P. S. (1993). A novel gene containing a trinucleotide repeat that is expanded and unstable on Huntington's disease chromosomes. *Cell*, *72*(6), 971–983. https://doi.org/10.1016/0092-8674(93)90585-E

Mana, S., & Chevalier, G. (2001). The fine organization of nigro-collicular channels with additional observations of their relationships with acetylcholinesterase in the rat. *Neuroscience*, *106*(2), 357–374. https://doi.org/10.1016/S0306-4522(01)00283-4

Mangiarini, L., Sathasivam, K., Seller, M., Cozens, B., Harper, A., Hetherington, C., Lawton, M., Trottier, Y., Lehrach, H., Davies, S. W., & Bates, G. P. (1996). Exon I of the HD gene with an expanded CAG repeat is sufficient to cause a progressive neurological phenotype in transgenic mice. *Cell*, *87*(3), 493–506. https://doi.org/10.1016/S0092-8674(00)81369-0

Marchi, V. (1886). Sulle degenerazioni consecutive all'estirpazione totale e parziale del cervelletto. *Riv Sper Freniat*, *12*, 50–56.

Martin, S. J., Grimwood, P. D., & Morris, R. G. M. (2000). Synaptic plasticity and memory: An evaluation of the hypothesis. In *Annual Review of Neuroscience* (Vol. 23, pp. 649–711). Annu Rev Neurosci. https://doi.org/10.1146/annurev.neuro.23.1.649

Matamales, M., McGovern, A. E., Mi, J. D., Mazzone, S. B., Balleine, B. W., & Bertran-Gonzalez, J. (2020). Local D2- To D1-neuron transmodulation updates goal-directed learning in the striatum. *Science*, *367*(6477), 549–555. https://doi.org/10.1126/science.aaz5751

McDonald, R. J., & White, N. M. (1993). A triple dissociation of memory systems: Hippocampus, amygdala, and dorsal striatum. *Behavioral Neuroscience*, *107*(1), 3–22. https://doi.org/10.1037//0735-7044.107.1.3

McDonald, R. J., & White, N. M. (1994). Parallel information processing in the water maze:

Evidence for independent memory systems involving dorsal striatum and hippocampus. *Behavioral and Neural Biology*, *61*(3), 260–270. https://doi.org/10.1016/S0163-1047(05)80009-3

McGeorge, A. J., & Faull, R. L. M. (1989). The organization of the projection from the cerebral cortex to the striatum in the rat. *Neuroscience*, *29*(3), 503–537. https://doi.org/10.1016/0306-4522(89)90128-0

McHaffie, J. G., Stanford, T. R., Stein, B. E., Coizet, V., & Redgrave, P. (2005). Subcortical loops through the basal ganglia. *Trends in Neurosciences*, *28*(8), 401–407. https://doi.org/10.1016/j.tins.2005.06.006

Menalled, L. B., Kudwa, A. E., Miller, S., Fitzpatrick, J., Watson-Johnson, J., Keating, N., Ruiz, M., Mushlin, R., Alosio, W., McConnell, K., Connor, D., Murphy, C., Oakeshott, S., Kwan, M., Beltran, J., Ghavami, A., Brunner, D., Park, L. C., Ramboz, S., & Howland, D. (2012). Comprehensive Behavioral and Molecular Characterization of a New Knock-In Mouse Model of Huntington's Disease: ZQ175. *PLoS ONE*, *7*(12). https://doi.org/10.1371/journal.pone.0049838

Menalled, L. B., Sison, J. D., Dragatsis, I., Zeitlin, S., & Chesselet, M.-F. (2003). Time course of early motor and neuropathological anomalies in a knock-in mouse model of Huntington's disease with 140 CAG repeats. *The Journal of Comparative Neurology*, *465*(1), 11–26. https://doi.org/10.1002/cne.10776

Miyamoto, Y., Katayama, S., Shigematsu, N., Nishi, A., & Fukuda, T. (2018). Striosome-based map of the mouse striatum that is conformable to both cortical afferent topography and uneven distributions of dopamine D1 and D2 receptor-expressing cells. *Brain Structure and Function*, *223*(9), 4275–4291. https://doi.org/10.1007/s00429-018-1749-3

Miyashita, Y. (2019). Perirhinal circuits for memory processing. In *Nature Reviews Neuroscience* (Vol. 20, Issue 10, pp. 577–592). Nature Publishing Group. https://doi.org/10.1038/s41583-019-0213-6

Moscovitch, M., Cabeza, R., Winocur, G., & Nadel, L. (2016). Episodic memory and beyond: The hippocampus and neocortex in transformation. *Annual Review of Psychology*, *67*, 105–134. https://doi.org/10.1146/annurev-psych-113011-143733

Moscovitch, M., Rosenbaum, R. S., Gilboa, A., Addis, D. R., Westmacott, R., Grady, C., McAndrews, M. P., Levine, B., Black, S., Winocur, G., & Nadel, L. (2005). Functional neuroanatomy of remote episodic, semantic and spatial memory: A unified account based on multiple trace theory. In *Journal of Anatomy* (Vol. 207, Issue 1, pp. 35–66). J

Anat. https://doi.org/10.1111/j.1469-7580.2005.00421.x

Murray, R. C., Gilbert, Y. E., Logan, A. S., Hebbard, J. C., & Horner, K. A. (2014). Striatal patch compartment lesions alter methamphetamine-induced behavior and immediate early gene expression in the striatum, substantia nigra and frontal cortex. *Brain Structure and Function*, *219*(4), 1213–1229. https://doi.org/10.1007/s00429-013-0559-x

Nauta, W. J. H., & Mehler, W. R. (1966). Projections of the lentiform nucleus in the monkey. In *Brain Research* (Vol. 1, Issue 1, pp. 3–42). Brain Res. https://doi.org/10.1016/0006-8993(66)90103-X

Naze, S., Humble, J., Zheng, P., Barton, S., Rangel-Barajas, C., Rebec, G. V., & Kozloski, J. R. (2018). Cortico-striatal cross-frequency coupling and gamma genesis disruptions in huntington's disease mouse and computational models. *ENeuro*, *5*(6). https://doi.org/10.1523/ENEURO.0210-18.2018

Nelson, A. B., & Kreitzer, A. C. (2014). Reassessing Models of Basal Ganglia Function and Dysfunction. *Annual Review of Neuroscience*, *37*(1), 117–135. https://doi.org/10.1146/annurev-neuro-071013-013916

Nopoulos, P. C., Aylward, E. H., Ross, C. A., Johnson, H. J., Magnotta, V. A., Juhl, A. R., Pierson, R. K., Mills, J., Langbehn, D. R., & Paulsen, J. S. (2010). Cerebral cortex structure in prodromal Huntington disease. *Neurobiology of Disease*, *40*(3), 544–554. https://doi.org/10.1016/j.nbd.2010.07.014

O'Hare, J. K., Ade, K. K., Sukharnikova, T., Van Hooser, S. D., Palmeri, M. L., Yin, H. H., & Calakos, N. (2016). Pathway-Specific Striatal Substrates for Habitual Behavior. *Neuron*, *89*(3), 472–479. https://doi.org/10.1016/j.neuron.2015.12.032

O'Hare, J. K., Li, H., Kim, N., Gaidis, E., Ade, K., Beck, J., Yin, H., & Calakos, N. (2017). Striatal fast-spiking interneurons selectively modulate circuit output and are required for habitual behavior. *ELife*, *6*. https://doi.org/10.7554/eLife.26231

O'Keefe, J., & Dostrovsky, J. (1971). The hippocampus as a spatial map. Preliminary evidence from unit activity in the freely-moving rat. *Brain Research*, *34*(1), 171–175. https://doi.org/10.1016/0006-8993(71)90358-1

Obeso, J. A., Rodríguez-Oroz, M. C., Benitez-Temino, B., Blesa, F. J., Guridi, J., Marin, C., & Rodriguez, M. (2008). Functional organization of the basal ganglia: therapeutic implications for Parkinson's disease. *Movement Disorders: Official Journal of the Movement Disorder Society*, *23 Suppl 3*, S548-559. https://doi.org/10.1002/mds.22062

Oertel, W. H., & Mugnaini, E. (1984). Immunocytochemical studies of GABAergic neurons in

rat basal ganglia and their relations to other neuronal systems. *Neuroscience Letters*, *47*(3), 233–238. https://doi.org/10.1016/0304-3940(84)90519-6

Owen, S. F., Berke, J. D., & Kreitzer, A. C. (2018). Fast-Spiking Interneurons Supply Feedforward Control of Bursting, Calcium, and Plasticity for Efficient Learning. *Cell*, *172*(4), 683-695.e15. https://doi.org/10.1016/j.cell.2018.01.005

Packard, M G, & McGaugh, J. L. (1996). Inactivation of hippocampus or caudate nucleus with lidocaine differentially affects expression of place and response learning. *Neurobiology of Learning and Memory*, *65*(1), 65–72. https://doi.org/10.1006/nlme.1996.0007

Packard, Mark G. (2009). Exhumed from thought: Basal ganglia and response learning in the plus-maze. In *Behavioural Brain Research* (Vol. 199, Issue 1, pp. 24–31). https://doi.org/10.1016/j.bbr.2008.12.013

Papoutsi, M., Labuschagne, I., Tabrizi, S. J., & Stout, J. C. (2014). The cognitive burden in Huntington's disease: pathology, phenotype, and mechanisms of compensation. *Movement Disorders : Official Journal of the Movement Disorder Society*, *29*(5), 673–683. https://doi.org/10.1002/mds.25864

Parent, A, & Hazrati, L. N. (1995). Functional anatomy of the basal ganglia. I. The cortico-basal ganglia-thalamo-cortical loop. *Brain Research. Brain Research Reviews*, *20*(1), 91–127. http://www.ncbi.nlm.nih.gov/pubmed/7711769

Parent, André. (1990). Extrinsic connections of the basal ganglia. In *Trends in Neurosciences* (Vol. 13, Issue 7, pp. 254–258). Trends Neurosci. https://doi.org/10.1016/0166-2236(90)90105-J

Parker, J. G., Marshall, J. D., Ahanonu, B., Wu, Y. W., Kim, T. H., Grewe, B. F., Zhang, Y., Li, J. Z., Ding, J. B., Ehlers, M. D., & Schnitzer, M. J. (2018). Diametric neural ensemble dynamics in parkinsonian and dyskinetic states. *Nature*, *557*(7704), 177–182. https://doi.org/10.1038/s41586-018-0090-6

Parsons, M. P., Li, S., & Kirouac, G. J. (2007). Functional and anatomical connection between the paraventricular nucleus of the thalamus and dopamine fibers of the nucleus accumbens. *Journal of Comparative Neurology*, *500*(6), 1050–1063. https://doi.org/10.1002/cne.21224

Parthasarathy, H. B., & Graybiel, A. M. (1997). Cortically driven immediate-early gene expression reflects modular influence of sensorimotor cortex on identified striatal neurons in the squirrel monkey. *Journal of Neuroscience*, *17*(7), 2477–2491. https://doi.org/10.1523/jneurosci.17-07-02477.1997

Patel, T. P., Man, K., Firestein, B. L., & Meaney, D. F. (2015). Automated quantification of neuronal networks and single-cell calcium dynamics using calcium imaging. *Journal of Neuroscience Methods*, *243*, 26–38. https://doi.org/10.1016/j.jneumeth.2015.01.020

Pavlov, I. P. (1927). Conditioned reflexes: An investigation of the physiological activity of the cerebral cortex. *Annals of Neurosciences*, *17*(3), 136. https://doi.org/10.5214/ans.0972-7531.1017309

Peak, J., Hart, G., & Balleine, B. W. (2019). From learning to action: the integration of dorsal striatal input and output pathways in instrumental conditioning. In *European Journal of Neuroscience* (Vol. 49, Issue 5, pp. 658–671). Blackwell Publishing Ltd. https://doi.org/10.1111/ejn.13964

Perrin, E., & Venance, L. (2019). Bridging the gap between striatal plasticity and learning. In *Current Opinion in Neurobiology* (Vol. 54, pp. 104–112). Elsevier Ltd. https://doi.org/10.1016/j.conb.2018.09.007

Pert, C. B., Kuhar, M. J., & Snyder, S. H. (1976). Opiate receptor: Autoradiographic localization in rat brain. *Proceedings of the National Academy of Sciences of the United States of America*, *73*(10), 3729–3733. https://doi.org/10.1073/pnas.73.10.3729

Peters, A., Steinmetz, N., Harris, K., & Carandini, M. (2019). Striatal activity reflects cortical activity patterns. *BioRxiv*, 703710. https://doi.org/10.1101/703710

Petryszyn, S., Parent, A., & Parent, M. (2018). The calretinin interneurons of the striatum: comparisons between rodents and primates under normal and pathological conditions. In *Journal of Neural Transmission* (Vol. 125, Issue 3, pp. 279–290). Springer-Verlag Wien. https://doi.org/10.1007/s00702-017-1687-x

Planert, H., Berger, T. K., & Silberberg, G. (2013). Membrane Properties of Striatal Direct and Indirect Pathway Neurons in Mouse and Rat Slices and Their Modulation by Dopamine. *PLoS ONE*, *8*(3). https://doi.org/10.1371/journal.pone.0057054

Planert, H., Szydlowski, S. N., Hjorth, J. J. J., Grillner, S., & Silberberg, G. (2010). Dynamics of synaptic transmission between fast-spiking interneurons and striatal projection neurons of the direct and indirect pathways. *The Journal of Neuroscience: The Official Journal of the Society for Neuroscience*, *30*(9), 3499–3507. https://doi.org/10.1523/JNEUROSCI.5139-09.2010

Poon, C.-S., & Schmid, S. (2012). Nonassociative Learning. In *Encyclopedia of the Sciences of Learning* (pp. 2475–2477). Springer US. https://doi.org/10.1007/978-1-4419-1428-6_1849

Postuma, R. B., & Dagher, A. (2005). Basal Ganglia Functional Connectivity Based on a Meta-Analysis of 126 Positron Emission Tomography and Functional Magnetic Resonance Imaging Publications. *Cerebral Cortex*, *16*(10), 1508–1521. https://doi.org/10.1093/cercor/bhj088

Pribram, K. H., Mishkin, M., Rosvold, H. E., & Kaplan, S. J. (1952). Effects on delayed-response performance of lesions of dorsolateral and ventromedial frontal cortex of baboons. *Journal of Comparative and Physiological Psychology*, *45*(6), 565.

Ragozzino, M. E., Jih, J., & Tzavos, A. (2002). Involvement of the dorsomedial striatum in behavioral flexibility: Role of muscarinic cholinergic receptors. *Brain Research*, *953*(1–2), 205–214. https://doi.org/10.1016/S0006-8993(02)03287-0

Ramirez, S., Liu, X., Lin, P.-A., Suh, J., Pignatelli, M., Redondo, R. L., Ryan, T. J., & Tonegawa, S. (2013). Creating a False Memory in the Hippocampus. *Science*, *341*(6144), 387–391. https://doi.org/10.1126/science.1239073

Ranen, N. G., Stine, O. C., Abbott, M. H., Sherr, M., Codori, A. M., Franz, M. L., Chao, N. I., Chung, A. S., Pleasant, N., Callahan, C., Kasch, L. M., Ghaffari, M., Chase, G. A., Kazazian, H. H., Brandt, J., Folstein, S. E., & Ross, C. A. (1995). Anticipation and instability of IT-15 (CAG)(N) repeats in parent-offspring pairs with Huntington disease. *American Journal of Human Genetics*, *57*(3), 593–602. /pmc/articles/PMC1801258/?report=abstract

Ranganath, C., & D'Esposito, M. (2001). Medial temporal lobe activity associated with active maintenance of novel information. *Neuron*, *31*(5), 865–873. https://doi.org/10.1016/S0896-6273(01)00411-1

Rangel-Barajas, C., & Rebec, G. V. (2018). Overview of Huntington's Disease Models: Neuropathological, Molecular, and Behavioral Differences. In *Current protocols in neuroscience* (Vol. 83, Issue 1, p. e47). NLM (Medline). https://doi.org/10.1002/cpns.47

Rao, V. R., & Finkbeiner, S. (2007). NMDA and AMPA receptors: old channels, new tricks. In *Trends in Neurosciences* (Vol. 30, Issue 6, pp. 284–291). Trends Neurosci. https://doi.org/10.1016/j.tins.2007.03.012

Raymond, L. A., André, V. M., Cepeda, C., Gladding, C. M., Milnerwood, A. J., & Levine, M. S. (2011). Pathophysiology of Huntington's disease: time-dependent alterations in synaptic and receptor function. *Neuroscience*, *198*, 252–273. https://doi.org/10.1016/j.neuroscience.2011.08.052

Rebec, G. V. (2018). Corticostriatal network dysfunction in Huntington's disease: Deficits in neural processing, glutamate transport, and ascorbate release. In *CNS Neuroscience and*

Therapeutics (Vol. 24, Issue 4, pp. 281–291). Blackwell Publishing Ltd. https://doi.org/10.1111/cns.12828

Redgrave, P., Rodriguez, M., Smith, Y., Rodriguez-Oroz, M. C., Lehericy, S., Bergman, H., Agid, Y., DeLong, M. R., & Obeso, J. A. (2010). Goal-directed and habitual control in the basal ganglia: implications for Parkinson's disease. *Nature Reviews. Neuroscience*, *11*(11), 760–772. https://doi.org/10.1038/nrn2915

Reiner, A., & Deng, Y. P. (2018). Disrupted striatal neuron inputs and outputs in Huntington's disease. In *CNS Neuroscience and Therapeutics* (Vol. 24, Issue 4, pp. 250–280). Blackwell Publishing Ltd. https://doi.org/10.1111/cns.12844

Ribak, C. E., Vaughn, J. E., & Roberts, E. (1979). The GABA Neurons and their axon terminals in rat corpus striatum as demonstrated by GAD immunocytochemistry. *Journal of Comparative Neurology*, *187*(2), 261–283. https://doi.org/10.1002/cne.901870203

Robbe, D. (2018). To move or to sense? Incorporating somatosensory representation into striatal functions. In *Current Opinion in Neurobiology* (Vol. 52, pp. 123–130). Elsevier Ltd. https://doi.org/10.1016/j.conb.2018.04.009

Robbins, T. W., & Costa, R. M. (2017). Habits. In *Current Biology* (Vol. 27, Issue 22, pp. R1200–R1206). Cell Press. https://doi.org/10.1016/j.cub.2017.09.060

Rosas, H. D., Tuch, D. S., Hevelone, N. D., Zaleta, A. K., Vangel, M., Hersch, S. M., & Salat, D. H. (2006). Diffusion tensor imaging in presymptomatic and early Huntington's disease: Selective white matter pathology and its relationship to clinical measures. *Movement Disorders*, *21*(9), 1317–1325. https://doi.org/10.1002/mds.20979

Rosen, G. D., & Williams, R. W. (2001). Complex trait analysis of the mouse striatum: Independent QTLs modulate volume and neuron number. *BMC Neuroscience*, *2*, 5. https://doi.org/10.1186/1471-2202-2-5

Rosenbaum, R. S., Köhler, S., Schacter, D. L., Moscovitch, M., Westmacott, R., Black, S. E., Gao, F., & Tulving, E. (2005). The case of K.C.: Contributions of a memory-impaired person to memory theory. In *Neuropsychologia* (Vol. 43, Issue 7, pp. 989–1021). Elsevier Ltd. https://doi.org/10.1016/j.neuropsychologia.2004.10.007

Rosenkilde, C. E. (1979). Functional heterogeneity of the prefrontal cortex in the monkey: a review. *Behavioral and Neural Biology*, *25*(3), 301–345. https://doi.org/10.1016/S0163-1047(79)90404-7

Ross, C. A., Aylward, E. H., Wild, E. J., Langbehn, D. R., Long, J. D., Warner, J. H., Scahill, R. I., Leavitt, B. R., Stout, J. C., Paulsen, J. S., Reilmann, R., Unschuld, P. G., Wexler, A., Margolis,

R. L., & Tabrizi, S. J. (2014). Huntington disease: Natural history, biomarkers and prospects for therapeutics. In *Nature Reviews Neurology* (Vol. 10, Issue 4, pp. 204–216). Nature Publishing Group. https://doi.org/10.1038/nrneurol.2014.24

Rossi, M. A., & Yin, H. H. (2012). Methods for studying habitual behavior in mice. *Current Protocols in Neuroscience*, *1*(SUPPL.60). https://doi.org/10.1002/0471142301.ns0829s60

Rothwell, P. E., Hayton, S. J., Sun, G. L., Fuccillo, M. V., Lim, B. K., & Malenka, R. C. (2015). Input- and Output-Specific Regulation of Serial Order Performance by Corticostriatal Circuits. *Neuron*, *88*(2), 345–356. https://doi.org/10.1016/j.neuron.2015.09.035

Rüb, U., Vonsattel, J. P. G., Heinsen, H., & Korf, H.-W. (2015). The neuropathological grading of Huntington's Disease (HD). In *Advances in Anatomy Embryology and Cell Biology* (Vol. 217, pp. 7–23). Springer Verlag. https://doi.org/10.1007/978-3-319-19285-7_2

Ryan, T. J., Roy, D. S., Pignatelli, M., Arons, A., & Tonegawa, S. (2015). Engram cells retain memory under retrograde amnesia. *Science*, *348*(6238), 1007–1013. https://doi.org/10.1126/science.aaa5542

Sadikot, A. F., & Rymar, V. V. (2009). The primate centromedian-parafascicular complex: Anatomical organization with a note on neuromodulation. In *Brain Research Bulletin* (Vol. 78, Issues 2–3, pp. 122–130). Brain Res Bull. https://doi.org/10.1016/j.brainresbull.2008.09.016

Saleeba, C., Dempsey, B., Le, S., Goodchild, A., & McMullan, S. (2019). A student's guide to neural circuit tracing. In *Frontiers in Neuroscience* (Vol. 13, Issue AUG, p. 897). Frontiers Media S.A. https://doi.org/10.3389/fnins.2019.00897

Schausberger, P., & Peneder, S. (2017). Non-associative versus associative learning by foraging predatory mites. *BMC Ecology*, *17*(1), 2. https://doi.org/10.1186/s12898-016-0112-x

Schilling, G., Becher, M. W., Sharp, A. H., Jinnah, H. A., Duan, K., Kotzuk, J. A., Slunt, H. H., Ratovitski, T., Cooper, J. K., Jenkins, N. A., Copeland, N. G., Price, D. L., Ross, C. A., & Borchelt, D. R. (1999). Intranuclear inclusions and neuritic aggregates in transgenic mice expressing a mutant N-terminal fragment of huntingtin. *Human Molecular Genetics*, *8*(3), 397–407. https://doi.org/10.1093/hmg/8.3.397

Schmidt, R., Leventhal, D. K., Mallet, N., Chen, F., & Berke, J. D. (2013). Canceling actions involves a race between basal ganglia pathways. *Nature Neuroscience*, *16*(8), 1118–1124. https://doi.org/10.1038/nn.3456

Schneider, S. A., Wilkinson, L., Bhatia, K. P., Henley, S. M. D., Rothwell, J. C., Tabrizi, S. J., &

Jahanshahi, M. (2010). Abnormal explicit but normal implicit sequence learning in premanifest and early huntington's disease. *Movement Disorders*, *25*(10), 1343–1349. https://doi.org/10.1002/mds.22692

Schröder, K. F., Hopf, A., Lange, H., & Thörner, G. (1975). Morphometrical-statistical structure analysis of human striatum, pallidum and subthalamic nucleus. *Journal Fur Hirnforschung*, *16*(4), 333–350. http://www.ncbi.nlm.nih.gov/pubmed/1214057

Scoville, W. B., & Milner, B. (1957). Loss of recent memory after bilateral hippocampal lesions. *Journal of Neurology, Neurosurgery, and Psychiatry*, *20*(1), 11–21. https://doi.org/10.1136/jnnp.20.1.11

Selemon, L. D., & Goldman-Rakic, P. S. (1985). Longitudinal topography and interdigitation of corticostriatal projections in the rhesus monkey. *Journal of Neuroscience*, *5*(3), 776–794. https://doi.org/10.1523/jneurosci.05-03-00776.1985

Sepers, M. D., & Raymond, L. A. (2014). Mechanisms of synaptic dysfunction and excitotoxicity in Huntington's disease. In *Drug Discovery Today* (Vol. 19, Issue 7, pp. 990–996). Elsevier Ltd. https://doi.org/10.1016/j.drudis.2014.02.006

Sharma, P., & Pienaar, I. S. (2018). The use of dreadds for dissecting the contribution of cellular and neural circuit mechanisms in models of neurodegenerative disease. In *Molecular-Genetic and Statistical Techniques for Behavioral and Neural Research* (pp. 565–596). Elsevier. https://doi.org/10.1016/B978-0-12-804078-2.00024-6

Shimizu, K., & Fukada, Y. (2017). Stereotaxic Surgery for Suprachiasmatic Nucleus Lesions in Mice. *BIO-PROTOCOL*, *7*(12). https://doi.org/10.21769/bioprotoc.2346

Shipp, S. (2017). The functional logic of corticostriatal connections. *Brain Structure & Function*, *222*(2), 669–706. https://doi.org/10.1007/s00429-016-1250-9

Sippy, T., Lapray, D., Crochet, S., & Petersen, C. C. H. (2015). Cell-Type-Specific Sensorimotor Processing in Striatal Projection Neurons during Goal-Directed Behavior. *Neuron*, *88*(2), 298–305. https://doi.org/10.1016/j.neuron.2015.08.039

Skinner, B. F. (1938). The behavior of organisms: an experimental analysis. In *The behavior of organisms: an experimental analysis.* Appleton-Century.

Smith, J. B., Klug, J. R., Ross, D. L., Howard, C. D., Hollon, N. G., Ko, V. I., Hoffman, H., Callaway, E. M., Gerfen, C. R., & Jin, X. (2016). Genetic-Based Dissection Unveils the Inputs and Outputs of Striatal Patch and Matrix Compartments. *Neuron*, *91*(5), 1069–1084. https://doi.org/10.1016/j.neuron.2016.07.046

Smith, K. S., & Graybiel, A. M. (2013). A dual operator view of habitual behavior reflecting

cortical and striatal dynamics. *Neuron*, *79*(2), 361–374. https://doi.org/10.1016/j.neuron.2013.05.038

Smith, Y., & Parent, A. (1986). Differential connections of caudate nucleus and putamen in the squirrel monkey (Saimiri sciureus). *Neuroscience*, *18*(2), 347–371. https://doi.org/10.1016/0306-4522(86)90159-4

Sprengelmeyer, R., Canavan, A. G. M., Lange, H. W., & Hömberg, V. (1995). Associative learning in degenerative neostriatal disorders: Contrasts in explicit and implicit remembering between Parkinson's and huntington's diseases. *Movement Disorders*, *10*(1), 51–65. https://doi.org/10.1002/mds.870100110

Squire, L. R., & Dede, A. J. O. (2015). Conscious and unconscious memory systems. *Cold Spring Harbor Perspectives in Medicine*, *5*(1). https://doi.org/10.1101/cshperspect.a021667

Squire, L. R., & Zola, S. M. (1996). Structure and function of declarative and nondeclarative memory systems. *Proceedings of the National Academy of Sciences of the United States of America*, *93*(24), 13515–13522. https://doi.org/10.1073/pnas.93.24.13515

Strick, P. L., Dum, R. P., & Mushiake, H. (1995). Basal Ganglia 'Loops' with the Cerebral Cortex. In *Functions of the Cortico-Basal Ganglia Loop* (pp. 106–124). Springer Japan. https://doi.org/10.1007/978-4-431-68547-0_7

Szydlowski, S. N., Pollak Dorocic, I., Planert, H., Carlén, M., Meletis, K., & Silberberg, G. (2013). Target selectivity of feedforward inhibition by striatal fast-spiking interneurons. *Journal of Neuroscience*, *33*(4), 1678–1683. https://doi.org/10.1523/JNEUROSCI.3572-12.2013

Takeuchi, T., Duszkiewicz, A. J., & Morris, R. G. M. (2014). The synaptic plasticity and memory hypothesis: Encoding, storage and persistence. In *Philosophical Transactions of the Royal Society B: Biological Sciences* (Vol. 369, Issue 1633). Royal Society. https://doi.org/10.1098/rstb.2013.0288

Tecuapetla, F., Jin, X., Lima, S. Q., & Costa, R. M. (2016). Complementary Contributions of Striatal Projection Pathways to Action Initiation and Execution. *Cell*, *166*(3), 703–715. https://doi.org/10.1016/j.cell.2016.06.032

Tecuapetla, F., Matias, S., Dugue, G. P., Mainen, Z. F., & Costa, R. M. (2014). Balanced activity in basal ganglia projection pathways is critical for contraversive movements. *Nature Communications*, *5*. https://doi.org/10.1038/ncomms5315

Tepper, J. M., & Bolam, J. P. (2004). Functional diversity and specificity of neostriatal interneurons. *Current Opinion in Neurobiology*, *14*(6), 685–692. https://doi.org/10.1016/j.conb.2004.10.003

Tepper, J. M., Tecuapetla, F., Koós, T., & Ibáñez-Sandoval, O. (2010). Heterogeneity and Diversity of Striatal GABAergic Interneurons. *Frontiers in Neuroanatomy*, *4*. https://doi.org/10.3389/fnana.2010.00150

Thorn, C. A., Atallah, H., Howe, M., & Graybiel, A. M. (2010). Differential Dynamics of Activity Changes in Dorsolateral and Dorsomedial Striatal Loops during Learning. *Neuron*, *66*(5), 781–795. https://doi.org/10.1016/j.neuron.2010.04.036

Thorndike, E. L. (1911). Animal intelligence; experimental studies,. In *Animal intelligence; experimental studies,*. The Macmillan Company,. https://doi.org/10.5962/bhl.title.55072

Threlfell, S., Lalic, T., Platt, N. J., Jennings, K. A., Deisseroth, K., & Cragg, S. J. (2012). Striatal dopamine release is triggered by synchronized activity in cholinergic interneurons. *Neuron*, *75*(1), 58–64. https://doi.org/10.1016/j.neuron.2012.04.038

Tonegawa, S., Morrissey, M. D., & Kitamura, T. (2018). The role of engram cells in the systems consolidation of memory. In *Nature Reviews Neuroscience* (Vol. 19, Issue 8, pp. 485–498). Nature Publishing Group. https://doi.org/10.1038/s41583-018-0031-2

Tonegawa, S., Pignatelli, M., Roy, D. S., & Ryan, T. J. (2015). Memory engram storage and retrieval. In *Current Opinion in Neurobiology* (Vol. 35, pp. 101–109). Elsevier Ltd. https://doi.org/10.1016/j.conb.2015.07.009

Tricomi, E., Balleine, B. W., & O'Doherty, J. P. (2009). A specific role for posterior dorsolateral striatum in human habit learning. *European Journal of Neuroscience*, *29*(11), 2225–2232. https://doi.org/10.1111/j.1460-9568.2009.06796.x

Tricomi, E. M., Delgado, M. R., & Fiez, J. A. (2004). Modulation of Caudate Activity by Action Contingency. *Neuron*, *41*(2), 281–292. https://doi.org/10.1016/S0896-6273(03)00848-1

Tripathy, S. P., & Öğmen, H. (2018). Sensory Memory Is Allocated Exclusively to the Current Event-Segment. *Frontiers in Psychology*, *9*(SEP), 1435. https://doi.org/10.3389/fpsyg.2018.01435

Tsujimoto, S., & Postle, B. R. (2012). The prefrontal cortex and oculomotor delayed response: A reconsideration of the mnemonic scotoma. *Journal of Cognitive Neuroscience*, *24*(3), 627–635. https://doi.org/10.1162/jocn_a_00171

Tulving, E. (1972). Episodic and semantic memory. In *Organization of memory* (New York:, pp. 381–403). http://alumni.media.mit.edu/~jorkin/generals/papers/Tulving_memory.pdf

Tulving, E. (1983). *Elements of Episodic Memory*. https://philpapers.org/rec/TULEOE

Tulving, E. (1985). Memory and consciousness. *Canadian Psychology/Psychologie Canadienne*, *26*(1), 1–12. https://doi.org/10.1037/h0080017

Valentin, V. V., Dickinson, A., & O'Doherty, J. P. (2007). Determining the neural substrates of goal-directed learning in the human brain. *Journal of Neuroscience*, *27*(15), 4019–4026. https://doi.org/10.1523/JNEUROSCI.0564-07.2007

Van Duijn, E., Craufurd, D., Hubers, A. A. M., Giltay, E. J., Bonelli, R., Rickards, H., Anderson, K. E., Van Walsem, M. R., Van Der Mast, R. C., Orth, M., & Landwehrmeyer, G. B. (2014). Neuropsychiatric symptoms in a European Huntington's disease cohort (REGISTRY). *Journal of Neurology, Neurosurgery and Psychiatry*, *85*(12), 1411–1418. https://doi.org/10.1136/jnnp-2013-307343

Vandaele, Y., Mahajan, N. R., Ottenheimer, D. J., Richard, J. M., Mysore, S. P., & Janak, P. H. (2019). Distinct recruitment of dorsomedial and dorsolateral striatum erodes with extended training. *ELife*, *8*. https://doi.org/10.7554/eLife.49536

Vicente, A. M., Galvão-Ferreira, P., Tecuapetla, F., & Costa, R. M. (2016). Direct and indirect dorsolateral striatum pathways reinforce different action strategies. In *Current Biology* (Vol. 26, Issue 7, pp. R267–R269). Cell Press. https://doi.org/10.1016/j.cub.2016.02.036

Vogt, C., & Vogt, O. (1920). *Zur Lehre der Erkrankungen des striären Systems*. JA Barth.

Vogt, C., & Vogt, O. (1941). Thalamus studies I-II. *Journal Fur Psychologie Und Neurologie*, *50*, 32–154.

Vonsattel, J. P. G., & DiFiglia, M. (1998). Huntington disease. *Journal of Neuropathology and Experimental Neurology*, *57*(5), 369–384. https://doi.org/10.1097/00005072-199805000-00001

Vonsattel, J. P., Myers, R. H., Stevens, T. J., Ferrante, R. J., Bird, E. D., & Richardson, E. P. (1985). Neuropathological classification of huntington's disease. *Journal of Neuropathology and Experimental Neurology*, *44*(6), 559–577. https://doi.org/10.1097/00005072-198511000-00003

Waldvogel, H. J., Kim, E. H., Tippett, L. J., Vonsattel, J. P. G., & Faull, R. L. M. (2014). The neuropathology of Huntington's disease. *Current Topics in Behavioral Neurosciences*, *22*, 33–80. https://doi.org/10.1007/7854_2014_354

Watkins, K. E., & Jenkinson, N. (2016). The Anatomy of the Basal Ganglia. In *Neurobiology of Language* (pp. 85–94). Elsevier. https://doi.org/10.1016/B978-0-12-407794-2.00008-0

Wilson, C. J. (1993). The generation of natural firing patterns in neostriatal neurons. *Progress in Brain Research*, *99*(C), 277–297. https://doi.org/10.1016/S0079-6123(08)61352-7

Wilson, C. J., & Groves, P. M. (1980). Fine structure and synaptic connections of the common spiny neuron of the rat neostriatum: A study employing intracellular injection of

horseradish peroxidase. *Journal of Comparative Neurology*, *194*(3), 599–615. https://doi.org/10.1002/cne.901940308

Wilson, C. J., & Groves, P. M. (1981). Spontaneous firing patterns of identified spiny neurons in the rat neostriatum. *Brain Research*, *220*(1), 67–80. https://doi.org/10.1016/0006-8993(81)90211-0

Wolff, S., Ko, R., & Ölveczky, B. (2019). Distinct roles for motor cortical and thalamic inputs to striatum during motor learning and execution. *BioRxiv*, 825810. https://doi.org/10.1101/825810

Xu, D., Hao, X., Wang, Z., Duan, Y., Liu, F., Marsh, R., Yu, S., & Peterson, B. S. (2012). A Virtual Radial Arm Maze for the Study of Multiple Memory Systems in a Functional Magnetic Resonance Imaging Environment. *The International Journal of Virtual Reality : A Multimedia Publication for Professionals*, *11*(2), 63–76. http://www.ncbi.nlm.nih.gov/pubmed/26366052

Yanagisawa, N. (2018). Functions and dysfunctions of the basal ganglia in humans. In *Proceedings of the Japan Academy Series B: Physical and Biological Sciences* (Vol. 94, Issue 7, pp. 275–304). Japan Academy. https://doi.org/10.2183/pjab.94.019

Yang, S. T., Shi, Y., Wang, Q., Peng, J. Y., & Li, B. M. (2014). Neuronal representation of working memory in the medial prefrontal cortex of rats. *Molecular Brain*, *7*(1), 61. https://doi.org/10.1186/s13041-014-0061-2

Yin, D., Valles, F. E., Fiandaca, M. S., Forsayeth, J., Larson, P., Starr, P., & Bankiewicz, K. S. (2009). Striatal volume differences between non-human and human primates. *Journal of Neuroscience Methods*, *176*(2), 200–205. https://doi.org/10.1016/j.jneumeth.2008.08.027

Yin, H. H., & Knowlton, B. J. (2004). Contributions of Striatal Subregions to Place and Response Learning. *Learning & Memory*, *11*(4), 459–463. https://doi.org/10.1101/lm.81004

Yin, H. H., & Knowlton, B. J. (2006). The role of the basal ganglia in habit formation. *Nature Reviews. Neuroscience*, *7*(6), 464–476. https://doi.org/10.1038/nrn1919

Yin, H. H., Knowlton, B. J., & Balleine, B. W. (2004). Lesions of dorsolateral striatum preserve outcome expectancy but disrupt habit formation in instrumental learning. *European Journal of Neuroscience*, *19*(1), 181–189. https://doi.org/10.1111/j.1460-9568.2004.03095.x

Yin, H. H., Knowlton, B. J., & Balleine, B. W. (2005). Blockade of NMDA receptors in the dorsomedial striatum prevents action-outcome learning in instrumental conditioning.

European Journal of Neuroscience, *22*(2), 505–512. https://doi.org/10.1111/j.1460-9568.2005.04219.x

Yin, H. H., Knowlton, B. J., & Balleine, B. W. (2006). Inactivation of dorsolateral striatum enhances sensitivity to changes in the action-outcome contingency in instrumental conditioning. *Behavioural Brain Research*, *166*(2), 189–196. https://doi.org/10.1016/j.bbr.2005.07.012

Yin, H. H., Mulcare, S. P., Hilário, M. R. F., Clouse, E., Holloway, T., Davis, M. I., Hansson, A. C., Lovinger, D. M., & Costa, R. M. (2009). Dynamic reorganization of striatal circuits during the acquisition and consolidation of a skill. *Nature Neuroscience*, *12*(3), 333–341. https://doi.org/10.1038/nn.2261

Yin, H. H., Ostlund, S. B., Knowlton, B. J., & Balleine, B. W. (2005). The role of the dorsomedial striatum in instrumental conditioning. *European Journal of Neuroscience*, *22*(2), 513–523. https://doi.org/10.1111/j.1460-9568.2005.04218.x

Résumé

La mémoire procédurale est la mémoire des habitudes motrices. Les ganglions de la base (GB), un groupe de structures impliqué dans les fonctions motrices et cognitives, sont responsables de la formation de cette mémoire. Le striatum, principale structure d'entrée des GB, joue un rôle central dans le transfert de l'information entre le cortex et les autres structures sous-corticales, assurant ainsi la sélection et l'intégration de l'information corticale au sein de boucles fonctionnelles parallèles. Lors d'un apprentissage procédural, le comportement est tout d'abord dirigé vers un but, impliquant les boucles associatives et le striatum dorsomédial (DMS), pour ensuite évoluer vers un comportement habituel automatique, impliquant les boucles sensorimotrices et le striatum dorsolatéral (DLS). L'anatomie des circuits et la dynamique des réseaux striataux au cours de l'apprentissage procédural ont été bien décrites. Cependant, comment la mémoire procédurale est précisément encodée au niveau des réseaux corticostriataux reste inconnu.

Dans mon travail de thèse, nous nous sommes intéressés à la caractérisation des dynamiques des réseaux corticostriataux impliqués dans l'apprentissage procédural et nous avons exploré l'existence de substrats neuronaux responsables de la formation de cette mémoire. Grâce à l'imagerie calcique *ex vivo* nous avons monitoré l'activité des réseaux corticostriataux durant les différentes phases d'apprentissage. Nous avons extrait et analysé les signaux calciques des neurones épineux moyens (MSNs), les neurones de sortie du striatum. Afin de distinguer les MSNs des autres neurones striataux, nous avons développé un classifieur basé sur les réponses calciques des neurones et leur morphologie. Nous avons montré qu'il existe une réorganisation spécifique des réseaux DMS pendant la première phase d'apprentissage moteur. L'activité dans le DMS est diminuée après un entraînement léger, avec une forte activité (HA) maintenue dans un petit groupe de cellules, et retournant à un niveau basal après un entrainement intense. Dans le DLS, la réorganisation est graduelle et localisée dans des 'clusters' d'activité (HA) après un entrainement intense. L'existence des cellules et clusters HA est directement corrélée à la qualité de l'apprentissage. Nous avons ensuite exploré les mécanismes sous-tendant cette réorganisation. Grâce à des enregistrements en patch-clamp nous avons examiné les propriétés des cellules et clusters HA et montré une augmentation du poids synaptique des afférences du cortex cingulaire sur les cellules HA dans le DMS après un entrainement léger. Des études de traçage anatomique ont montré des changements plus robustes dans le DLS avec une augmentation du nombre de projections du cortex somatosensoriel après entrainement intense. Une stratégie cFos-TRAP couplée à la chimiogénétique nous a permis d'inhiber spécifiquement les cellules et clusters HA, et montrer que cela affecte l'apprentissage moteur. Ceci montre la nécessité de ces cellules dans les premières et dernières phases de l'apprentissage moteur respectivement.

Ensuite, notre but était d'explorer s'il existe des déficits d'apprentissage moteur dans une phase présymptomatique dans un modèle murin de la maladie de Huntington (HD), et d'examiner l'association de ces déficits à des altérations au niveau des réseaux corticostriataux. Nous avons d'abord montré qu'il existait des déficits dans la dernière phase d'apprentissage dans ce modèle murin. Grâce à l'imagerie calcique *ex vivo*, nous avons observé une altération des réseaux du DMS et du DLS dans des conditions naïve ainsi qu'une absence de réorganisation des réseaux après l'apprentissage. Ainsi, ces résultats confirment l'importance de la réorganisation des réseaux pour l'apprentissage moteur.

L'ensemble de ce travail offre de nouvelles perspectives quant au rôle des réseaux corticostriataux et leur réorganisation dans l'apprentissage moteur. La nécessité des cellules HA et des clusters ouvrent les portes du monde de l'engramme dans les réseaux striataux.

Mots-clés: Ganglions de la base, striatum dorsomédial, striatum dorsolatéral, apprentissage moteur, réseaux corticostriataux.

Abstract

Procedural memory is the memory of habits, involved in the acquisition and maintenance of new motor skills. The neural substrates underlying this memory are the basal ganglia (BG), a group of structures involved in motor and cognitive functions. The input nucleus of the BG is the striatum, earning it a central role in relaying information between the cortex and other subcortical structures, thus ensuring the selection and integration of cortical information within parallel functional loops. Procedural learning first follows a goal-directed behavior mediated by the associative loops, including the dorsomedial striatum (DMS), which is then transferred to an automatic behavior where habit is formed and mediated by the sensorimotor loops including the dorsolateral striatum (DLS). The anatomy and the evolution of the dynamics of the striatal networks has been well described during procedural learning, and the involvement of each striatal territory in a specific phase of learning established. However, how procedural learning is encoded at the level of the corticostriatal networks remains unknown.

During my PhD work, we were interested in characterizing the dynamics of the corticostriatal networks involved in motor skill learning and determining the neural correlates responsible for the formation of this memory. We first used two-photon *ex vivo* calcium imaging to monitor the activity of the networks during the different phases of procedural learning. First we extracted the calcium responses of only medium spiny neurons (MSNs), the striatal output neurons. To distinguish MSNs from other striatal neurons, we developed a cell-sorting classifier based on the calcium responses of neurons and their morphology. We showed a specific reorganization of the DMS networks during the early phase, and the DLS during the late phase of motor skill learning. In DMS, the activity of the networks decreased after early training and returned to a basal level after late training. The main activity of the DMS networks was held by a group of highly active (HA) cells. In DLS, the reorganization of the activity was gradual and localized in small clusters of activity after late training. We then examined the properties of the HA cells in DMS and clusters in DLS. The existence of HA cells and clusters are directly correlated to the performance of the animals. Whole-cell patch-clamp recordings allowed us to characterize electrophysiological properties of HA bells and determine an increase of the synaptic weight of cingulate cortex inputs to HA cells in DMS after early learning. Anatomical tracing showed more robust changes in the DLS with an increase of the number of somatosensory projections to the DLS after late training. Using an AAV cFos-TRAP strategy coupled to chemogenetics, we inhibited HA and cluster cells, leading to impaired motor learning. These experiments thus highlighted the necessity of these cells in early and late phases of motor skill learning respectively.
Next we wanted to explore if deficits in motor skill learning occur in a premotor-symptomatic phase of a mouse model of Huntington's disease (HD), and if they would be associated to dysfunctions in the corticostriatal networks. We first showed deficits in the late phase of motor skill learning in a mouse model of HD. Using *ex vivo* two-photon calcium imaging, we explored the DMS and DLS networks and we observed an alteration of both networks in naïve HD animals and in addition, an absence of reorganization upon motor skill learning. These results confirm the importance of the reorganization of the networks in motor skill learning.

Altogether, this work provides a new insight on the role of the corticostriatal networks and their reorganization in motor skill learning. The necessity of HA and cluster cells opens the door of the 'engram' world to the striatal networks.
Key words: Basal ganglia, dorsomedial striatum, dorsolateral striatum, motor skill learning, corticostriatal networks.